Title

The Discovery and Characterization of Covalent Stereoselective Sulfinyl Aziridines as Destabilizing Degraders of the Oncogenic Transcription Factor MYC

ISBN

9798189277153

Author

Rosen, Hannah Trella

Publication Date

2026-05-01

Peer reviewed|Thesis/dissertation

The Discovery and Characterization of Covalent Stereoselective Sulfinyl Aziridines as Destabilizing Degraders of the Oncogenic Transcription Factor MYC

By

Hannah Trella Rosen

A dissertation submitted in partial satisfaction of the

Requirements for the degree of

Doctor of Philosophy

in

Molecular Toxicology

in the

Graduate Division

of the

University of California, Berkeley

Committee in charge:

Professor Daniel K. Nomura, Chair

Professor Andreas Stahl

Professor Thomas J. Maimone

Spring 2026

Abstract

The Discovery and Characterization of Covalent Stereoselective Sulfinyl Aziridines as Destabilizing Degraders of the Oncogenic Transcription Factor MYC

by

Hannah Trella Rosen

Doctor of Philosophy in Molecular Toxicology

University of California, Berkeley

Professor Daniel K. Nomura, Chair

Drug discovery has changed greatly over time. Humanity once derived most medications from natural products and now we can treat a person by gene-editing their cells within their body. It is only recently that the scientific community even understands what proteins cause specific phenotypes or diseases. This work explores the challenges of modern drug discovery and the solution that is presented in the form of covalency. In addition, the relevant biology and druggability of the oncogenic transcription factor MYC is discussed. Lastly, this dissertation discusses the development and characterization of covalent stereoselective sulfinyl aziridines that act as destabilizing degraders against MYC.

Chapter 1 provides an overview on drug development and the use of covalent small molecules to overcome challenges in discovery and target identification. This section discusses the nature of covalent binding and how it differs from traditional inhibitor modalities. Briefly, workflows in chemoproteomics and bio-orthogonal chemistry are highlighted.

Chapter 2 focuses on the biology and efforts to drug the oncogene, MYC. Nonmalignant MYC biology and the subsequent transition to malignancy is evaluated. Similarly, the complexity of MYC cancer biology and its involvement in almost every area of cell biology. Brief discussions of previous efforts to drug MYC are included with a focus on small molecule modalities.

Chapter 3 describes the discovery and characterization of covalent stereoselective sulfinyl aziridine small molecules that act upon MYC as destabilizing degraders. This work builds upon previous literature to exploit the intrinsic disorder of many transcription factors as a vulnerability for their targeted degradation. I screen a library of stereochemically paired small molecules made by Dr. Kelvin Li, evaluating for MYC degradation. Upon discovery of the hit molecule KL2-236, I characterize the mechanism of degradation through proteasomal rescue studies as well as characterize the interaction between KL2-236 and MYC through multiple chemical biology approaches. I establish KL2-236 as a destabilizing degrader and use site directed mutagenesis to determine the site of modification of KL2-236 on MYC. I show on-target downstream effects of MYC

degradation leading to a reduction in MYC transcriptional activity and MYC target genes by transcriptomics. Dr. Kelvin Li used structure-activity relationship to synthesize over 180 analogs of KL2-236 and I tested the analogs to find a more potent and effective MYC degrader in KL4-219A. I fully characterize KL4-219A and find that it is more potent than the initial hit compound, but also selective for MYC in proteome wide analysis. Overall, this work reveals a novel ligandable site within MYC and indicates that certain intrinsically disordered regions within transcription factors, such as MYC, can be interrogated by isomerically unique chiral small molecules, leading to destabilization and degradation.

Table of Contents

Dedication

To my friends and family

Without your love and support, I do not believe I would be where I am today.

To my former self

Damn it's a lot of hard work, but it's so worth it. You don't know how much there is to learn or how far you will come, but it will all work out in the end.

For Barbara Rosen

Cancer is cruel and you have gone too soon. Every day following your diagnosis, this dissertation has been dedicated to you.

Acknowledgements

Mom and Dad – I love you more than I have the words to describe and I hope I can convey that I would not have this dissertation without you both. Mom, you have shown me what it looks like to be a powerful woman in science, having both the career and the family. You listen to me when times are tough, ground me in reality and never fail to make me feel loved. I cannot wait to join you as the second doctor in the family! Dad, I know science isn't exactly your thing, but you have done so much to learn and support me regardless. I know that if I call, we can talk for hours about my work, even if you get lost. Your wisdom is always on my mind as I haven't made a figure in years where I don't consider principles of design. I am so lucky to have parents who both understand my goals, support me in reaching them, and have set me up for success in more ways than I can count. I hope you read this work and kvell.

Leah and Olivia – I wouldn't be me without you. I have only known what it is to be your big sister and it's one of my favorite titles. I am so proud of you both and I am so excited to see what comes next. Leah, you inspire me to be more creative, look at furniture with a critical eye and let loose when I can. Olivia, you remind me that knowledge is power, animals are better than people and of course the differences between antler and horn. Even when I am annoying, you love and support me. I am eternally grateful.

Paul – My puffin buddy, my partner in life, my best friend, my teammate and my biggest supporter. We have been through a lot together over the last 9 years and it was not always smooth sailing. We weathered the pandemic, long distance, and more and for that, I am incredibly proud of us. I have always told people I came to Berkeley because it was best for my career and although that is true, I would be lying if I didn't say that I came to Berkeley for you too. I can't wait to marry you and to see what adventures come our way. I love you so much!

Margot – According to legend, you were Paul's friend first and although that might be true, I will maintain that we became friends all on our own. I will forever be grateful that I had a friendly face during my first weeks in lab. You are one of the kindness most genuine people I know, and I am so glad you are in my life. I hope you never learn how to spell or stop saying "love you" when we hang up the phone.

Melissa – My best friend! There are no other words to describe it. We are separated by thousands of miles and yet I know when we are together, everything falls into place as if no time has passed. You are the handiest, most hard working and dedicated person I have ever met, truly. I love you and I hope with the core of my being that we live closer together in the future.

Kelvin – I could not have asked for a better collaborator. Working with you has been an honor and a privilege. I am so proud of what we have done together. Thank you for never laughing at my lack of chemistry knowledge and for always walking down the hill to give me compounds. I am so grateful for your skills and to be your friend.

Alice – You have been a constant balancing and grounding force in my life for over a decade. You have watched me grow, literally and figuratively and I know that I would not have this dissertation without your time and support. Thank you from the bottom of my heart.

Taylor, Melissa, and Aman – The four of us have seen it all together. I feel so lucky that I came into this lab with such amazing scientists and friends. You all have taught me so much. When things are difficult, I have taken comfort in knowing I am not alone and we can always vent to each other.

Brynne – You showed me all the best parts of mentorship with very few of the downsides. I am so proud of the work we have done together and to watch you grow as a scientist and independent thinker. I got so lucky that you happen to be in my NST 11 section and that you always read instructions. I can't wait to see what your future holds and know I am always there to support you.

Nomura Labmates of past and present – Bridget, Alicia, Margot, Ethan, Anand, Ellie, Vienna, Lauren, Kosuke, Chris, and Isaac – I am so grateful for you all. You guys have constantly pushed me to be a better scientist. You have shown me what an amazing lab culture can look like and I am forever grateful. Late nights in IGI would not be tolerable without your company. The laughs and occasionally tears that we have shared are invaluable to me. Thank you!

Emma, Pete, and Ann – Thank you for opening your family to me. I could not be happier to be part of such a loving, caring, and silly family, full of inside jokes, songs, and portmanteaus.

Hong – I have said it before, but I will say it again. You gave me the scientific foundation from which I have built this dissertation on. I would not be the scientist I am today without your mentorship. Thank you for all that you have done for me.

Professor Dan Nomura – I would not be here without your guidance, determination and passion. I remember sitting in your office on my first day and you suggested we go after MYC. I literally thought you were insane because it's the holy grail and I did not think I would have the skills to tackle such a challenge. Well, I am happy to say you were right and I was wrong. Thank you for your support.

List of Figures

List of Abbreviations

ABPP	Activity-Based Protein Profiling
AKT	Protein Kinase B
ASO	Antisense Oligonucleotide
BCA	Bicinchoninic Acid
BET	Bromodomain and extra-terminal domain
bHLHZ	Basic Heliz-Loop-Helix Leucine Zipper
BRD4	Bromodomain-containing protein 4
BSA	Bovine Serum Albumin
BTZ	Bortezomib
CDCA4	Cell division cycle-associated protein 4
CDK7	Cyclin-Dependent Kinase 7
CDK9	Cyclin-Dependent Kinase 9
cDNA	Complementary DNA
CETSA	Cellular Thermal Shift Assay
CTNNB1	Beta-Catenin
CuAAC	Copper(I)-Catalyzed Azide-Alkyne Cycloaddition
DAPI	4',6'-diamidino-2-phenylindole
DCM	Dichloromethane
DDA	Data-dependent Acquisition
DMAP	4-(Demethylamino)pyridine
D_{max}	Maximum Degradation
DMEDA	N,N'-Dimethylethylenediamine
DMEM	Dulbecco's Modified Eagle Medium
DMF	Dimethylformamide
DMSO	Dimethyl sulfoxide
DNA	Deoxyribose Nucleaic Acid
DTT	Dithiothreitol
E-Box	Enhancer Box
E2F	Early 2 Factor
EC_{50}	Half Maximal Effective Concentration
EDTA	Ethylenediaminetetraacetic acid
ELISA	Enzyme-Linked Immunosorbent Assay
ESI	Electrospray Ionization
EtOAc	Ethyl acetate
EtOH	Ethanol

FBS	Fetal Bovine Serum
FOXA1	Forkhead Box Protein A1
G1	Gap 1 phase
G2M	Gap 2 Mitosis transition
G3BP1	Ras-GTPase-activating protein (GAP)-binding protein 1
GAPDH	Glyceraldehyde-3-phosphate dehydrogenase
GSEA	Gene Set Enrichment Analysis
GSH	Glutathione
HCl	Hydrochloric Acid
HEPES	4-(2-hydroxyethyl)-1-piperazineethanesulfonic acid
HiBiT	High-affinity Binary Technology
HPLC	High Phase Liquid Chromatography
HRP	Horseradish Perioxidase
IA-alkyne	Iodoacetimide-Alkyne
ID1	Inhibitor of DNA Binding 1
IFNα	Interferon alpha
IFNγ	Interferon gamma
IL6	Interleukin 6
IPTG	Isopropyl β-D-1-thiogalactopyranoside
IR	Infrared Spectroscopy
JAK	Janus kinases
K_d	Equilibrium dissociation constant
K_{off}	Dissociation rate constant
K_{on}	Association rate constant
LC-MS	Liquid Chromatography-Mass Spectrometry
LC-MS/MS	Liquid Chromatography-tandem Mass Spectrometry
LgBiT	Large Binary Technology
MAX	Myc-associated factor x
MCL1	Myeloid Cell Leukemia 1
MeCN	Acetonitrile
mRNA	messenger RNA
MS/MS	Tandem Mass Spectrometry
MsCl	Methanesulfonyl Chloride

mTORC1	Mechanistic Target of Rapamycin Complex 1
NaCl	Sodium Chloride
NaOH	Sodium Hydroxide
NP-40	Nonidet P-40
Opti-MEM	Optimized Minimum Essential Medium
p15	p15(INK4b)
p21	p21 Waf1/Cip1
PBS	Phosphate-Buffered Solution
PBST	Phosphate-Buffered Solution with Tween 20
PI3K	Phosphatidylinositol 3-kinase
POI	Protein of Interest
RIPA	Radioimmunoprecipitation Assay (buffer)
RNA	Ribose Nucleic Acid
RPMI1640	Roswell Park Memorial Institute (RPMI medium)
rRNA	Ribosomal RNA
SDS	Sodium Dodecyl Sulfate
SDS/PAGE	Sodium Dodecyl Sulfate-Polyacrylamide Gel Electrophoresis
SEC buffer	Size Exclusion Chromatography
STAT3	Signal Transducer and Activator of Transcription 3
TBST	Tris-Buffered Solution with Tween 20
TBTA	Tris(benzyltriazolylmethyl)amine
tBuOH	Tert-butyl alcohol
TEAB	Tetraethylammonium bromide
TEAD	Transcriptional Enhanced Associate Domain
TEV	Tobacco Etch Virus
TFA	Trifluoroacetic acid
TGX	Tris-Glycine eXtended
THF	Tetrahydrofuran
THPTA	Tris(3-hydroxypropyltriazolylmethyl)amine
TLC	Thin-Layer Chromatography
T_m	Melting Temperature
TMB	3,3',5,5'-tetramethylbenzidine
TMT	Tandem Mass Tag
Tris	Tris(hydroxymethyl)aminomethane

UV	Ultraviolet
Wnt	Wingless-releated integration site
WT	Wild-type

Chapter 1 – Covalency and Chemoproteomics as a Strategy to Overcome Challenges in Modern Drug Discovery

1.1 Challenges in Drug Discovery

Historically, drug discovery used small molecules to inhibit a disease-causing protein by designing a compound that fit into a binding pocket. This strategy is contingent on the protein of interest (POI) having a defined hydrophobic cavity or cleft. Modern medicine has moved forward significantly such that today, most disease-causing proteins with known binding pockets for which an inhibitor *can* be designed, *have* been designed and made. The problem now stems from the harsh reality that a significant portion of disease-causing proteins do not have this exploitable binding pocket and thus traditional noncovalent small molecule inhibitors are no longer suitable.[1,2] These POIs are now known as "undruggable" and require the full spectrum of scientific approaches to target them.

Traditional noncovalent drugs bind to proteins reversibly. This noncovalent interaction occurs when the molecule is associated with the protein through means such as van der waals forces, hydrogen bonding and electrostatic interactions. These interactions are not strong enough to permanently form a drug-protein complex but rather equilibrate between an "on" and "off" state or residence time. The binding affinity of the molecule to a POI is defined as the dissociation constant of the drug-protein complex (K_d) in which the equilibrium constant of the rate of dissociation of the complex (k_{off}) is divided by the rate of association of the complex (k_{on})(**Figure 1.1.a**).[3] This metric is similar to the inhibitory constant used for noncovalent inhibitors (K_i).[3] To maintain inhibition of the POI, the molecule must possess a high K_i or strong binding affinity to the protein.[4] Drugs with strong binding affinity must have high on-rates with a relatively low off-rates. For proteins that have shallow or non-existent binding pockets, noncovalent drug interactions may not be sufficient for tight binding, high residence time in the drug-protein complex, and thus ineffectively inhibited.

A strategy to overcome challenges with low binding affinity drugs can be the use of covalency. Covalent drugs possess a reactive functional group, also known as a "warhead" which reacts with a POI. There are many types of covalent warheads but often are electrophilic which react with nucleophilic amino acid side chains such as cysteine, lysine, tyrosine and serine.[5] Covalent drug binding occurs in two steps. The first step is the formation of the drug-protein complex by noncovalent interactions (K_i) and the second step is the reaction of the warhead with the protein to irreversibly form a covalent bond between the drug and protein (k_{inact}).[6] The rate of drug binding for a covalent molecule is calculated as k_{inact} divided by K_i with k_{inact} directly indicating the reactivity of the warhead and K_i as the noncovalent binding affinity (**Figure 1.1.b**).[6] Covalency overcomes the challenges of unstable low affinity drug-protein interactions because the complex can no longer dissociate following the formation of the covalent bond. Once the reaction has occurred, the protein is permanently inhibited until endogenous turnover occurs and new protein is synthesized.

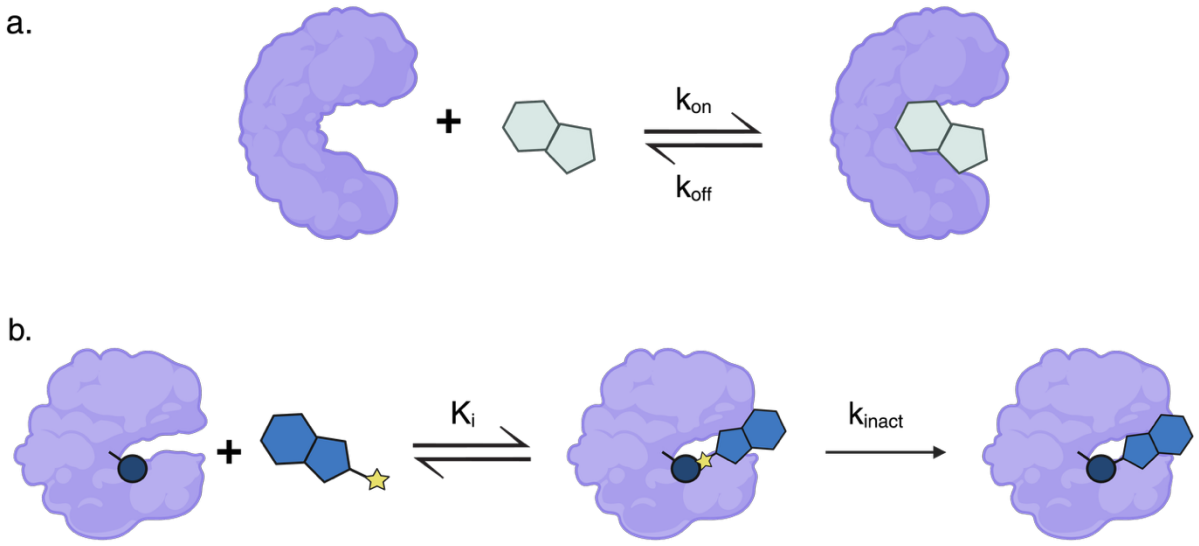

Figure 1.1: Binding Kinetics in Noncovalent vs. Covalent Inhibitors. a. Noncovalent inhibitors bind reversibly, at the rate defined by the inhibitory constant (K_i), a type of dissociation constant. **b.** Covalent inhibitors bind in two steps: the first is reversible, noncovalent-type interaction with the POI, then during the second step, the reactive warhead (yellow star) reacts with the reactive functional group of the protein (blue circle). This second step is irreversible and results in the formation of a covalent bond between the POI and covalent compound.

1.2 Chemoproteomic Workflow Enabled by Covalent Molecules

Besides stabilizing weak protein-drug interactions in cells, covalency can be used to simplify and improve target identification using chemoproteomics. Since the covalent molecule is permanently bound to a POI, downstream applications in which protein structure is disrupted will not affect molecular binding. To profile proteome-wide reactivity of covalent compounds, activity-based protein profiling (ABPP) can be used.[7] Established by Ben Cravatt's lab, ABPP involves competition of a covalent compound of interest by a covalent probe, which can be functionalized in a variety of ways for further utility. Functionalization can include the addition of an affinity handle for enrichment, fluorophore for imaging, or bio-orthogonal functional group. To identify the targets of the covalent compound of interest, proteins undergo tryptic digestion and analysis of the resulting dissolved peptides by liquid chromatography couples with mass spectrometry (LC-MS). In some cases, using a covalent molecule already functionalized with an alkyne handle may be preferable and used instead. After intact cells or proteome are incubated with an alkyne functionalized compound, azide containing molecules are attached through a copper(I)-catalyzed azide-alkyne cycloaddition (CuAAC).[8] Proteins may then be enriched, undergo tryptic digest, and peptides analyzed by LC-MS/MS. Peptides analyzed by LC-MS/MS have the potential to provide valuable information about site of modification, protein engagement, and levels of protein expression across the proteome.

Chapter 2 – MYC: The Undruggable High Value Oncology Target

2.1 Introduction

MYC was first discovered as a cellular homolog of a viral oncogene from an avian virus that causes leukemia and sarcoma in chickens in the 1970s.[9,10] The MYC family includes regulator genes and proto oncogenes that encode for transcription factors including N-MYC, L-MYC and C-MYC.[11] C-MYC (termed MYC henceforth) is a universal transcription amplifier that regulates almost every physiological process in a cell including cell cycle, metabolism, proliferation, differentiation and apoptosis.[12] Under normal cellular conditions, MYC acts as a transcription factor, binds to MAX (MYC-associated factor X) and the complex translocate into the nucleus to bind at E-Box consensus sequences with high affinity and other non-consensus sites with lower affinity.[11] This binding event relieves the transcriptionally paused RNA polymerase and actives transcriptional elongation.[11] MYC expression levels are normally tightly controlled, but when dysregulated, MYC has been associated with many diseases, including numerous types of cancer.[12] Some estimates indicate that MYC may be dysregulated in around 70% of all human cancers.[13] Because of the high occurrence of MYC dysregulation in cancer, it is considered a high-value target for drug discovery. To properly target such an important protein, understanding its complex biology is paramount to success.

2.2 MYC in Cancer Biology

The areas of cell biology in which MYC plays a direct role are too numerous to describe in extensive detail, especially in context of cancer. For example, in normal physiology, over-expression of MYC increases sensitivity to apoptosis.[14,15] However, under MYC activation, the cell can overcome physiological barriers to promote cancer cell survival through several interdependent cell-intrinsic mechanisms.[16] These include protein and ribosomal biosynthesis, metabolism, proliferation, autophagy, cell adhesion, gene instability and angiogenesis (Figure 2.2).[16] Moreover, MYC enforces out of control cell proliferation by giving cancer cells the ability to re-enter the cell cycle[14] and advances cells through the cell cycle by bypassing cell cycle checkpoints.[17] MYC can antagonize the expression of p15 and p21, key cell cycle checkpoint proteins.[18] It has also been shown that MYC target genes are responsible for cell growth including rRNA transcription and processing, ribosomal protein transcription and translation, and translation initiation.[19] If the cell has an increased capacity to produce translational machinery and protein itself, it can more easily grow and divide. Another major change resulting from MYC dysregulation is a global rewiring of multiple metabolic pathways including glycolysis.[11] More specifically, MYC-transformed cells have an increased glucose utilization and increased expression of key glycolytic enzymes.[11] All of these phenomena are tissue specific and developmentally contextual which further complicates the nature of MYC cancer biology. Despite these challenges, MYC presents itself as a fantastic candidate for drug discovery due to its overwhelming importance in cancer biology.

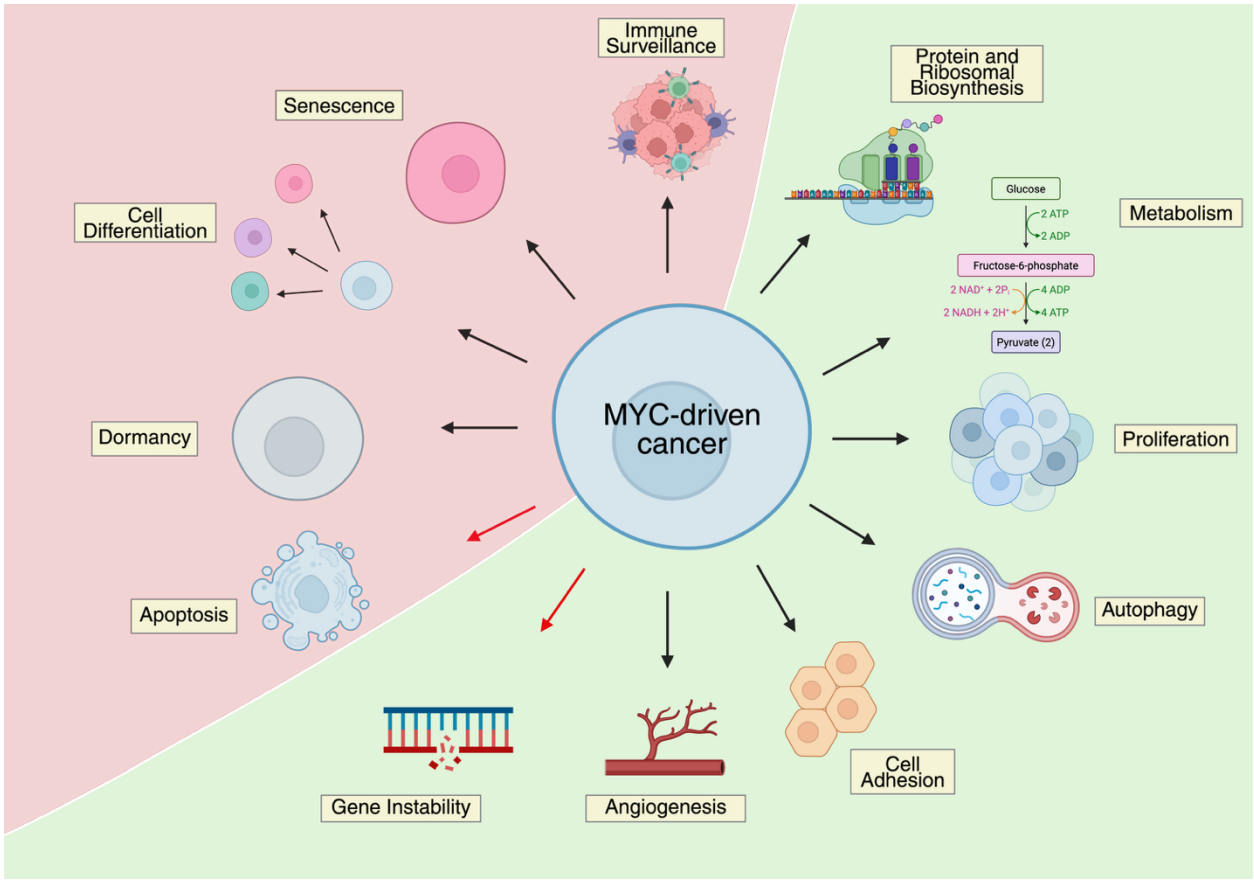

Figure 2.2: The Grand Orchestrator of the Hallmarks of Cancer. MYC regulates several cancer cell-intrinsic pathways to promote cancer cell growth and survival (green area). MYC also simultaneously blocks cellular protective mechanisms such as differentiation and senescence, thereby promoting cancer progression (red area). Paradoxically, MYC induces cellular processes such as apoptosis and chromosomal instability that can be detrimental to cancer cell survival (red arrows). All these hallmarks of cancer are regulated by MYC in unison to drive cancer progression.

2.3 Previous efforts toward targeting MYC

Although MYC may be considered a high value target for drug discovery, for most of its known existence, it has been considered an undruggable protein. The traditional approach to targeting a protein or enzyme is to develop a small molecule that fits into its binding pocket to inhibit the activity of the protein or enzyme. This methodology cannot be applied to MYC because significant portions of the protein are intrinsically disordered, meaning they lack a fixed, ordered structure.[20] There is no easily accessible binding pocket for which to develop a small molecule against. Because of this problem, the scientific advancement toward targeting MYC have been met with mixed success and a variety of approaches.

The very first attempt at targeting MYC was in 1988 with an antisense oligo (**Figure 2.3**).[21] The authors report that with the expression of antisense oligo, they see an increase in cells arrested in G1.[21] The authors do not outwardly consider this advancement to be therapeutic but rather aim to fundamentally understand how MYC dysregulation changes

cellular differentiation. But given their initial success with antisense oligonucleotides, Inex Pharmaceuticals developed INX-3280 against MYC in 1999 (**Figure 2.3**). The preclinical studies showed no significant toxicities in cynomolgus monkeys.[22] Phase I clinical trial was started in 2000 but discontinued in 2002 when it was unsuccessfully repurposed as an anti-restenosis medication.[23] Since this first attempt, at least five other clinical trials to directly inhibit MYC have occurred and all have been discontinued.[24]

Another major advancement toward targeting MYC has come from a mini protein modality. In 1998, Omomyc was originally designed and developed for use as a MYC dominant negative tool (**Figure 2.3**).[25] Scientists would transfect cells with viral constructs containing Omomyc and repeatedly saw MYC inhibition. It could also be applied to transgenic murine models where inducible expression of Omomyc would show decreased tumor proliferation and metastasis.[26] It's mechanism of action is threefold, all of which inhibit MYC function. Omomyc can bind to MAX thereby displacing endogenous MYC. It can also form homodimers with itself and block the E-box binding sites on DNA. Lastly it's able to bind directly with MYC thereby sequestering it in protein complexes that are unable to bind DNA.[25,27] Because this mini-protein was used to study MYC cancer biology before it was developed for medicinal applications, by the time there was interest in moving towards commercial ventures, there was a large body of evidence that systemic MYC inhibition was feasible and had a favorable therapeutic window.[24] Only in 2021 did scientists discovery that purified Omomyc was intrinsically cell penetrating and could itself be a viable candidate for clinical development.[28] To date, Omomyc is the only MYC-targeting effort to successfully complete Phase I trials and begin Phase II and Phase Ib.[24] Despite these promising results, there still remains an unmet need for a direct-acting drug against MYC.

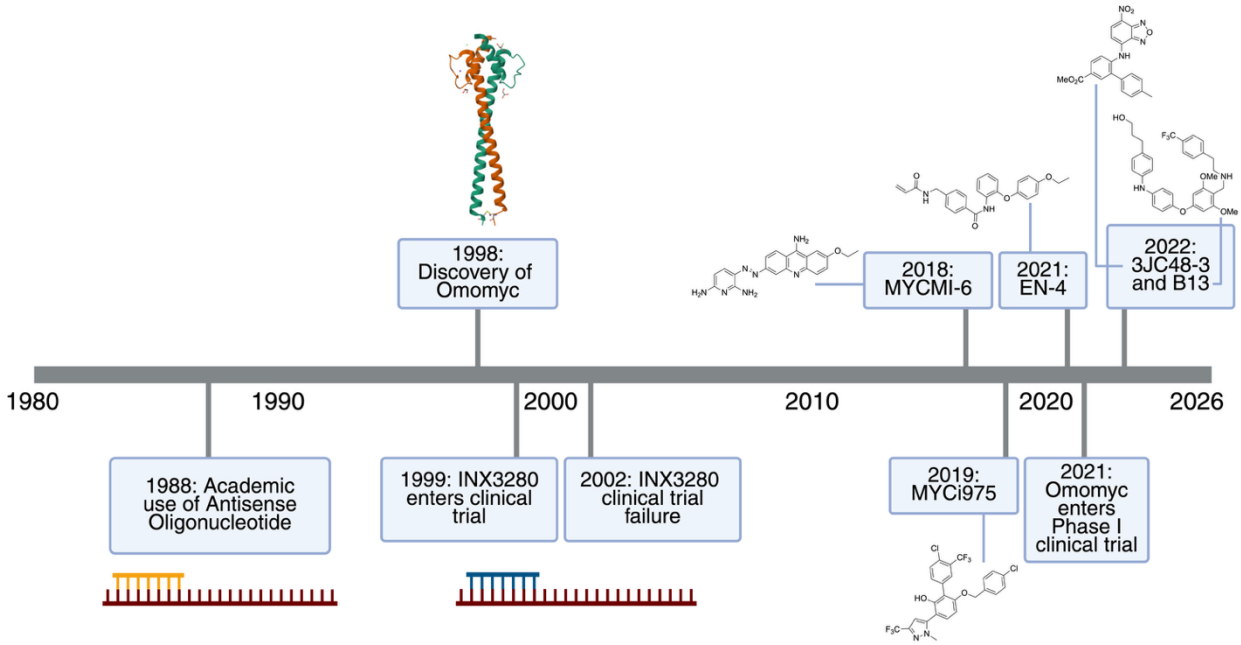

Figure 2.3: Timeline of Select MYC-Targeting Drug Candidates. A timeline from 1980 to present (2026) indicating key discoveries towards targeting MYC. The first ASO and proof of

concept toward lowering MYC protein levels was developed in 1988. In 1998 the mini-protein Omomyc was developed as a dominant negative for MYC studies. Following the first ASO study, INX3280 was developed against MYC but failed clinical trials a few years after starting in 2002. More recently, there have been several small molecule efforts to target MYC including EN-4 from the Nomura Lab.

Small molecule inhibitors remain a valuable tool in the arsenal of drug discovery with which to target MYC. Despite its lack of secondary and tertiary structure when not in a complex biological system, many efforts have been made to drug MYC using small molecules recently. In 2018, Castell et. al. developed MYCMI-6 which binds within the basic helix-loop-helix leucine zipper (bHLHZ) domain with an IC50 of 0.5μM in neuroblastoma tumor xenograft model (**Figure 2.3**).[29] In 2019, using an *in-silico* screen, MYCi975 was developed and shown to block MYC-MAX interaction and caused reduction in tumor growth in mouse allograft models of MYC-dependent prostate cancer (**Figure 2.3**).[30] This preliminary work has been expanded significantly and appears promising for clinical development. Towards this effort, Shukla et. al. have developed 3JC48-3 and have shown decreased prostate cancer cell growth and viability *in-vitro* as well as anti-tumor activity *in-vivo* (**Figure 2.3**).[31] Similarly, another MYC-MAX dimerization inhibitor has been developed, B13, showing cytotoxicity against colorectal cancer cells *in-vitro* and decreased growth in mouse tumor xenograft models (**Figure 2.3**).[32] Unfortunately, 3JC48-3 and B13 have not been shown to prove direct MYC inhibition. Direct-acting MYC engagement remains challenging and an area in which drug development could expand.

Nevertheless, the Nomura lab has strived to develop a direct-acting MYC ligand and found initial success in the work of Dr. Alexander Cioffi and Dr. Lydia Boike. They found a covalent small molecule, EN4, which targets C171 of MYC, causing downregulation of MYC target genes and impairing tumor growth in a mouse xenograft model of MDA-MB-231 breast cancer cells (**Figure 2.3**).[33] It is with this work that the basis for my dissertation is founded upon.

Chapter 3 – Discovery of Sulfinyl Aziridines as Stereoselective Covalent Destabilizing Degraders of the Oncogenic Transcription Factor MYC

This chapter is based on the *Angewandte Chemie International Edition* publication "Sulfinyl Aziridines as Stereoselective Covalent Destabilizing Degraders of the Oncogenic Transcription Factor MYC" [34] and has been adapted with the permission from all co-authors.

3.1 Summary

While MYC is a significant oncogenic transcription factor driver of cancer, directly targeting MYC has remained challenging due to its intrinsic disorder and poorly defined structure, deeming it "undruggable." Whether transient pockets formed within unstructured regions of proteins can be selectively targeted with small molecules remains an outstanding challenge. Here, we developed a stereochemically-paired spirocyclic oxindole aziridine covalent library and screened this library for degradation of MYC. We identified a hit covalent ligand KL2-236, bearing a unique sulfinyl aziridine warhead, that engaged MYC as pure MYC/MAX protein complex and in cancer cells to destabilize MYC, inhibit MYC transcriptional activity and degrade MYC in a proteasome-dependent manner through targeting intrinsically disordered C203 and D205 residues. Notably, this reactivity was most pronounced for specific stereoisomers of KL2-236 with a diastereomer KL4-019 that was largely inactive. Mutagenesis of both C203 and D205 completely attenuated KL2-236-mediated MYC degradation. We also optimized our KL2-236 hit compound to generate a more potent, selective, and durable MYC degrader KL4-219A. Our results reveal a novel ligandable site within MYC and indicate that certain intrinsically disordered regions within transcription factors, such as MYC, can be interrogated by isomerically unique chiral small molecules, leading to destabilization and degradation.

3.2 Introduction

Among "undruggable" targets that have been identified, transcription factors have represented a particularly challenging class of targets for drug discovery due to the presence of large regions of intrinsic disorder and poorly defined structures for many members. Whether these unstructured regions of transcription factors have ligandable sites that can be pharmacologically targeted in a selective manner is often unclear.[35] MYC has been a particularly elusive target for direct targeting due to its high degree of intrinsic disorder and poorly defined structure. [36–38] Several therapeutic strategies have indirectly targeted MYC or the MYC pathway. MYC is a nuclear transcription factor that drives the expression of genes required for cell growth, metabolism, and survival, and it is one of the most frequently amplified oncogenes in human malignancies.[38,39] Through required heterodimerization with MAX, MYC binds E-box sequences to activate its targets. Because of MYC's key role in tumor development, extensive efforts have focused on developing agents that either block MYC directly or interfere with pathways that control it.[37,38,40,41] Such strategies include impeding MYC transcription with bromodomain and extraterminal (BET) family inhibitors or CDK7/9 inhibitors[42], reducing MYC translation via mTORC1 or AKT/PI3K inhibitors, preventing MYC-MAX dimer formation [37,38], and inhibiting BRD4 with inhibitors such as JQ1 and GSK525762 that disrupt BRD4 binding at acetylated chromatin regions necessary for MYC transcription. Small-molecule microarray approaches have also uncovered MAX/MAX homostabilizers that sequester MAX away from MYC, thereby impairing MYC's transcriptional function,[43] and small-molecule inhibitors have been developed that disrupt the WDR5 and MYC protein interaction.[44–47] Nevertheless, directly targeting MYC remains challenging due to its predominantly disordered structure and lack of prominent binding pockets, earning it the reputation of being "undruggable".

Over the past several decades, covalent chemoproteomic approaches such as activity-based protein profiling (ABPP) have arisen as powerful approaches for uncovering unique, cryptic, allosteric, or shallow ligandable sites that can be accessed with covalently-acting small molecules through balancing reactivity with binding affinity.[33,48–53] There have also been several successes in using covalent chemistry to target transcription factors, including against a palmitoylation site cysteine in the Hippo pathway transcription factor TEAD [54], a cysteine within the Wnt pathway transcription factor CTNNB1[51], and most recently, a cysteine in FOXA1 to rewire its transcriptional specificity.[52] Recently, we have also uncovered a covalent ligand EN4 that targets an allosteric cysteine, C171 (or C186, depending on the MYC isoform and associated protein sequence) to cause destabilization of MYC and subsequent inhibition of MYC/MAX binding to DNA and MYC transcriptional activity in cells, leading to downregulation of MYC target genes, and anti-proliferative and anti-tumorigenic effects.[33] The Bar-Peled lab has also previously used covalent chemoproteomics profiling with scout ligands across a panel of cancer cell lines to identify ligandable sites across the proteome, including in MYC.[53] Some of these covalent ligands, including EN4, have been shown to target intrinsically disordered cysteines within these proteins.[33] However, whether there is an actionable binding pocket or non-covalent interactions recognized by these molecules versus whether the binding occurs mainly through reactivity-driven binding has been less clear. One strategy to begin to address this question is through the use of stereochemically matched compound libraries composed of either enantio- and/or diastereomerically matched compounds that allow the direct comparisons between these stereoisomers to determine if stereoselective interactions exist in the bioconjugation of the corresponding protein target with the electrophilic fragment. Previous studies from Cravatt, Vinogradova, and others have extensively exemplified such studies using various chemical scaffolds such as tryptoline-based acrylamides and spirocyclic acrylamides.[49,52,55–58]

In this study, we discovered that spirocyclic oxindole-based sulfinyl aziridines can stereoselectively modulate MYC levels and thus inhibit MYC transcriptional activity in cells. We synthesized a small library of covalent ligands bearing electrophilic aziridine-derived warheads of variable reactivity coupled with stereochemical pairing. Through this effort, we identified and optimized a covalent ligand that directly engages an intrinsically disordered cysteine in MYC in a stereoselective manner and, as a result, leads to MYC destabilization and proteasome-dependent degradation in cells.

3.3 Results

3.3.1 Synthesis & Screening of Stereochemically Paired Covalent Ligand Library

We synthesized a small library of stereochemically well-defined aziridines bearing tunable sulfonyl and sulfinyl warhead activating groups surrounding a conserved spirocyclic oxindole core–a privileged motif in drug discovery **(**Figure 3.1**a**). [59–64] While oxindole-based sulfonyl aziridines have been shown to react with indoles, thiols, alcohols, and amines in a flask, their utility and limitations (toxicity, GSH stability, etc.) are unexplored in cellular, proteome-wide contexts as required for covalent drug discovery. [65,66] This fact,

together with the observation that their sulfinyl congeners are even less interrogated in similar contexts, prompted us to synthesize and interrogate these novel chiral probes in a cellular setting with the knowledge that aziridines and related azirines are recognized electrophiles with a range of reactivities toward numerous amino-acid side-chains. [65–68]

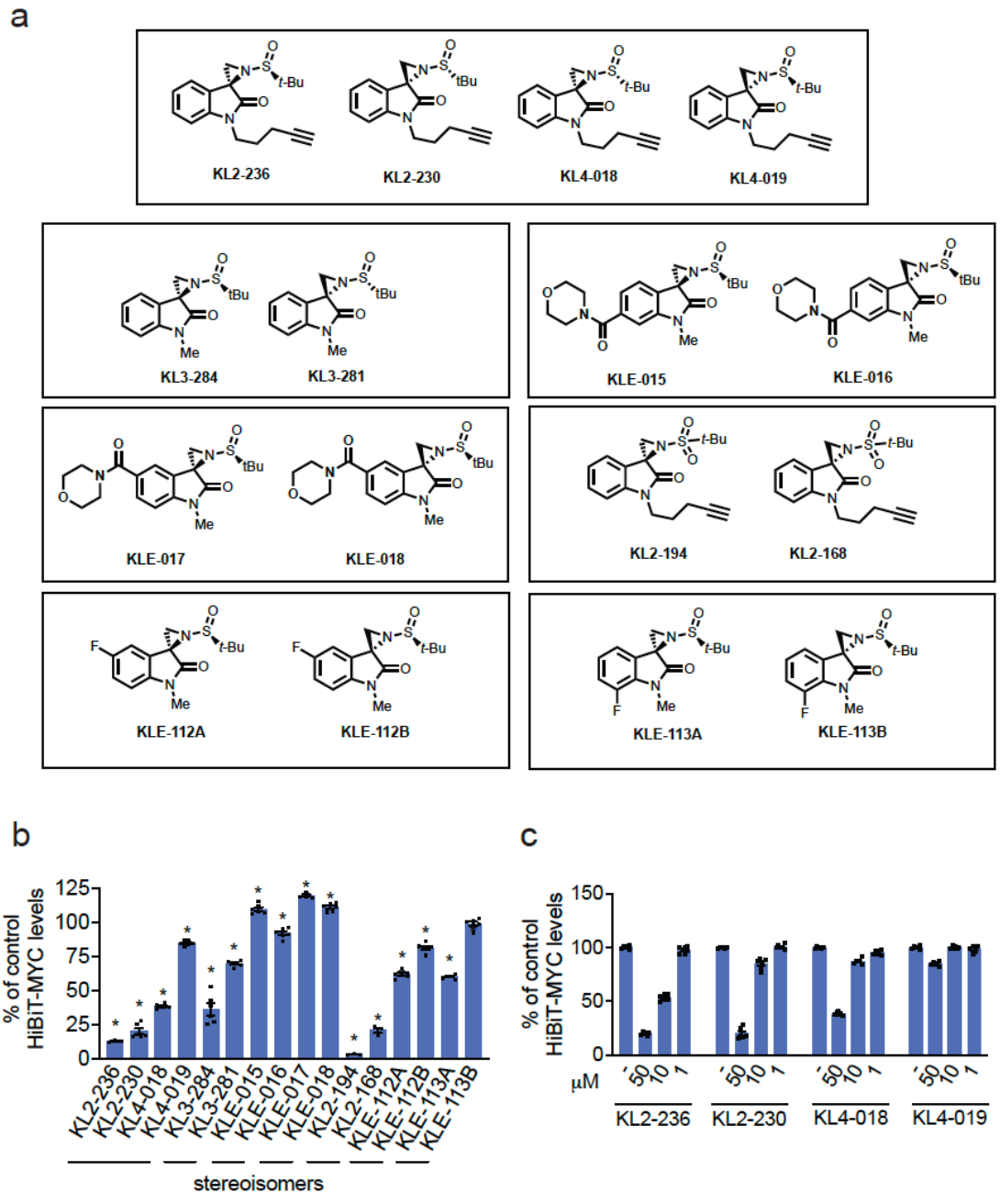

Figure 3.1: Screening a covalent ligand library for stereoselective MYC

oxindole aziridine covalent ligand library. **(b)** HiBiT-MYC HEK293-LgBiT cellular screen for MYC degraders. HiBiT-MYC HEK293-LgBiT cells were treated with DMSO vehicle or covalent compound (50 μM) for 24 h, and MYC levels were detected with the Nano-Glo HiBiT Lytic Detection System. **(c)** Dose-response of KL2-236 and its isomers in HiBiT-MYC cells. HiBiT-MYC

HEK293-LgBiT cells were treated with DMSO vehicle, KL2-236, KL2-230, KL4-018, or KL4-019 for 24 h, and MYC levels were detected with the Nano-Glo HiBiT Lytic Detection System. Data in **(b,c)** are presented as individual replicate values and average ± sem percent of DMSO vehicle-treated controls. Significance is expressed as *p<0.05 compared to DMSO vehicle-treated controls.

We screened this bespoke covalent library in HEK293 cells expressing a HiBiT tag on the endogenous loci of MYC to identify molecules that lowered HiBiT-MYC levels **(**Figure 3.1**b).** From an initial small library-screen, we were pleased to identify several molecules that significantly lowered HiBiT-MYC levels by >50 % – KL2-236, KL2-230, KL4-018, KL3-284, KL2-168, and KL2-194 **(**Figure 3.1**b).** While substituents appended to the oxindole ring generally decreased activity (i.e., KLE-017/KLE-018, KLE-015/KLE-016, KLE-112A/KLE-112B, KLE-113A/KLE-113B), initial modifications to the oxindole nitrogen were tolerated (see KL3-284). Interestingly, enantiomeric sulfonyl aziridine-containing compounds KL2-194 and KL2-168 showed only modest differences in their ability to attenuate HiBiT-MYC levels and were also significantly cytotoxic, thus limiting their further use **(**Figure 3.1**b,** Figure 3.2**a)**. In contrast, however, KL2-236, which possessed a sulfinyl activating group of attenuated reactivity, showed interesting patterns of stereoselective and dose-responsive HiBiT-MYC loss compared to its three stereoisomers **(**Figure 3.1**c)**. While KL2-236 is the most active stereoisomer in the series, its enantiomer KL2-230 also showed comparable activity. A diastereomer of these compounds, KL4-018, showed attenuated activity; however, its enantiomer, KL4-019, was largely inactive. This pattern of stereoselective activity also held for oxindoles KL3-284 and KL3-281, KLE-112A and KLE-112B, and KLE-113A and KLE-113B. None of the other compounds screened, including the four stereoisomers KL2-236, KL2-230, KL4-018, or KL4-019, showed more than 25 % impairment in cell viability **(**Figure 3.2**a)**.

We next tested the chemoselectivity of the four sulfinyl aziridine stereoisomers alongside the sulfonyl aziridine KL2-194 with an artificial peptide bearing 15 of the 20 amino acids, including most nucleophilic amino acids, to assess amino acid reactivity preferences. We found that these compounds only reacted with cysteine and not with any other nucleophilic amino acid, including glutamic/aspartic acids, serines, tyrosines, threonines, lysines, or methionines in this experiment **(**Figure 3.2**b).** As expected, KL2-194, which possesses a more highly-oxidized sulfur atom, was more reactive than the four stereoisomers KL2-236, KL2-230, KL4-018, and KL4-019 **(**Figure 3.2**b-3.2c)**. The higher reactivity of the sulfonyl aziridine KL2-194 compared to the sulfinyl aziridine counterparts is consistent with the higher degree of cytotoxicity observed with KL2-194. We also tested the *in vitro* stability of KL2-236 and KL4-019 in the presence of glutathione (GSH) and observed comparable GSH half-lives of 50.6 minutes for KL2-236 and 59.4 minutes for KL4-019, respectively. These values are longer than previously reported *in vitro* GSH stability of clinically approved covalent drugs such as afatinib and neratinib with GSH half-lives of ~30 minutes.[69] Overall, while our cellular data showed pronounced bioactivity differentiation between KL2-236 and its diastereomer KL4-019, these two compounds showed similar inherent reactivity with cysteine in a linear artificial peptide and with GSH. Moreover, our data also demonstrated that these sulfonyl aziridines were preferentially

cysteine reactive, although we cannot rule out potential adducts that may form with other nucleophilic amino acids that may be reversible or unstable using traditional mass spectrometry approaches **(**Figure 3.2**c**).

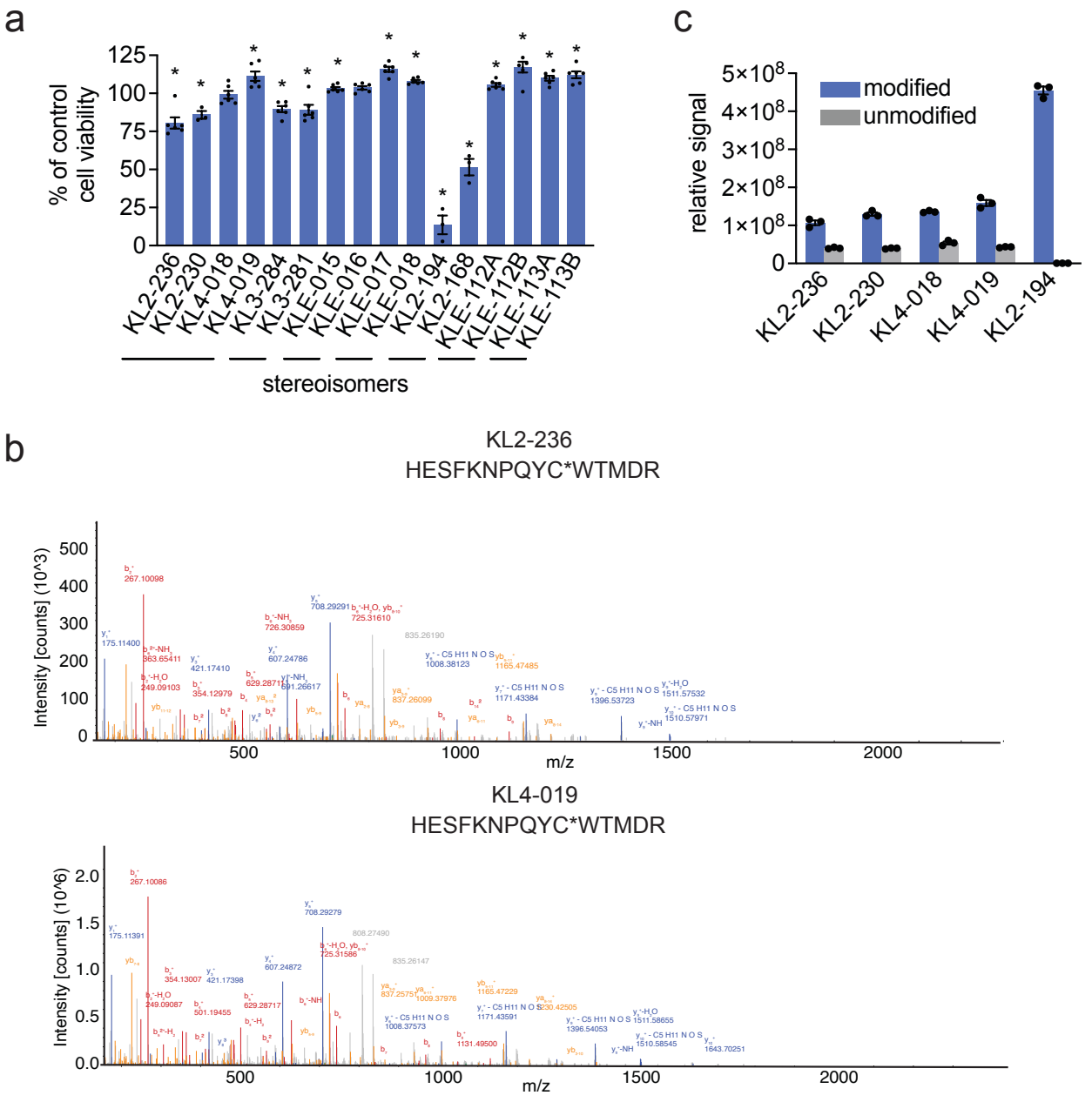

Figure 3.2: Effects of Covalent Screening Compounds on Cell Viability and KL2-236 Adduct on MYC (a) Cell viability. LgBiT-MYC HEK293 cells were treated with DMSO vehicle or covalent compound (50 μM) for 24 h, and cell viability was assessed by CellTiter-Glo. **(b)** Reaction of KL2-236 and KL4-019 (50 μM) with artificial peptide HESFKNPQYCWTMDR (1 μM, 1 hr). Shown are MS/MS spectra showing that only the cysteine was modified. **(c)** Relative reactivity of KL2-236, KL2-230, KL4-018, KL4-019, and KL2-194 (50 μM) with HESFKNPQACWTMDR (1 μM, 1 hr) where the mass spectrometry signal of the modified peptide

was quantified by measuring area under the curve. Shown are the mass spectrometry signals for modified and unmodified peptides.

Given that oxindole KL2-236 showed the best activity in reducing MYC without deleterious cytotoxicity and possessed a diastereomeric negative control compound (KL4-019), we prioritized downstream biological studies using this molecule. Confirming that HiBiT-MYC loss was through proteasome-mediated degradation rather than transcriptional downregulation, we observed significant attenuation of KL2-236-mediated HiBiT-MYC loss upon pre-treatment of cells with the proteasome inhibitor bortezomib **(**Figure 3.3**a)**. We also demonstrated dose-responsive loss of HiBiT-MYC with KL2-236, but not with KL4-019, with an 50 % effective concentration (EC_{50}) value of 9.3 μM and >50 μM, respectively **(**Figure 3.3**b)**. We further confirmed the proteasome-dependent degradation of endogenous MYC with KL2-236, but not with inactive stereoisomer KL4-019, in wild-type HEK293 cells **(**Figure 3.3**c-3.3f)**. We also demonstrated proteasome-mediated loss of MYC with KL2-236 treatment in more cancer-relevant PSN1 pancreatic cancer cells with MYC amplification **(**Figure 3.3**g-3.3h)**.[70] We also synthesized unreactive analogs of KL2-236, including four stereoisomeric pairs of reduced, ring-opened analogs lacking an aziridine as well as analogs possessing an oxazolidinone instead of the sulfinyl aziridine warhead **(**Figure S1**a)**. None of these unreactive analogs degraded HiBiT-MYC, suggesting the importance of covalency in the degradation of MYC **(**Figure S1**b)**.

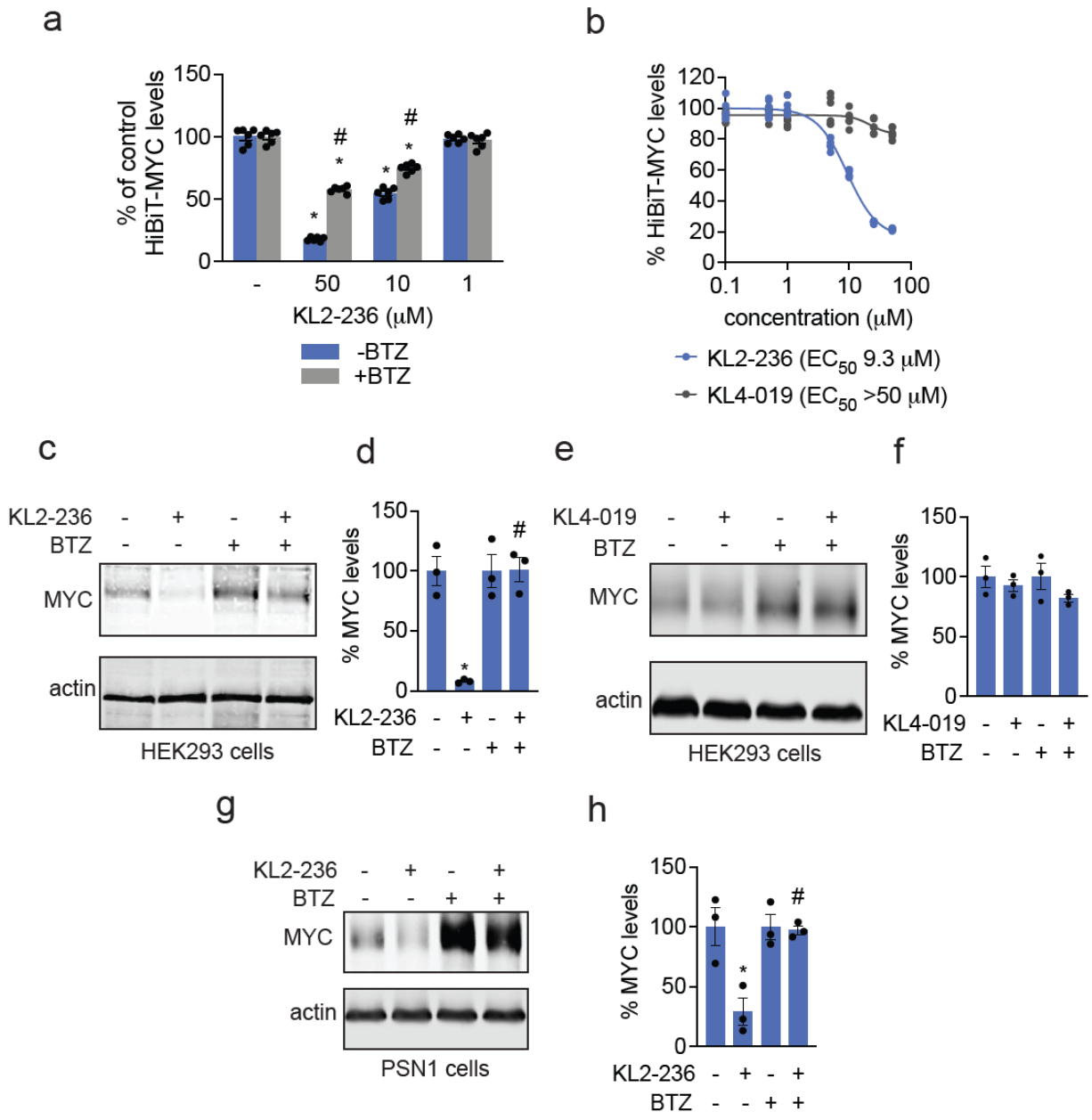

Figure 3.3: Characterization of KL2-236 and its Stereoisomers. **(a)** Proteasome-

proteasome inhibitor bortezomib (500 nM) for 1 hr before treatment of DMSO vehicle or KL2-236 for 24 h, and MYC levels were detected by luminescence. **(b)** Dose-response of HiBiT-MYC degradation. HiBiT-MYC HEK293-LgBiT cells were treated with DMSO vehicle, KL2-236, or KL4-019 for 24 h, and MYC levels were detected by luminescence. **(c,d,e,f)** MYC degradation in HEK293 cells. HEK293 cells were treated with DMSO vehicle or bortezomib (500 nM) for 1 hr before treatment of DMSO vehicle or KL2-236 **(c,d)** or KL4-019 (50 μM) **(e,f)** for 24 h and MYC and loading control actin levels were assessed by Western blotting **(c,e)** and quantified **(d,f)**. **(g,h)** MYC degradation in PSN1 pancreatic cancer cells. PSN1 cells were treated with DMSO vehicle or bortezomib (500 nM) for 1 hr before treatment with DMSO vehicle or KL2-236 for 2 h, and MYC

and loading control actin levels were assessed by Western blotting **(g)** and quantified **(h)**. Blots in **(c,e)** represent n=3 biologically independent replicates per group. Bar graphs in **(a,d,f,h)** show individual replicate values and average ± sem. Significance in **(a,d,f,h)** is shown as *p<0.05 compared to vehicle-treated controls and #p<0.05 compared to the respective KL2-236-treated groups.

3.3.2 Characterizing KL2-236 Interactions with MYC

We next sought to determine whether KL2-236 directly interacted with MYC *in vitro* or in cancer cells. Given that KL2-236 had an alkyne handle for directly conjugating analytical handles through copper-catalyzed azide-alkyne cycloaddition (CuAAC), we exploited this feature to characterize its interactions using ABPP-based approaches. We first demonstrated direct covalent labeling of pure human full-length MYC in the MYC/MAX protein complex in a dose-responsive manner, visualized through CuAAC-mediated conjugation of a rhodamine fluorophore and gel-based ABPP **(**Figure 3.4**a-3.4b)**. Strikingly, stereoselective labeling was also observed between KL2-236 and KL4-019, even at this pure MYC/MAX protein complex level **(**Figure 3.4**c-3.4d)**. We also demonstrated direct covalent binding to pure MYC without MAX as well **(**Figure S2**a)**. We did not observe any labeling of MAX.

To understand where our molecule was binding to MYC, we assessed the KL2-236 modification site in the MYC/MAX pure protein complex through mass spectrometry (MS) analysis of KL2-236-modified MYC pepsin digests. The only modification found was on cysteine C203 **(**Figure S2**b-S2c)**. These data showed direct and covalent binding of KL2-236 to MYC *in vitro*.

We next assessed direct MYC target engagement in living cells. Treating PSN1 cells with KL2-236, appending a biotin enrichment handle through CuAAC under denaturing conditions, and avidin-enriching KL2-236-modified proteins, we observed significant and stereoselective MYC enrichment with KL2-236 treatment over both the less active diastereomer KL4-019 and vehicle-treated controls **(**Figure 3.4**e-3.4f).** Using an orthogonal enzyme-linked immunosorbent assay (ELISA)-ABPP approach wherein we treated HiBiT-MYC expressing DLD-1 cells with KL2-236 or KL4-019, appended a biotin handle by CuAAC under denaturing conditions, captured and immobilized HiBiT-MYC using a HiBiT antibody, and reading out compound-engaged HiBiT-MYC by streptavidin-HRP, we also observed dose-responsive and significant stereoselective KL2-236 engagement of MYC-HiBiT over KL4-019 **(**Figure 3.4**g;** Figure S2**d)**. Through quantitative chemoproteomic profiling of KL2-236-enriched targets, we identified 437 proteins enriched by $\log_2$>0.8 with p<0.003, including MYC out of 1048 proteins quantified **(**Figure 3.4**h; Table S1)**.

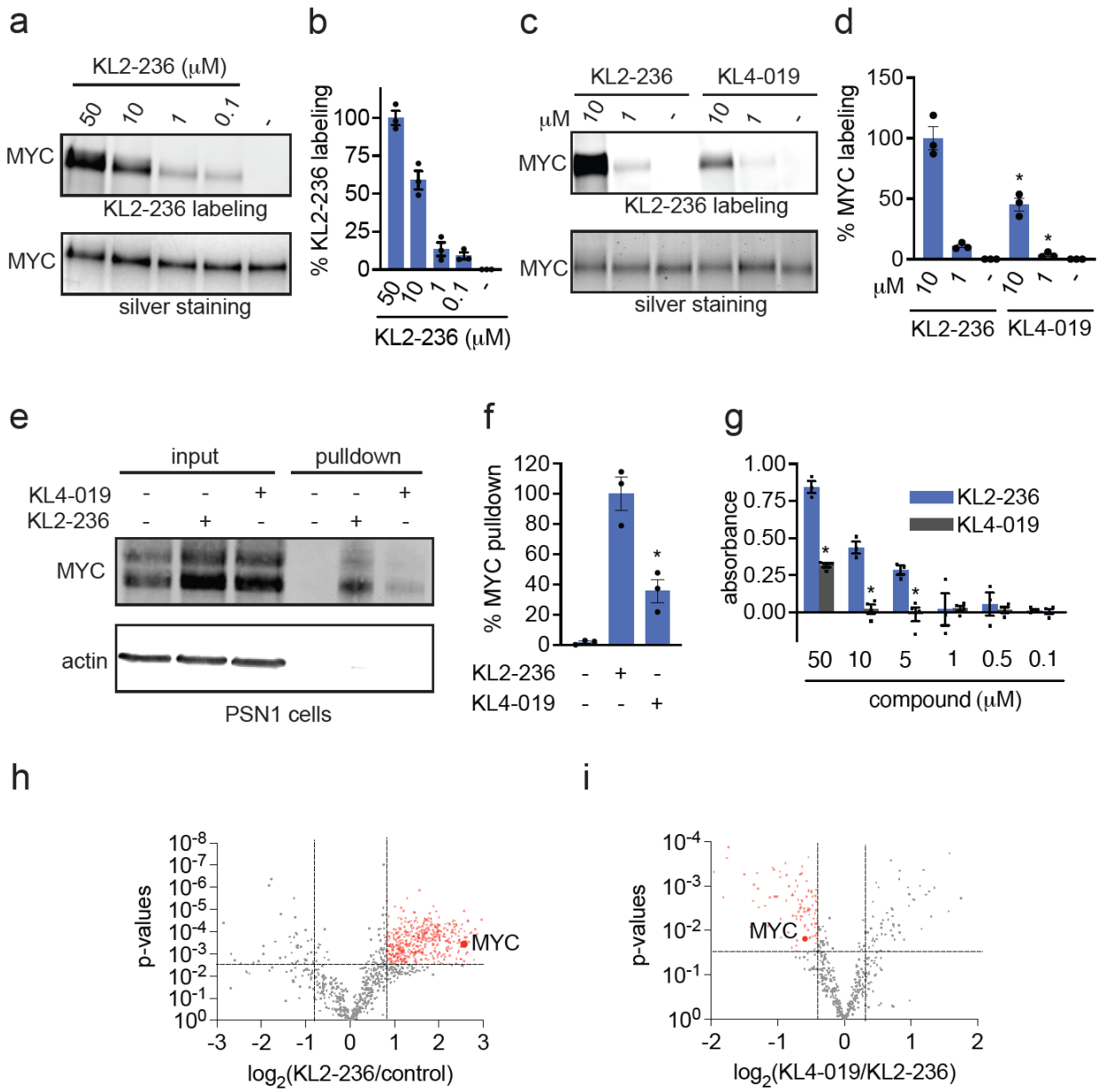

Figure 3.4: Characterization of KL2-236 Interactions with MYC. (a,b,c,d) Gel-based protein complex was treated with DMSO vehicle, KL2-236, or KL4-019 for 1 h, after which probe-modified protein was subjected to CuAAC with an azide conjugated rhodamine, separated by SDS/PAGE and visualized by in-gel fluorescence **(a,c)** and quantified **(b,d)**. Gels were silver stained to account for MYC protein loading. **(e,f)** KL2-236 versus KL4-019 engagement of MYC in PSN1 cells. PSN1 cells were pretreated with BTZ (500 nM) for 1 hour before treatment with DMSO vehicle, KL2-236 (50 μM) or KL4-019 (50 μM) for 2 h, after which probe-modified proteins were subjected to CuAAC with an azide-functionalized biotin, after which probe-modified proteins were enriched with avidin beads, eluted, and input and pulldown eluate was separated by SDS/PAGE and MYC and negative control protein actin were detected by Western blotting **(e)** and quantified **(f)**. **(g)** ELISA-ABPP assessment of KL2-236 versus KL4-019 cellular engagement of MYC in DLD-1 MYC-HiBiT expressing cells. DLD-1 MYC HiBiT expressing cells were treated

with DMSO vehicle, KL2-236, or KL4-019 for 1 h after which probe-modified proteins were appended with a biotin handle by CuAAC, and HiBiT-MYC was captured and immobilized on plate using a HiBiT antibody and then compound-engaged HiBiT-MYC was detected by streptavidin HRP. **(h,i)** KL2-236 versus DMSO **(h)** or KL2-236 versus KL4-019 **(i)** chemoproteomic profiling in PSN1 cells. PSN1 cells were pretreated with BTZ (500 nM) for 1 hour before treatment with DMSO vehicle, KL2-236 (50 μM) or KL4-019 (50 μM) for 2 h, after which probe-modified proteins were subjected to CuAAC with an azide-functionalized biotin, after which probe-modified proteins were enriched with avidin beads, eluted, and input and pulldown eluate was tryptically digested and analyzed and quantified by LC-MS/MS. Gels, blots, and data in **(a-i)** represent n=3-4 biologically independent replicates per group. Data for **(h,i)** can be found in **Tables S1-S2.**

MYC and 101 other proteins were also enriched by KL2-236 more significantly than KL4-019 **(**Figure 3.4**i, Table S2).** Among these off-targets that were stereoselectively engaged were highly abundant enzymes that bear a catalytic and hyper-reactive cysteine, such as glyceraldehyde-3-phosphate dehydrogenase (GAPDH) **(Table S2)**[71] To confirm that GAPDH was indeed an off-target that was stereoselectively and functionally engaged by KL2-236, and not non-specific capture, we showed that GAPDH was inhibited by KL2-236, more so than KL4-019 **(**Figure 3.5**).** Interestingly, the stereoselectivity of GAPDH inhibition differed from that of MYC showing less GAPDH inhibition with KL2-230 and KL4-019, compared to KL2-236 and KL4-018 **(**Figure 3.5**).** While these data showed that KL2-236 had several hundred off-targets and relatively poor selectivity, they also demonstrated direct stereoselective engagement of MYC with KL2-236 over its isomer, KL4-019, in cells. Given the significant challenges faced in directly targeting MYC, we were still intrigued by the stereoselective engagement of MYC observed in living cells.

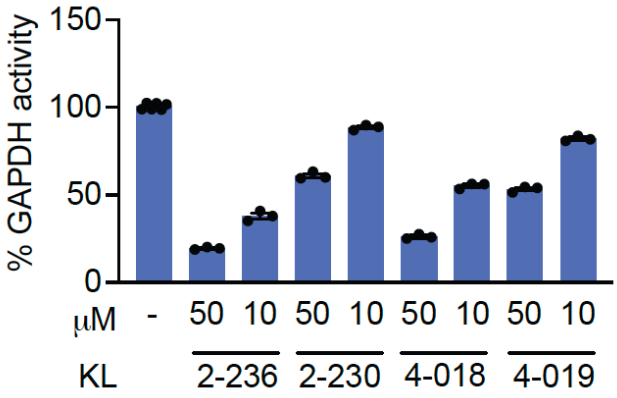

Figure 3.5: GAPDH activity assay. GAPDH activity was assessed using a kit with pure human GAPDH protein. GAPDH was treated with DMSO vehicle or compounds for 1 h after which activity was read out according to manufacturer protocols. Bar graph shows individual replicate and average ± sem values from n=3-6 biologically independent replicates per group.

To further demonstrate MYC engagement in cells by KL2-236, we performed a cellular thermal shift assay (CETSA) in PSN1 cells. Instead of observing the stabilization of MYC thermal stability, we found a significant destabilization of MYC thermal stability with KL2-236 treatment in PSN1 cells with a 6.4°C shift in the temperature at which 50 % of MYC was stable (T_m) from 51.8°C to 45.4°C **(**Figure 3.6**a-3.6b)**. This destabilization of MYC by KL2-236 was reminiscent of our previously discovered covalent destabilizing MYC degrader EN4 and our destabilizing CTNNB1 degrader NF764, indicating that KL2-236 was degrading MYC through a similar destabilizing degradation mechanism compared to traditional PROTACs and molecular glue degraders.[33,51,72,73]

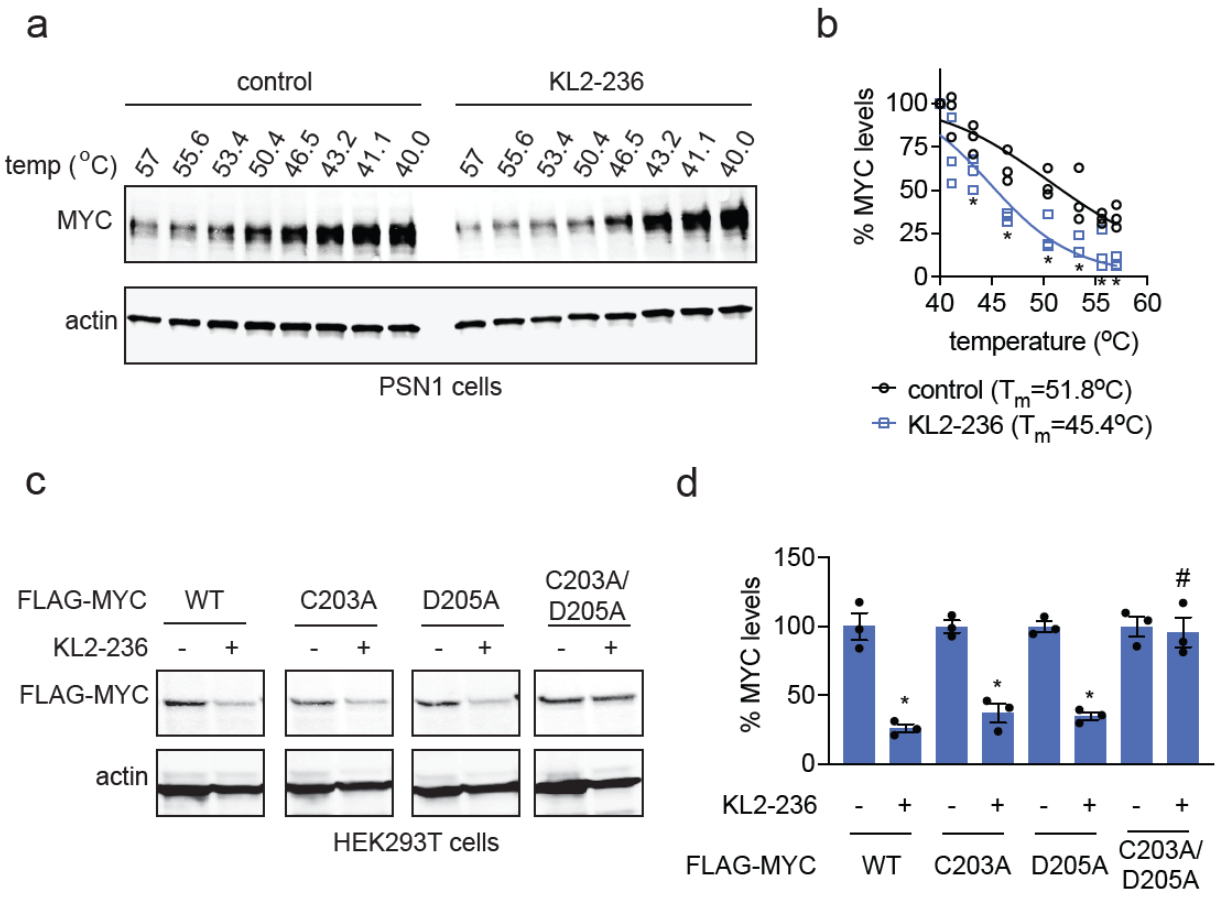

Figure 3.6: Understanding Mechanism Through Which KL2-236 Degrades MYC. (a,b) Cellular Thermal Shift Assay (CETSA) of KL2-236 on MYC and negative control actin in PSN1 cells. PSN1 cells were treated with DMSO vehicle or KL2-236 (50 μM) for 4 h. Cells were then heated at the designated temperatures, cells were harvested and lysed, insoluble proteins were pelleted, and soluble proteins were separated by SDS/PAGE and MYC, and negative control actin levels were detected by Western blotting (a) and quantified (b). (c,d) FLAG-MYC degradation with KL2-236 treatment. HEK293T cells stably expressing FLAG-MYC wild-type (WT), C203A, D205A, or C203A/D205A were treated with DMSO vehicle or KL2-236 (50 μM) for 24 h after which proteins were separated by SDS/PAGE and FLAG-MYC and loading control actin were detected (c) and quantified (d) by Western blotting. Blots in (a,c) represent n=3 biologically independent replicates per group. Data in (b) shows individual replicate values. Data in (d) shows individual replicate and average ± sem values. Significance in (b,d) expressed *p<0.05 compared to vehicle-treated controls and #p<0.05 compared to KL2-236 treated FLAG-MYC WT control groups in (d).

To assess whether KL2-236 engagement of C203 was responsible for MYC degradation, we determined whether mutagenesis of C203 to alanine would attenuate MYC loss. Disappointingly, KL2-236 still degraded MYC C203A to the same extent as the wild-type protein in HEK293T cells **(**Figure 3.6**c-3.6d)**. We next sought to address whether there might be neighboring residues proximal to C203 that KL2-236 could react with in the

absence of C203 or residues that may coordinate the reactivity of C203. We performed mass spectrometry-based activity-based protein profiling (MS-ABPP) with KL2-236 as a probe to understand its site-specific and sequence-specific reactivity in complex PSN1 proteomes **(Figure 3.7a-3.7c; Table S3).**

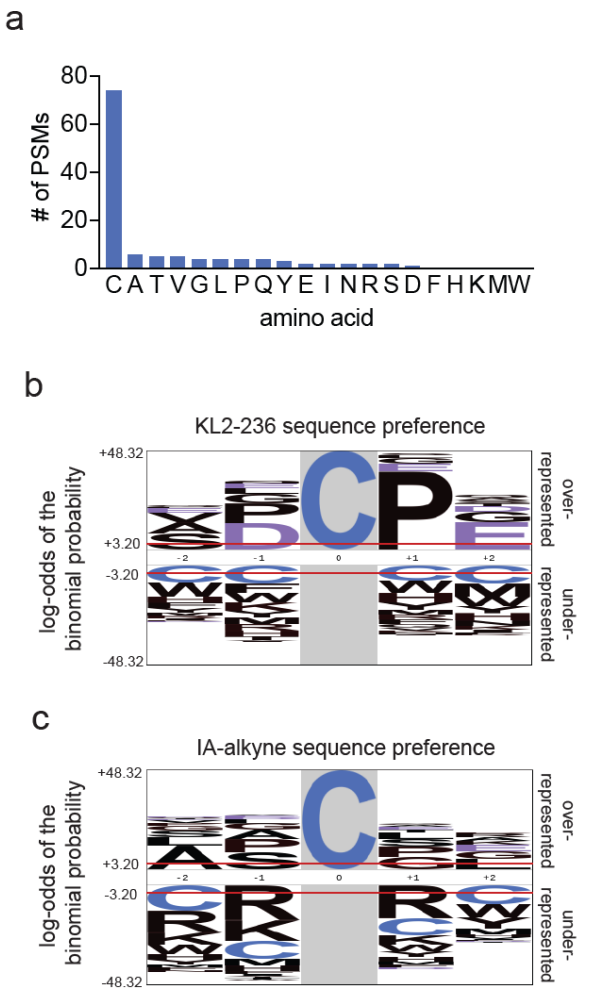

Figure 3.7: Chemoproteomic characterization of KL2-236 modified sites. (a) MS-ABPP analysis of KL2-236 (50 μM) in PSN1 cells. PSN1 cells were pre-treated with proteasome inhibitor (500 nM) for 1 h and then co-treated with KL2-236 (50 μM) for 4 h. Cells were then lysed and probe-modified proteins were subjected to CuAAC with a desthiobiotin-functionalized avidin, after which probe-modified proteins were enriched with avidin beads, eluted, pulldown eluate was tryptically digested and probe-modified peptides were eluted and analyzed and quantified by LC-MS/MS. Data can be found in **Table S3.** Shown is the modification preference for KL2-236 in PSN1 proteomes, showing chemoselectivity for cysteines. **(b,c)** KL2-236 versus IA-alkyne sequence preference around modified cysteines. KL2-236 data are derived from **(a)** and **Table S3**. IA-alkyne probe-modification were taken from previously published datasets from labeling in MDA-MB-231 human breast cancer cells[74]. Data are from n=3 biologically independent replicates per group.

Unfortunately, we were unable to capture the KL2-236 modified tryptic MYC peptide, likely due to the long length of the C203-bearing tryptic peptide and the relatively low abundance of MYC. However, we successfully captured several hundred KL2-236-modified peptides from complex proteomes of other proteins **(Table S3)**. By using an unbiased approach to determine the amino acid labeling preferences of KL2-236, we still observed a high chemoselectivity for cysteine over any other amino acid **(Figure 3.7a; Table S3)**. When we performed sequence preference analysis of neighboring residues to the KL2-236-modified cysteines, we found a preference for acidic residues such as aspartic or glutamic acid either -1 or +2 from the modified cysteine **(Figure 3.7b; Table S3)**. Upon analyzing a previously published chemoproteomic profiling dataset using a

broadly reactive alkyne-functionalized iodoacetamide (IA-alkyne) probe [75], we did not observe this preference (

Figure **3.7c; Table S3**). Indeed, C203 is also flanked by E202 and D205. We were unable to identify E202 or D205 modifications with KL2-236, but we conjectured that these adducts may be potentially reversible. Interestingly, upon modeling this region in MYC with AlphaFold [76,77] while the region where C203 resides is generally disordered, there is relatively higher confidence around D205, where D205 is hydrogen-bonded with a neighboring S207 in a helix **(**Figure 3.8**).**

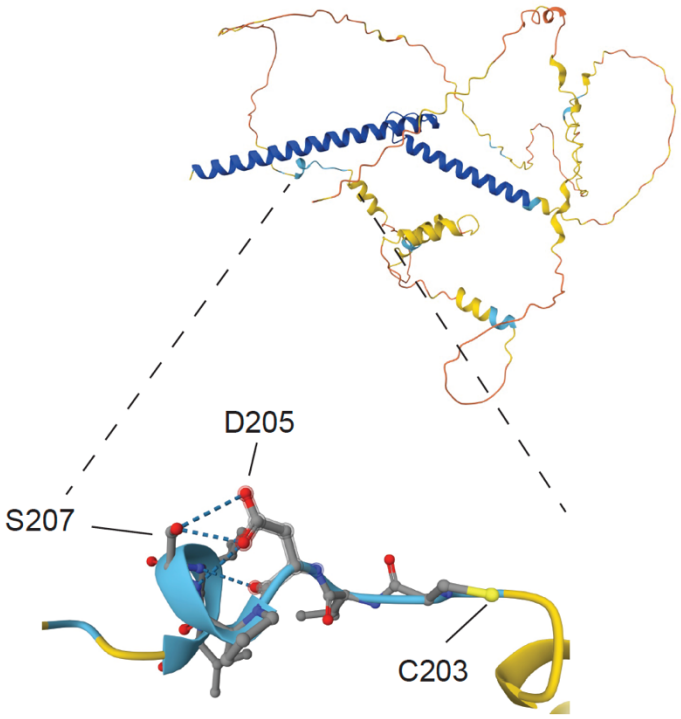

Figure 3.8: Alpha-fold modeling of MYC. Shown is an alpha-fold model of human MYC with an expanded region showing C203, D205, and S207.

We fully recognize that AlphaFold trains its model on existing structures and that all MYC-containing entries include MAX and may thus bias predictions of MYC structure towards helical structure. We also acknowledge that structural insights into this largely disordered region of MYC are purely speculative. Nonetheless, we postulated that one of these acidic residues, particularly D205, could activate the C203 thiol, making it more nucleophilic and hyper-reactive, and that KL2-236 could also potentially react with one of these acidic residues in the absence of C203. Alternatively, one of these acidic residues could be required for protonation of the chiral sulfoxide and subsequent positioning of the electrophile for covalent bond formation. Also, another possibility was that in the absence of C203, KL2-236 may be able to react with E202 or D205.

Mutagenesis of E202 or D205 alone also did not attenuate MYC degradation from KL2-236 treatment **(**Figure 3.6**c-3.6d;** Figure 3.9**a-3.9b)**. However, we observed complete attenuation of MYC degradation with the MYC D205A/C203A double mutant **(**Figure 3.6**c-3.6d)**. We did not observe this rescue with the MYC E202A/C203A mutant **(**Figure 3.9**a-3.9b)**. Overall, our results suggest that in addition to C203, D205 is involved in the reactivity and activity of KL2-236 with MYC. Thus, while KL2-236 is a pathfinder molecule,

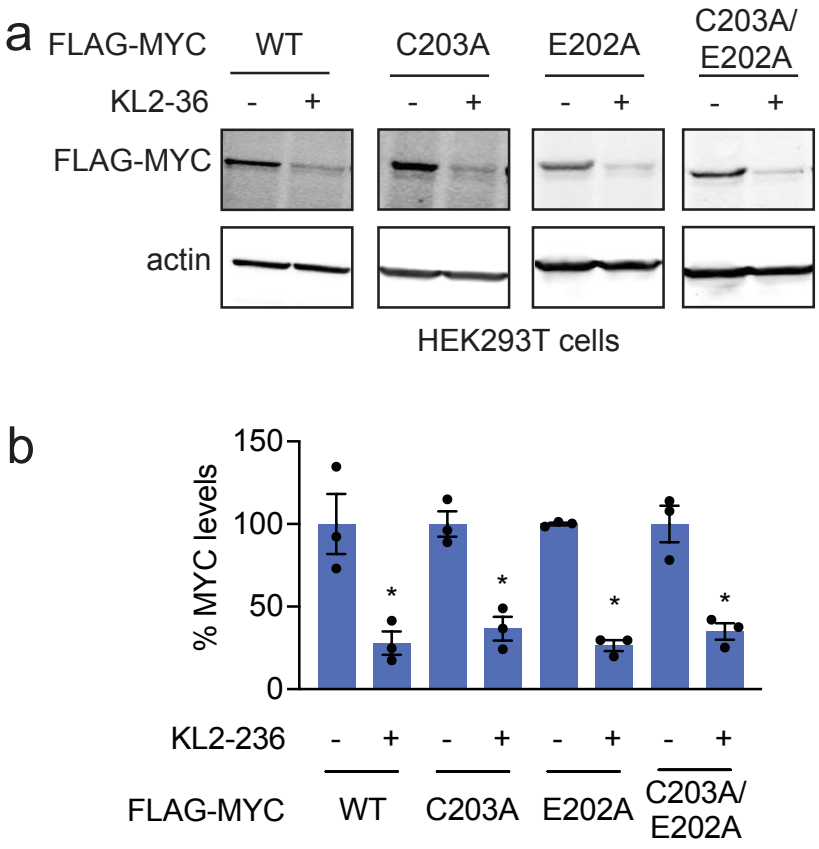

we have demonstrated that the observed degradation of MYC is mediated through on-target activity, resulting from direct engagement of MYC.

Figure 3.9: Continued Mechanistic Investigation of KL2-236 (a,b) HEK293T cells stably expressing FLAG-MYC wild-type (WT), C203A, E202A, C203A/E202A were treated with DMSO vehicle or KL2-236 (50 μM) for 24 h after which proteins were separated by SDS/PAGE and FLAG-MYC and loading control actin were detected and quantified by Western blotting. Blots represent n=3 biologically independent replicates per group. Data shows individual replicate values. Bar graph shows individual replicate and average ± sem values. Significance in expressed *p<0.05 compared to vehicle-treated controls.

3.3.3 Impact of KL2-236 on MYC Transcriptional Activity

Thus far, we have shown that KL2-236 stereoselectively engages MYC *in vitro* and in cells at C203, potentially involving D205, to destabilize and degrade MYC in a proteasome-dependent manner. We next wanted to understand whether KL2-236 impairs MYC transcriptional activity and downregulates MYC target genes in cancer cells. KL2-236, but not the inactive isomer KL4-019, dose-responsively inhibited MYC luciferase reporter transcriptional activity in HEK293T cells with an EC_{50} of 4.5 μM versus >50 μM, respectively **(**Figure 3.10**a).** KL2-236 treatment in PSN1 cancer cells significantly modulated >280 transcript levels **(**Figure 3.10**b; Table S4).** Consistent with KL2-236 action on inhibiting and degrading MYC, gene set enrichment analysis (GSEA) of significantly modulated genes revealed the most significant pathway affected with the lowest normalized enrichment score as MYC targets, followed by IFNα response, E2F targets, oxidative phosphorylation, and IFNγ response **(**Figure 3.10**c-3.10d;** Figure 3.11**a; Table S4).**

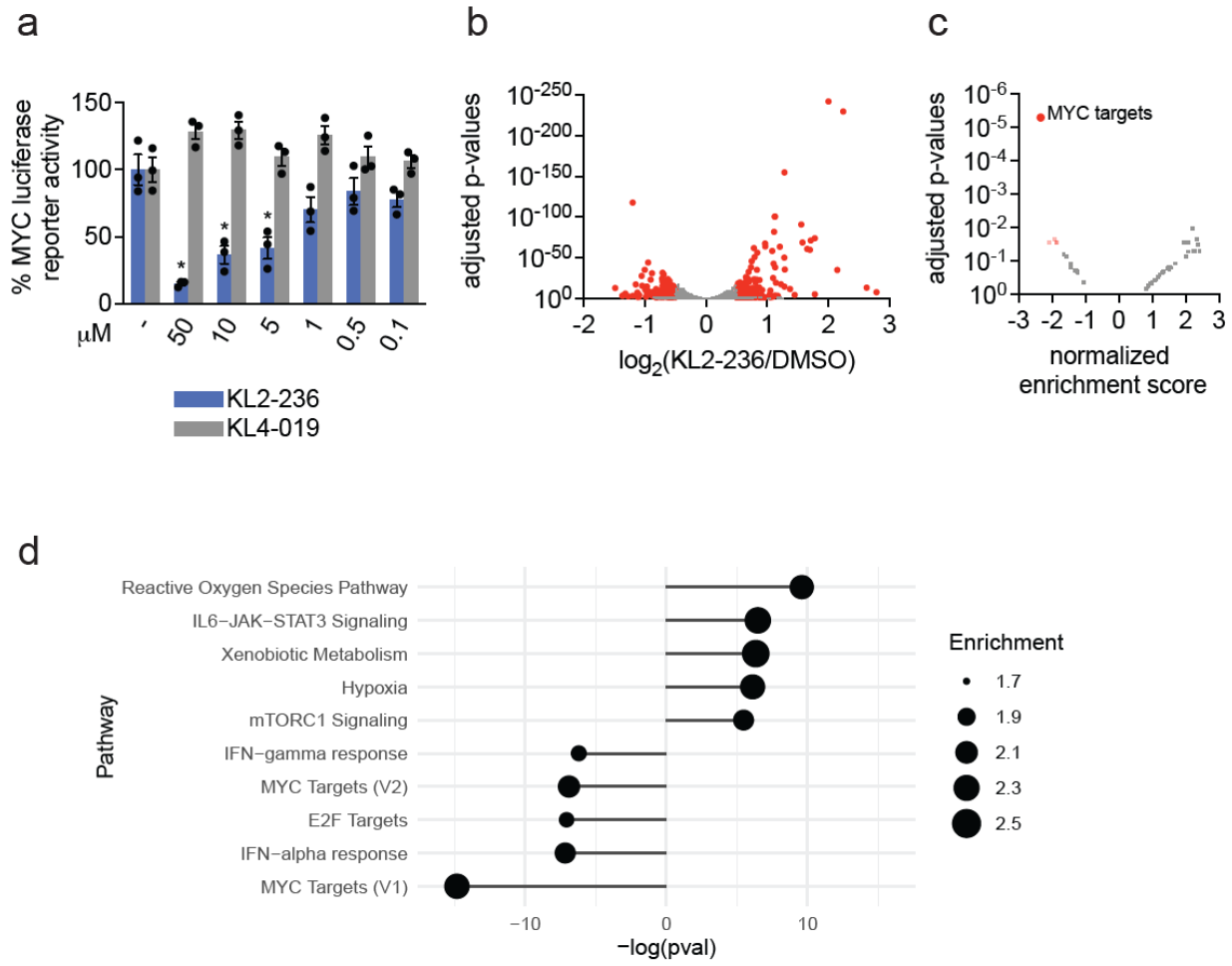

Figure 3.10: Functional Effects of KL2-236 on MYC Transcriptional Activity. **(a)** MYC luciferase reporter transcriptional activity in HEK293T cells. HEK293T cells expressing an MYC luciferase reporter were treated with DMSO vehicle, KL2-236, or KL4-019 for 24 h, after which MYC transcriptional activity was read out by luminescence. **(b)** RNA sequencing of KL2-236 in PSN1 cells. PSN1 cells were treated with DMSO vehicle or KL2-236 (50 μM) for 2 h. Resulting RNA from treated cells were sequenced and quantified. Shown in red are significantly altered transcripts ($p<0.05$, $<\log_2 -0.5$ or $> \log_2 0.5$). Data are in Table S4. **(c,d)** Gene enrichment analysis shows significantly altered pathways and normalized enrichment scores, detailed in Table S4. These plots highlight the directionality, significance, and amount of enrichment of the top- and bottom- five pathways. "Enrichment" represents the Normalized Enrichment Score. Data in **(a-d)** are from n=3 biologically independent replicates per group. Data in **(a)** shows individual replicate and average ± sem values. Significance in **(a)** expressed *$p<0.05$ compared to vehicle-treated controls.

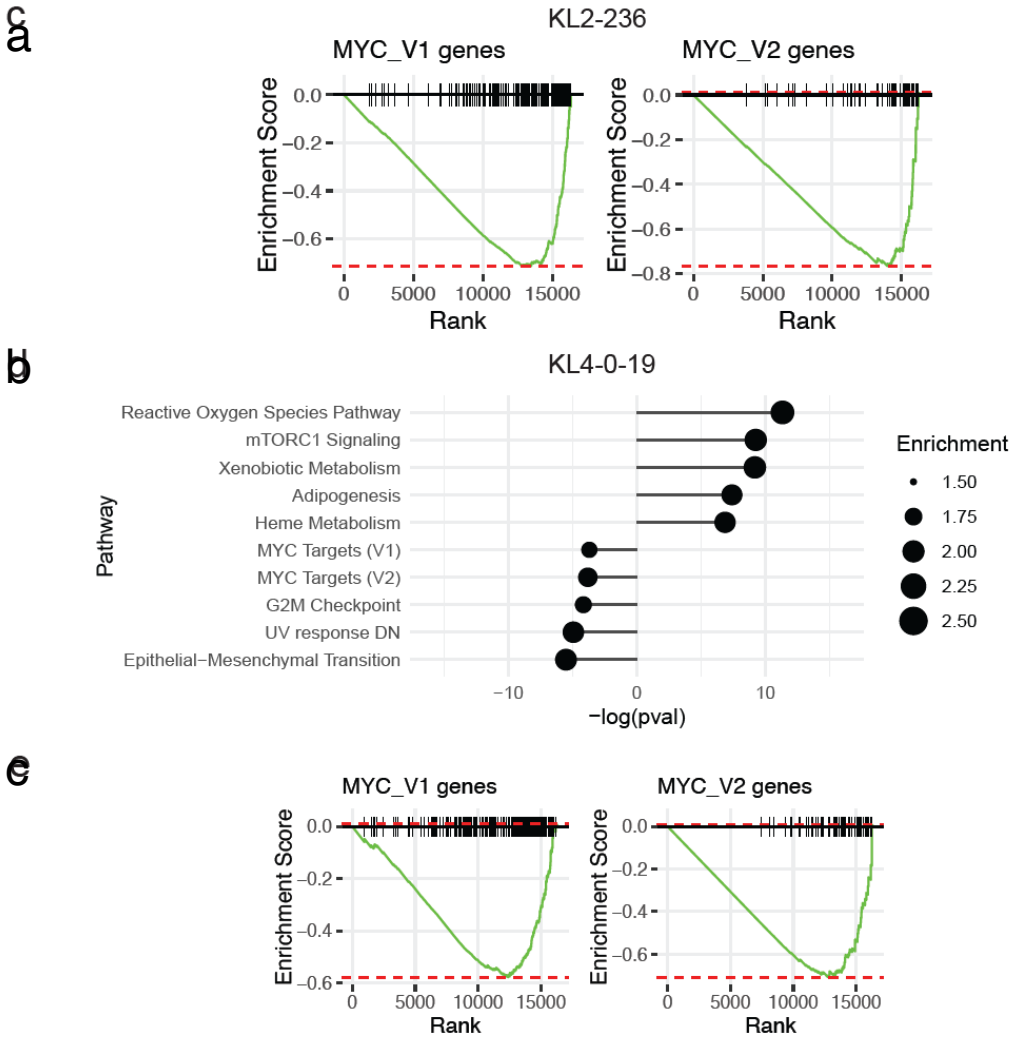

Figure 3.11: Transcriptional Pathway Analysis of KL2-236 and KL4-019 (a) Enrichment plots for MYC target genes from RNA seq analysis described in Figure 3.10b-3.10d and Table S4. **(b)** Gene enrichment analysis shows significantly altered pathways and normalized enrichment scores, detailed in Table S4 from PSN1 cells treated with DMSO vehicle or KL4-019 (50 μM) for 2h. These plots highlight the directionality, significance, and amount of enrichment of the top- and bottom- five pathways. "Enrichment" represents the Normalized Enrichment Score. **(c)** Enrichment plots for MYC target genes from RNA seq analysis described in Table S4 from PSN1 cells treated with DMSO vehicle or KL4-019 (50 μM) for 2h.

In contrast, while MYC target genes do tend to be at the end of the ranks in MYC target gene enrichment plots, they are not significantly repressed in GSEA testing against randomized permutations **(**Figure 3.11**a; Table S4).** While MYC target genes are enriched in the top and bottom five enriched pathways, it is not the most significantly enriched pathway, and MYC target genes show much less statistical significance compared to what is observed with KL2-236 **(**Figure 3.11**a-3.11b; Table S4).** Overall, while the global transcriptomic comparison of KL2-236 and KL4-019 compared to DMSO vehicle-treated controls does not show absolute stereoselective effects, MYC target

genes are more significantly enriched with KL2-236 compared with KL4-019 treatment in GSEA. This is consistent with our pure protein and intracellular MYC engagement data comparing KL2-236 to KL4-019, showing that both compounds engage MYC, but KL2-236 labels and engages MYC to a higher degree compared to KL4-019 **(**Figure 3.4**c-3.4i)**. Our data collectively demonstrated that KL2-236 engages and degrades MYC, inhibits MYC transcriptional activity, and downregulates MYC target genes in cells.

3.3.4 Improving the Durability of MYC Degradation

While we showed compelling results with KL2-236 of a covalent molecule that stereoselectively engages MYC directly in cells to destabilize, degrade, and inhibit MYC, KL2-236 only shows acute loss of MYC in the first 2-6 hours of treatment with recovery of MYC protein levels by 12 h in PSN1 cancer cells where MYC turnover is rapid **(**Figure 3.12**)**. Indeed, this feature of MYC (rapid turnover) presents a known challenge for small molecule drug discovery efforts.[78] In addition, KL2-236 had many off-targets at concentrations required for MYC degradation. Thus, we sought to develop a more potent, selective, and durable MYC degrader. The reaction of spirocyclic oxindole sulfonyl aziridines with nucleophiles is proposed to involve *in situ* aziridinium ion formation generated using the oxindole nitrogen.[65,66] As such, we suspected that substituents on nitrogen would be important in modulating the protein reactivity of these sulfinyl aziridines as well. We generated analogs with various alterations to this site and assessed structure-activity relationships in degrading HiBiT-MYC in cells, assessing both the EC_{50} potency of degradation and the maximal percent degradation (D_{max}) **(**Figure 3.13**).** As expected, groups that remove electron density from the oxindole nitrogen (see: KLE-142, KLE-144, and KLE-138) were largely inactive, as was the free N-H oxindole compound KL6-030. Likewise, a highly potent compound was achieved through attachment of an electron-rich *para*-anisole ring (see: KL4-219A). The *ortho*-anisole isomer (KL6-019A), which is twisted out of planarity and displays atropisomerism, was less active. Compound KL5-289A, which lacks the phenyl ring found in KL4-219A (and instead possesses a direct N–OMe linkage), also showed dampened activity as did related ethers KLE-217A and alkyne probe KL6-085A. These findings suggest that steric and/or physicochemical properties are important parameters in addition to electronic effects.

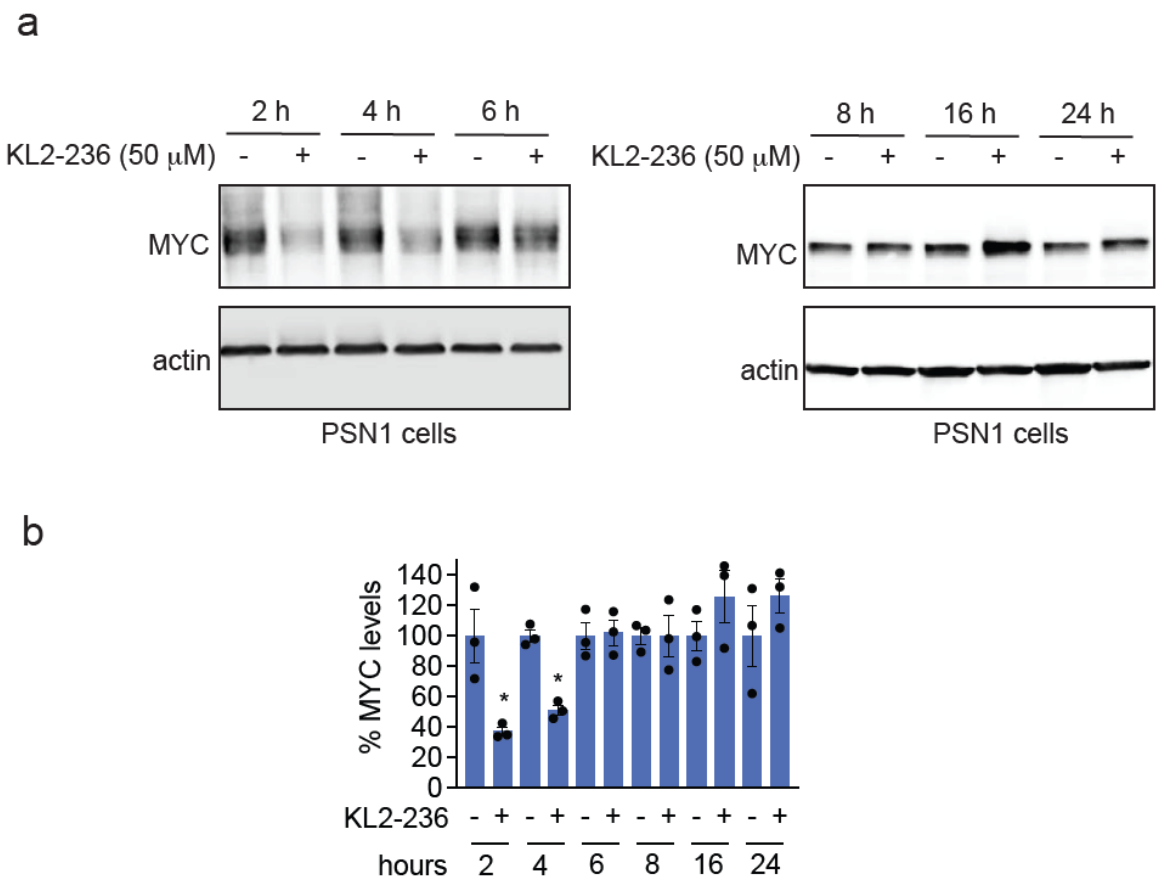

Figure 3.12: Time-course of KL2-236 degradation of MYC in PSN1 cells. (**a,b**) Time-course of KL2-236 degradation of MYC in PSN1 cells. PSN1 cells were treated with DMSO vehicle or KL2-236 (50 μM) for 24 h. Proteins were separated by SDS/PAGE and MYC and loading control actin levels were detected by Western blotting **(a)** and quantified **(b)**. Blots are representative of n=3 biologically independent replicates/group. Bar graph shows individual replicate values and average ± sem. Significance expressed as *p<0.05 compared to vehicle-treated controls at each time-point.

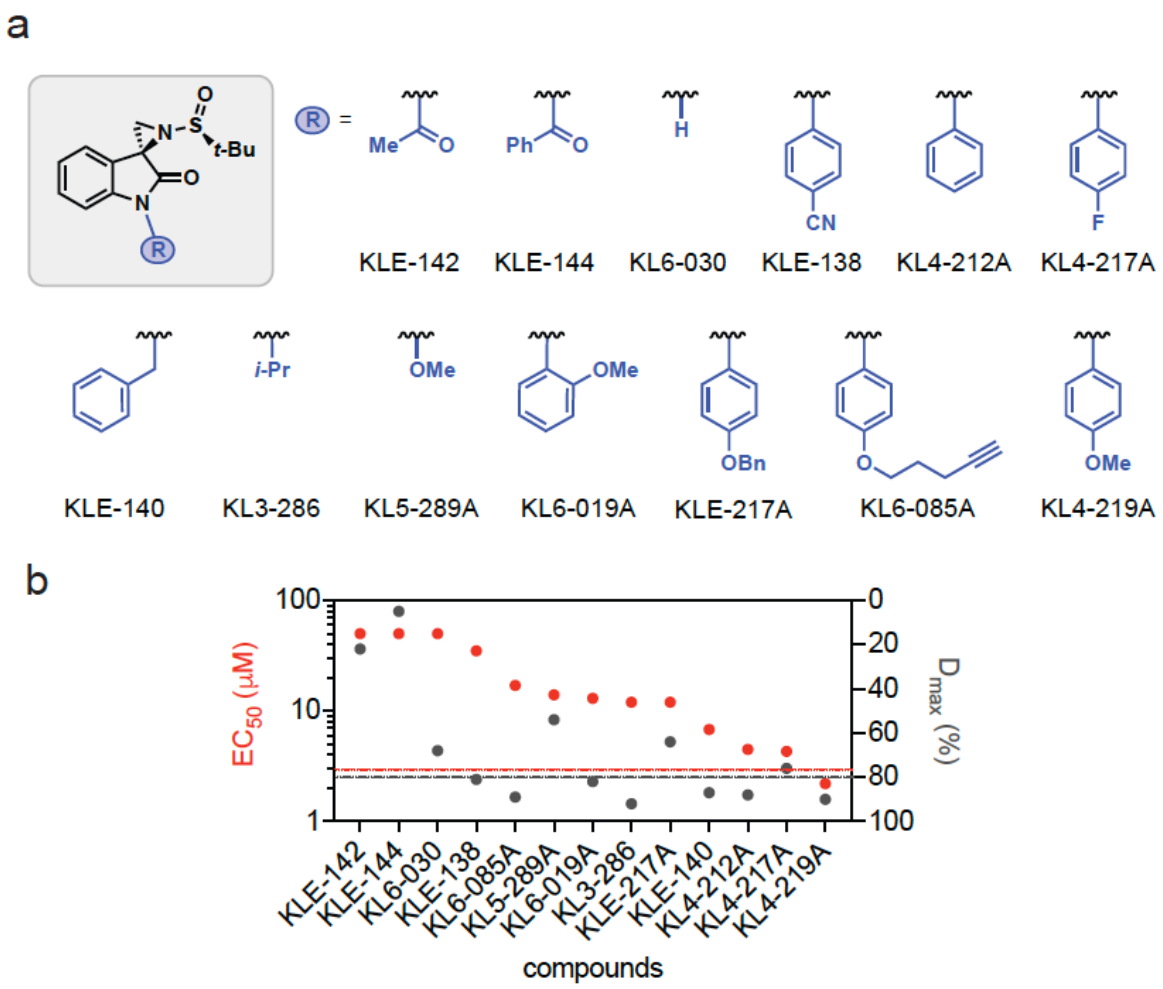

Figure 3.13: Structure-activity relationship of sulfinyl aziridines. (a) Analogs of KL2-236. **(b)** HiBiT-MYC HEK293-LgBiT cells were pre-treated DMSO vehicle or compound in dose-response experiments for 24 h, and HiBiT-MYC levels were detected by luminescence. D_{max} and EC_{50} of degradation were calculated and plotted. Data are from n=3 biologically independent replicates/group.

Gratifyingly, we found that KL4-219A showed more potent and durable degradation of MYC with an EC_{50} of 1.7 μM and continued MYC loss after 24 h of treatment in PSN1 cells without showing any cytotoxicity **(**Figure 3.13**;** Figure 3.14**a-3.14d;** Figure 3.15**).** Like KL2-236, we also observed diminished HiBiT-MYC degradation and inhibition of MYC transcriptional reporter activity with the diastereomeric compound KL4-219B, compared to KL4-219A **(**Figure 3.14**a-3.14b,** Figure 3.14**e).** KL4-219A showed an EC50 of 0.93 μM for inhibition of MYC transcriptional activity, compared to >50 μM with KL4-219B **(**Figure 3.14**e)**. Similar to KL2-236, KL4-219A also significantly destabilized MYC in thermal shift assays **(**Figure 3.14**f-3.14g).**

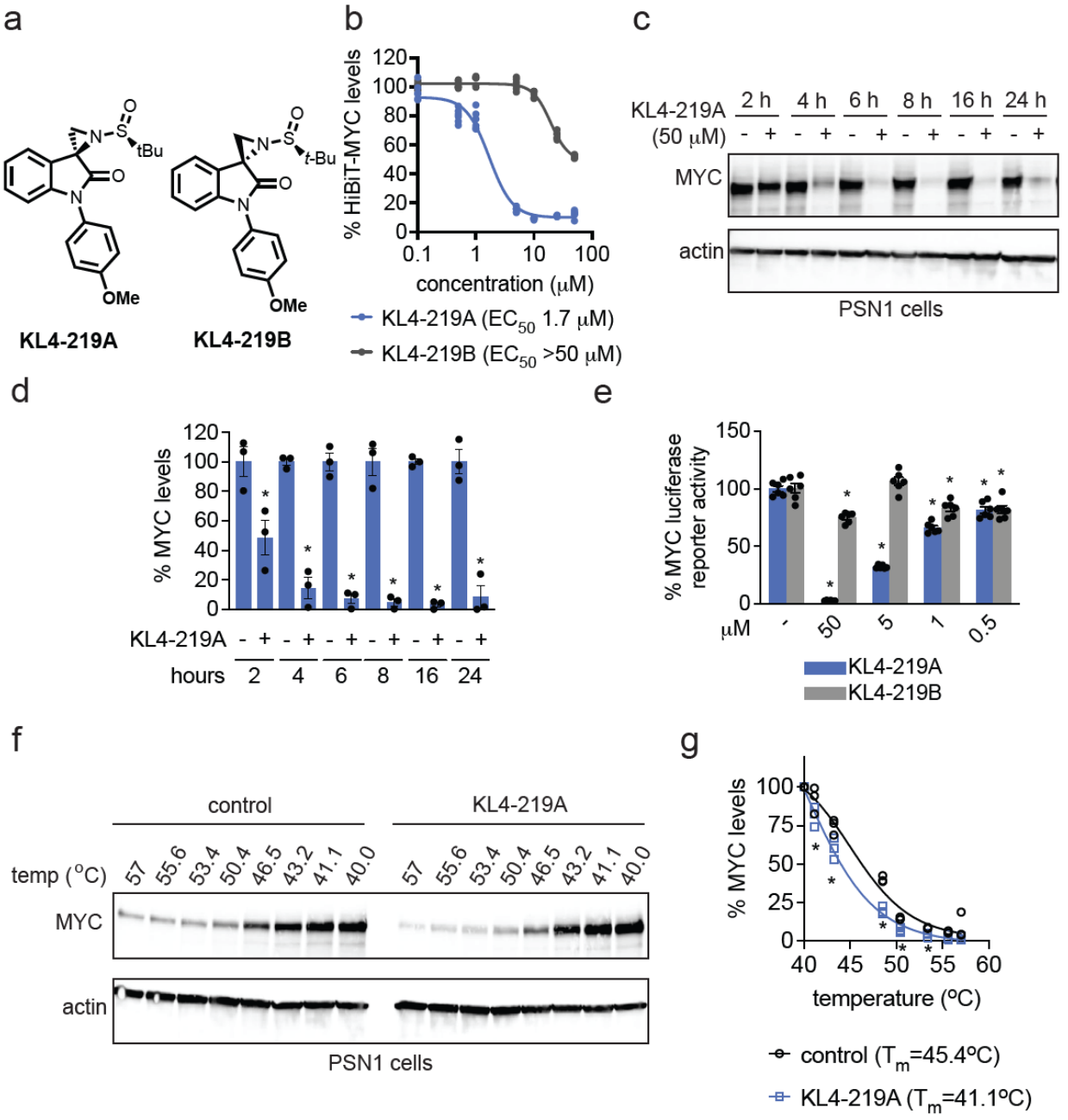

Figure 3.14: More Durable Analog of KL2-236: KL4-219A. **(a)** Structure of KL4-219A and diastereomer KL4-219B. **(b)** HiBiT-MYC HEK293-LgBiT cell dose-response with KL4-219A/B. HiBiT-MYC HEK293-LgBiT cells were treated with DMSO vehicle, KL4-219A, or KL4-219B for 24 h, and MYC levels were detected with the Nano-Glo HiBiT Lytic Detection System. **(c,d)** Time-course of KL4-219A-mediated MYC degradation in PSN1 cells. PSN1 cells were treated with a DMSO vehicle or KL4-219A (50 μM) at designated times, and MYC and loading control actin levels were assessed by Western blotting **(c)** and quantified **(d). (e)** MYC luciferase reporter transcriptional activity in HEK293T cells. HEK293T cells expressing an MYC luciferase reporter were treated with DMSO vehicle, KL4-219A, KL4-219B for 24 h, after which MYC transcriptional activity was read out by luminescence. **(f,g**) CETSA of KL4-219A on MYC and

negative control actin in PSN1 cells. PSN1 cells were treated with DMSO vehicle or KL4-219A (50 μM) for 4 h. Cells were then heated at the designated temperatures, cells were harvested and lysed, insoluble proteins were pelleted, and soluble proteins were separated by SDS/PAGE and MYC, and negative control actin levels were detected by Western blotting **(f)** and quantified **(g)**. Data or blots in **(b-g)** represent n=3-6 biologically independent replicates per group. The blots are representative. The bar and line graphs in **(b,d,e,g)** show individual replicate values and average ± sem for bar graphs and average for line. Significance is shown as *p<0.05 compared to vehicle-treated controls for each group.

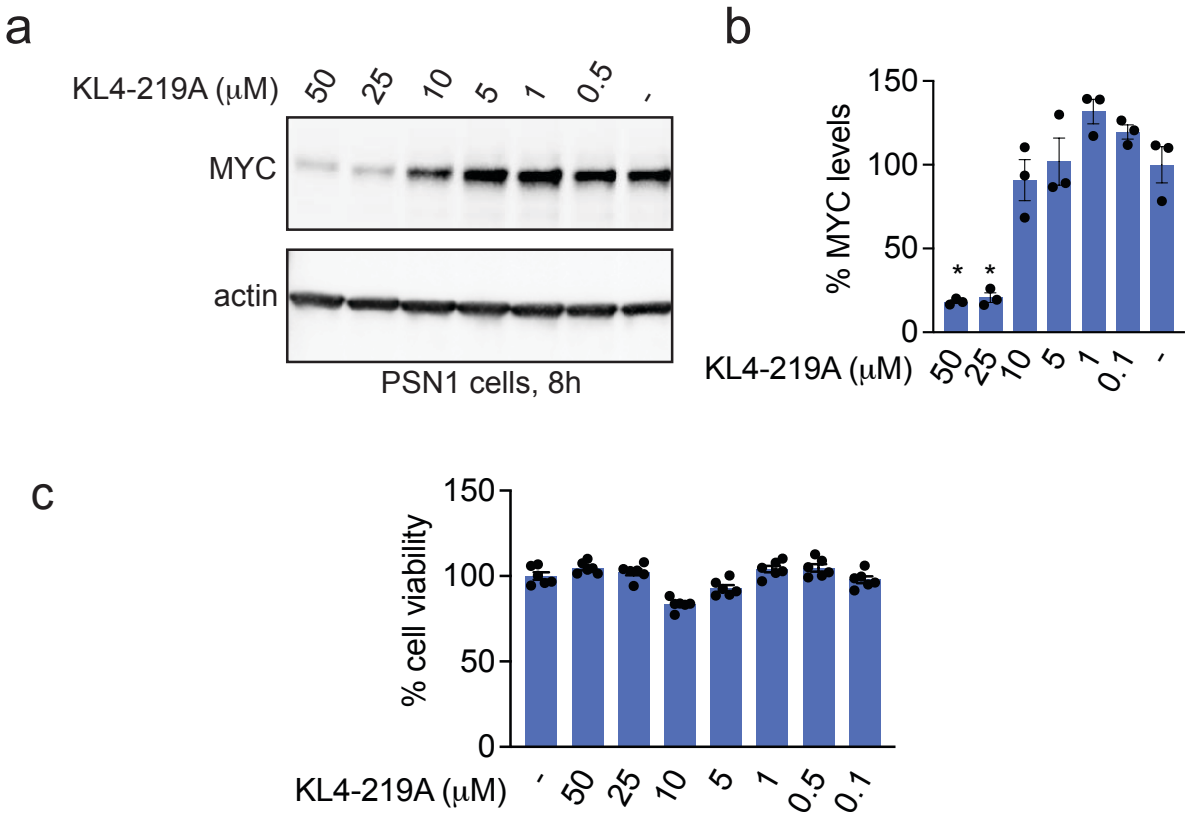

Figure 3.15: Characterization of KL4-219A (a-b) PSN1 cells were treated with a DMSO vehicle or KL4-219A for 8h, and MYC and loading control actin levels were assessed by Western blotting **(a)** and quantified **(b). (c)** PSN1 cells were treated with KL4-219A for 24 hours in a dose responsive manner and cell viability was assessed by CellTiter-Glo 2.0. Blot shown in **(a)** is representative of n=3 biologically independent replicates/group. Bar graphs in **(b)** show individual replicate values and average ± sem. Data in bar graphs have been normalized against average of DMSO control.

The loss of MYC conferred by KL4-219A was attenuated upon pre-treatment of cells with a proteasome inhibitor, confirming proteasome-dependence of MYC loss, whereas no MYC degradation was observed with KL4-219B treatment **(**Figure 3.16**).** Confirming a similar mechanism of action as KL2-236, we showed that MYC degradation was still observed in wild-type and single mutants C203A or D205A, but was completely attenuated in C203A and D205A-double mutant MYC-expressing cells **(Figure 3.17).**

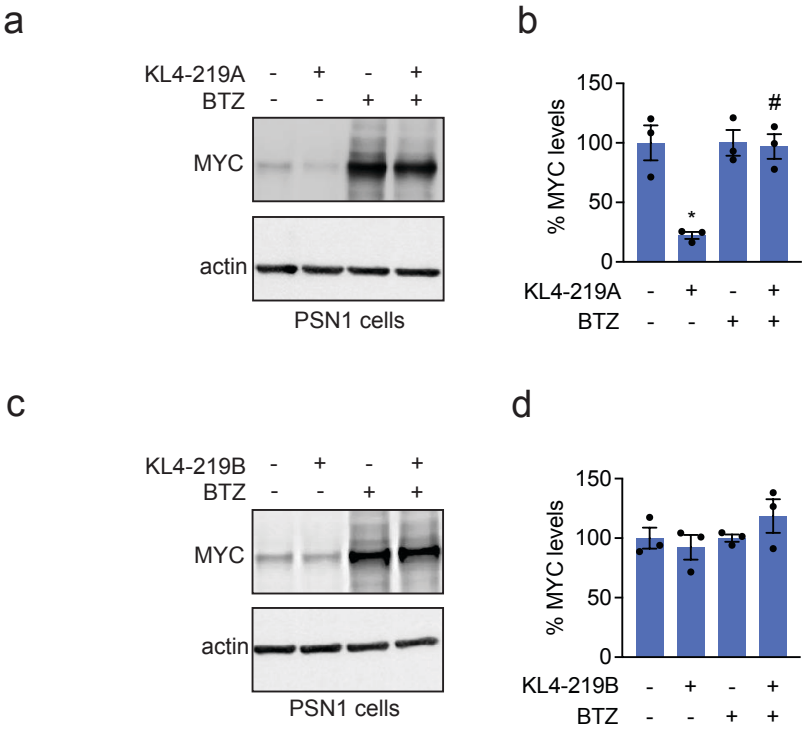

Figure 3.16: Proteasomal Dependent Degradation of MYC by KL4-219A and KL4-219B (a,b,c,d) Proteasome-dependence of MYC degradation. PSN1 cells were pretreated with a DMSO vehicle or bortezomib (BTZ) (200 nM) for 1 hr prior to treatment of cells with a DMSO vehicle or KL4-219A or KL4-219B (25 μM) for 6h. MYC and loading control actin levels were assessed by Western blotting **(a,c)** and quantified **(b,d)**. Blots shown in **(a,c)** are representative of n=3 biologically independent replicates/group. Bar graphs in **(b,d)** show individual replicate values and average ± sem. Data in bar graphs have been normalized against average of DMSO control for DMSO and KL4-219A/B treatment groups and normalized against average of BTZ treatment for BTZ and BTZ and KL4-219A/B treatment groups. Statistical significance is shown as *p<0.05 compared to DMSO-treated controls and #p<0.05 compared to KL4-219A-treated groups.

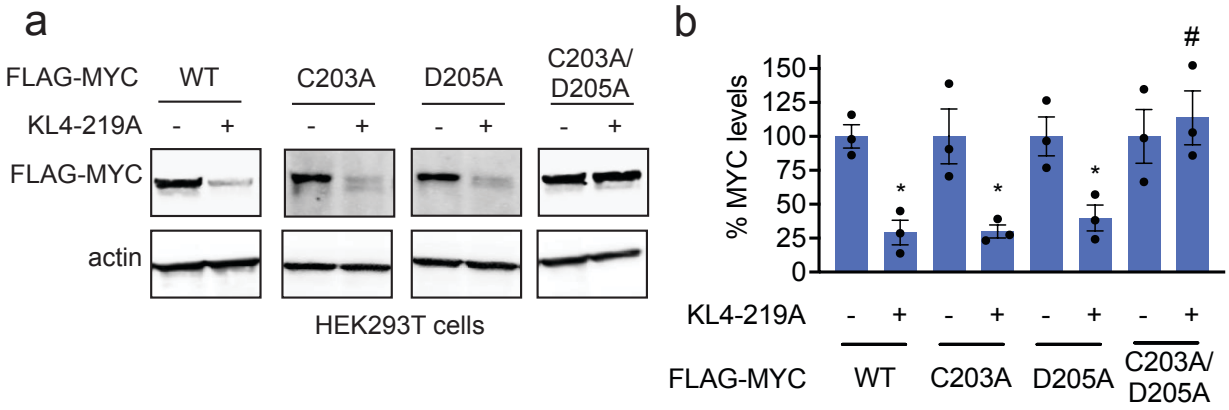

Figure: 3.17 Mechanistic Investigation of KL4-219A (a,b) FLAG-MYC degradation with KL4-219A treatment. HEK293T cells stably expressing FLAG-MYC wild-type (WT), C203A, D205A, or C203A/D205A were treated with DMSO vehicle or KL4-219A (50 μM) for 24 h after which proteins were separated by SDS/PAGE and FLAG-MYC and loading control actin were detected **(a)** and quantified **(b)** by Western blotting. Data or blots in **(a)** represent n=3 biologically independent replicates per group. The bar and line graphs in **(b)** show individual replicate values and average ± sem values or average values, respectively from n=3 biologically independent

replicates per group. Significance is shown as *p<0.05 compared to vehicle-treated controls and #p<0.05 compared to KL4-219A-treated FLAG-MYC wild-type cells.

Interestingly, these analogs, which induced more long-lasting degradation, had shorter *in vitro* GSH half-lives (19.3 and 26.3 minutes for KL4-219A and KL4-219B, respectively) as compared to KL2-236 and KL4-019. Thus, the sustained MYC degradation observed with KL4-219A may be related to the kinetics of degradation or other physicochemical parameters (such as permeability and potency) rather than warhead stability. We further showed that analogs of KL4-219A and KL4-219B that lack a reactive warhead—KL6-278A and KL6-278B, respectively—did not degrade MYC **(**Figure 3.18**).** Previous studies have suggested that electrophiles may cause cell stress and induce the formation of stress granules, which could complicate the interpretation of protein degradation.[79] We found that neither KL2-236 nor KL4-219A causes stress granule formation at concentrations used in this study compared to the positive control sodium arsenite **(**Figure 3.19**).**

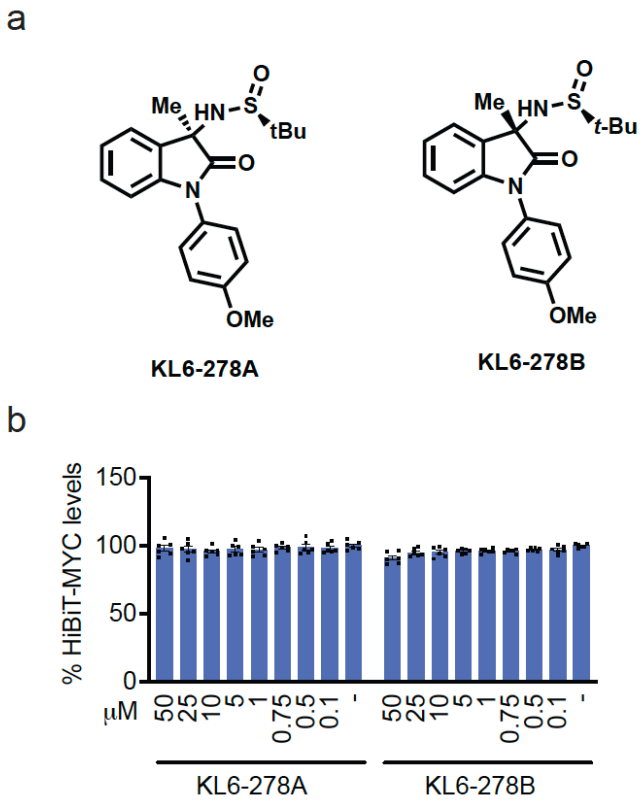

Figure 3.18: Dose-response of HiBiT-MYC degradation by KL6-278A & KL6-278B which lack an aziridine. (a) Structures of unreactive analogs of KL4-219A/B—KL6-278A and KL6-278B. **(b)** HiBiT-MYC HEK293-LgBiT cells were treated with DMSO vehicle, KL6-278A, or KL6-278B for 24 h, and MYC levels were detected by luminescence. Data shown are individual replicate values and average ± sem from n=6 biologically independent replicates/group.

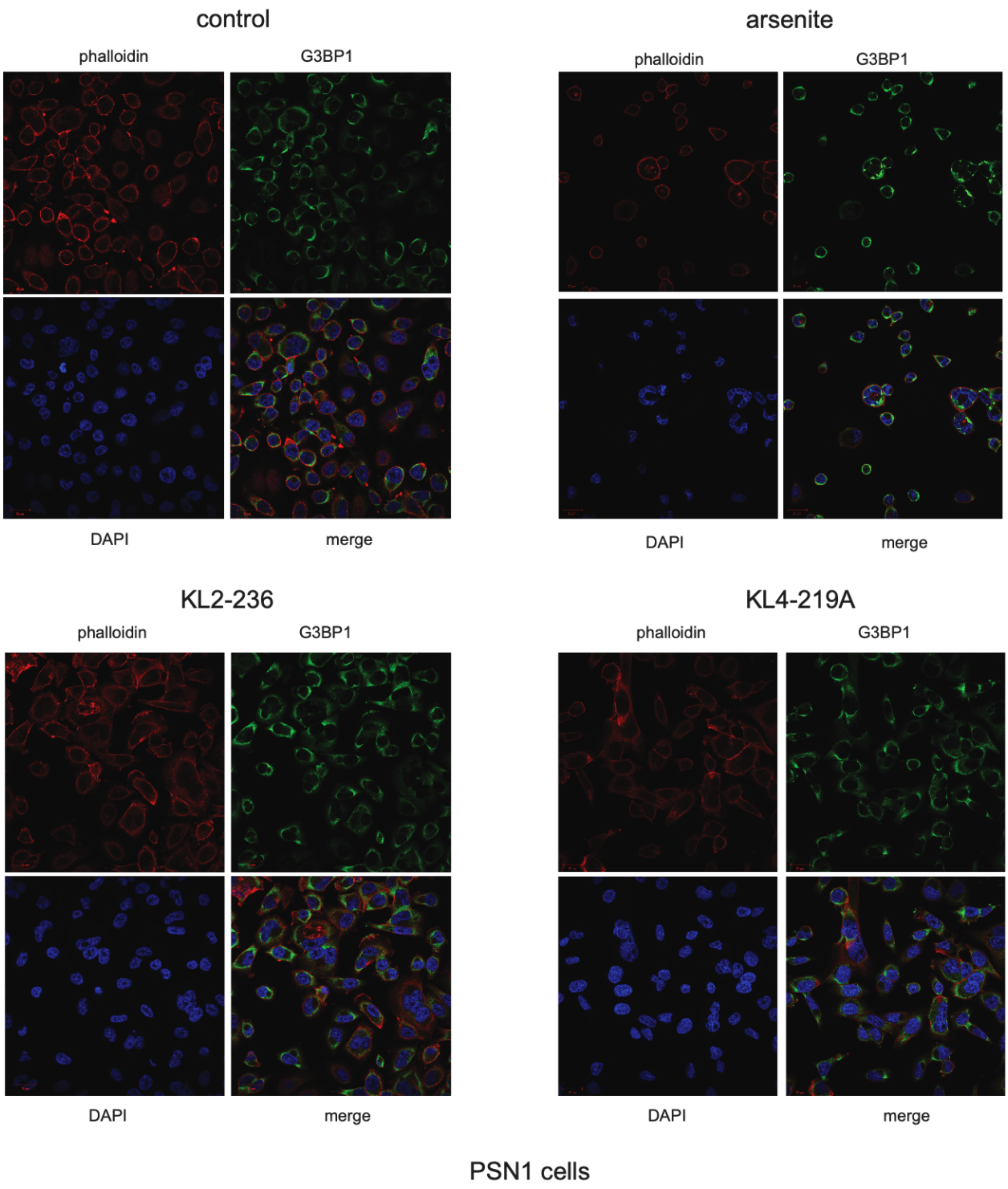

Figure 3.19: Stress Granule Assessment PSN1 cells were treated with DMSO vehicle, KL2-

and visualized for actin marker phalloidin, G3BP1, or nuclear marker DAPI by microscopy. Shown are the individual channels and merged channels. Data are representative of n=3 biologically independent replicates per group.

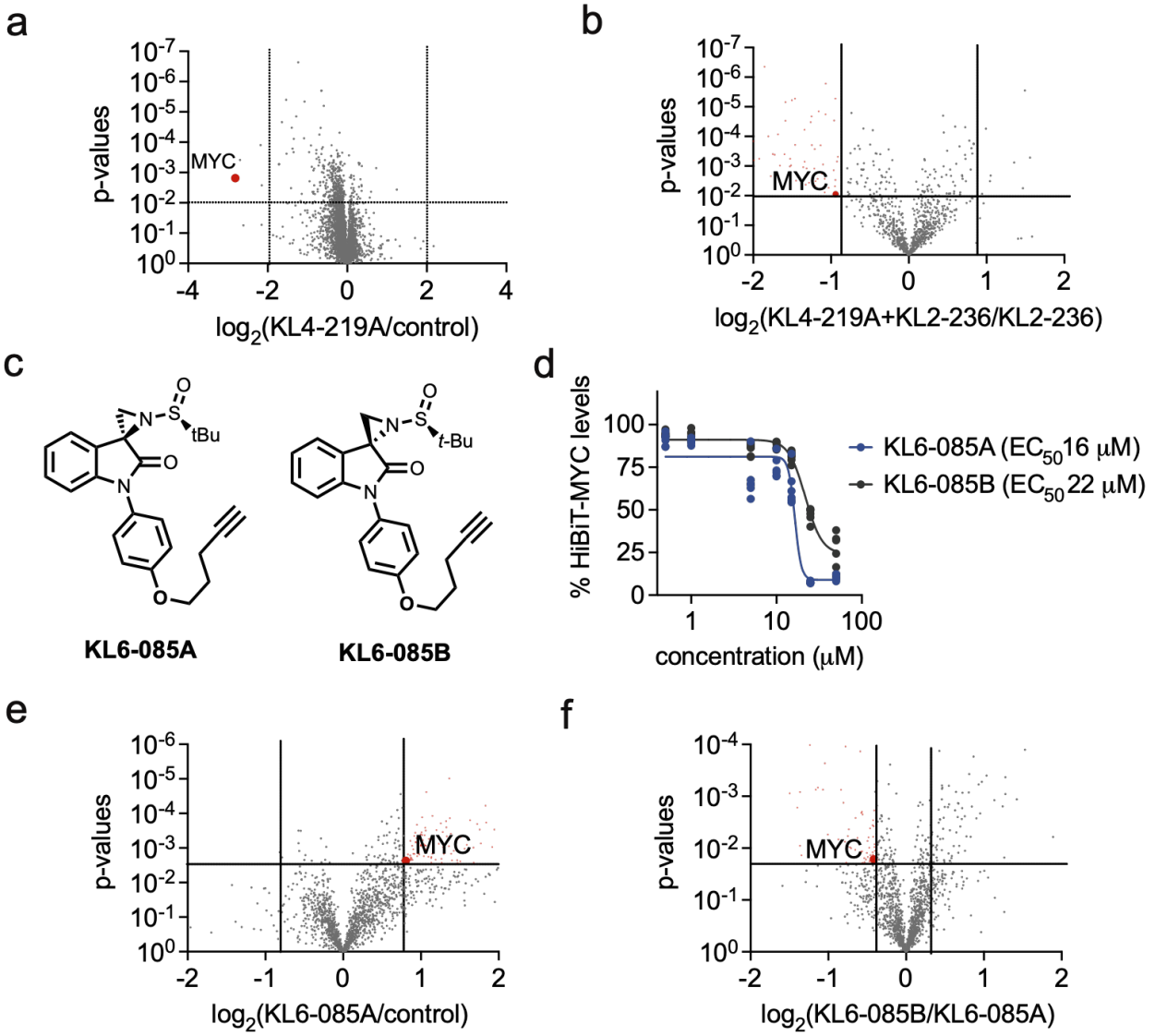

Figure 3.20: Chemoproteomic Characterization of KL4-219A (a) Quantitative proteomic (50 μM) for 8h. Protein level changes were assessed by TMT-based quantitative proteomic methods. Shown in red is MYC. **(b)** Chemoproteomic profiling of KL4-219A. PSN1 cells were pre-treated with proteasome inhibitor bortezomib (500 nM) for 30 min prior to treatment with DMSO vehicle or KL4-219A (100 μM) for 1 h and then treatment with KL2-236 (25 μM) for 4 h, after which resulting cell lysates were subjected to CuAAC mediated appendage of a azide-functionalized biotin handle, probe-modified proteins were enriched, tryptically digested, and analyzed by TMT-based quantitative proteomics. Shown in red are proteins that were significantly enriched and were outcompeted by KL4-219A. **(c)** Structure of KL6-085A and diastereomer KL6-085B. **(d)** HiBiT-MYC HEK293-LgBiT cell dose-response with KL6-085A/B. HiBiT-MYC HEK293-LgBiT cells were treated with DMSO vehicle, KL6-085A, or KL6-085B for 24 h, and MYC levels were detected with the Nano-Glo HiBiT Lytic Detection System. **(e,f)** KL6-085A versus DMSO **(e)** or KL6-085A versus KL6-085B **(f)** chemoproteomic profiling in PSN1 cells. PSN1 cells were pretreated with BTZ (500 nM) for 1 hour before treatment with DMSO vehicle, KL6-085A (50 μM)

or KL6-085B (50 μM) for 2 h, after which probe-modified proteins were subjected to CuAAC with an azide-functionalized biotin, after which probe-modified proteins were enriched with avidin beads, eluted, and input and pulldown eluate was tryptically digested and analyzed and quantified by LC-MS/MS. Data for **(a,b,e,f)** are in **Tables S5-S8.**

Given that our original hit compound KL2-236 showed hundreds of off-targets, we sought to assess whether KL4-219A was more selective. First, we performed global quantitative proteomic profiling to assess the selectivity of MYC degradation. We were pleased to see that KL4-219A showed highly selective degradation of MYC with only 3 other proteins that were significantly lowered—MCL1, CDCA4, and ID1 **(**Figure 3.20**a; Table S5).** Interestingly, MCL1 has been shown to be a direct MYC target gene.[80] Second, chemoproteomic profiling of KL4-219A-outcompeted proteins from KL2-236 enrichment showed significant out competition of MYC; among >968 proteins quantified, only 65 other proteins were significantly outcompeted by KL4-219A pre-treatment **(**Figure 3.20**b, Table S6)**. We also tested alkyne-functionalized analogs of KL4-219A and KL4-219B--KL6-085A and KL6-085B, respectively **(**Figure 3.20**c)**. These probes showed stereoselective degradation of HiBiT-MYC, albeit with attenuated potencies **(**Figure 3.20**d)**. Chemoproteomic profiling with KL6-085A showed significant MYC enrichment compared to vehicle-treated controls, with 98 other off-targets, considerably less than the >400 off-targets observed with KL2-236 **(**Figure 3.20**e; Table S7)**. Comparative chemoproteomic profiling between KL6-085B and KL6-085A showed significant stereoselective engagement of MYC, with only 56 other off-targets showing stereoselective engagement, compared to >100 off-targets comparing KL4-019 and KL2-236 **(**Figure 3.20**f; Table S8).** Overall, we developed an improved stereoselective MYC degrader, KL4-219A. While this molecule still possesses several off-targets, it shows improved potency and selectivity to our original hit molecule and is an important pathfinder molecule for future optimization studies.

3.4 Discussion

Our findings address a longstanding challenge in chemical biology and oncology by demonstrating that MYC, a notoriously “undruggable” oncogenic transcription factor with extensive intrinsic disorder, can indeed be directly and stereoselectively targeted. Through a focused covalent library of stereochemically defined electrophiles, we discovered the hit compound KL2-236, which engages MYC at C203 with contribution from the neighboring D205 with distinct selectivity to its isomers to trigger proteasome-mediated degradation of MYC. While the nature of the interactions between these small molecules and MYC remains unclear at the molecular level, this study further highlights the power of chiral, covalent molecules to interrogate structurally undefined proteins. We also introduce the sulfinyl aziridine as a robust, protein-reactive electrophilic warhead with desirable stability, modulable reactivity, and opportunities for direct at-warhead stereochemical tuning. The engagement of KL2-236 relative to KL4-019, even at the pure protein complex level, also further underscores the importance of expanding stereochemical space in covalent warhead design for targeting intrinsically disordered

protein regions beyond that of just enantiomers, as a greater number of stereocenters may be required for observable compound differentiation.[49,52] Spirocyclic oxindole sulfonyl aziridines react with nucleophiles under mild aqueous conditions owing to hydrogen-bond activation of the sulfonyl group with water.[65,66] This could suggest context-specific, two-point activation for the even less reactive sulfinyl aziridines reported herein, whereby acidic protein residues position or activate the chiral sulfoxide before covalent bond formation occurs. Such a mechanism would be sensitive to local chiral environments found in dynamic structures within intrinsically disordered regions, in accordance with our stereochemical findings. Alternatively, sulfinyl aziridines may react with aspartic or glutamic acids in certain contexts as well, but these adducts might be reversible or unstable and thus difficult to detect with typical proteomics methods.

Because MYC is a central driver of growth and metabolism in various cancers, even modest decreases in MYC protein levels can have broad anticancer effects. By mapping the binding sites and confirming their importance in MYC degradation through mutagenesis studies, we uncovered a cooperative role for C203 and D205 in KL2-236-mediated MYC degradation, suggesting that residue adjacency and local electrostatics can significantly influence small-molecule reactivity within disordered protein regions. Consistent with this mechanism, KL2-236 not only degraded MYC but also demonstrably reduced its transcriptional activity—underscoring the central role of structural destabilization in achieving functional inhibition of an intrinsically disordered transcription factor.

Moreover, we improved upon the liability of KL2-236 in only achieving acute and transient MYC degradation through the development of KL4-219A, which exhibits enhanced degradation durability. Furthermore, KL2-236 showed a high number of off-targets, whereas KL4-219A shows far fewer off-targets and shows exceptional selectivity for MYC degradation. Such iterative optimization exemplifies the power of rational medicinal chemistry approaches for improving the potency, selectivity, and temporal profile of covalent degraders. These differences in durability are likely driven by structural modifications that influence MYC engagement, covalent bond formation, proteasomal processing, and the stability and half-life of the molecule. Nonetheless, KL4-219A is still not of sufficient potency or selectivity and still requires further medicinal chemistry efforts for future translational applications. We can also not rule out potential confounding effects of these off-targets in the biological effects reported here for both KL2-236 and KL4-219A.

Another major question to be addressed in future work surrounds the mechanism by which MYC is degraded. We have not yet been able to identify an E3 ligase responsible for the observed proteasome-mediated degradation of MYC. We postulate that the destabilization may cause partial unfolding of MYC either exposing a degron that is recognized by an E3 ligase, or general quality control E3 ligases that recognize unfolded proteins. Future functional genomic screens to identify the mechanism of degradation of MYC, and more broadly these classes of destabilizing degraders will be important for the future translatability of these molecules.

Further characterization of KL4-219A and more potent, selective, and metabolically stable analogs, particularly in physiologically relevant animal models, will be critical for translating these proof-of-concept findings into potential therapeutic interventions. Delineating how the surrounding protein environment in living systems affects compound reactivity and specificity will deepen our understanding of covalent ligand-protein interactions in intrinsically disordered regions. By demonstrating that intrinsically disordered proteins harbor exploitable cryptic sites, this work opens new vistas for targeting one of the most recalcitrant classes of oncogenic transcription factors.

3.5 Biological Experimental Methods

3.5.1 Chemicals

Bortezomib (C835570) was purchased from Cayman. Chapter 3.6 describes the synthesis and characterization of the covalent library.

3.5.2 Cell Culture

c-MYC HiBiT cells were commercially purchased from Promega (CS302396) in a HEK293-LgBiT background. HEK293T and PSN1 cells were obtained from UC Berkeley's Biosciences Divisional Services Cell Culture Facility. LgBiT cells and HEK293T cells were cultured in DMEM (Corning 10-013-CV) with 10% Fetal Bovine Serum (FBS) (Corning 35-010-CV). PSN1 cells were cultured in RPMI1640 (Gibco 11875093) with 10% FBS. Cells were maintained at 37°C with 5% CO_2.

3.5.3 Screening and Testing of Covalent Ligands with HiBiT-MYC Cells

Covalent ligand screen and dose responses were conducted using the Nano-Glo HiBiT Lytic Detection System (Promega N3040) and CellTiter-Glo 2.0 Assay (G9242). c-MYC-HiBiT cells were seeded at 25,000 cells per well in a 96-well plate (Corning 3917) in 99μL of media and were left to adhere overnight. Cells were then pre-treated or treated with 1 μL of DMSO stock solutions containing varying concentrations of the compound under the conditions described. The Nano-Glo HiBiT Lytic Detection System and Cell Titer Glo 2.0 were used per the manufacturer's instructions (1:1 media to reagent). Plates were incubated in the dark for 10 minutes before their luminescence readout on the Tecan Spark plate reader (30086376).

3.5.4 GSH Stability Assay

GSH stability assays were performed as previously reported.[81]

3.5.5 Western Blotting

Cells were seeded overnight in 6 well plates (800,000 cells/well) or 6cm dishes (1,200,000 cells/dish). Media was aspirated, replaced with media containing DMSO or compound, and treated for the indicated length. Cells were then washed twice with PBS before harvesting by scraping. Cells were collected and pelleted, and PBS was aspirated. Pelleted cells were lysed using RIPA buffer (ThermoScientific 89900) containing protease inhibitor cocktail (Pierce A32955) and Benzonase (Millipore 70746-3 at 25-29 unit/mL) at 37°C for 10 minutes. Sample protein concentrations were normalized using BCA Protein

Assay (Pierce 23225) to run 20-50 μg per well depending on the desired protein target. Samples were boiled for 7 minutes at 95°C after the addition of 4x reducing Laemmli SDS sample loading buffer and run on precast 4-20% Criterion TGX gels (Bio-Rad) in 1x TGX buffer (Bio-Rad 1610734). Proteins were resolved by SDS/PAGE and transferred to 0.2 μm nitrocellulose membrane using the Bio-Rad Trans-Blot Turbo Transfer system (Bio-Rad, 1704150 and 1704271). Membranes were blocked with 5% Bovine Serum Albumin (BSA) (bioWORLD 22070008-6) in Tris-buffered saline containing Tween 20 solution (TBST)(ThermoFisher J77500.K8) for 1 hour at room temperature. Blots were then probed with primary antibody solution overnight at 4°C. Antibodies used in this study were c-MYC (Abcam, AB32072), b-Actin (Cell Signaling Technology, 8H10D10 or Cell Signaling Technology, D6A8), and DDDDK tag (Cell Signaling Technology, 9A3) were diluted 1:1000 in 5% BSA in TBST. Membranes were then washed 3 times with TBST, followed by 1 hour of incubation with a secondary antibody solution in the dark at room temperature. Secondary antibodies used in this study include IRDye680RD Goat anti-Mouse IgG (LicorBio, 926-68070) and IRDye800CW Goat anti-Rabbit IgG (LicorBio 926-32211) diluted 1:10,000 in 5% BSA in TBST solution. Before imaging, membranes were washed an additional 3 times with TBST. Western blots were visualized using an Odyssey DLx Imager (LICORbio) and ChemiDoc MP Imaging System (Bio-Rad).

3.5.6 Pure Protein Labeling with Covalent Ligands and Probes

MYC/MAX pure protein (0.5 μg/50 μL in PBS) was treated with DMSO vehicle or KL2-236 or KL4-019 at 37 °C for 30 minutes. A master mix of the click reagents was prepared such that each replicate would receive 0.25 μL of Rhodamine Azide (5mM stock in DMSO, Click Chemistry Tools, AZ109-5), 1 μL of copper (II) sulfate (50mM stock in water, Sigma-Aldrich, 203165), 3 μL of TBTA (1.7 mM in 4:1 tBuOH/DMSO, TCI Chemicals, T2993) and 1 μL of TCEP (50 mM in water freshly prepared, ThermoScientific, 20491). Samples were vortexed and incubated at room temperature for 1 hour, after which 30 μL of 4x reducing Laemmli SDS sample loading buffer was added to each replicate and boiled at 95 °C for 10 minutes. Samples were cooled to room temperature, loaded into a precast 4-20% Criterion TGX gel (Bio-Rad), and run in 1x TGX buffer (Bio-Rad 1610734). Proteins were resolved by SDS/PAGE. Probe-labeled proteins were analyzed by in-gel fluorescence using the ChemiDoc MP Imaging system (Bio-Rad). Gels were silver-stained using the Pierce Silver Stain Kit (ThermoScientific, 24612) per manufacturer instructions and imaged on the ChemiDoc MP Imaging System (Bio-Rad).

3.5.7 Expression and Purification of MYC/MAX

MYC (residues 1-439, isoform 1) without any purification tags was cloned into a pET derived vector for expression in *E. coli*. MAX (residues 2-160) with an N-terminal STREP tag, followed by a TEV cleavage site was cloned into a pET derived vector for expression in *E. coli*.

MYC

MYC was expressed in BL21 cells as inclusion bodies by induction with 1 mM IPTG at an OD_{600} of 0.6-0.8 at 37 °C for 4 h. Cells were lysed with a high pressure homogenizer (Emulsiflex C3, Avestin) in lysis buffer (50 mM Tris/HCl pH 8.0, 5 mM DTT, 5 mM

Benzamidine-HCl, 5 mM EDTA) and inclusion bodies were collected by centrifugation at 16,000 x *g* at 4 °C for 30 min. Inclusion bodies were washed once with lysis buffer and collected by centrifugation at 16,000 x *g* at 4 °C for 30 min. Inclusion bodies were washed a second time with water and collected by centrifugation at 16,000 x *g* at 4 °C for 30 min. Protein concentration in inclusion bodies was determined by HPLC analysis after dissolving in 6 M guanidine chloride. Inclusion bodies were dissolved in inclusion body buffer (25 mM HEPES/NaOH pH 7.6, 15 % glycerol, 300 mM NaCl, 0.1 mM EDTA, 1 mM DTT, 7 M Urea), clarified by centrifugation at 25,000 x *g* at 4 °C for 30 min and the supernatant was flash frozen in small aliquots at a final protein concentration of 5 mg/mL.

MAX

MAX was expressed in BL21 cells by induction with 0.15 mM IPTG at an OD_{600} of 2.2 at 18 °C for 16 h. Cells were lysed with a high pressure homogenizer (Emulsiflex C3, Avestin) in lysis buffer (50 mM Tris/HCl pH 7.5, 300 mM NaCl, 1 mM TCEP, 1 mM EDTA, 0.1 % Triton-X100) and the supernatant was cleared by centrifugation at 40,000 x *g* at 4 °C for 40 min. The supernatant was loaded on a prepacked StrepTrap HP column (Cytiva), washed with 5 CV of wash buffer (50 mM Tris/HCl pH 7.5, 300 mM NaCl) and bound protein was eluted with 5 CV elution buffer (50 mM Tris/HCl pH 7.5, 300 mM NaCl, 2.5 mM d-desthiobiotin).
The STREP-tag was removed by cleavage with TEV protease at RT for 4 h. MAX was further purified by anion exchange on a HiTrapQ column. The salt concentration in the TEV-cleaved sample was reduced to 25 mM NaCl by dilution with 50 mM Tris/HCl pH 8.3. The sample was loaded onto the HiTrapQ HP column, washed with 5 CV of HiTrapQ A buffer (50 mM Tris/HCl pH 8.3, 25 mM NaCl) and eluted with a gradient from 0-100 % HiTrapQ buffer B (50 mM Tris/HCl pH 8.3, 1000 mM NaCl) over 20 CV. Peak fractions were pooled, concentrated with a 10 kDa MWCO spin concentrator (Millipore) and further purified by size exclusion chromatography on a Superdex 200 16/60 PG column equilibrated in SEC buffer (50 mM Tris/HCl pH 7.5, 150 mM NaCl). Peak fractions were pooled and concentrated to >5 mg/mL with a 10 kDa MWCO spin concentrator (Millipore).

MYC-MAX

MYC/MAX was obtained by refolding MYC from inclusion bodies in presence of purified MAX. All steps were carried out at 4 °C. MYC/MAX were mixed at equal molar ratios and the sample was diluted to a final protein concentration of 0.25 mg/mL in refolding buffer (25 mM HEPES/NaOH pH 7.6, 15 % glycerol, 300 mM NaCl, 0.1 mM EDTA, 1 mM DTT, 6 M Urea). The complex was refolded by a stepwise dialysis (3 M Urea, 1 M Urea, 0.5 M Urea) with 10x buffer excess for each step over 1 h to 1.5 h. The final buffer exchange in 25 mM HEPES/NaOH pH 7.6, 15% glycerol, 300 mM NaCl, 0.1 mM EDTA, 1 mM DTT was performed over night with 30x buffer excess. The sample was further purified on a Heparin HP column, washed with 10 CV of Heparin HP A buffer (25 mM Tris/HCl, pH 8, 200 mM NaCl), 10% Heparin buffer B (25 mM Tris/HCl, pH 8, 2000 mM NaCl) and eluted with a gradient from 10-100 % Heparin buffer B (25 mM Tris, pH 8, 2000 mM NaCl) over 10 CV. The sample was concentrated using a 10 kDa MWCO spin concentrator (Millipore) and further purified by SEC on a Superdex75 16/60 column in SEC buffer

(20 mM HEPES/NaOH pH7.0, 300 mM NaCl, 2 mM TCEP). Peak fractions containing a 1:1 molar ratio of MYC:MAX based on LC/MS analysis were pooled, flash frozen in liquid nitrogen and stored at -80 °C until use.

3.5.8 Peptide Mapping Using Online Pepsinolysis LC-MS/MS

MYC(1-439)/MAX(2-160) (1 μM) protein was labeled with 50 μM KL2-236 in 20 mM HEPES, pH 7.0, 300 mM NaCl buffer for 1 hour at room temperature. The mixture as then directly injected on to LC-MS system. Peptide mapping was performed using tandem online pepsin digestion and reversed-phase separation coupled to an Orbitrap Q Exactive mass spectrometer. Samples were injected onto an immobilized-pepsin column (Waters Enzymate BEH Pepsin, 2.1 mm × 30 mm) with resulting peptic peptides collected and separated by reversed-phase (C18) (Agilent ZORBAX Extend-C18, 1.0 mm × 150 mm, 3.5 μm particle size). The eluting peptides were then analyzed using data-dependent tandem MS acquisition (DDA). Samples (10 μL, 10 pmol) were injected at 0.25 mL/min in 0.1% formic acid in water for 4 min with resulting peptic peptides collected on the C18 trap cartridge. The pepsin column is then switched from the flow stream and peptides are eluted at 0.12 mL/min using a gradient of 8–40% B (0–14 min), followed by 70% B (2 min) and equilibration back to 2% B (Mobile Phase A = 0.1% formic acid, B = acetonitrile with 0.1% formic acid). Tandem MS spectra were acquired using the following DDA settings (Full MS Scan: 70,000 Resolution, AGC Target 3e6, *m/z* 370–1200 ddMS2 Settings; 17,500 resolution, AGC Target 1e5, max IT 50 ms, Isol window 2.0 *m/z*, NCE 30, Charge Exclusion >5, Min AGC Targe 8e4, and dynamic exclusion off).

3.5.9 Pulldown of MYC and Covalent Ligands for Western Blotting Detection

Pelleted cells were lysed by probe sonication on ice in PBS containing a protease inhibitor cocktail (Pierce A32955). Samples were centrifuged at 10,000 g at 4 °C for 10 minutes to remove cellular debris. Lysate protein concentrations were measured using BCA Protein Assay (Pierce 23225) and normalized to 5 mg/mL in 500 μL of PBS with protease inhibitor cocktail. A master mix of the click reagents was prepared such that each replicate would receive 10 μL of biotin picolyl azide (10 mM stock in DMSO, Sigma-Aldrich, 900912), 10 μL of copper (II) sulfate (50 mM stock in water, Sigma-Aldrich, 203165), 30 μL of TBTA (1.7 mM in 4:1 tBuOH/DMSO, TCI Chemicals, T2993) and 10 μL of TCEP (50mM in water freshly prepared, ThermoScientific, 20491). Samples were vortexed and incubated on a rotator at room temperature for 1 hour. Proteins were pelleted by centrifugation (6500 g) at room temperature for 5 minutes. The supernatant was removed, 500 μL of cold methanol was added, and samples underwent three cold methanol washes with centrifugation to pellet proteins and sonication for resuspension. Pelleted proteins were redissolved in 200 μL of PBS with 1.2% SDS (w/v) by sonication. Samples were heated to 90°C for 5 minutes, and 5μL of the sample was removed and saved for input (diluted to 60 μL and 20 μL of 4x reducing Laemmli SDS sample loading buffer). 55 μL (per sample) of streptavidin-agarose beads (ThermoFisher, 20353) were washed with PBS using a Micro-Bio Spin Column (Bio-Rad, 7326204) and vacuum manifold. 500 μL of PBS was added to the dissolved proteins, and then the washed beads were added to each sample using two washes of 250 μL of PBS. Samples were incubated on a rotator at 4°C

overnight. Samples were then put in a 37°C bath to redissolve SDS for 5 minutes, and then beads were pelleted by centrifugation at 1400 g for 5 min. The supernatant was removed, and beads were washed with 0.2% SDS in PBS (w/v) for 10 minutes on a rotator at room temperature. The supernatant was removed, and pelleted beads were moved to Micro-Bio Spin Columns using two washes of PBS. Beads were washed on a vacuum manifold three times with PBS and then three times with water. The beads were then moved to screw cap Eppendorf tubes with PBS, centrifuged, and the supernatant removed. 30 μL of 1x reducing Laemmli SDS sample loading buffer was added to each sample and then boiled at 95 °C for 15 minutes to elute proteins from beads. Samples and corresponding inputs were run on precast 4-20% Criterion TGX gels (Bio-Rad) in 1x TGX buffer (Bio-Rad 1610734). Proteins were resolved by SDS/PAGE and transferred to 0.2 μm nitrocellulose membrane using the Bio-Rad Trans-Blot Turbo Transfer system (Bio-Rad, 1704150 and 1704271). Membranes were blocked with 5% Bovine Serum Albumin (BSA) (bioWORLD 22070008-6) in Tris-buffered saline containing Tween 20 solution (TBST)(ThermoFisher J77500.K8) for 1 hour at room temperature. Blots were then probed with primary antibody solution overnight at 4 °C. Antibodies used in this study were c-MYC (Abcam, AB32072) and B-Actin (Cell Signaling Technology, 8H10D10), were diluted 1:1000 in 5% BSA in TBST. Membranes were then washed 3 times with TBST, followed by 1 hour of incubation with a secondary antibody solution in the dark at room temperature. Secondary antibodies used in this study include IRDye680RD Goat anti-Mouse IgG (LicorBio, 926-68070) and IRDye800CW Goat anti-Rabbit IgG (LicorBio 926-32211) diluted 1:10,000 in 5% BSA in TBST solution. Before imaging, membranes were washed an additional 3 times with TBST. Western blots were visualized using an Odyssey DLx Imager (LICORbio).

3.5.10 Quantitative Global TMT Proteomics

Cells were treated with either DMSO vehicle or compound (KL4-219A 50 μM for 8 h) and lysed by sonication in PBS with protease inhibitor cocktail (Pierce A32955). Briefly, 100 μg protein from each sample was reduced, alkylated and tryptically digested overnight. Individual samples were then labeled with isobaric tags using commercially available TMTsixplex (ThermoFisher Scientific, P/N 90061) kits, in accordance with the manufacturer's protocols. Tagged samples (20 μg per sample) were combined, dried using a vacuum concentrator at 30 °C, resuspended in 300 μL 0.1% TFA in water, and fractionated using high pH reverse-phased peptide fractionation kits (ThermoFisher Scientific, P/N 84868) according to the manufacturer's protocol. Fractions were dried using vacuum concentrator at 30 °C, resuspended in 25 μL 0.1% formic acid in water, and analyzed by LC-MS/MS as previously described.[82,83]

3.5.11 Pulldown TMT Proteomics Experiments with Covalent Ligand/Probes

Cells were seeded at 15 million cell/dish in 15 cm dishes (1 dish per replicate). All cells were pre-treated with 500 nM of Bortezomib for 1 hour. Cells were then treated with compound at 50μM final concentration and incubated for an additional 4 hours. Cells were then washed twice with PBS, scraped, and collected. Cells were pelleted by centrifugation, and the supernatant was removed. Cells were lysed by probe sonication

on ice in PBS containing a protease inhibitor cocktail (Pierce A32955). Samples were centrifuged at 10,000 g at 4 °C for 10 minutes to remove cellular debris. Lysate protein concentrations were measured using BCA Protein Assay (Pierce 23225) and normalized. A master mix of the click reagents was prepared such that each replicate would receive 10 μL of biotin picolyl azide (10 mM stock in DMSO, Sigma-Aldrich, 900912), 10 μL of copper (II) sulfate (50 mM stock in water, Sigma-Aldrich, 203165), 30 μL of TBTA (1.7 mM in 4:1 tBuOH/DMSO, TCI Chemicals, T2993) and 10 μL of TCEP (50 mM in water freshly prepared, ThermoScientific, 20491). Samples were vortexed and incubated on a rotator at room temperature for 1 hour. To each sample, 100% acetonitrile was added to the final concentration of 80% and mixed by inversion to precipitate proteins. Proteins were pelleted by centrifugation at 21,000 g at 4 °C for 10 minutes. The supernatant was removed, 500 μL of cold methanol was added, and samples underwent three cold methanol washes with centrifugation to pellet proteins and sonication for resuspension. After the final wash, the pellets were left to air dry for 10 minutes. Proteins were redissolved in 1 mL of PBS with 1.2% SDS (w/v) by sonication. Samples were then heated to 90°C for 5 minutes, and 5 mL of PBS was transferred to 15 mL tubes. 170 μL of streptavidin-agarose beads (ThermoFisher, 20353) were added to each sample and incubated at 4°C overnight with constant rotation. Samples were then put in a 37°C bath to redissolve SDS for 5 minutes, and then beads were pelleted by centrifugation at 1400 g for 5 min. The supernatant was removed, and beads were washed with 0.2% SDS in PBS (w/v) for 10 minutes on a rotator at room temperature. The supernatant was removed, and pelleted beads were moved to Micro-Bio Spin Columns using two washes of PBS. Beads were washed on a vacuum manifold four times with PBS and then four times with water. The beads were then moved to screw cap Eppendorf tubes with two 250 μL washes of 6 M Urea in PBS. To each sample, 25 μL of DTT (30 mg/mL in water) was added and incubated at 65 °C for 20 minutes, gently mixing every 5 minutes. Samples were cooled to room temperature, and then 25 μL of iodoacetamide (400 mM in water)(G-Biosciences RC-150) was added and incubated at 37 °C for 30 minutes with constant agitation. Samples were then diluted with PBS, centrifuged, the supernatant removed, rewashed with PBS, and then washed once with 500 μL of 50 mM TEAB (ThermoScientific 90114), and the supernatant removed. Beads were resuspended in 100 μL of 50 mM TEAB, and 4 μL of sequencing grade trypsin (0.5 mg/mL, Promega, V5111) was added to each sample. Samples were digested at 37°C overnight with constant agitation. Samples (beads and liquid) were then moved to a Micro-Bio Spin Column and centrifuged at 2000 g for 2 min at RT to collect flow through. Quantification of peptides was done using the Thermo Scientific Pierce Quantitative Colorimetric Peptide Assay (ThermoScientific, 23275). 100 μL of each sample was for TMT labeling. TMT labels (ThermoScientific, 90061, or A58332) were equilibrated with anhydrous acetonitrile, and 20 μL of each tag was added to a corresponding replicate. The reaction was incubated at room temperature for 1 hour on a rotating mixer and then quenched with 5% hydroxylamine for 15 minutes at room temperature. Peptides were dried down by Vacufuge (Eppendorf, 022820168) at 30 °C until dry. Samples were then resuspended in 50 μL of 0.1% Trifluoroacetic acid (TFA) in water and combined. Using the previously recorded concentrations, 100 μg of peptides were then fractionated according to the

manufacturer's protocol using the Thermo Fisher High pH Reverse Phase Fractionation Kit (ThermoScientific, 84868). Following fractionation, samples were dried down using Vacufuge at 30°C and then resuspended in 25 μL of 0.1% formic acid in water by vortexing and bath sonication. Samples were centrifuged at 20,000 g for 10 minutes at 4 °C and the supernatant were transferred into an LCMS vial with a glass insert (ThermoScientific, 6PME03C1SP) and capped. Samples were analyzed by LC-MS/MS as previously described.[82,83]

3.5.12 ELISA-ABPP

For capture plate preparation, the HiBiT capture antibody (Promega N7200) was diluted down to 2.5 μg/mL in ELISA coating buffer A (Invitrogen CB07100) and 100 μL were dispensed into each well of a Nunc MaxiSorp flat bottom 96-well plate (Thermo 473768) and incubated overnight at 4C. The following day, the plate was washed once with 200μL PBST (Boston BioProducts IBB-171) and blocked with 200 μL SuperBlock (Thermo 37515) for 1 hour at room temperature. Blocking buffer was removed, plate was washed three times with 200 μL PBST, and coated plate was used immediately for ELISA-ABPP.

For the ELISA-ABPP method, 96-well cell culture plates (Corning 3596) were coated with 100 μL of 0.1 mg/mL poly-D-lysine (Sigma Aldrich P7280-5MG) in PBS for 3 hours at room temperature followed by two 200 μL washes with PBS. DLD1 cells expressing HiBiT-MYC were seeded at 75,000 cells per well in complete media (RPMI, 10% FBS, 1% Penn/Strep, 10 μg/mL blasticidin) and incubated overnight (37 °C, 5% CO_2) to allow cells to attach. The next day, the media was removed and replaced with 75 μL complete media followed with 25 μL of a 4x stock of the oxindoles in complete media and incubated for 1 hour at 37°C, 5%CO_2. After incubation, the media was removed, and cells were washed once with 200 μL warm cell imaging solution (Thermo A59688DJ) followed with addition of 100 μL lysis buffer consisting of 1% n-dodecyl-β-D-maltopyranoside (Anatrace D310-25GM) in cell imaging solution containing complete EDTA-free protease inhibitors (Sigma Aldrich 4693132001) and lysed for 1 hour at room temperature with constant mixing. During lysis, reporter biotin click reagents were prepared by dissolving 100 mg THPTA (Vector 1010-5G) into 5 mL of water, 100 mg ascorbate (Sigma Aldrich 11140-5G) into 5mL water, 20mg copper sulfate (Sigma Aldrich 451657-10G) into 5 mL water, and 125μL 10 mM biotin picolyl azide (Vector 1167-100MG) into 5 mL of water. The individual click components were combined and 50 μL of the click mix was added to each well containing protein lysate and incubated for 1 hour at room temperature. The click reaction was quenched with the addition of 12.5 μL 0.5 M EDTA (Sigma Aldrich 324506-100ML) and centrifuged at 3000xg for 15 minutes at 4 °C. After centrifugation, 130 μL of clarified lysate was transferred to "Capture Plate" and incubated overnight at 4C with gentle mixing. After incubation, capture plates were washed five times with 200 μL PBST. Following final wash, 50 μL of streptavidin-HRP (CST 3999S) was added at a 1:1000 dilution and incubated for 1 hour at room temperature. After incubation, capture plate was washed five times with 200μL PBST followed with addition of 135μL of TMB substrate (Thermo N301) with a 5-minute incubation at room temperature with gentle mixing. Following incubation, the reaction was quenched with addition of 50 μL TMB stop solution

(Thermo N600) and strong shaking for a few seconds followed by reading absorbance at 450 nm on PHERAstar FS (BMG Labtech).

3.5.13 Generating Cells Expressing FLAG-Wild Type or Mutant MYC

Human MYC constructs were customized and purchased from GenScript. The customized construct was in a pGenLenti backbone and MYC had a C-terminal DYKDDDDK (FLAG) tag. All mutant constructs were ordered from GenScript, which maintained a pGenLenti backbone and C-terminal DYKDDDDK tag.

These constructs were then used to generate both transient and stable FLAG-MYC-expressing cells. For stable cell generation, lentiviral infection was used. Before transfection, HEK293T cells were conditioned in complete media containing heat-inactivated FBS. For lentivirus production, FLAG-tagged wild type c-MYC or FLAG-tagged MYC mutant plasmids (GenScript), psPAX2 (Addgene, 12260) and pMD2.G (Addgene, 12259) were transfected into HEK293T cells using Lipofectamine 2000 (ThermoFisher, 11668027) in Opti-MEM (Gibco, 31985062). The virus-containing medium was collected and filtered (0.45 μm PES) after 48 hours. The virus was then used to infect new HEK293T with a 1:1000 dilution of Polybrene (Sigma-Aldrich, TR-1003-G). After 48 hours, infected cells were selected with puromycin (Abcam, ab141453) (1.5 μg/mL for HEK293T cells. After 4 days of the selection, cells were recovered by replacing puromycin-containing media with fresh media.

For transient expression of Flag-Wildtype or Mutant MYC, HEK293T cells were seeded at 300,000 cell/well in 6-well plates or 3 million cells/dish in 15cm dishes. 24 hours post seeding, cells were conditioned in complete media containing heat inactivated FBS. For transient transfection, FLAG-tagged wild type c-MYC or FLAG-tagged MYC mutant plasmids (GenScript) were transfected into HEK293T cells using Lipofectamine 2000 (ThermoFisher, 11668027) in Opti-MEM (Gibco, 31985062). 24 hours post transfection, cells used for downstream application.

3.5.14 Luciferase Reporter Assay

MYC luciferase reporter assay was purchased from Qiagen (CCS-012L) and performed according to the manufacturer's protocol with minor alterations. Before transfection, HEK293T cells were seeded into a 96-well plate (Corning 3917) at 30,000 cells/well in 100 μL of media. Negative control, positive control, or MYC luciferase reporter construct were diluted in Opti-MEM medium (1 μL DNA into 25 μL Opti-MEM per well). Attractene (Qiagen, 301005) was diluted in Opti-MEM (1 μL Attractene into 25 μL Opti-MEM per well). DNA and diluted Attractene were gently mixed in a 1:1 ratio and then incubated at room temperature for 20 minutes undisturbed. 50 μL of DNA-Attractene mixture was added to each well in triplicate. 24 hours post-transfection, media was carefully aspirated from each well, and 75 μL of media containing either DMSO or compound was added. After 24 hours of compound treatment, Dual-Glo luciferase assay (Promega, E2920) was used according to the manufacturer's protocol for luminescent readout. Firefly and Renilla luminescence were read on a Tecan Spark plate reader. Background luminescence levels were subtracted using a blank control, and then Firefly: Renilla was calculated for each well.

3.5.15 Cellular Thermal Shift Assay (CETSA)

PSN1 cells were harvested by scraping from a 10 cm dish after 1 hour at 50 μM compound treatment. Cells were resuspended in PBS containing protease inhibitor cocktail and 50 μM compound and then aliquoted into eight 0.2 mL PCR strips with 100 μL per tube. PCR strips were designated a temperature via a gradient program on Bio-Rad's T100 Thermal cycler (Bio-Rad, 1861096). Samples were heated at their respective temperatures (57 °C, 55.6 °C, 53.4 °C, 50.4 °C, 46.5 °C, 43.2 °C, 41.1 °C, 40 °C) for 3 minutes and then at 25 °C for 3 minutes. Immediately following, cells were snap-lysed using liquid nitrogen (3 freeze-thaw cycles). Cell debris, along with any precipitated and aggregated proteins, were removed by centrifugation at 20,000 g for 20 minutes at 4 °C. 80 μL of supernatant was transferred to new PCR strips, 26.6 μL of 4x reducing Laemmli SDS sample loading buffer was added to each sample and boiled at 95°C for 10 minutes. 12 μL of each sample with buffer were loaded per well and run on precast 4-20% Criterion TGX gels (Bio-Rad) in 1x TGX buffer (Bio-Rad 1610734). Proteins were resolved by SDS/PAGE and transferred to 0.2μm nitrocellulose membrane using the Bio-Rad Trans-Blot Turbo Transfer System (Bio-Rad, 1704150 and 1704271). Membranes were blocked with 5% Bovine Serum Albumin (BSA) (bioWORLD 22070008-6) in Tris-buffered saline containing Tween 20 solution (TBST) (Thermo Fisher J77500.K8) for 1 hour at room temperature. Blots were then probed with primary antibody solution overnight at 4 °C. Antibodies used in this study were c-MYC (Abcam, AB32072) band -Actin (Cell Signaling Technology, 8H10D10), diluted 1:1000 in 5% BSA in TBST. Membranes were washed 3 times with TBST, followed by 1 hour of incubation with a secondary antibody solution in the dark at room temperature. Secondary antibodies used in this study include IRDye680RD Goat anti-Mouse IgG (LicorBio, 926-68070) and IRDye800CW Goat anti-Rabbit IgG (LicorBio 926-32211) diluted 1:10,000 in 5% BSA in TBST solution. Before imaging, membranes were washed an additional 3 times with TBST. Western blots were visualized using an Odyssey DLx Imager (LICORbio).

3.5.16 RNA Extraction

PSN1 cells were seeded at 1,200,000 cells/dish in a 6 cm dish and allowed to adhere overnight. Aspirate media, replace it with media containing DMSO or compound, and treat it for 2 hours. After treatment, cells were washed twice with PBS before harvesting by scraping. Cells were collected into a 1.7 mL Eppendorf tube and centrifuged to collect pellet cells. PBS supernatant was aspirated, and the cell pellet was further processed. The Monarch Total RNA Miniprep kit (New England Biolabs, T2010S) was used to harvest total RNA and was followed according to the manufacturer's protocols.

3.5.17 RNA Sequencing

Library preparation and sequencing were performed by the QB3-Berkeley Genomics core

quality was assessed on an Agilent 2100 Bioanalyzer. We then enriched for mRNA using NEB oligo-dT beads (E7490L), and assessed the mRNA quality on an Agilent 4200 TapeStation. Libraries were prepared using the KAPA RNA Hyper Prep kit (Roche

then extended via 11 cycles of PCR using unique dual indexing primers into full-length Illumina adapters. Library quality was checked on an AATI (now Agilent) Fragment Analyzer, and samples were then transferred to the Vincent J. Coates Genomics Sequencing Laboratory (GSL), where samples were pooled with other FGL prepared

validate coverage on an Illumina MiSeq 25 Single Read Nano Run. Subsequently, the pool was adjusted to meet required throughputs per sample and then run on 1 lane of an Illumina 150 Paired End NovaSeq X 25B flowcell. Samples were demultiplexed and converted into fastq files on local GSL servers using Illumina BCLConvert Software. RNA libraries were sequenced generating 30-40 million 150bp paired end reads per sample (average 36 million reads).

3.5.18 Analysis of RNA Sequencing Data

Fastq files were processed using the Exon Quantification Pipeline (v2.5)[84], in which reads were aligned to the human genome (GRCh38) using STAR (version 2.7.3a)[85] with an average of 32.9 million reads mapped per sample (89-92%), and gene counts were generated. Prior to differential expression analysis, DESeq2 (v1.44.0)[86] normalized gene read counts (vsn; v3.72.0)[87] were visualized, and one outlier sample was removed from subsequent analysis due to high read count variability. When downstream analysis was repeated with this outlier included, results were consistent with the outlier-removed analysis, and conclusions were not changed. Differential expression analysis was performed using DESeq2 comparing KL2-236 versus DMSO. Genes with an adjusted p-value of less than 0.05 and a log2(Fold Change) less than -0.5 or greater than 0.5 were considered significantly differentially expressed. To examine gene set enrichments, DESeq2 results were filtered for a baseMean of 15 counts and ranked using -log10(p-value)*sign(log2 Fold Change), then MSigDB Hallmark gene sets (v7.5.1)[88] were tested for gene set enrichment using the fGSEA multi-level implementation (v1.30.0).[89] Significant genes with positive fold-changes were at the beginning of the rank list (ranks close to 1) and significant genes with negative fold-changes were at the end of the list (ranks close to 16000). To ensure GSEA reproducibility, 50 permutations were run and the summary statistics for those results are shown in Table S4.

3.5.19 Assessment of Stress Granules

PSN1 cells were seeded in 4-well glass bottom cell culture dishes at 100,000 cells/well (Greiner Bio, 627870). The treated cells were fixed with 4% paraformaldehyde in PBS (Cell Signaling Technology, 47746P) for 15 minutes at room temperature and then blocked with Blocking Buffer (Cell Signaling Technology, 12411) for one hour at room temperature. Samples were further incubated with primary antibodies in Antibody Dilution Buffer (Cell Signaling Technology, 12378S) either overnight at 4°C or at room temperature for 1 hour. Following primary antibody incubation, cells were washed 3 times with PBS and then incubated in secondary antibody in Antibody Dilution Buffer for 1 hour at room temperature. Antibodies used in this experiment include G3BP1 (BD Biosciences, 611126), Phalloidin-iFluor 594 Conjugate (Abcam, ab176757) and Anti-mouse IgG (H+L), F(ab')2 Fragment (Alexa Fluor 488 Conjugate) (Cell Signaling Technology, 4408S). Upon completion of immunostaining, a few drops of ProLong Gold Antifade reagent with DAPI

(Invitrogen P36941) were added to each well. Images were captured using a Zeiss LSM880 FCS microscope with a 63x oil objective.

3.5.20 Flag Pulldown

HEK293T cells were seeded at 3 million cells/dish in 15 cm dishes. Following transient transfection in with FLAG-tagged wild type c-MYC or FLAG-tagged MYC mutant plasmids (GenScript), cells were washed with ice cold PBS twice then lysed on ice with Pierce IP Lysis Buffer (ThermoFisher 87787) with protease inhibitor cocktail (Pierce A32955). Samples were centrifuged at 20,000 g at 4 °C for 15 minutes to remove cellular debris. Supernatant was collected for pulldown. Pierce Anti-DYKDDDDK Magnetic Agarose beads (ThermoFisher A36797) were prepared according to the manufacturer's protocol. 100 μL of magnetic beads were added to each sample and incubated for 5 hours at 25°C while mixing. Flag-protein was then eluted from beads using the Gentle Elution Protocol according to manufacturer's instructions (ThermoFisher A36806) and used for downstream applications.

3.5.21 Whole Proteome Site of Labeling

Cells were seeded at 15 million cell/dish in 15 cm dishes (1 dish per replicate). All cells were pre-treated with 500 nM of Bortezomib for 1 hour. Cells were then treated with compound at 50μM final concentration and incubated for an additional 4 hours. Cells were then washed twice with PBS, scraped, and collected. Cells were pelleted by centrifugation, and the supernatant was removed. Cells were lysed in RIPA buffer (ThermoScientific 89900) containing a protease inhibitor cocktail (Pierce A32955) and 50mM Iodoacetamide (G-Biosciences RC-150). Lysate protein concentrations were measured using BCA Protein Assay (Pierce 23225) and normalized to 2 mg/mL such that each replicate contained 4 mg of total protein. A master mix of the click reagents was prepared such that each replicate would receive 55 μL of copper (II) sulfate (50 mM stock in water, Sigma-Aldrich, 203165), 170 μL of TBTA (1.7 mM in 4:1 tBuOH/DMSO, TCI Chemicals, T2993) and 55 μL of TCEP (50 mM in water freshly prepared, ThermoScientific, 20491). 120 μL of master mix was added to each tube and mixed followed by 5 μL of desthiobiotin azide.[90] Samples were vortexed and incubated on a mixer at 37°C for 1 hour. To each sample, 100% acetonitrile was added to the final concentration of 80% and mixed by inversion to precipitate proteins. Proteins were pelleted by centrifugation at 21,000 g at 4 °C for 10 minutes. The supernatant was removed, 4 mL of 80% EtOH was added, and samples underwent two 80% EtOH washes with centrifugation to pellet proteins and sonication for resuspension. After the final wash, the pellets were left to air dry for 10 minutes. Proteins were redissolved in 600 μL 8 M urea (dissolved in 50 mM HEPES buffer) and then diluted with 50 mM HEPES for a final concentration of 2 M urea. 50 μL of streptavidin-agarose beads (ThermoFisher, 20353) were added to each sample with 2.4 mL of 0.2% NP-40 and incubated at 4°C overnight with constant rotation. Beads were pelleted by centrifugation at 1400 g for 5 min. The supernatant was removed, and beads were resuspended in 1.2 mL of 0.1% NP-40 in PBS (w/v) and moved to a low-bind tube. Beads were pelleted by centrifugation at 1400 g for 5 min and the supernatant was removed. Samples underwent an additional two washes with 0.1% NP-40 in PBS. Then samples were washed three times with PBS and three

times with water. After the final wash, supernatant was aspirated, and beads resuspended in 600 μL of 8 M urea (dissolved in 50 mM HEPES buffer). To each sample, 30 μL of DTT (30 mg/mL in water) was added and incubated at 37 °C for 45 minutes with shaking. Samples were cooled to room temperature, and then 30 μL of iodoacetamide (400 mM in water) (G-Biosciences RC-150) was added and incubated at room temperature for 30 minutes with constant agitation. Beads were then diluted with 1.8 mL of 50 mM HEPES buffer, centrifuged, the supernatant removed. Beads were resuspended in 400 μL 2 M urea (dissolved in 50 mM HEPES buffer) and 8 μL of sequencing grade trypsin (0.5 mg/mL, Promega, V5111) was added to each sample. Samples were digested at 37°C overnight with constant agitation. Samples (beads and liquid) were then diluted with 800 μL 0.1% NP-40 in PBS and moved to a Micro-Bio Spin Column. Beads were washed on a vacuum manifold three times with 0.1% NP-40 in PBS, then three times with PBS and then two times with water. The Micro-Bio Spin Column was moved into a 2 mL low-binding tube. Beads were incubated in 300 μL of elution buffer (0.1% formic acid in 50% acetonitrile) for 10 minutes. Samples were centrifuged at 1,400 g for 3 minutes and the flowthrough retained. The elution steps were repeated a total of three times and then all three flowthrough fractions were recombined, and peptides were dried down by Vacufuge (Eppendorf, 022820168) at 30 °C until dry. Samples were then resuspended in 25 μL of 0.1% formic acid in water and then centrifuged at 20,000 g for 10 minutes at 4 °C and the supernatant were transferred into an LCMS vial with a glass insert (ThermoScientific, 6PME03C1SP) and capped. Samples were analyzed by LC-MS/MS. The amino acid reactivity and selectivity of KL2-236 was determined as described previously.[75]

3.6 Synthetic Methods and Characterization

3.6.1 General Procedures

All reactions were performed in flame- or oven-dried glassware under a positive pressure of nitrogen or argon, unless otherwise noted. Air- and moisture-sensitive liquids were transferred via syringe. When indicated, solvents or reagents were degassed by sparging with argon for 10 minutes in an ultrasound bath at 25 °C. Volatile solvents were removed under reduced pressure using rotary evaporation below 35 °C. Analytical and preparative thin-layer chromatography (TLC) were performed using glass plates pre-coated with silica gel (0.25-mm, 60-Å pore size, Merck TLC Silicagel 60 F254) impregnated with a fluorescent indicator (254 nm). TLC plates were visualized by exposure to ultraviolet light (UV) and then were stained by submersion in an ethanolic *p*-anisaldehyde solution, ceric ammonium molybdate solution, or potassium permanganate solution followed by brief heating on a hot plate. Flash column chromatography was performed with silica gel purchased from Fisher Scientific (Fisher Chemical™, 60 Å, 230-400 mesh, 40-63 µm). Synthetic procedures used to prepare oxindole sulfonyl and sulfinyl aziridines were adapted from the prior methods of Hajra and co-workers.[65]

Commercial solvents and reagents were used as received with the following exceptions. Anhydrous tetrahydrofuran (THF), dichloromethane (DCM), dimethylformamide (DMF), and acetonitrile (MeCN) were obtained by passage through activated alumina columns. 1,4-dioxane (dioxane), triethylamine (NEt_3), *N*,*N*'-dimethylethylenediamine (DMEDA),

and methanesulfonyl chloride (MsCl) were distilled over calcium hydride and stored under argon over activated 4Å molecular sieve beads. 4-(dimethylamino)pyridine (DMAP) was recrystallized from toluene and stored under argon.

Optical rotations were measured on a Perkin-Elmer 241 polarimeter at the D line (path length: 1 dm, cell volume: 1 mL, c in g/mL). The instrument was warmed up for 30 minutes before use. Optical rotations were conducted at room temperature, where room temperature is defined between 25 ºC to 30 ºC unless otherwise noted. Proton nuclear magnetic resonance (^{1}H NMR) spectra and carbon nuclear magnetic resonance (^{13}C NMR) spectra were recorded on Bruker AV 400 (400MHz/101MHz) Bruker NEO 500 (500 MHz/126MHz), Bruker AV 500 (500 MHz/126 MHz), Bruker AV 600 (600 MHz/151 MHz), and Bruker AV 700 (700 MHz/176 MHz) NMR spectrometers at 23 °C. Proton chemical shifts are expressed as parts per million (ppm, δ scale) and are referenced to residual solvent ($CHCl_3$: δ 7.26, C_6D_5H: δ 7.16), unless stated otherwise. Carbon chemical shifts are expressed as parts per million (ppm, δ scale) and are referenced to the solvent ($CDCl_3$: δ 77.16, C_6D_6: δ 128.06), unless stated otherwise. Data is represented as follows: chemical shift, multiplicity (s = singlet, d = doublet, dd = doublet of doublets, ddd, doublet of doublet of doublet, dt = doublet of triplets, t = triplet, td = triplet of doublets, tt = triplet of triplets, q = quartet, p = pentet, hept = heptet, m = multiplet, br = broad), coupling constant (*J*) in Hertz (Hz), and integration. Infrared (IR) spectra were recorded on a Bruker Alpha FT-IR spectrometer as thin films and are reported in frequency of absorption (cm^{-1}). Only selected resonances are reported. High-resolution mass spectra were obtained at the Lawrence Berkeley National Laboratory Catalysis Center using a Perkin Elmer AxION 2 TOF mass spectrometer with electrospray ionization (ESI) and by the QB3/chemistry mass spectrometry facility at the University of California, Berkeley using a Finnigan LTQFT mass spectrometer (Thermo Electron Corporation) with electrospray ionization (ESI).

3.6.2 Compound Preparation and Characterization Data

General procedure A: Synthesis of *N*-sulfinyl spiroaziridines (KL2-236, KL2-230, KL4-018, KL4-019, KL3-284, KL3-281, KLE-015, KLE-016, KLE-017, KLE-108, KLE-112A, KLE-112B, KLE-113A, KLE-113B). *i.* To a mixture of substituted isatin (0.250 mmol, 1 equiv.) and (*S*)-*tert*-butanesulfinamide (37.9 mg, 0.313 mmol, 1.25 equiv.) in anhydrous DCM (1 mL) at 20 °C was added $Ti(OR)_4$ (0.500 mmol, 2 equiv., R = Me, Et, or *i*-Pr) upon which the color of the mixture immediately darkened. The reaction vessel was sealed with Teflon tape and the reaction mixture was heated to 50 °C for 4 hours with stirring. The reaction was cooled to room temperature and diluted with EtOAc (3 mL). Excess $Ti(OR)_4$ was quenched by the addition of saturated *aq*. $NaHCO_3$ (2 mL), and the emulsion formed was vigorously stirred for 10 minutes at which point a white *aq*. suspension of TiO_2 separated. The mixture was filtered through a pad of celite and rinsed with EtOAc until colorless. The orange filtrate was washed with brine (10 mL), dried over Na_2SO_4, and concentrated *in vacuo* to yield the crude sulfinimine as a red oil that solidified upon standing. The crude sulfinimine was used immediately without further purification.

ii. A mixture of Me_3SOI (110 mg, 0.500 mmol, 2 equiv.), Cs_2CO_3 (163 mg, 0.500 mmol, 2 equiv.), and powdered, activated 4Å molecular sieves (ca. 75 mg) in anhydrous MeCN (1

mL) was heated to 50 °C and stirred for 0.5 hours. After cooling to 20 °C, a solution of the crude sulfinimine (0.250 mmol, 1 equiv.) in anhydrous MeCN (1 mL) was added, and additional MeCN (2 x 0.5 mL) was used for quantitative transfer. The orange-colored reaction mixture was stirred at 20 °C for 1 hour during which the orange color gradually disappeared. The suspension, which was often beige-colored but sometimes green, blue, or purple, was filtered through a pad of celite, rinsing with EtOAc, to remove the 4Å molecular sieves. The filtrate was then washed with brine (5 mL), dried over Na_2SO_4, and concentrated in vacuo. The crude residue was purified by flash column chromatography on silica gel (20% →33% → 50% EtOAc–hexanes) then preparative TLC (15% EtOAc–toluene or 25% EtOAc–toluene) to yield (*S*,*S*)- and (*S*,*R*)-spiroaziridines respectively as white or yellow solids. The combined yield of the two diastereomers ranged from 40% to 60%, and the *d.r.* ranged from 3:1 to 4:1 (*S*,*S*):(*S*,*R*).

General procedure B: Synthesis of *N*-sulfonyl aziridines (KL2-194 and KL2-168). To a solution of the *N*-sulfinyl aziridine (0.1 mmol, 1 equiv.) in DCM (1 mL) at 20 °C was added *m*-CPBA (77%, 67.2 mg, 0.300 mmol, 3 equiv.). The reaction mixture was stirred at 20 °C for 1 hour, then excess *m*-CPBA was quenched by addition of saturated *aq*. $Na_2S_2O_3$ (1 mL) and saturated *aq*. $NaHCO_3$ (1 mL). The biphasic mixture was vigorously stirred for 10 min., then the aqueous layer was extracted with EtOAc (3 x 2 mL). The combined organic layers were washed with brine (2 mL), dried over Na_2SO_4, then concentrated in vacuo. The crude residue was purified by two rounds of preparative TLC (33% EtOAc–hexanes then 15% EtOAc–toluene) to yield the *N*-sulfonyl aziridine as a white solid in 70% to 90% yield.

General procedure C: Synthesis of morpholine amides (KLE-015, KLE-016, KLE-017, KLE-018). *i.* To a solution of aryl ester (0.100 mmol, 1 equiv.) in a 1:9 mixture of H_2O:dioxane (1 mL) at 20 °C was added LiOH ·H_2O (21.0 mg, 0.500 mmol, 5 equiv.). The reaction mixture was stirred at 60 °C for 1.5 h, allowed to cool to 20 °C, then diluted with EtOAc (2 mL). Excess LiOH was quenched by addition of *aq.* HCl (1.0 M, 1 mL), and the aqueous layer was extracted with EtOAc (5 x 1 mL). The combined organic layers were washed with brine (2 mL), dried over Na_2SO_4, then concentrated in vacuo to yield crude carboxylic acid as a yellow solid. The crude carboxylic acid was used immediately without further purification.

ii. To a mixture of the crude carboxylic acid and HOBt (14.9 mg, 0.110 mmol, 1.1 equiv.) in DCM (1 mL) at 20 °C was added morpholine (34.5 µL, 0.400 mmol, 4 equiv.) then DCC (22.7 mg, 0.110 mmol, 1.1 equiv.). The reaction mixture, which immediately turned cloudy, was stirred at 20 °C for 6 h, then filtered through a pad of celite and concentrated in vacuo. The crude residue was purified by two rounds of preparative TLC (EtOAc then 66% EtOAc–toluene + 5% MEOH) to yield the morpholine amides as colorless or slightly yellow oils or solids.

General Procedure D: Synthesis of *N*-acyl oxindoles (KLE-142 and KLE-144). To a solution of KL6-030 (10.0 mg, 0.0378 mmol, 1 equiv.) in anhydrous DCM (0.150 mL) at 20 °C was added Cs_2CO_3 (24.8 mg, 0.0757 mmol, 2 equiv.), DMAP (0.5 mg, 0.004 mmol, 0.1 equiv.) and acyl chloride (0.06 mmol, 1.5 equiv.). The reaction mixture was stirred at

20 °C for 3 h, then diluted with EtOAc (0.5 mL). The HCl generated was quenched by addition of saturated *aq*. $NaHCO_3$ (1 mL), and the aqueous layer was extracted with EtOAc (3 x 1 mL). The combined organic layers were dried over Na_2SO_4 and concentrated in vacuo. The crude residue was purified by two rounds of preparative TLC (33% EtOAc–hexane then 16% EtOAc–toluene) to yield the *N*-acyl oxindole as a colorless oil or white solid in 85% to quantitative yield.

General Procedure E: Synthesis of spiro-oxazolidinones (**KL2-237** and **KL3-082**). To a solution of *N*-sulfinyl aziridine (0.1 mmol, 1 equiv.) in dioxane (1 mL) at 0 °C was added a solution of HCl in dioxane (4.0 M, 1.00 mL). The reaction mixture was stirred for 10 minutes, then poured into *aq.* $NaHCO_3$ (10 mL) and stirred for a further 10 minutes. The mixture was extracted with EtOAc (3 x 2 mL), dried over Na_2SO_4, and concentrated in vacuo. The crude residue was purified two rounds of preparative TLC (66% EtOAc–hexanes then 30% EtOAc–toluene) to yield the spiro-oxazolidinone as a white solid in 70-75% yield.

General Procedure F: Synthesis of *N*-sulfonyl oxazolidinones (**KL2-243** and **KL3-013**). To a solution of spiro-oxazolidinone (0.05 mmol, 1 equiv.) in anhydrous DCM (0.5 mL) was added TsCl (0.1 mmol, 2 equiv.) then Cs_2CO_3 (0.2 mmol, 4 equiv.). The reaction mixture was stirred at 40 °C for 2 hours, cooled to 20 °C, then diluted with EtOAc (2 mL) and brine (2 mL). The aqueous layer was extracted with EtOAc (3 x 1 mL), then the combined organic layers were washed with brine (2 mL), dried over Na_2SO_4, and concentrated in vacuo. The crude residue was purified by two rounds of preparative TLC (33% EtOAc–hexanes then 15% EtOAc–toluene) to yield the *N*-tosyl oxazolidinone as a white solid in 60-75% yield.

General Procedure G: Synthesis of α-methyl sulfinamides (**KL6-274A**, **KL6-274B**, **KL6-275A**, **KL6-275B**, **KL6-278A**, and **KL6-278B**). Crude sulfinimine (General Procedure A i.) was quickly passed through a short silica plug (50% EtOAc–hexanes) to remove excess *tert*-butanesulfinamide. N.B., sulfinimine hydrolysis occurs upon prolonged exposure to silica gel. To a solution of partially purified sulfinimine (0.1 mmol, 1 equiv.) in THF (0.4 mL) at –78 °C was added a suspension of $MeCeCl_2$ in THF (0.1 M, 0.1 mmol, 1.2 equiv.) dropwise. The reaction mixture was allowed to warm slowly to 20 °C, remaining in the cooling bath, while stirring for 16 hours, over which the color turned brown. The reaction mixture was diluted with EtOAc (1 mL), and excess $MeCeCl_2$ was quenched by addition of brine (1 mL). The aqueous layer was extracted with EtOAc (3 x 1 mL), then the combined organic layers were washed with brine (2 mL), dried over Na_2SO_4, and concentrated in vacuo. The crude residue was purified by two rounds of preparative TLC (75% EtOAc–hexanes then 60% EtOAc–toluene) to yield (*S*,*S*)- and (*S*,*R*)-sulfinamides respectively as white solids. The combined yield of the two diastereomers ranged from 30% to 60%, and the d.r. ranged from 1:1 to 1:1.6 (*S*,*S*):(*S*,*R*).

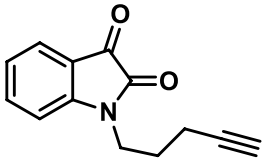

SI-1. Requisite Isatin used for the preparation of KL2-236, KL2-230, KL4-018, KL4-019, KL2-194, and KL2-168 : Cs_2CO_3 (652 mg, 2.00 mmol, 2 equiv.) was added to a solution of 1*H*-indole-2,3-dione (147 mg, 1.00 mmol, 1 equiv.) in anhydrous DMF (4 mL) at 20 °C. The deep purple-colored reaction mixture was stirred for five minutes, then pent-4-yn-1-yl methanesulfonate[93] (1.50 mmol, 1.5 equiv.) was added dropwise. The reaction mixture was stirred at 20 °C for 16 h, then diluted with EtOAc (10 mL). Excess Cs_2CO_3 was quenched with *aq.* HCl (1.0 M, 5 mL), and the aqueous layer was extracted with EtOAc (3 x 5 mL). The combined organic layers were washed with washed with 5% *aq*. LiCl (2 x 10 mL) and brine (10 mL) then dried over Na_2SO_4 and concentrated in vacuo. The crude residue was purified by flash column chromatography on silica gel (20%→33% EtOAc–hexanes) to yield the *N*-alkylated isatin **SI-1** (171.0 mg, 80.2%) as an orange solid. **^{1}H NMR** (700 MHz, $CDCl_3$) δ 7.63 – 7.57 (m, 2H), 7.12 (t, *J* = 7.5 Hz, 1H), 7.00 (d, *J* = 7.9 Hz, 1H), 3.86 (t, *J* = 7.3 Hz, 2H), 2.32 (td, *J* = 6.8, 2.6 Hz, 2H), 2.04 (t, *J* = 2.6 Hz, 1H), 1.94 (p, *J* = 6.9 Hz, 2H); **^{13}C NMR** (151 MHz, $CDCl_3$) δ 183.48, 158.44, 151.08, 138.53, 125.65, 123.88, 117.76, 110.23, 82.88, 69.86, 39.30, 26.12, 16.30; **IR** (thin film) ν_{max}: 1736, 1610, 1469, 1353, 1170 cm^{-1}; **HRMS** (ESI-TOF) *m/z*: $[M+H]^+$ calcd for $C_{13}H_{11}NO_2$: 214.0863, found 214.0863.

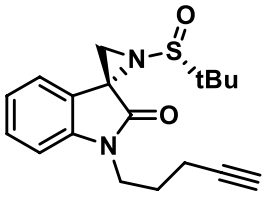

KL2-230: Prepared by general procedure A with **SI-1** (47.1 mg, 0.221 mmol), (*R*)-*tert*-butanesulfinamide, and Ti(O*i*-Pr)$_4$. **Yield**: 24.0 mg, 33%. **^{1}H NMR** (600 MHz, $CDCl_3$) δ 7.67 – 7.61 (m, 1H), 7.34 (td, *J* = 7.8, 1.2 Hz, 1H), 7.07 (td, *J* = 7.6, 1.0 Hz, 1H), 7.01 (dt, *J* = 7.9, 0.8 Hz, 1H), 3.93 – 3.84 (m, 2H), 3.37 (s, 1H), 2.78 (s, 1H), 2.30 (td, *J* = 6.9, 2.7 Hz, 2H), 2.02 (t, *J* = 2.7 Hz, 1H), 1.94 (p, *J* = 7.1 Hz, 2H), 1.31 (s, 9H); **^{13}C NMR** (126 MHz, $CDCl_3$) δ 171.90, 144.71, 129.64, 125.44, 122.81, 121.70, 108.99, 83.15, 69.53, 58.63, 44.30, 39.60, 31.33, 26.38, 22.59, 16.36; **IR** (thin film) ν_{max} 3249, 2953, 1727, 1611, 1468, 1372, 1173, 1078, 941, 765 cm^{-1}; $[\alpha]_D^{25}$ = –217.6° (c 0.0013 g/ml, $CHCl_3$); **HRMS** (ESI-TOF) *m/z*: $[M+H]^+$ calcd for $C_{18}H_{23}N_2O_2S$: 331.1475, found 331.1475.

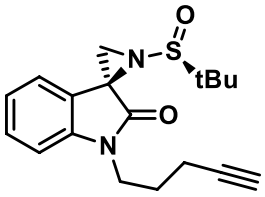

KL2-236: Prepared by general procedure A with **SI-1** (47.1 mg, 0.221 mmol), (*R*)-*tert*-butanesulfinamide, and Ti(O*i*-Pr)$_4$. **Yield**: 27.2 mg, 37%. **^{1}H NMR**, **^{13}C NMR**, and **IR** data matched that of **KL2-230**; $[\alpha]_D^{25}$ = +240.5° (c 0.0037 g/ml, $CHCl_3$); **HRMS** (ESI-TOF) *m/z*: $[M+H]^+$ calcd for $C_{18}H_{23}N_2O_2S$: 331.1475, found 331.1475.

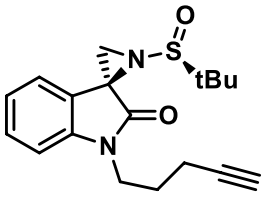

KL4-018: Prepared by general procedure A with **SI-1** (47.1 mg, 0.221 mmol), (*S*)-*tert*-butanesulfinamide, and Ti(O*i*-Pr)$_4$. **Yield**: 6.5 mg, 8.9%. **^{1}H NMR** (700 MHz, $CDCl_3$) δ 7.35 (ddd, *J* = 8.7, 6.0, 2.1 Hz, 1H), 7.12 – 7.05 (m, 2H), 6.99 (d, *J* = 7.9 Hz, 1H), 3.93 (dt, *J* = 14.4, 7.3 Hz, 1H), 3.86 (dt, *J* = 14.3, 7.2 Hz, 1H), 3.35 (s, 1H), 2.69 (s, 1H), 2.29 (td, *J* = 7.0, 2.7 Hz, 2H), 2.02 (t, *J* = 2.6 Hz, 1H), 1.94 (p, *J* = 7.1 Hz, 2H), 1.24 (s, 9H); **^{13}C NMR** (151 MHz, $CDCl_3$) δ 171.05, 143.60, 129.59, 125.31, 122.87, 121.98, 108.80, 83.18, 69.54, 57.89, 45.96, 39.75, 36.04, 26.57, 22.21,

16.37; **IR** (thin film) ν_{max}: 3251, 2926, 1719, 1617, 1468, 1366, 1173, 938, 758 cm^{-1}; $[\alpha]_D^{25}$ = –126.0° (c 0.001 g/ml, $CHCl_3$); **HRMS** (ESI-TOF) *m/z*: $[M+H]^+$ calcd for $C_{18}H_{23}N_2O_2S$: 331.1475, found 331.1476.

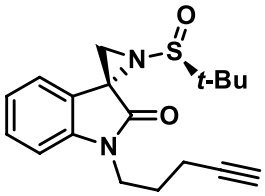

KL4-019: Prepared by general procedure A with **SI-1** (47.1 mg, 0.221 mmol), (*S*)-*tert*-butanesulfinamide, and Ti(O*i*-Pr)$_4$. **Yield**: 6.8 mg, 9.3%. **^{1}H NMR**, **^{13}C NMR**, and **IR** data matched that of **KL4-018**; $[\alpha]_D^{25}$ = +117.0° (c 0.001 g/ml, $CHCl_3$); **HRMS** (ESI-TOF) *m/z*: $[M+H]^+$ calcd for $C_{18}H_{23}N_2O_2S$: 331.1475, found 331.1476.

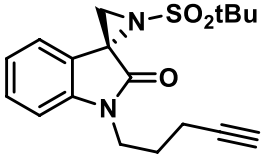

KL2-168: Prepared by general procedure B with **KL2-230** (38.2 mg, 0.116 mmol). **Yield**: 28.5 mg, 70.9%. **^{1}H NMR** (700 MHz, $CDCl_3$) δ 7.57 (br, 1H), 7.35 (td, *J* = 7.8, 1.2 Hz, 1H), 7.08 (td, *J* = 7.6, 1.0 Hz, 1H), 6.99 (d, *J* = 7.9 Hz, 1H), 3.89 (hept, *J* = 7.2 Hz, 2H), 3.31 (s, 1H), 3.16 (s, 1H), 2.30 (tt, *J* = 6.7, 2.6 Hz, 2H), 2.04 (t, *J* = 2.7 Hz, 1H), 1.94 (p, *J* = 7.1 Hz, 2H), 1.52 (s, 9H). **^{13}C NMR** (151 MHz, C_6D_6) δ 169.87, 144.91, 129.87, 125.82, 122.50, 121.52, 108.85, 83.17, 69.71, 61.17, 46.27, 41.24, 39.45, 26.32, 23.88, 16.20; **IR** (thin film) ν_{max}: 3358, 2923, 2853, 1728, 1613, 1469, 1313, 1122, 958, 788 cm^{-1}; $[\alpha]_D^{25}$ = –17.1° (c 0.00082 g/ml, $CHCl_3$); **HRMS** (ESI-TOF) *m/z*: $[M+H]^+$ calcd for $C_{18}H_{23}N_2O_3S$: 347.1424, found 347.1426.

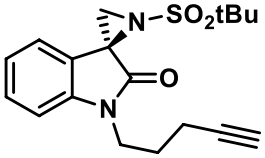

KL2-194: Prepared by general procedure B with **KL2-236** (31.2 mg, 0.0944 mmol). **Yield**: 28.1mg, 85.9%. **^{1}H NMR**, **^{13}C NMR**, and **IR** data matched that of **KL2-168**; $[\alpha]_D^{25}$ = +21.0° (c 0.001 g/ml, $CHCl_3$); **HRMS** (ESI-TOF) *m/z*: $[M+H]^+$ calcd for $C_{18}H_{23}N_2O_3S$: 347.1424, found 347.1426.

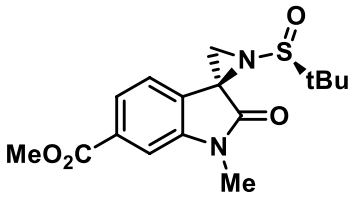

SI-2: Prepared by general procedure A with methyl 1-methyl-2,3-dioxoindoline-6-carboxylate[94] (50 mg, 0.228 mmol), (*S*)-*tert*-butanesulfinamide, and Ti(OMe)$_4$. **Yield**: 18.7 mg, 24%. **^{1}H NMR** (700 MHz, $CDCl_3$) δ 7.78 (dd, *J* = 8.0, 1.5 Hz, 1H), 7.73 (d, *J* = 7.9 Hz, 1H), 7.56 (d, *J* = 1.5 Hz, 1H), 3.95 (s, 3H), 3.44 (s, 1H), 3.33 (s, 3H), 2.84 (s, 1H), 1.31 (s, 9H); **^{13}C NMR** (151 MHz, $CDCl_3$) δ 171.58, 166.63, 145.65, 131.51, 126.94, 125.21, 124.54, 109.28, 58.88, 52.57, 44.27, 31.75, 27.07, 22.58; **IR** (thin film) ν_{max}: 2954, 2360, 1721, 1620, 1454, 1247, 1099, 938, 766 cm^{-1}; $[\alpha]_D^{25}$ = +308.0° (c 0.001 g/ml, $CHCl_3$); **HRMS** (ESI-TOF) *m/z*: $[M+H]^+$ calcd for $C_{16}H_{21}N_2O_4S$: 337.1217, found 337.1217.

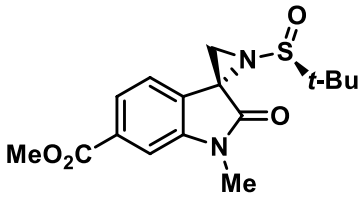

SI-3: Prepared by general procedure A with methyl 1-methyl-2,3-dioxoindoline-6-carboxylate (50 mg, 0.228 mmol), (*S*)-*tert*-butanesulfinamide, and Ti(OMe)$_4$. **Yield**: 4.4 mg, 5.7%. **^{1}H NMR** (700 MHz, $CDCl_3$) δ 7.81 (dd, *J* = 7.7, 1.4 Hz, 1H), 7.55 (d, *J* = 1.5 Hz, 1H), 7.15 (d, *J* = 7.6 Hz, 1H), 3.95 (s, 3H), 3.40 (s, 1H), 3.34 (s, 3H), 2.75 (s, 1H), 1.24 (s, 9H); **^{13}C NMR** (151 MHz, $CDCl_3$) δ 170.71, 166.60, 144.44, 131.61, 130.27, 124.77, 121.66, 109.25, 58.08, 52.59, 45.86, 36.30, 27.09, 22.18; **IR** (thin film) ν_{max}: 2954, 2360, 1718, 1624,

1453, 1246, 1084, 767 cm^{-1}; $[\alpha]_D^{25}$ = +78.7° (c 0.0015 g/ml, $CHCl_3$); **HRMS** (ESI-TOF) *m/z*: $[M+H]^+$ calcd for $C_{16}H_{21}N_2O_4S$: 337.1217, found 337.1219.

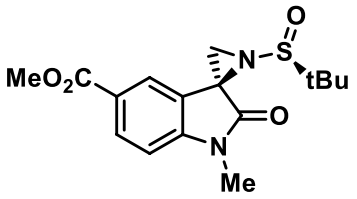

SI-4: Prepared by general procedure A with methyl 1-methyl-2,3-dioxoindoline-5-carboxylate[95] (94.0 mg, 0.429 mmol), (*S*)-*tert*-butanesulfinamide, and $Ti(OMe)_4$. **Yield**: 50.0 mg, 35%. **^{1}H NMR** (700 MHz, $CDCl_3$) δ 8.30 (s, 1H), 8.12 (dd, *J* = 8.2, 1.7 Hz, 1H), 6.97 (d, *J* = 8.2 Hz, 1H), 3.90 (s, 3H), 3.46 (s, 1H), 3.32 (s, 3H), 2.83 (s, 1H), 1.32 (s, 9H); **^{13}C NMR** (151 MHz, $CDCl_3$) δ 172.28, 166.80, 149.24, 132.36, 126.57, 125.08, 121.74, 108.48, 58.86, 52.40, 44.02, 31.52, 27.08, 22.65; **IR** (thin film) ν_{max}: 2922, 2360, 1716, 1617, 1365, 1266, 1106, 934, 768 cm^{-1}; $[\alpha]_D^{25}$ = +42.0° (c 0.001 g/ml, $CHCl_3$); **HRMS** (ESI-TOF) *m/z*: $[M+H]^+$ calcd for $C_{16}H_{21}N_2O_4S$: 337.1217, found 337.1218.

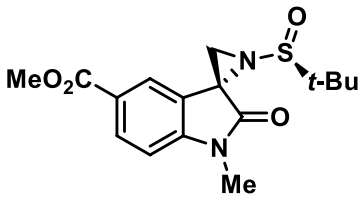

SI-5: Prepared by general procedure A with methyl 1-methyl-2,3-dioxoindoline-5-carboxylate[95] (94.0 mg, 0.429 mmol), (*S*)-*tert*-butanesulfinamide, and $Ti(OMe)_4$. **Yield**: 15.5 mg, 10.7%. **^{1}H NMR** (700 MHz, $CDCl_3$) δ 8.10 (dd, J = 8.2, 1.7 Hz, 1H), 7.73 (s, 1H), 6.94 (d, J = 8.2 Hz, 1H), 3.92 (s, 3H), 3.40 (s, 1H), 3.32 (s, 3H), 2.74 (s, 1H), 1.26 (s, 9H); **^{13}C NMR** (151 MHz, $CDCl_3$) δ 171.31, 166.69, 148.11, 132.11, 125.39, 125.08, 122.99, 108.20, 58.14, 52.33, 45.50, 35.79, 27.09, 22.19; **IR** (thin film) ν_{max}: 2953, 2360, 1715, 1623, 1367, 1265, 1099, 767 cm^{-1}; $[\alpha]_D^{25}$ = +190.6° (c 0.0027 g/ml, $CHCl_3$); **HRMS** (ESI-TOF) *m/z*: $[M+H]^+$ calcd for $C_{16}H_{21}N_2O_4S$: 337.1217, found 337.1219.

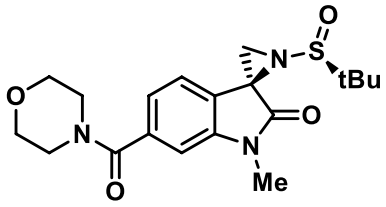

KLE-015: Prepared by general procedure C with **SI-2** (6.1 mg, 0.019 mmol). **Yield**: 2.8 mg, 38%. **^{1}H NMR** (500 MHz, $CDCl_3$) δ 7.68 (d, *J* = 7.7 Hz, 1H), 7.05 (dd, *J* = 7.7, 1.4 Hz, 1H), 7.02 (d, *J* = 1.4 Hz, 1H), 3.91 – 3.44 (br, 8H), 3.42 (s, 1H), 3.29 (s, 3H), 2.83 (s, 1H), 1.31 (s, 9H); **^{13}C NMR** (151 MHz, $CDCl_3$) δ 171.71, 169.75, 146.05, 136.80, 125.21, 123.53, 121.22, 107.97, 67.02, 58.83, 48.46, 44.13, 42.82, 31.40, 27.00, 22.59; **IR** (thin film) ν_{max}: 2922, 2361, 1732, 1622, 1463, 1249, 1113, 765 cm^{-1}; $[\alpha]_D^{25}$ = +226.0° (c 0.001 g/ml, $CHCl_3$); **HRMS** (ESI-TOF) *m/z*: $[M+H]^+$ calcd for $C_{19}H_{26}N_3O_4S$: 392.1639, found 392.1641.

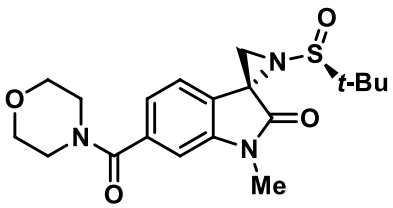

KLE-016: Prepared by general procedure C with **SI-3** (7.7 mg, 0.024 mmol). **Yield**: 6.7 mg, 71%. **^{1}H NMR** (500 MHz, $CDCl_3$) δ 7.12 (d, *J* = 7.9 Hz, 1H), 7.07 (dd, *J* = 7.5, 1.3 Hz, 1H), 7.00 – 6.96 (m, 1H), 3.91 – 3.42 (br, 8H), 3.37 (s, 1H), 3.30 (s, 3H), 2.73 (s, 1H), 1.24 (s, 9H); **^{13}C NMR** (151 MHz, $CDCl_3$) δ 170.83, 169.77, 144.80, 136.93, 126.91, 121.80, 121.37, 107.68, 67.02, 58.02, 45.79, 36.22, 27.03, 22.18; **IR** (thin film) ν_{max}: 2923, 1724, 1624, 1463, 1247, 1113 cm^{-1}; $[\alpha]_D^{25}$ = +120.0° (c 0.001 g/ml, $CHCl_3$); **HRMS** (ESI-TOF) *m/z*: $[M+H]^+$ calcd for $C_{19}H_{26}N_3O_4S$: 392.1639, found 392.1641.

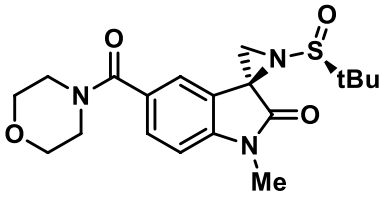

KLE-017: Prepared by general procedure C with **SI-4** (7.4 mg, 0.023 mmol). **Yield**, 3.1 mg, 34%. **^{1}H NMR** (500 MHz, $CDCl_3$) δ 7.72 (d, J = 1.6 Hz, 1H), 7.57 (dd, J = 8.1, 1.7 Hz, 1H), 6.98 (d, J = 8.1 Hz, 1H), 3.68 (br, 8H), 3.41 (s, 1H), 3.30 (s, 3H), 2.82 (s, 1H), 1.30 (s, 9H); **^{13}C NMR** (151 MHz, $CDCl_3$) δ 171.94, 169.91, 146.90, 130.35, 129.70, 124.51, 121.29, 109.04, 66.99, 58.79, 44.16, 31.23, 27.03, 22.59; **IR** (thin film) ν_{max}: 2920, 1731, 1616, 1422, 1250, 1112, 923, 764 cm^{-1}; **$[\alpha]_D^{25}$** = +486.7° (c 0.00015 g/ml, $CHCl_3$); **HRMS** (ESI-TOF) *m/z*: $[M+H]^+$ calcd for $C_{19}H_{26}N_3O_4S$: 392.1639, found 392.1641.

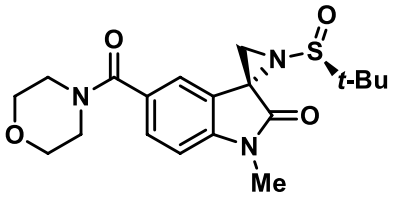

KLE-018: Prepared by general procedure C with **SI-5** (8.6 mg, 0.027 mmol). **Yield**: 2.8 mg, 26%. **^{1}H NMR** (700 MHz, $CDCl_3$) δ 7.44 (dd, *J* = 8.0, 1.7 Hz, 1H), 7.21 (br, 1H), 6.92 (d, *J* = 8.0 Hz, 1H), 3.70 (br, 8H), 3.36 (d, *J* = 11.9 Hz, 1H), 3.31 (s, 3H), 2.74 (s, 1H), 1.25 (s, 9H); **^{13}C NMR** (151 MHz, $CDCl_3$) δ 171.04, 170.02, 145.73, 129.76, 129.23, 125.48, 121.63, 108.27, 67.00, 58.14, 45.66, 36.06, 27.06, 22.23; **$[\alpha]_D^{25}$** = +54.0° (c 0.0005 g/ml, $CHCl_3$); **HRMS** (ESI-TOF) *m/z*: $[M+H]^+$ calcd for $C_{19}H_{26}N_3O_4S$: 392.1639, found 392.1639.

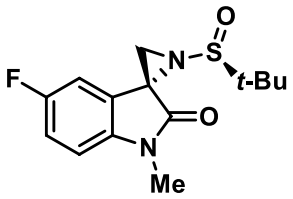

KLE-112B: Prepared by general procedure A with 5-fluoro-1-methyl-1*H*-indoline-2,3-dione[96] (30 mg, 0.167 mmol), (*S*)-*tert*-butanesulfinamide, and Ti(O*i*-Pr)$_4$. **Yield**: 4.7 mg, 9.5%. **^{1}H NMR** (700 MHz, $CDCl_3$) δ 7.09 – 7.02 (m, 1H), 6.82 (m, 2H), 3.36 (s, 1H), 3.28 (s, 3H), 2.68 (s, 1H), 1.24 (s, 9H); **^{13}C NMR** (151 MHz, $CDCl_3$) δ 170.73, 159.51 (d, J = 241.5 Hz), 140.09 (d, J = 2.1 Hz), 126.89 (d, J = 8.2 Hz), 115.81 (d, J = 23.8 Hz), 109.97 (d, J = 25.7 Hz), 109.21 (d, J = 8.0 Hz), 57.97, 46.03 (d, *J* = 2.2 Hz), 35.97, 26.99, 22.14; **IR** (thin film) ν_{max}: 2925, 1719, 1493, 1367, 1277, 1089, 945 cm^{-1}; **$[\alpha]_D^{25}$** = +231.8° (c 0.00073 g/ml, $CHCl_3$); **HRMS** (ESI-TOF) *m/z*: $[M+H]^+$ calcd for $C_{14}H_{18}FN_2O_2S$: 297.1068, found 297.1069.

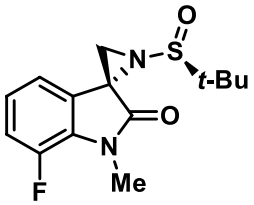

KLE-113B: Prepared by general procedure A with 7-fluoro-1-methyl-1*H*-indoline-2,3-dione[97] (89.6 mg, 0.500 mmol), (*S*)-*tert*-butanesulfinamide, and Ti(O*i*-Pr)$_4$. **Yield**: 21.0 mg, 14.2%. **^{1}H NMR** (700 MHz, $CDCl_3$) δ 7.07 (ddd, *J* = 11.4, 8.4, 1.0 Hz, 1H), 7.00 (td, *J* = 7.9, 4.3 Hz, 1H), 6.85 (d, *J* = 7.4 Hz, 1H), 3.49 (d, *J* = 2.6 Hz, 3H), 3.36 (s, 1H), 2.67 (s, 1H), 1.24 (s, 9H); **^{13}C NMR** (151 MHz, $CDCl_3$) δ 170.70, 147.89 (d, J = 244.4 Hz), 130.73 (d, J = 9.1 Hz), 128.15, 123.54 (d, J = 6.5 Hz), 122.39 (d, J = 6.7 Hz), 117.56 (d, J = 19.3 Hz), 57.96, 45.92 (d, J = 3.3 Hz), 36.34, 29.43 (d, J = 5.5 Hz), 22.14; **IR** (thin film) ν_{max}: 2925, 2361, 1728, 1479, 1371, 1238, 1098, 972, 731 cm^{-1}; **$[\alpha]_D^{25}$** = +142.5° (c 0.00027 g/ml, $CHCl_3$); **HRMS** (ESI-TOF) *m/z*: $[M+H]^+$ calcd for $C_{14}H_{18}FN_2O_2S$: 297.1068, found 297.1069.

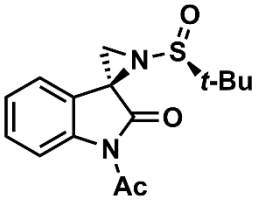

KLE-142: Prepared by general procedure D with **KL6-030** (10.0 mg, 0.0378 mmol) and acetyl chloride. **Yield**: 9.4 mg, 85%. **^{1}H NMR** (500 MHz, $CDCl_3$) δ 8.36 (dt, *J* = 8.3, 0.8 Hz, 1H), 7.66 (dd, *J* = 7.8, 1.4 Hz, 1H), 7.42 – 7.38 (m, 1H), 7.23 (td, *J* = 7.6, 1.1 Hz, 1H), 3.42 (s, 1H), 2.86 (s, 1H), 2.71 (s, 3H), 1.31 (s, 9H); **^{13}C NMR** (126 MHz, $CDCl_3$) δ 172.74, 170.64, 141.92, 130.10, 125.59, 124.73, 120.87, 117.13, 58.87, 44.76, 32.70, 26.91, 22.55; **IR** (thin film) ν_{max}: 2927, 1768, 1607, 1465, 1275, 1183, 1085, 954, 766 cm^{-1}; $[\alpha]_D^{25}$ = +268.5° (c 0.003 g/ml, $CHCl_3$); **HRMS** (ESI-TOF) *m/z*: $[2M+NH_4]^+$ calcd for $C_{30}H_{40}N_5O_6S_2$: 630.2415, found 630.2422.

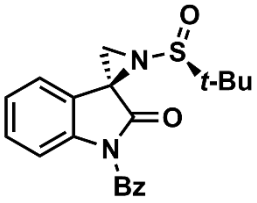

KLE-144: Prepared by general procedure D with **KL6-030** (10.0 mg, 0.0378 mmol) and benzoyl chloride. **Yield**: 13.5 mg, 96%. **^{1}H NMR** (500 MHz, $CDCl_3$) δ 7.94 (dt, *J* = 8.2, 0.8 Hz, 1H), 7.77 – 7.73 (m, 2H), 7.69 (dd, *J* = 7.8, 1.3 Hz, 1H), 7.63 – 7.57 (m, 1H), 7.50 – 7.46 (m, 2H), 7.44 (td, *J* = 8.0, 1.4 Hz, 1H), 7.25 (td, *J* = 7.7, 1.1 Hz, 1H), 3.43 (s, 1H), 2.83 (s, 1H), 1.29 (s, 9H); **^{13}C NMR** (126 MHz, $CDCl_3$) δ 171.51, 169.02, 141.98, 133.97, 133.23, 130.04, 129.65, 128.38, 125.39, 125.04, 121.35, 115.72, 58.85, 44.81, 32.69, 22.49; **IR** (thin film) ν_{max}: 3056, 2927, 1769, 1467, 1265, 1173, 1077, 731 cm^{-1}; $[\alpha]_D^{25}$ = +213.5° (c 0.002 g/ml, $CHCl_3$); **HRMS** (ESI-TOF) *m/z*: $[2M+NH_4]^+$ calcd for $C_{40}H_{44}N_5O_6S_2$: 754.2728, found 754.2707.

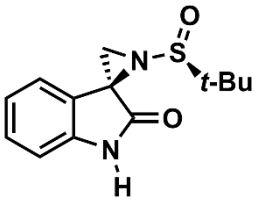

KL6-030: Prepared by general procedure A with 1*H*-indole-2,3-dione (23.0 mg, 0.156 mmol), (*S*)-*tert*-butanesulfinamide, and $Ti(OEt)_4$. **Yield**: 20.0 mg, 48%. ^{1}H NMR (500 MHz, $CDCl_3$) δ 7.98 – 7.67 (m, 1H), 7.63 (d, *J* = 7.7 Hz, 1H), 7.29 (td, *J* = 7.8, 1.2 Hz, 1H), 7.07 (td, *J* = 7.8, 1.1 Hz, 1H), 6.95 (d, *J* = 7.9 Hz, 0H), 3.39 (s, 1H), 2.80 (s, 1H), 1.31 (s, 8H); **^{13}C NMR** (126 MHz, $CDCl_3$) δ 173.99, 142.46, 129.66, 125.64, 122.99, 121.93, 110.79, 58.61, 44.73, 31.36, 22.56; **IR** (thin film) ν_{max}: 3209, 2962, 1725, 1620, 1470, 1217, 1057, 933, 732 cm^{-1}; $[\alpha]_D^{25}$ = +256.5° (c 0.002 g/ml, $CHCl_3$); **HRMS** (ESI-TOF) *m/z*: $[2M+NH_4]^+$ calcd for $C_{26}H_{36}N_5O_4S_2$: 546.2203, found 546.2228.

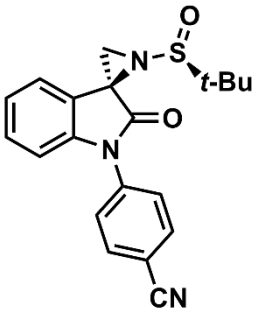

KLE-138: To a suspension of **KL6-030** (9.8 mg, 0.038 mmol), CuI (0.8 mg, 0.004 mmol, 0.1 equiv.), K_2CO_3 (10.5 mg, 0.076 mmol, 2 equiv.).), 4-bromobenzonitrile (10.3 mg, 0.057 mmol, 1.5 equiv.), and activated 4Å molecular sieves (ca. 10 mg) in anhydrous toluene (0.38 mL) at 20 °C was added DMEDA (1 µL, 0.009, 0.24 mmol) upon which the mixture darkened in color. The reaction mixture was heated to 80 °C, stirred for 16 h, then cooled to room temperature and diluted with EtOAc (1 mL). The reaction mixture was filtered through a pad of silica and rinsed with EtOAc (3 x 1 mL), then the brown filtrate was concentrated in vacuo. The crude residue was purified by two rounds of preparative TLC (33% EtOAc–hexane then 16% EtOAc–toluene) to yield **KLE-138** (1.9 mg, 14%) as a white solid. **^{1}H NMR** (500 MHz, $CDCl_3$) δ 7.88 – 7.80 (m, 2H), 7.75 (dd, *J* = 7.7, 1.3 Hz, 1H), 7.69 – 7.62 (m, 2H), 7.32 (td, *J* = 7.8, 1.3 Hz, 1H), 7.17 (td, *J* = 7.7, 1.0 Hz, 1H), 7.00

(d, *J* = 8.0 Hz, 1H), 3.48 (s, 1H), 2.89 (s, 1H), 1.33 (s, 9H); **^{13}C NMR** (151 MHz, $CDCl_3$) δ 171.03, 143.84, 138.43, 133.68, 129.69, 126.85, 125.99, 124.22, 121.55, 118.25, 111.78, 110.07, 58.93, 44.49, 29.85, 22.62; **IR** (thin film) ν_{max}: 2923, 2230, 1742, 1605, 1510, 1465, 1373, 1200, 1080, 937, 843, 764 cm^{-1}; **$[\alpha]_D^{25}$** = +127.5° (c 0.008 g/ml, $CHCl_3$); **HRMS** (ESI-TOF) *m/z*: $[2M+NH_4]^+$ calcd for $C_{40}H_{42}N_7O_4S_2$: 748.2734, found 748.2743.

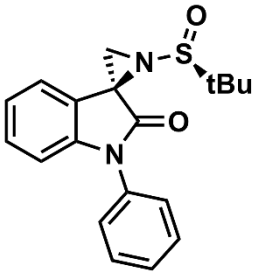

KL4-212A: Prepared by general procedure A with 1-phenyl-1*H*-indoline-2,3-dione[98] (40.0 mg, 0.179 mmol), (*S*)-*tert*-butanesulfinamide, and Ti(O*i*-Pr)$_4$. **Yield**: 17.2 mg, 28%. **^{1}H NMR** (500 MHz, $CDCl_3$) δ 7.72 (dd, *J* = 7.6, 1.3 Hz, 1H), 7.57 – 7.50 (m, 2H), 7.48 – 7.39 (m, 3H), 7.27 (td, *J* = 7.8, 1.3 Hz, 1H), 7.11 (td, *J* = 7.7, 1.1 Hz, 1H), 6.91 (dt, *J* = 8.0, 0.8 Hz, 1H), 3.46 (s, 1H), 2.88 (s, 1H), 1.34 (s, 9H); **^{13}C NMR** (151 MHz, $CDCl_3$) δ 171.18, 145.40, 134.27, 129.78, 129.52, 128.40, 126.69, 125.52, 123.36, 121.43, 110.15, 58.76, 44.53, 31.75, 22.61. **IR** (thin film) ν_{max}: 2923, 1736, 1612, 1466, 1373, 1080, 936, 761 cm^{-1}; **$[\alpha]_D^{25}$** = +237.8° (c 0.0009 g/ml, $CHCl_3$); **HRMS** (ESI-TOF) *m/z*: $[2M+NH_4]^+$ calcd for $C_{38}H_{44}N_5O_4S_2$: 698.2829, found 698.2834.

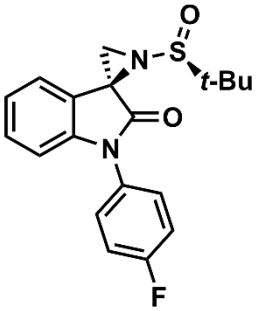

KL4-217A: Prepared by general procedure A with 1-(4-fluorophenyl)-1*H*-indoline-2,3-dione[98] (21.3 mg, 0.0884 mmol), (*S*)-*tert*-butanesulfinamide, and Ti(O*i*-Pr)$_4$. **Yield**: 12.2 mg, 40%. **^{1}H NMR** (500 MHz, $CDCl_3$) δ 7.73 (dd, *J* = 7.7, 1.3 Hz, 1H), 7.46 – 7.39 (m, 2H), 7.29 (td, *J* = 7.8, 1.3 Hz, 1H), 7.25 – 7.19 (m, 2H), 7.12 (td, *J* = 7.6, 1.0 Hz, 1H), 6.86 (dt, *J* = 8.0, 0.8 Hz, 1H), 3.46 (s, 1H), 2.87 (s, 1H), 1.34 (s, 9H). **^{13}C NMR** (151 MHz, $CDCl_3$) δ 171.32, 162.14 (d, *J* = 248.4 Hz), 145.27, 130.17 (d, *J* = 3.2 Hz), 129.59, 128.65 (d, *J* = 8.8 Hz), 125.62, 123.52, 121.39, 116.83 (d, *J* = 23.1 Hz), 109.94, 58.80, 44.46, 31.80, 22.61; **IR** (thin film) ν_{max}: 2926, 2360, 1736, 1611, 1513, 1466, 1381, 1244, 1157, 1080, 937, 831, 762 cm^{-1}; **$[\alpha]_D^{25}$** = +40.0° (c 0.007 g/ml, $CHCl_3$); **HRMS** (ESI-TOF) *m/z*: $[2M+NH_4]^+$ calcd for $C_{38}H_{42}F_2N_5O_4S_2$: 734.2641, found 734.2668.

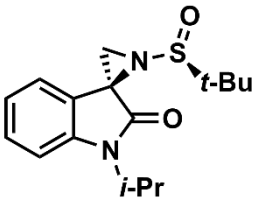

KL3-286: Prepared by general procedure A with 1-(propan-2-yl)-1*H*-indole-2,3-dione[99] (18.2 mg, 0.0962 mmol), (*S*)-*tert*-butanesulfinamide, and Ti(OEt)$_4$. **Yield**: 14.3 mg, 49%. **^{1}H NMR** (400 MHz, $CDCl_3$) δ 7.65 (dd, *J* = 7.7, 1.3 Hz, 1H), 7.31 (td, *J* = 7.8, 1.3 Hz, 1H), 7.08 (dt, *J* = 8.1, 0.8 Hz, 1H), 7.04 (td, *J* = 7.6, 1.0 Hz, 1H), 4.67 (hept, *J* = 7.0 Hz, 1H), 3.35 (s, 1H), 2.76 (s, 1H), 1.51 (t, *J* = 6.9 Hz, 6H), 1.30 (s, 9H); **^{13}C NMR** (126 MHz, $CDCl_3$) δ 171.40, 144.13, 129.33, 125.45, 122.30, 122.12, 110.49, 58.63, 44.57, 44.31, 31.53, 22.61, 19.60, 19.56; **IR** (thin film) ν_{max}: 2975, 1720, 1609, 1467, 1360, 1224, 1076, 942, 762 cm^{-1}; **$[\alpha]_D^{25}$** = +57.0° (c 0.003 g/ml, $CHCl_3$); **HRMS** (ESI-TOF) *m/z*: $[2M+NH_4]^+$ calcd for $C_{32}H_{48}N_5O_4S_2$: 630.3142, found 630.3120.

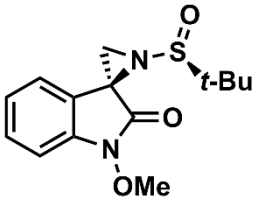

KL5-289A: Prepared by general procedure A with 1-methoxy-1*H*-indole-2,3-dione[100] (7.8 mg, 0.044 mmol), (*S*)-*tert*-butanesulfinamide, and Ti(O*i*-Pr)$_4$. **Yield**: 2.7 mg, 21%. **^{1}H NMR** (700 MHz, $CDCl_3$) δ 7.64 (d, *J* = 7.6 Hz, 1H), 7.37 (t, *J* = 7.7 Hz, 1H), 7.11 (t, *J* = 7.7 Hz, 1H), 7.08 (d, *J* = 8.0 Hz, 1H), 4.07 (s, 3H), 3.39 (s, 1H), 2.82 (s, 1H), 1.31 (s, 9H); **^{13}C NMR** (151 MHz, $CDCl_3$) δ 166.54, 141.95, 129.80, 125.70, 123.51, 118.74, 107.96, 64.02, 58.79, 43.11, 30.92, 22.58; **IR** (thin film) ν_{max}: 2923, 2843, 2359, 1744, 1616, 1465, 1321, 1226, 1084, 1045, 963, 947, 914, 759 cm^{-1}; $[\alpha]_D^{25}$ = +88.0° (c 0.001 g/ml, $CHCl_3$); **HRMS** (ESI-TOF) *m/z*: $[2M+NH_4]^+$ calcd for $C_{28}H_{40}N_5O_6S_2$: 606.2415, found 606.2415.

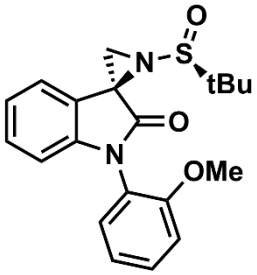

KL6-019A: Prepared by general procedure A with 1-(2-methoxyphenyl)-1*H*-indoline-2,3-dione[101] (25 mg, 0.0987 mmol), (*S*)-*tert*-butanesulfinamide, and Ti(O*i*-Pr)$_4$. **Yield**: 11.7 mg, 32%, 5:4 a.r. **^{1}H NMR** (400 MHz, $CDCl_3$) δ 7.74 – 7.64 (m, 1H), 7.43 (tt, *J* = 8.4, 2.2 Hz, 1H), 7.36 (dd, *J* = 7.6, 1.7 Hz, 0.56H), 7.30 (dd, *J* = 8.0, 1.7 Hz, 0.44H), 7.22 (dt, *J* = 7.8, 1.4 Hz, 1H), 7.13 – 7.04 (m, 3H), 6.62 – 6.55 (m, 1H), 3.79 (s, 1.33H), 3.77 (s, 1.67H), 3.46 (s, 0.56H), 3.45 (s, 0.44H), 2.88 (s, 0.56H), 2.88 (s, 0.44H), 1.34 (s, 5H), 1.33 (s, 4H). **^{13}C NMR** (151 MHz, $CDCl_3$) δ 171.31, 171.24, 155.64, 155.59, 145.87, 145.81, 130.53, 130.45, 129.79, 129.62, 129.42, 129.38, 125.18, 122.88, 122.85, 122.73, 122.68, 121.34, 121.29, 121.26, 112.71, 112.62, 110.34, 110.27, 58.70, 58.60, 55.92, 55.87, 44.66, 44.58, 31.68, 31.60, 22.65, 22.57. **IR** (thin film) ν_{max}: 3487, 3059, 2960, 2359, 1738, 1613, 1508, 1466, 1377, 1310, 1281, 1252, 1219, 1080, 1022, 937, 756 cm^{-1}; $[\alpha]_D^{25}$ = +200.5° (c 0.004 g/ml, $CHCl_3$); **HRMS** (ESI-TOF) *m/z*: $[2M+NH_4]^+$ calcd for $C_{40}H_{48}N_5O_6S_2$: 758.3041, found 758.3035.

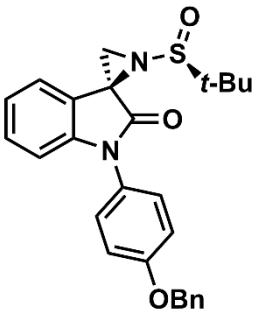

KLE-217A: Prepared by general procedure A with 1-(4-benzyloxyphenyl)-1*H*-indoline-2,3-dione[102] (217 mg, 0.659 mmol), (*S*)-*tert*-butanesulfinamide, and Ti(O*i*-Pr)$_4$. **Yield**: 72.7 mg, 25%. **^{1}H NMR** (500 MHz, $CDCl_3$) δ 7.71 (dd, *J* = 7.6, 1.2 Hz, 1H), 7.48 – 7.44 (m, 2H), 7.44 – 7.39 (m, 2H), 7.38 – 7.32 (m, 3H), 7.26 (td, *J* = 7.8, 1.3 Hz, 1H), 7.14 – 7.08 (m, 3H), 6.85 (d, *J* = 7.6 Hz, 1H), 5.12 (s, 2H), 3.45 (s, 1H), 2.87 (s, 1H), 1.34 (s, 9H); **^{13}C NMR** (126 MHz, $CDCl_3$) δ 171.39, 158.63, 145.80, 136.69, 129.52, 128.80, 128.27, 128.09, 127.61, 127.05, 125.44, 123.22, 121.36, 115.97, 110.07, 70.43, 58.74, 44.48, 31.68, 22.61; **IR** (thin film) ν_{max}: 3464, 2926, 2360, 1736, 1611, 1513, 1465, 1381, 1244, 1080, 1023, 937, 831, 762 cm^{-1}; $[\alpha]_D^{25}$ = +193.5° (c 0.002 g/ml, $CHCl_3$); **HRMS** (ESI-TOF) *m/z*: $[2M+NH_4]^+$ calcd for $C_{52}H_{56}N_5O_6S_2$: 910.3667, found 910.3664.

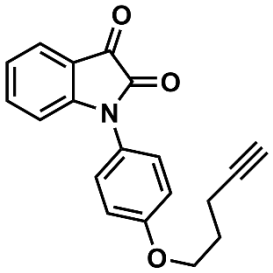

SI-6: To a solution of 1-bromo-4-(4-pentyn-1-yloxy)benzene[103] (1.6914 g, 7.074 mmol, 1.5 equiv.) in anhydrous DMF (13.9 mL) was added 1*H*-indole-2,3-dione (694 mg, 4.72 mmol, 1 equiv.) and CuO (703 mg, 9.43 mmol, 2 equiv.). The reaction mixture was heated to 155 °C and stirred for 8 h. N.B. longer reaction times result in reduced yields. Upon cooling to 20 °C, the reaction mixture was filtered through a pad of silica and rinsed with EtOAc until colorless. The filtrate was washed with *aq*. HCl (1.0 M, 20 mL) and 5% *aq*. LiCl (2 x 20 mL), then the combined aqueous washes were extracted with EtOAc. The aqueous layers were washed with brine, dried over Na_2SO_4, and concentrated in vacuo to a dark red and brown oil that solidified upon standing. The crude residue was purified by was purified by flash column chromatography on silica gel (20%→33% EtOAc–hexanes) to yield *N*-arylated isatin **SI-6** (66.4 mg, 5%) as an orange solid. **^{1}H NMR** (600 MHz, $CDCl_3$) δ 7.67 (ddd, *J* = 7.4, 1.4, 0.6 Hz, 1H), 7.52 (td, *J* = 7.8, 1.4 Hz, 1H), 7.34 – 7.28 (m, 2H), 7.15 (td, *J* = 7.5, 0.9 Hz, 1H), 7.09 – 7.03 (m, 2H), 6.83 (dt, *J* = 8.1, 0.7 Hz, 1H), 4.13 (t, *J* = 6.1 Hz, 2H), 2.44 (td, *J* = 7.0, 2.7 Hz, 2H), 2.07 – 2.02 (m, 2H), 1.99 (t, *J* = 2.7 Hz, 1H); **^{13}C NMR** (151 MHz, $CDCl_3$) δ 183.26, 159.20, 157.78, 152.24, 138.44, 127.63, 125.62, 125.55, 124.28, 117.63, 115.93, 111.32, 83.36, 69.22, 66.64, 28.17, 15.28; **IR** (thin film) ν_{max}: 3464, 3286, 3065, 2928, 1736, 1610, 1511, 1465, 1371, 1298, 1247, 1045, 926, 829, 755 cm^{-1}; **HRMS** (ESI-TOF) *m/z*: $[2M+NH_4]^+$ calcd for $C_{38}H_{34}N_3O_6$: 628.2442, found 628.2435.

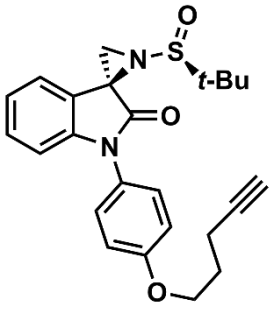

KL6-085A: Prepared by general procedure A with **SI-6** (48.9 mg, 0.160 mmol), (*S*)-*tert*-butanesulfinamide, and Ti(O*i*-Pr)$_4$. **Yield**: 26.0 mg, 38%**^{1}H NMR** (400 MHz, $CDCl_3$) δ 7.70 (dd, *J* = 7.6, 1.3 Hz, 1H), 7.40 – 7.30 (m, 2H), 7.26 (td, *J* = 7.7, 1.2 Hz, 1H), 7.09 (td, *J* = 7.7, 1.1 Hz, 1H), 7.06 – 6.99 (m, 2H), 6.84 (d, *J* = 7.9 Hz, 1H), 4.12 (t, *J* = 6.0 Hz, 2H), 3.45 (s, 1H), 2.87 (s, 1H), 2.44 (td, *J* = 6.9, 2.6 Hz, 2H), 2.08 – 2.01 (m, 2H), 1.99 (q, *J* = 2.2 Hz, 1H), 1.33 (s, 9H); **^{13}C NMR** (151 MHz, $CDCl_3$) δ 171.39, 158.78, 145.87, 129.52, 128.09, 126.88, 125.45, 123.20, 121.38, 115.63, 110.05, 83.43, 69.16, 66.57, 58.74, 44.49, 31.68, 28.22, 22.62, 15.29; **IR** (thin film) ν_{max}: 3295, 3251, 2956, 1731, 1610, 1512, 1466, 1378, 1246, 1157, 1078, 935, 833, 762 cm^{-1}; $\mathbf{[\alpha]_D^{25}}$ = +189.4° (c 0.005 g/ml, $CHCl_3$); **HRMS** (ESI-TOF) *m/z*: $[M+H]^+$ calcd for $C_{24}H_{27}N_2O_3S$: 423.1737, found 423.1736.

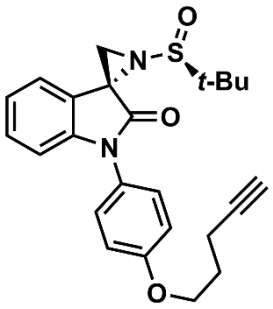

KL6-085B: Prepared by general procedure A with **SI-6** (48.9 mg, 0.160 mmol), (*S*)-*tert*-butanesulfinamide, and Ti(O*i*-Pr)$_4$. **Yield**: 8.2 mg, 12%. **^{1}H NMR** (700 MHz, $CDCl_3$) δ 7.37 – 7.32 (m, 2H), 7.28 (tt, *J* = 8.0, 1.0 Hz, 1H), 7.15 (br, 1H), 7.11 (t, *J* = 7.4 Hz, 1H), 7.05 – 7.00 (m, 2H), 6.87 (d, *J* = 7.9 Hz, 1H), 4.12 (t, *J* = 6.1 Hz, 2H), 3.42 (s, 1H), 2.78 (s, 1H), 2.44 (td, *J* = 7.0, 2.7 Hz, 2H), 2.04 (p, *J* = 6.2 Hz, 2H), 1.99 (td, *J* = 2.7, 0.8 Hz, 1H), 1.28 – 1.25 (m, 9H); **^{13}C NMR** (151 MHz, $CDCl_3$) δ 170.53, 158.71, 144.54, 129.48, 127.82, 126.90, 124.99, 123.29, 122.08, 115.53, 109.88, 83.45, 69.15,

66.60, 57.93, 46.22, 36.73, 28.24, 22.23, 15.31; **IR** (thin film) ν_{max}: 3294, 2925, 2363, 1729, 1616, 1514, 1466, 1376, 1248, 1199, 1091, 930, 833, 758 cm^{-1}; $[\alpha]_D^{25}$ = +57.0° (c 0.001 g/ml, $CHCl_3$); **HRMS** (ESI-TOF) *m/z*: $[2M+NH_4]^+$ calcd for $C_{48}H_{56}N_5O_6S_2$: 862.3667, found 862.3653.

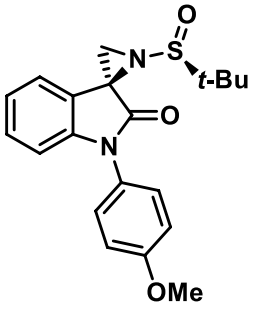

KL4-219A: Prepared by general procedure A with 1-(4-methoxyphenyl)-1*H*-indoline-2,3-dione[98] (16.6 mg, 0.0656 mmol), (*S*)-*tert*-butanesulfinamide, and Ti(O*i*-Pr)$_4$. **Yield**: 9.2 mg, 38%. **^{1}H NMR** (600 MHz, $CDCl_3$) δ 7.71 (d, *J* = 7.6 Hz, 1H), 7.37 – 7.32 (m, 2H), 7.26 (t, 1H), 7.10 (td, *J* = 7.6, 1.0 Hz, 1H), 7.07 – 7.01 (m, 2H), 6.84 (d, *J* = 7.9 Hz, 1H), 3.86 (s, 3H), 3.45 (s, 1H), 2.87 (s, 1H), 1.33 (s, 9H); **^{13}C NMR** (151 MHz, $CDCl_3$) δ 171.42, 159.47, 145.89, 129.53, 128.10, 126.86, 125.45, 123.21, 121.39, 115.08, 110.06, 58.75, 55.69, 44.50, 31.69, 22.63; **IR** (thin film) ν_{max}: 2959, 2360, 1735, 1611, 1514, 1250, 1080, 938, 759 cm^{-1}; $[\alpha]_D^{25}$ = +189.0° (c 0.001 g/ml, $CHCl_3$); **HRMS** (ESI-TOF) *m/z*: $[M+H]^+$ calcd for $C_{20}H_{23}N_2O_3S$: 371.1424, found 371.1424.

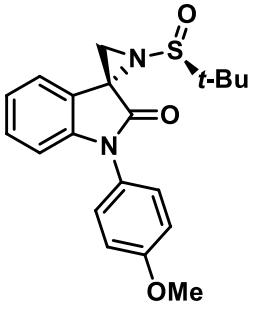

KL4-219B: Prepared by general procedure A with 1-(4-methoxyphenyl)-1*H*-indoline-2,3-dione[98] (16.6 mg, 0.0656 mmol), (*S*)-*tert*-butanesulfinamide, and Ti(O*i*-Pr)$_4$. **Yield**: 2.7 mg, 11%. **^{1}H NMR** (700 MHz, $CDCl_3$) δ 7.37 – 7.33 (m, 2H), 7.28 (td, *J* = 7.8, 1.4 Hz, 1H), 7.15 (s, 1H), 7.11 (t, *J* = 7.4 Hz, 1H), 7.05 – 7.00 (m, 2H), 6.87 (d, *J* = 7.9 Hz, 1H), 3.86 (s, 3H), 3.42 (s, 1H), 2.78 (s, 1H), 1.27 (s, 9H); **^{13}C NMR** (126 MHz, $CDCl_3$) δ 170.54, 159.37, 144.53, 129.48, 127.82, 126.85, 124.98, 123.30, 122.04, 114.95, 109.88, 57.94, 55.70, 46.20, 36.71, 22.22.; **IR** (thin film) ν_{max}: 2924, 2361, 1727, 1615, 1514, 1251, 1091, 923, 751 cm^{-1}; $[\alpha]_D^{25}$ = +63.8° (c 0.00091 g/ml, $CHCl_3$); **HRMS** (ESI-TOF) *m/z*: $[M+H]^+$ calcd for $C_{20}H_{23}N_2O_3S$: 371.1424, found 371.1427.

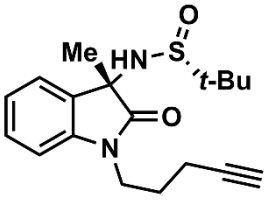

KL6-274A. Prepared by general procedure G with **SI-1** (8.8 mg, 0.041 mmol), (*R*)-*tert*-butanesulfinamide, and Ti(O*i*-Pr)$_4$. **Yield**: 4.0 mg, 30%. **^{1}H NMR** (500 MHz, $CDCl_3$) δ 7.35 (td, *J* = 7.8, 1.3 Hz, 1H), 7.29 (dd, *J* = 7.5, 1.3 Hz, 1H), 7.10 (td, *J* = 7.6, 1.0 Hz, 1H), 6.99 (dt, *J* = 7.9, 0.8 Hz, 1H), 4.12 (br, 1H), 3.88 (dt, *J* = 14.3, 7.2 Hz, 1H), 3.79 (dt, *J* = 14.3, 7.3 Hz, 1H), 2.39 – 2.24 (m, 2H), 2.02 (t, *J* = 2.6 Hz, 1H), 1.95 (p, *J* = 7.0 Hz, 2H), 1.56 (s, 3H), 1.19 (s, 9H); **^{13}C NMR** (151 MHz, $CDCl_3$) δ 178.23, 143.08, 129.96, 128.96, 125.15, 122.88, 109.19, 83.59, 69.38, 60.44, 55.98, 39.18, 26.08, 25.28, 22.79, 16.21; **IR** (thin film) ν_{max}: 3430, 3244, 2927, 1715, 1613, 1489, 1469, 1371, 1175, 1069, 753 cm^{-1}; $[\alpha]_D^{25}$ = –65.0° (c 0.001 g/ml, $CHCl_3$); **HRMS** (ESI-TOF) *m/z*: $[2M+NH_4]^+$ calcd for $C_{36}H_{52}N_5O_4S_2$: 682.3455, found 682.3433.

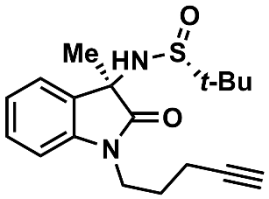

KL6-274B. Prepared by general procedure G with **SI-1** (8.8 mg, 0.041 mmol), (*R*)-*tert*-butanesulfinamide, and Ti(O*i*-Pr)$_4$. **Yield**: 4.0 mg, 30%. **^{1}H NMR** (500 MHz, $CDCl_3$) δ 7.52 (dd, *J* = 7.4, 1.2 Hz, 1H), 7.34 (td, *J* = 7.8, 1.2 Hz, 1H), 7.12 (td, *J* = 7.6, 1.0 Hz, 1H), 6.95 (dt, *J* = 7.8, 0.8 Hz, 1H), 3.89 – 3.75 (m, 2H), 3.79 (br, 1H), 2.29 – 2.23 (m, 2H), 2.03 (t, *J* = 2.6 Hz, 1H), 1.92 (p, *J* = 7.1 Hz, 2H), 1.66 (s, 3H), 1.15 (s, 9H); **^{13}C NMR** (151 MHz, $CDCl_3$) δ 176.92, 142.18, 130.54, 129.73, 125.38, 123.15, 108.88, 83.10, 69.54, 61.22, 56.48, 39.16, 26.38, 25.61, 22.48, 16.20; **IR** (thin film) ν_{max}: 3435, 3255, 2927, 1717, 1612, 1489, 1469, 1366, 1176, 1058, 753 cm^{-1}; $[\alpha]_D^{25}$ = –67.0° (c 0.001 g/ml, $CHCl_3$); **HRMS** (ESI-TOF) *m/z*: $[2M+NH_4]^+$ calcd for $C_{36}H_{52}N_5O_4S_2$: 682.3455, found 682.3427.

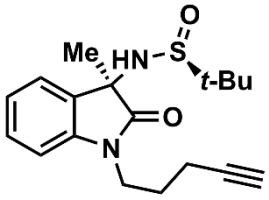

KL6-275A. Prepared by general procedure G with **SI-1** (24.3 mg, 0.114 mmol), (*S*)-*tert*-butanesulfinamide, and Ti(O*i*-Pr)$_4$. **Yield**: 6.5 mg, 17%. **^{1}H NMR**, **^{13}C NMR**, and **IR** data matched that of **KL6-274A**; $[\alpha]_D^{25}$ = +58.0° (c 0.001 g/ml, $CHCl_3$); **HRMS** (ESI-TOF) *m/z*: $[2M+NH_4]^+$ calcd for $C_{36}H_{52}N_5O_4S_2$: 682.3455, found 682.3429.

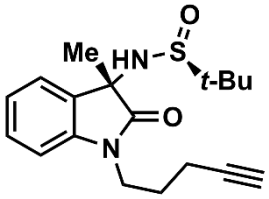

KL6-275B. Prepared by general procedure G with **SI-1** (24.3 mg, 0.114 mmol), (*S*)-*tert*-butanesulfinamide, and Ti(O*i*-Pr)$_4$. **Yield**: 10.2 mg, 27%. **^{1}H NMR**, **^{13}C NMR**, and **IR** data matched that of **KL6-274B**; $[\alpha]_D^{25}$ = +59.0° (c 0.001 g/ml, $CHCl_3$); **HRMS** (ESI-TOF) *m/z*: $[2M+NH_4]^+$ calcd for $C_{36}H_{52}N_5O_4S_2$: 682.3455, found 682.3446.

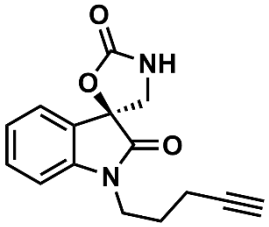

KL2-237. Prepared by general procedure E with **KL2-230** (204 mg, 0.617 mmol). **Yield**: 116 mg, 70%. **^{1}H NMR** (600 MHz, C_6D_6) δ 6.96 (dd, *J* = 7.4, 1.2 Hz, 1H), 6.93 (td, *J* = 7.8, 1.3 Hz, 1H), 6.70 (td, *J* = 7.6, 0.9 Hz, 1H), 6.32 (d, *J* = 7.8 Hz, 1H), 5.53 (br, 1 H), 3.34 (d, *J* = 9.1, 1H), 3.31 – 3.21 (m, 2H), 2.88 (d, *J* = 9.1 Hz, 1H), 1.76 (td, *J* = 6.9, 2.7 Hz, 2H), 1.69 (t, *J* = 2.6 Hz, 1H), 1.44 – 1.29 (m, 2H); **^{13}C NMR** (151 MHz, C_6D_6) δ 172.96, 158.44, 143.70, 131.08, 127.15, 125.00, 123.40, 108.90, 83.11, 78.83, 69.70, 47.87, 39.06, 26.11, 16.08; **IR** (thin film) ν_{max}: 3289, 2925, 1770, 1728, 1616, 1470, 1374, 1171, 1081, 755 cm^{-1}; $[\alpha]_D^{25}$ = –10.0° (c 0.001 g/ml, $CHCl_3$); **HRMS** (ESI-TOF) *m/z*: $[2M+NH_4]^+$ calcd for $C_{30}H_{32}N_5O_6$: 558.2347, found 558.2330.

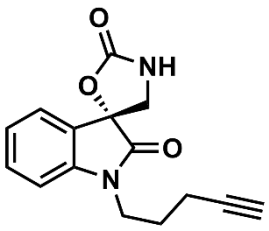

KL3-082. Prepared by general procedure E with **KL2-236** (318 mg, 0.962 mmol). **Yield**: 191.3 mg, 74%. **^{1}H NMR**, **^{13}C NMR**, and **IR** data matched that of **KL2-237**; $[\alpha]_D^{25}$ = +12.5° (c 0.002 g/ml, $CHCl_3$); **HRMS** (ESI-TOF) *m/z*: $[2M+NH_4]^+$ calcd for $C_{30}H_{32}N_5O_6$: 558.2347, found 558.2353.

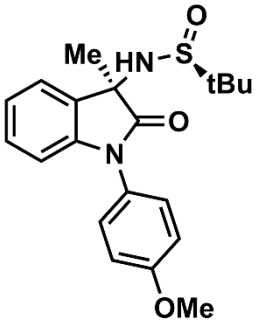

KL6-278A. Prepared by general procedure G with 1-(4-methoxyphenyl)-1*H*-indoline-2,3-dione[98] (28.4 mg, 0.112 mmol), (*S*)-*tert*-butanesulfinamide, and Ti(O*i*-Pr)$_4$. **Yield**: 5.0 mg, 12%. **^{1}H NMR** (700 MHz, $CDCl_3$) δ 7.40 – 7.37 (m, 2H), 7.36 – 7.33 (m, 1H), 7.28 (td, *J* = 7.7, 1.3 Hz, 1H), 7.12 (td, *J* = 7.5, 1.0 Hz, 1H), 7.03 – 6.99 (m, 2H), 6.78 (d, *J* = 8.2 Hz, 1H), 4.24 (br, 1H), 3.84 (s, 3H), 1.67 (s, 3H), 1.23 (s, 9H); **^{13}C NMR** (151 MHz, $CDCl_3$) δ 178.02, 159.46, 144.51, 129.93, 128.43, 128.34, 127.03, 125.22, 123.22, 115.08, 110.13, 60.56, 55.92, 55.68, 25.15, 22.87; **IR** (thin film) ν_{max}: 3430, 3236, 2925, 1725, 1612, 1514, 1467, 1377, 1249, 755cm^{-1}; **$[\alpha]_D^{25}$** = +83.0° (c 0.001 g/ml, $CHCl_3$); **HRMS** (ESI-TOF) *m/z*: $[2M+NH_4]^+$ calcd for $C_{40}H_{52}N_5O_6S_2$: 762.3354, found 762.3339.

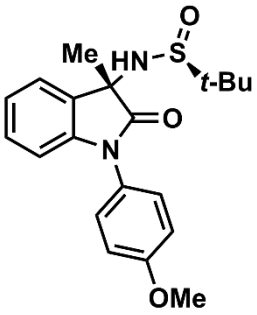

KL6-278B. Prepared by general procedure G with 1-(4-methoxyphenyl)-1*H*-indoline-2,3-dione[98] (28.4 mg, 0.112 mmol), (*S*)-*tert*-butanesulfinamide, and Ti(O*i*-Pr)$_4$. **Yield**: 8.0 mg, 19%. **^{1}H NMR** (700 MHz, $CDCl_3$) δ 7.58 (ddd, *J* = 7.4, 1.3, 0.5 Hz, 1H), 7.31 – 7.29 (m, 2H), 7.27 (td, *J* = 7.8, 1.3 Hz, 1H), 7.15 (td, *J* = 7.5, 1.0 Hz, 1H), 7.06 – 7.01 (m, 2H), 6.79 (dt, *J* = 7.8, 0.8 Hz, 1H), 3.92 (br, 1H), 3.86 (s, 3H), 1.77 (s, 3H), 1.18 (s, 9H). **^{13}C NMR** (151 MHz, $CDCl_3$) δ 176.56, 159.49, 143.38, 130.13, 129.62, 127.99, 126.74, 125.42, 123.54, 115.12, 109.91, 61.45, 56.56, 55.71, 25.91, 22.52; **IR** (thin film) ν_{max}: 3444, 3234, 2926, 1730, 1668, 1610, 1465, 1511, 1371, 1249, 1033, 835, 762 cm^{-1}; **$[\alpha]_D^{25}$** = +96.0° (c 0.001 g/ml, $CHCl_3$); **HRMS** (ESI-TOF) *m/z*: $[2M+NH_4]^+$ calcd for $C_{40}H_{52}N_5O_6S_2$: 762.3354, found 762.3357.

3.7 Distribution of Credit

Portions of this chapter have been reproduced in Rosen, H.T.; Li, K. et. al. *Angew. Chem. Int. Ed.* 2025, *64* (48). The idea of exploring sulfinyl aziridines as covalent drug leads along with strategies for exploring SAR were developed in collaboration with Dr. Kelvin Li and Professor Dr. Thomas Maimone. All synthetic work in this chapter was carried out by Dr. Kelvin Li and Erin Li with guidance from Professor Dr. Thomas Maimone. Initial project ideation and target choice were developed by Dr. Daniel Nomura. The direction of the project was a collaborative effort between me and Dr. Daniel Nomura. Most molecular biology, cell biology and chemoproteomics experiments were performed by me and my undergraduate student Brynne Currier. The synthetic peptide experiment in **Figure 3.2c-3.2d** was carried out by Scott Brittan (Novartis Biomedical Research). The ELISA in **Figure 3.4g** was completed by Francisco Garcia (Novartis Biomedical Research). Christian Stieger (UC Berkeley) assisted with the analysis of data presented in **Figure 3.7a**. Diana Beard (Novartis Biomedical Research) completed the RNAseq analysis in **Figure 3.10b-3.10d** and **Figure 3.11a-3.11c**. Sandra Haenni-Holzinger (Novartis Biomedical Research) developed the protocol for purification of MYC/MAX as well as completed the purification.

Concluding Remarks

Over the last millennium, drug discovery has undergone drastic changes. Some of the most common and first-line treatments for disease are molecules where the mechanism of action remains unknown. Humanity has entered the phase of pharmaceutical development where it is no longer sufficient to show that use of a medicine causes a phenotypic outcome. We have no choice but to elucidate the complex mechanisms of biology and pathology to accurately and selectively target disease-causing proteins. This dissertation discusses some of the biggest challenges in modern drug discovery and presents solutions in the form of covalent chemoproteomic methodologies. Chemoproteomics allows for more advanced target identification of both disease-causing proteins, but also potential therapeutics against a specific target. The introduction to the application of bio-orthogonal chemistry and its numerous utilities are presented in this work.

In addition, one of the highlights of this dissertation has been to understand the complex biology that MYC participates in. There is not a single area of cell biology in which MYC or its target genes are not found, modulated, and often altered in a cancer context. A key principle in the field of toxicology is the importance of how biology should behave under certain conditions, and then how the alteration of conditions leads to a toxic outcome. Although my dissertation does not cover toxicology-specific topics, the approach to the work remains the same. To be able to target MYC, we must understand its basic biology and then build upon that knowledge to develop novel therapeutics. In this work, I present a select group of historical MYC modulating strategies that set the stage for my contributions to the field.

This dissertation described the discovery and characterization of covalent stereoselective sulfinyl aziridine small molecules that act upon MYC as destabilizing degraders. This work expanded upon previous literature to exploit the intrinsic disorder of many transcription factors as a vulnerability for their targeted degradation. I screened a library of stereochemically paired small molecules, evaluated MYC degradation, while counter-screening for cell viability. I discovered KL2-236 and found that its diastereomers showed less degradation with one diastereomer KL4-019 acting as a negative control for further experimentation. I show that sulfinyl aziridines are a robust, protein-reactive electrophilic warhead with favorable stability for drug development. I characterized the mechanism of degradation through proteasomal rescue studies. I evaluated the interaction between KL2-236 and MYC through multiple chemical biology approaches including activity-based protein profiling (ABPP), ELIZA, and pulldown immunoblots. I established KL2-236 as a destabilizing degrader by cellular thermal shift assay (CETSA) and used site directed mutagenesis to determine the site of modification of KL2-236 on MYC as C203/D205. I show on-target downstream effects of MYC degradation leading to a reduction in MYC transcriptional activity by luciferase reporter assay and MYC target genes by transcriptomics. I collaborated with an amazing chemist who synthesized over 180 analogs of KL2-236 and I subsequently tested them for potency and cell viability. We used structure-activity relationship to find a more potent and effective MYC degrader in KL4-219A. I fully characterize KL4-219A and find that it is both more potent than the initial

hit compound, and more selective for MYC in proteome wide analysis. This work represents the ability to drug a notorious “undruggable” oncogenic transcription factor, and it shows the value in using chiral covalent small molecules to interrogate structurally undefined proteins.

References

1. Dang, C. V., Reddy, E. P., Shokat, K. M. & Soucek, L. Drugging the 'undruggable' cancer targets. *Nat. Rev. Cancer* **17**, 502–508 (2017).
2. Xie, X. *et al.* Recent advances in targeting the "undruggable" proteins: from drug discovery to clinical trials. *Signal Transduct. Target. Ther.* **8**, 335 (2023).
3. Nelson, D. L., Cox, M. M. & Lehninger, A. L. *Lehninger Principles of Biochemistry*. (W.H. Freeman and Company ; Macmillan Higher Education, New York, NY : Houndmills, Basingstoke, 2017).
4. Hopkins, A. L. & Groom, C. R. The druggable genome. *Nat. Rev. Drug Discov.* **1**, 727–730 (2002).
5. Gehringer, M. & Laufer, S. A. Emerging and Re-Emerging Warheads for Targeted Covalent Inhibitors: Applications in Medicinal Chemistry and Chemical Biology. *J. Med. Chem.* **62**, 5673–5724 (2019).
6. De Cesco, S., Kurian, J., Dufresne, C., Mittermaier, A. K. & Moitessier, N. Covalent inhibitors design and discovery. *Eur. J. Med. Chem.* **138**, 96–114 (2017).
7. Liu, Y., Patricelli, M. P. & Cravatt, B. F. Activity-based protein profiling: The serine hydrolases. *Proc. Natl. Acad. Sci.* **96**, 14694–14699 (1999).
8. Rostovtsev, V. V., Green, L. G., Fokin, V. V. & Sharpless, K. B. A stepwise huisgen cycloaddition process: copper(I)-catalyzed regioselective 'ligation' of azides and terminal alkynes. *Angew. Chem.* **41**, 2596–2599 (2002).
9. Duesberg, P. H. & Vogt, P. K. Avian acute leukemia viruses MC29 and MH2 share specific RNA sequences: Evidence for a second class of transforming genes. *Proc. Natl. Acad. Sci. U. S. A.* **76**, 1633–1637 (1979).
10. Sheiness, D. & Bishop, J. M. DNA and RNA from Uninfected Vertebrate Cells Contain Nucleotide Sequences Related to the Putative Transforming Gene of Avian Myelocytomatosis Virus. *J. Virol.* **31**, 514–521 (1979).
11. Stine, Z. E., Walton, Z. E., Altman, B. J., Hsieh, A. L. & Dang, C. V. MYC, Metabolism, and Cancer. *Cancer Discov.* **5**, 1024–1039 (2015).
12. Jha, R. K., Kouzine, F. & Levens, D. MYC function and regulation in physiological perspective. *Front. Cell Dev. Biol.* **11**, 1268275 (2023).
13. Llombart, V. & Mansour, M. R. Therapeutic targeting of "undruggable" MYC. *EBioMedicine* **75**, 103756 (2021).
14. Kaczmarek, L., Hyland, J. K., Watt, R., Rosenberg, M. & Baserga, R. Microinjected c-myc as a Competence Factor. *Science* **228**, 1313–1315 (1985).
15. Shi, Y. *et al.* Role for c-myc in Activation-Induced Apoptotic Cell Death in T Cell Hybridomas. *Science* **257**, 212–214 (1992).
16. Dhanasekaran, R. *et al.* The MYC oncogene — the grand orchestrator of cancer growth and immune evasion. *Nat. Rev. Clin. Oncol.* **19**, 23–36 (2022).

17. Bretones, G., Delgado, M. D. & León, J. Myc and cell cycle control. *Biochim. Biophys. Acta* **1849**, 506–516 (2015).
18. García-Gutiérrez, L., Delgado, M. D. & León, J. MYC Oncogene Contributions to Release of Cell Cycle Brakes. *Genes* **10**, 244 (2019).
19. Schmidt, E. V. The role of c-myc in cellular growth control. *Oncogene* **18**, 2988–2996 (1999).
20. Das, S. K., Lewis, B. A. & Levens, D. MYC: a complex problem. *Trends Cell Biol.* **33**, 235–246 (2023).
21. Prochownik, E. V., Kukowska, J. & Rodgers, C. c-myc antisense transcripts accelerate differentiation and inhibit G1 progression in murine erythroleukemia cells. *Mol. Cell. Biol.* **8**, 3683–3695 (1988).
22. Webb, M. S. *et al.* Toxicity and Toxicokinetics of a Phosphorothioate Oligonucleotide Against the c-myc Oncogene in Cynomolgus Monkeys. *Antisense Nucleic Acid Drug Dev.* **11**, 155–163 (2001).
23. Kutryk, M. J. B. *et al.* Local intracoronary administration of antisense oligonucleotide against c-myc for the prevention of in-stent restenosis: Results of the randomized investigation by the thoraxcenter of antisense dna using local delivery and ivus after coronary stenting (ITALICS) trial. *J. Am. Coll. Cardiol.* **39**, 281–287 (2002).
24. Whitfield, J. R. & Soucek, L. MYC in cancer: from undruggable target to clinical trials. *Nat. Rev. Drug Discov.* **24**, 445–457 (2025).
25. Soucek, L. *et al.* Design and properties of a Myc derivative that efficiently homodimerizes. *Oncogene* **17**, 2463–2472 (1998).
26. Massó-Vallés, D. & Soucek, L. Blocking Myc to Treat Cancer: Reflecting on Two Decades of Omomyc. *Cells* **9**, 883 (2020).
27. Soucek, L. *et al.* Omomyc, a potential Myc dominant negative, enhances Myc-induced apoptosis. *Cancer Res.* **62**, 3507–3510 (2002).
28. Beaulieu, M.-E. *et al.* Intrinsic cell-penetrating activity propels Omomyc from proof of concept to viable anti-MYC therapy. *Sci. Transl. Med.* **11**, eaar5012 (2019).
29. Castell, A. *et al.* A selective high affinity MYC-binding compound inhibits MYC:MAX interaction and MYC-dependent tumor cell proliferation. *Sci. Rep.* **8**, 10064 (2018).
30. Han, H. *et al.* Small Molecule MYC Inhibitors Suppress Tumor Growth and Enhance Immunotherapy. *Cancer Cell* **36**, 483-497.e15 (2019).
31. Shukla, S. *et al.* 3JC48-3 (methyl 4'-methyl-5-(7-nitrobenzo[c][1,2,5]oxadiazol-4-yl)-[1,1'-biphenyl]-3-carboxylate): a novel MYC/MAX dimerization inhibitor reduces prostate cancer growth. *Cancer Gene Ther.* **29**, 1550–1557 (2022).
32. Huang, Q. *et al.* Synthesis and biological evaluation of a novel c-Myc inhibitor against colorectal cancer via blocking c-Myc/Max heterodimerization and disturbing its DNA binding. *Eur. J. Med. Chem.* **243**, 114779 (2022).

33. Boike, L. *et al.* Discovery of a Functional Covalent Ligand Targeting an Intrinsically Disordered Cysteine within MYC. *Cell Chem. Biol.* **28**, 4-13.e17 (2021).
34. Rosen, H. T. *et al.* Sulfinyl Aziridines as Stereoselective Covalent Destabilizing Degraders of the Oncogenic Transcription Factor MYC. *Angew. Chem. Int. Ed.* **64**, e202508518 (2025).
35. Henley, M. J. & Koehler, A. N. Advances in targeting 'undruggable' transcription factors with small molecules. *Nat. Rev. Drug Discov.* **20**, 669–688 (2021).
36. Meyer, N. & Penn, L. Z. Reflecting on 25 years with MYC. *Nat. Rev. Cancer* **8**, 976–990 (2008).
37. Chen, H., Liu, H. & Qing, G. Targeting oncogenic Myc as a strategy for cancer treatment. *Signal Transduct. Target. Ther.* **3**, 5 (2018).
38. McKeown, M. R. & Bradner, J. E. Therapeutic Strategies to Inhibit MYC. *Cold Spring Harb. Perspect. Med.* **4**, a014266 (2014).
39. Kress, T. R., Sabò, A. & Amati, B. MYC: connecting selective transcriptional control to global RNA production. *Nat. Rev. Cancer* **15**, 593–607 (2015).
40. Dang, C. V., Reddy, E. P., Shokat, K. M. & Soucek, L. Drugging the 'undruggable' cancer targets. *Nat. Rev. Cancer* **17**, 502–508 (2017).
41. Whitfield, J. R., Beaulieu, M.-E. & Soucek, L. Strategies to Inhibit Myc and Their Clinical Applicability. *Front. Cell Dev. Biol.* **5**, (2017).
42. Olson, C. M. *et al.* Pharmacological perturbation of CDK9 using selective CDK9 inhibition or degradation. *Nat. Chem. Biol.* **14**, 163–170 (2018).
43. Struntz, N. B. *et al.* Stabilization of the Max Homodimer with a Small Molecule Attenuates Myc-Driven Transcription. *Cell Chem. Biol.* **26**, 711-723.e14 (2019).
44. Mitchell, K. *et al.* WDR5 represents a therapeutically exploitable target for cancer stem cells in glioblastoma. *Genes Dev.* **37**, 86–102 (2023).
45. Ding, J. *et al.* Discovery of Potent Small-Molecule Inhibitors of WDR5-MYC Interaction. *ACS Chem. Biol.* **18**, 34–40 (2023).
46. Ding, J. *et al.* Discovery and Structure-Based Design of Inhibitors of the WD Repeat-Containing Protein 5 (WDR5)–MYC Interaction. *J. Med. Chem.* **66**, 8310–8323 (2023).
47. Meyer, C. T. *et al.* Expanded profiling of WD repeat domain 5 inhibitors reveals actionable strategies for the treatment of hematologic malignancies. *Proc. Natl. Acad. Sci.* **121**, e2408889121 (2024).
48. Backus, K. M. *et al.* Proteome-wide covalent ligand discovery in native biological systems. *Nature* **534**, 570–574 (2016).
49. Vinogradova, E. V. *et al.* An activity-guided map of electrophile-cysteine interactions in primary human T cells. *Cell* **182**, 1009-1026.e29 (2020).
50. Spradlin, J. N., Zhang, E. & Nomura, D. K. Reimagining Druggability Using Chemoproteomic Platforms. *Acc. Chem. Res.* **54**, 1801–1813 (2021).

51. Gowans, F. A. *et al.* Covalent Degrader of the Oncogenic Transcription Factor β-Catenin. *J. Am. Chem. Soc.* 10.1021/jacs.4c05174 (2024) doi:10.1021/jacs.4c05174.
52. Won, S. J. *et al.* Redirecting the pioneering function of FOXA1 with covalent small molecules. *Mol. Cell* **84**, 4125-4141.e10 (2024).
53. Takahashi, M. *et al.* DrugMap: A quantitative pan-cancer analysis of cysteine ligandability. *Cell* **187**, 2536-2556.e30 (2024).
54. Fan, M. *et al.* Covalent disruptor of YAP-TEAD association suppresses defective Hippo signaling. *eLife* **11**, e78810 (2022).
55. Lazear, M. R. *et al.* Proteomic discovery of chemical probes that perturb protein complexes in human cells. *Mol. Cell* **83**, 1725-1742.e12 (2023).
56. Scott, K. A. *et al.* Covalent Targeting of Splicing in T Cells. *Cell Chem. Biol.* **32**, 201-218.e17 (2025).
57. Ogasawara, D. *et al.* Chemical tools to expand the ligandable proteome: Diversity-oriented synthesis-based photoreactive stereoprobes. *Cell Chem. Biol.* **31**, 2138-2155.e32 (2024).
58. Liu, Z. *et al.* Proteomic ligandability maps of spirocycle acrylamide stereoprobes identify covalent ERCC3 degraders. *J. Am. Chem. Soc.* **146**, 10393–10406 (2024).
59. Hajra, S., Aziz, S. M., Jana, B., Mahish, P. & Das, D. Synthesis of Chiral Spiro-Aziridine Oxindoles via Aza-Corey–Chaykovsky Reaction of Isatin Derived N-tert-Butanesulfinyl Ketimines. *Org. Lett.* **18**, 532–535 (2016).
60. Khetmalis, Y. M., Shivani, M., Murugesan, S. & Chandra Sekhar, K. V. G. Oxindole and its derivatives: A review on recent progress in biological activities. *Biomed. Pharmacother.* **141**, 111842 (2021).
61. Yu, B., Yu, D.-Q. & Liu, H.-M. Spirooxindoles: Promising scaffolds for anticancer agents. *Eur. J. Med. Chem.* **97**, 673–698 (2015).
62. Kaur, M., Singh, M., Chadha, N. & Silakari, O. Oxindole: A chemical prism carrying plethora of therapeutic benefits. *Eur. J. Med. Chem.* **123**, 858–894 (2016).
63. Badillo, J. J., Hanhan, N. V. & Franz, A. K. Enantioselective synthesis of substituted oxindoles and spirooxindoles with applications in drug discovery. *Curr. Opin. Drug Discov. Devel.* **13**, 758–776 (2010).
64. Boddy, A. J. & Bull, J. A. Stereoselective synthesis and applications of spirocyclic oxindoles. *Org. Chem. Front.* **8**, 1026–1084 (2021).
65. Hajra, S., Singha Roy, S., Aziz, S. M. & Das, D. Catalyst-Free “On-Water” Regio- and Stereospecific Ring-Opening of Spiroaziridine Oxindole: Enantiopure Synthesis of Unsymmetrical 3,3′-Bisindoles. *Org. Lett.* **19**, 4082–4085 (2017).
66. Hajra, S., Singha Roy, S., Biswas, A. & Saleh, S. A. Catalyst-Free Ring Opening of Spiroaziridine Oxindoles by Heteronucleophiles: An Approach to the Synthesis of Enantiopure 3-Substituted Oxindoles. *J. Org. Chem.* **83**, 3633–3644 (2018).

67. Ma, N. *et al.* 2H-Azirine-Based Reagents for Chemoselective Bioconjugation at Carboxyl Residues Inside Live Cells. *J. Am. Chem. Soc.* **142**, 6051–6059 (2020).
68. Jiang, L. *et al.* Abstract 526: RMC-9805, a first-in-class, mutant-selective, covalent and oral KRASG12D(ON) inhibitor that induces apoptosis and drives tumor regression in preclinical models of KRASG12D cancers. *Cancer Research* (2023) doi:10.1158/1538-7445.AM2023-526.
69. Shibata, Y. & Chiba, M. The Role of Extrahepatic Metabolism in the Pharmacokinetics of the Targeted Covalent Inhibitors Afatinib, Ibrutinib, and Neratinib. *Drug Metab. Dispos.* **43**, 375–384 (2015).
70. Yamada, H., Yoshida, T., Sakamoto, H., Terada, M. & Sugimura, T. Establishment of a human pancreatic adenocarcinoma cell line (PSN-1) with amplifications of both c-*myc* and activated c-Ki-*ras* by a point mutation. *Biochem. Biophys. Res. Commun.* **140**, 167–173 (1986).
71. Talwar, D. *et al.* The GAPDH redox switch safeguards reductive capacity and enables survival of stressed tumour cells. *Nat. Metab.* **5**, 660–676 (2023).
72. London, N. Covalent Proximity Inducers. *Chem. Rev.* **125**, 326–368 (2025).
73. Gerry, C. J. & Schreiber, S. L. Unifying principles of bifunctional, proximity-inducing small molecules. *Nat. Chem. Biol.* **16**, 369–378 (2020).
74. Zanon, P. R. A. *et al.* Profiling the proteome-wide selectivity of diverse electrophiles. https://doi.org/10.33774/chemrxiv-2021-w7rss-v2 (2021) doi:10.33774/chemrxiv-2021-w7rss-v2.
75. Zanon, P. R. A. *et al.* Profiling the proteome-wide selectivity of diverse electrophiles. *Nat. Chem.* **17**, 1712–1721 (2025).
76. Varadi, M. *et al.* AlphaFold Protein Structure Database: massively expanding the structural coverage of protein-sequence space with high-accuracy models. *Nucleic Acids Res.* **50**, D439–D444 (2022).
77. Jumper, J. *et al.* Highly accurate protein structure prediction with AlphaFold. *Nature* **596**, 583–589 (2021).
78. Mark, K. G. *et al.* Orphan quality control shapes network dynamics and gene expression. *Cell* **186**, 3460-3475.e23 (2023).
79. Julio, A. R. *et al.* Delineating cysteine-reactive compound modulation of cellular proteostasis processes. *Nat. Chem. Biol.* **21**, 693–705 (2025).
80. Labisso, W. L. *et al.* MYC directs transcription of MCL1 and eIF4E genes to control sensitivity of gastric cancer cells toward HDAC inhibitors. *Cell Cycle* **11**, 1593–1602 (2012).
81. Lorthiois, E. *et al.* JDQ443, a Structurally Novel, Pyrazole-Based, Covalent Inhibitor of KRASG12C for the Treatment of Solid Tumors. *J. Med. Chem.* **65**, 16173–16203 (2022).

82. Toriki, E. S. *et al.* Rational Chemical Design of Molecular Glue Degraders. *ACS Cent. Sci.* **9**, 915–926 (2023).
83. Lim, M. *et al.* DCAF16-Based Covalent Handle for the Rational Design of Monovalent Degraders. *ACS Cent. Sci.* **10**, 1318–1331 (2024).
84. Schuierer, S. & Roma, G. The exon quantification pipeline (EQP): a comprehensive approach to the quantification of gene, exon and junction expression from RNA-seq data. *Nucleic Acids Res.* **44**, e132 (2016).
85. Dobin, A. *et al.* STAR: ultrafast universal RNA-seq aligner. *Bioinformatics* **29**, 15–21 (2013).
86. Love, M. I., Huber, W. & Anders, S. Moderated estimation of fold change and dispersion for RNA-seq data with DESeq2. *Genome Biol.* **15**, 550 (2014).
87. Huber, W., von Heydebreck, A., Sültmann, H., Poustka, A. & Vingron, M. Variance stabilization applied to microarray data calibration and to the quantification of differential expression. *Bioinformatics* **18**, S96–S104 (2002).
88. Liberzon, A. *et al.* The Molecular Signatures Database Hallmark Gene Set Collection. *Cell Syst.* **1**, 417–425 (2015).
89. Korotkevich, G. *et al.* Fast gene set enrichment analysis. 060012 Preprint at https://doi.org/10.1101/060012 (2021).
90. Stieger, C. E. *et al.* DFT-Guided Discovery of Ethynyl-Triazolyl-Phosphinates as Modular Electrophiles for Chemoselective Cysteine Bioconjugation and Profiling. *Angew. Chem. Int. Ed.* **61**, e202205348 (2022).
91. Hodgson, D. M., Kloesges, J. & Evans, B. Asymmetric Synthesis of Terminal N - tert -Butylsulfinyl Aziridines from Organoceriums and an α-Chloroimine. *Org. Lett.* **10**, 2781–2783 (2008).
92. Hodgson, D. M., Kloesges, J. & Evans, B. Asymmetric Synthesis of Terminal N-tert-Butylsulfinyl Aziridines from Organoceriums and an α-Chloroimine. *Org. Lett.* **10**, 2781–2783 (2008).
93. Liu, Z., Derosa, J. & Engle, K. M. Palladium(II)-Catalyzed Regioselective syn-Hydroarylation of Disubstituted Alkynes Using a Removable Directing Group. *J. Am. Chem. Soc.* **138**, 13076–13081 (2016).
94. Qi, D. *et al.* Photoinduced Synthesis of Functionalized Oxacyclic Spirooxindoles Via Ring Expansion. *Org. Lett.* **25**, 506–511 (2023).
95. Chandra, A., Yadav, N. R. & Moorthy, J. N. Facile synthesis of isatins by direct oxidation of indoles and 3-iodoindoles using NIS/IBX. *Tetrahedron* **75**, 2169–2174 (2019).
96. Ngo, H. X. *et al.* Potent 1,2,4-Triazino[5,6b]indole-3-thioether Inhibitors of the Kanamycin Resistance Enzyme Eis from Mycobacterium tuberculosis. *ACS Infect. Dis.* **4**, 1030–1040 (2018).

97. Luo, Q. *et al.* Enantioselective Synthesis of Spiro[cyclopentane-1,3′-oxindole] Scaffolds with Five Consecutive Stereocenters. *Org. Lett.* **26**, 6402–6406 (2024).
98. Coppola, G. M. N-Arylation of isatins. A direct route to N-arylisatoic anhydrides. *J. Heterocycl. Chem.* **24**, 1249–1251 (1987).
99. Jeankumar, V. U. *et al.* Discovery and structure optimization of a series of isatin derivatives as Mycobacterium tuberculosis chorismate mutase inhibitors. *Chem. Biol. Drug Des.* **83**, 498–506 (2014).
100. Pedras, M. S. C., Suchy, M. & Ahiahonu, P. W. K. Unprecedented chemical structure and biomimetic synthesis of erucalexin, a phytoalexin from the wild crucifer Erucastrum gallicum. *Org. Biomol. Chem.* **4**, 691–701 (2006).
101. Sun, J., Liu, B. & Xu, B. Copper-catalyzed tandem oxidative cyclization of arylacetamides: efficient access to N-functionalized isatins. *RSC Adv.* **3**, 5824–5827 (2013).
102. Jiang, Q., Natrajan, A., Sharpe, D., Wong, W.-J. & Law, S.-J. Chemiluminescent Substrates of Hydrolytic Enzymes Such as Phosphatases. (2001).
103. Cornelissen, L., Vercruysse, S., Sanhadji, A. & Riant, O. Copper-Catalyzed Vinylsilane Allylation. *Eur. J. Org. Chem.* **2014**, 35–38 (2014).

Appendices

Appendix 1: Supplemental Figures

a

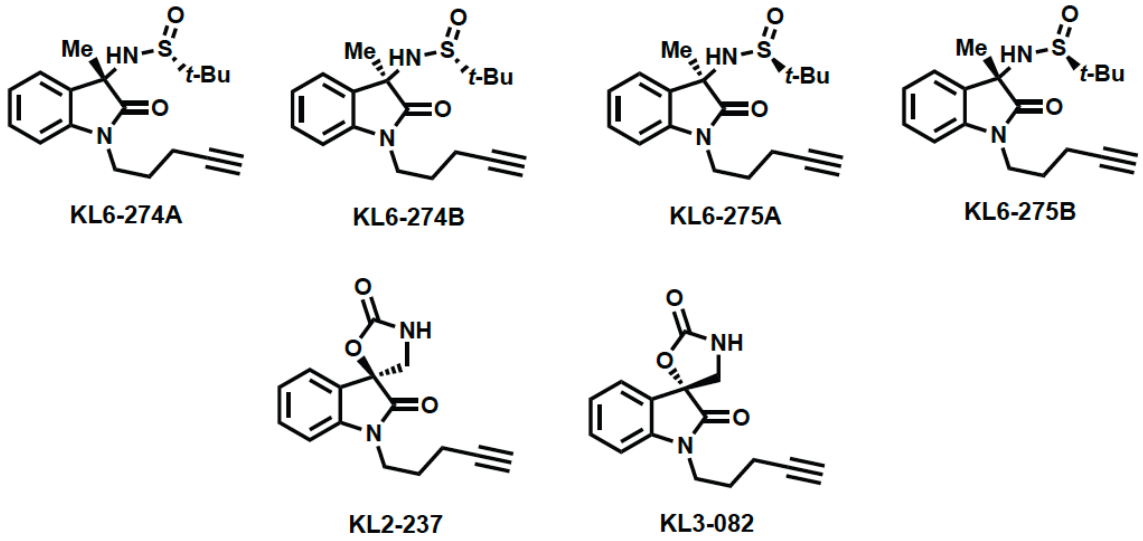

b

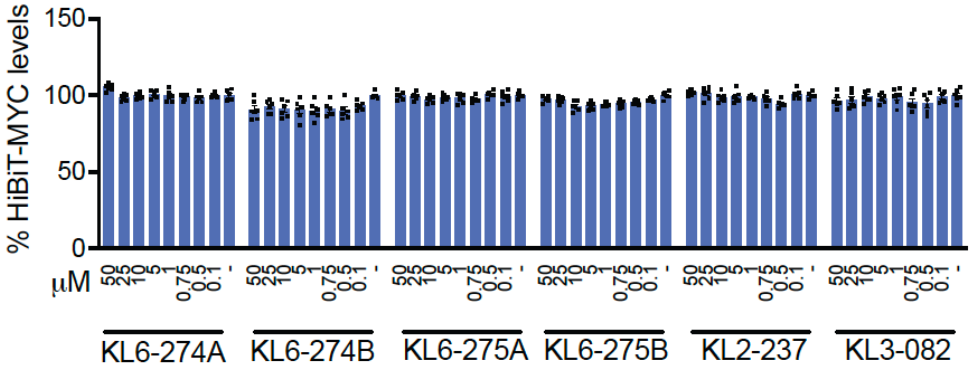

Figure S1: Dose-response of HiBiT-MYC degradation with analogs lacking an aziridine. (a) Structures of unreactive analogs of KL2-236 and their stereoisomers. **(b)** HiBiT-MYC HEK293-LgBiT cells were treated with DMSO vehicle or compounds for 24 h, and HiBiT-MYC levels were detected by luminescence. Data shown are individual replicate values and average ± sem from n=6 biologically independent replicates/group.

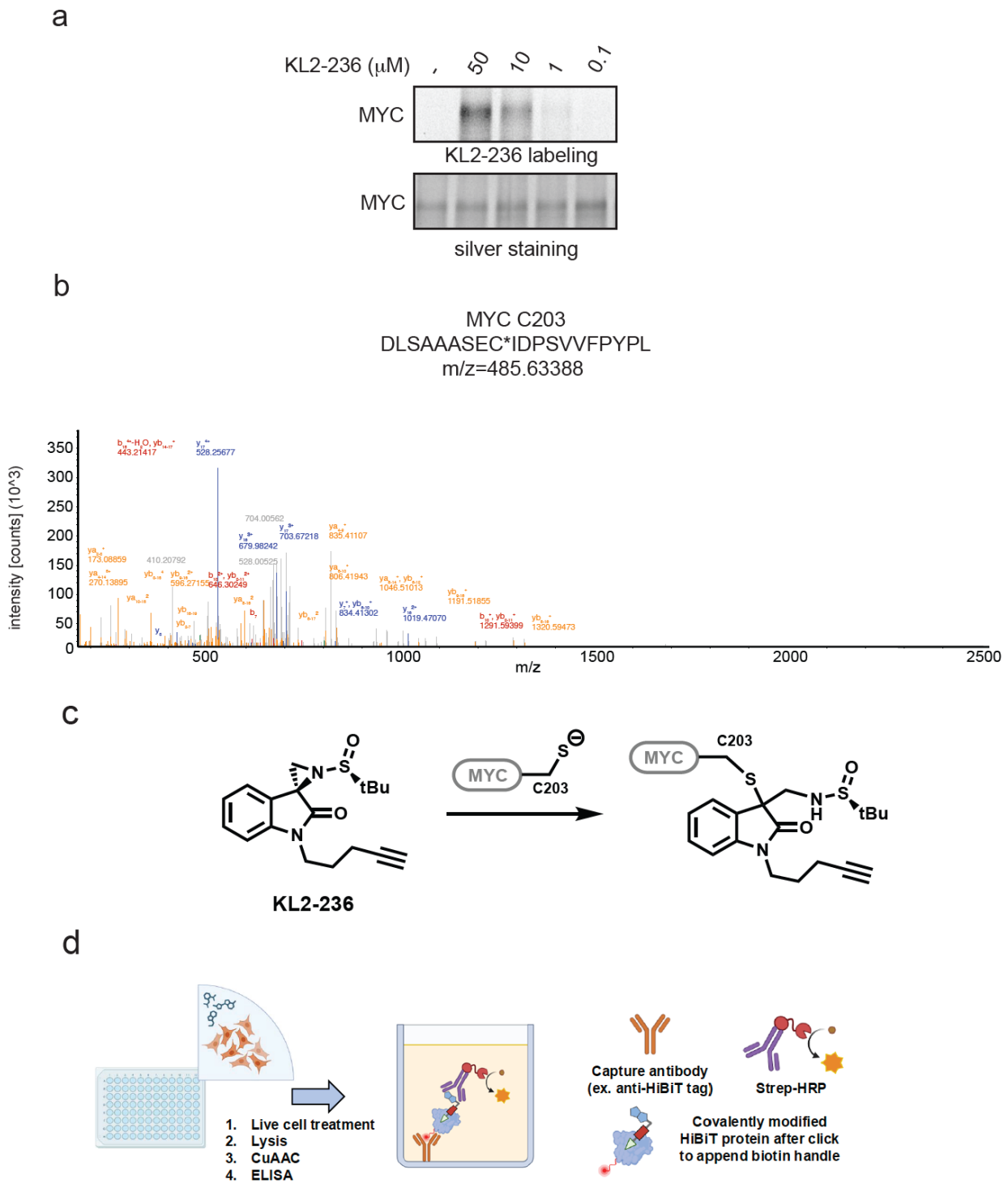

Figure S2: Characterization of KL2-236 binding to MYC. (a) Gel-based ABPP of KL2-236 with pure human MYC protein. Pure MYC human protein was treated with DMSO vehicle or KL2-236 for 1 h, after which probe-modified protein was subjected to CuAAC with an azide conjugated rhodamine, separated by SDS/PAGE and visualized by in-gel fluorescence **(a)**. Gels were silver-stained to account for MYC protein loading. **(b)** Reaction of KL2-236 with MYC based on incubation of KL2-236 (50 μM, 1 hr) with pure human MYC/MAX protein (1 μM), digestion of

the complex with pepsin, and analysis of probe-modified peptides by LC-MS/MS**.** Shown is the MS/MS spectra of the KL2-236 modified peptide. **(c)** Shown are the possible KL2-236 adducts on MYC C203. **(d)** Schematic of ELISA-ABPP based on data shown in Figure 3.4**g**. Data in **(a,b)** are representative from an n=3 biologically independent replicates per group.

Appendix 2: Supporting Tables Legends

All supporting tables have been included in the online submission of this dissertation but can also be found at https://onlinelibrary.wiley.com/doi/10.1002/anie.202508518 under Supporting Information.

Table S1. Chemoproteomic Profiling of KL2-236. Chemoproteomic profiling of KL2-236 versus DMSO vehicle-treatment in PSN1 cells. PSN1 cells were pretreated with BTZ for 1 hr before treatment with DMSO vehicle or KL2-236 (50 μM) for 4 h, after which probe-modified proteins were subjected to CuAAC with an azide-functionalized biotin, after which probe-modified proteins were enriched with avidin beads, eluted, pulldown eluate was tryptically digested and analyzed and quantified by LC-MS/MS. Data are from n=3 biologically independent replicates per group.

Table S2. Chemoproteomic Profiling of KL2-236 versus KL4-019. Chemoproteomic profiling of KL2-236 versus KL4-019-treatment in PSN1 cells. PSN1 cells were pretreated with BTZ for 1 hr before treatment with KL2-236 (50 μM) or KL4-019 (50 μM) for 4 h, after which probe-modified proteins were subjected to CuAAC with an azide-functionalized biotin, after which probe-modified proteins were enriched with avidin beads, eluted, pulldown eluate was tryptically digested and analyzed and quantified by LC-MS/MS. Data are from n=3 biologically independent replicates per group.

Table S3. MS-ABPP of KL2-236 labeling of PSN1 proteomes. Chemoproteomic profiling of KL2-236 (50 μM) in PSN1 cell lysate. PSN1 cells were pre-treated with proteasome inhibitor (500 nM) for 1 h and then co-treated with KL2-236 (50 μM) for 4 h. Cells were then lysed and probe-modified proteins were subjected to CuAAC with a desthiobiotin-functionalized avidin, after which probe-modified proteins were enriched with avidin beads, eluted, pulldown eluate was tryptically digested and probe-modified peptides were eluted and analyzed and quantified by LC-MS/MS. Also shown are IA-alkyne probe-modification data as a comparison taken from previously published

Table S4. RNA Sequencing of KL2-236 Treatment in PSN1 Cells. RNA sequencing of KL2-236 and KL4-019 in PSN1 cells. PSN1 cells were treated with DMSO vehicle or KL2-236 of KL4-019 (50 μM) for 2 h. Resulting RNA from treated cells were sequenced and quantified. Gene enrichment analysis shows significantly altered pathways and normalized enrichment scores. This table also includes raw counts, enrichment rankings, and GSEA permutations.

Table S5. Quantitative Proteomic Profiling of KL4-219A. Quantitative proteomic profiling of KL4-219A in PSN1 cells. PSN1 cells were treated with DMSO vehicle or KL4-219A (50 μM) for 8h. Protein level changes were assessed by TMT-based quantitative proteomic methods. Data are from n=3 biologically independent replicates/group.

Table S6. Chemoproteomic Profiling of KL4-219A Against KL2-236 Pulldown. PSN1 cells were pre-treated with proteasome inhibitor bortezomib (500 nM) for 30 min prior to treatment with DMSO vehicle or KL4-219A (100 μM) for 1 h and then treatment with KL2-236 (25 μM) for 4 h, after which resulting cell lysates were subjected to CuAAC mediated appendage of an azide-functionalized biotin handle, probe-modified proteins were enriched, tryptically digested, and analyzed by TMT-based quantitative proteomics.

Table S7. Chemoproteomic Profiling of KL6-085A. Chemoproteomic profiling of KL6-

BTZ for 1 hr before treatment with DMSO vehicle or KL6-085A (50 μM) for 24 h, after which probe-modified proteins were subjected to CuAAC with an azide-functionalized biotin, after which probe-modified proteins were enriched with avidin beads, eluted, pulldown eluate was tryptically digested and analyzed and quantified by LC-MS/MS. Data are from n=3 biologically independent replicates per group.

Table S8. Chemoproteomic Profiling of KL6-085A versus KL6-085B. Chemoproteomic profiling of KL6-085A versus KL6-085B-treatment in PSN1 cells. PSN1 cells were pretreated with BTZ for 1 hr before treatment with KL6-085A (50 μM) or KL6-085B (50 μM) for 24 h, after which probe-modified proteins were subjected to CuAAC with

avidin beads, eluted, pulldown eluate was tryptically digested and analyzed and quantified by LC-MS/MS. Data are from n=3 biologically independent replicates per group.

Appendix 3: Raw Images

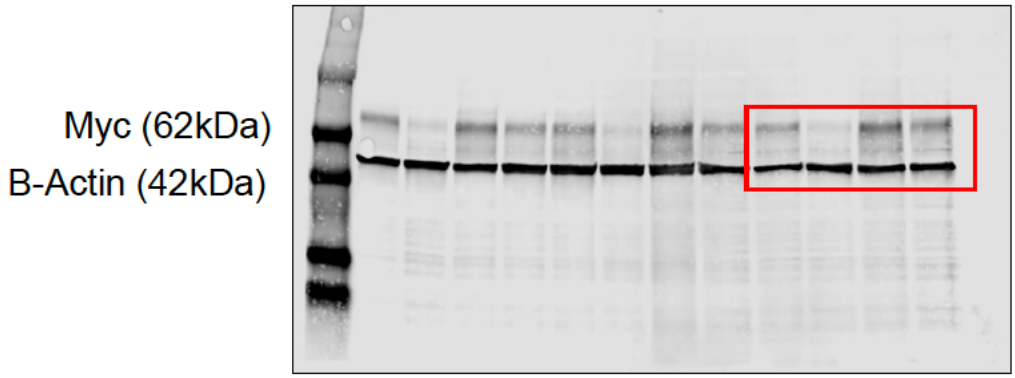

Appendix 3 Figure 1: Raw Image Blot in Figure 3.3c

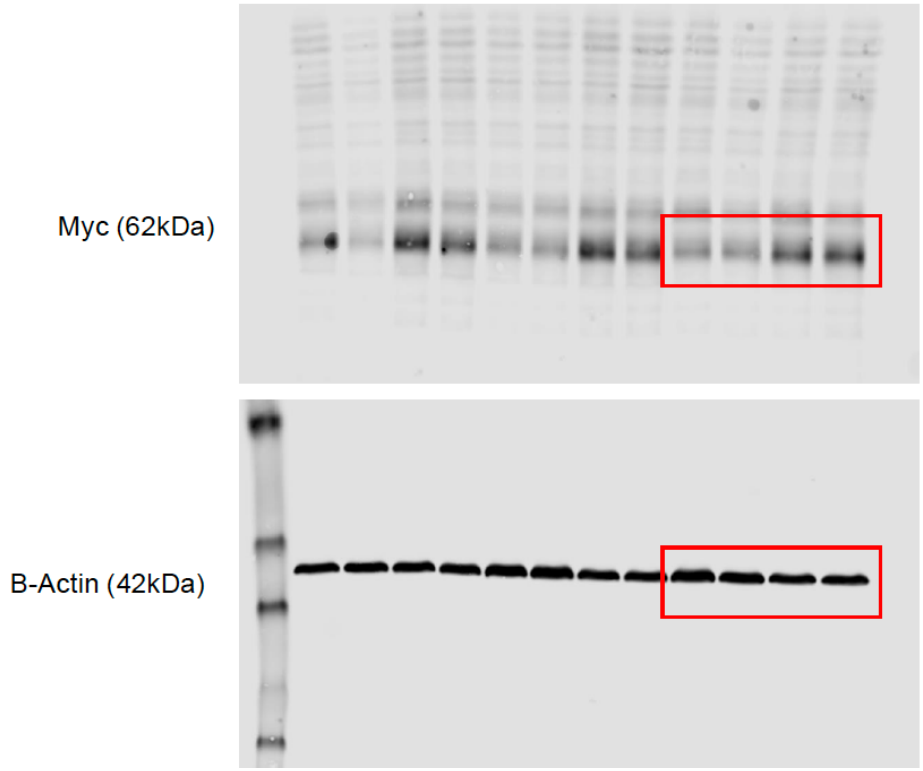

Appendix 3 Figure 2: Raw Image for Blot in Figure 3.3e

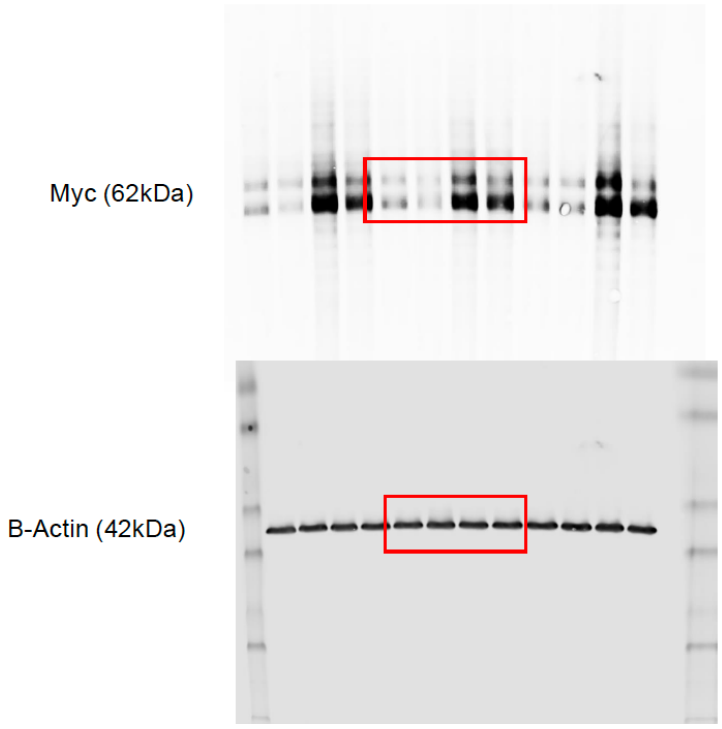

Appendix 3 Figure 3: Raw Image for Blot in Figure 2.2g

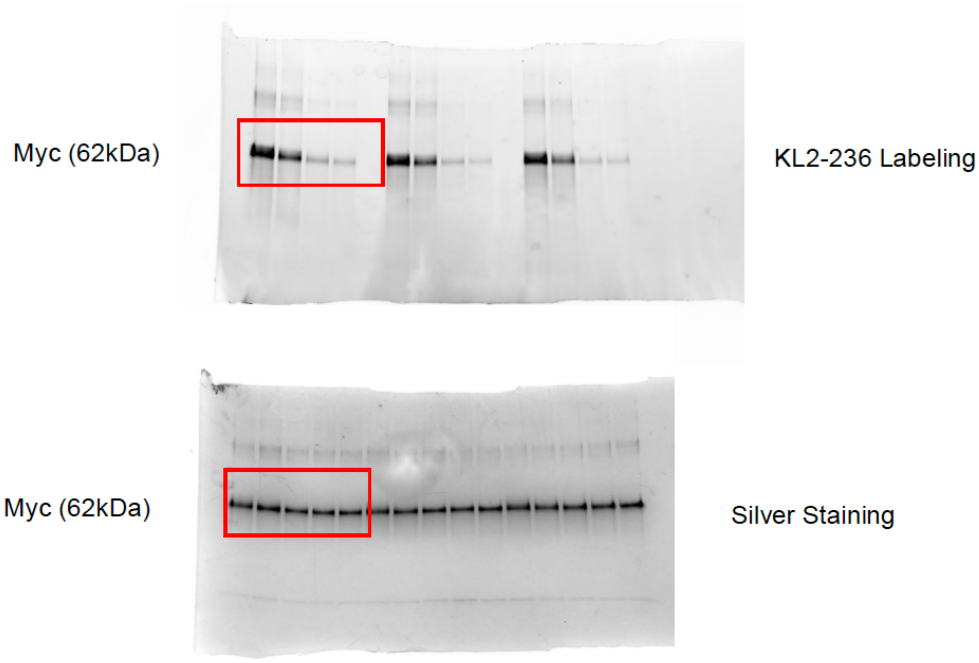

Appendix 3 Figure 4: Raw Image for Gel in Figure 3.4a

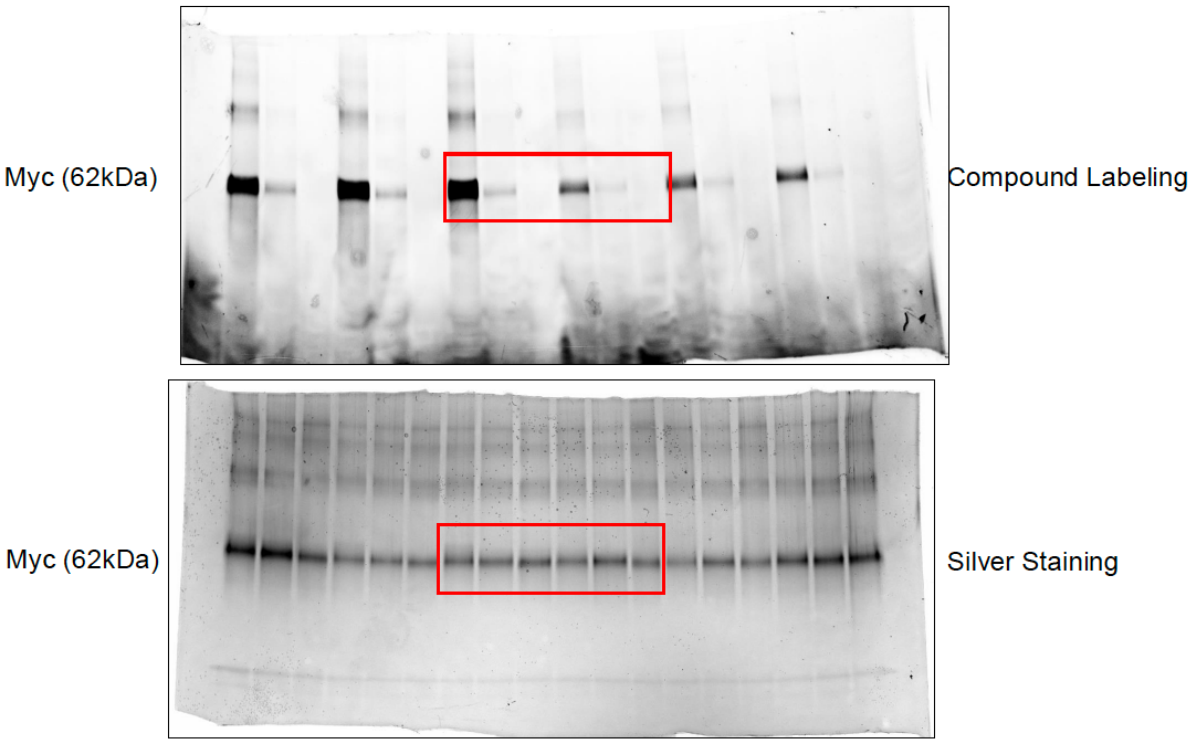

Appendix 3 Figure 5: Raw Image for Gel in Figure 4.3c

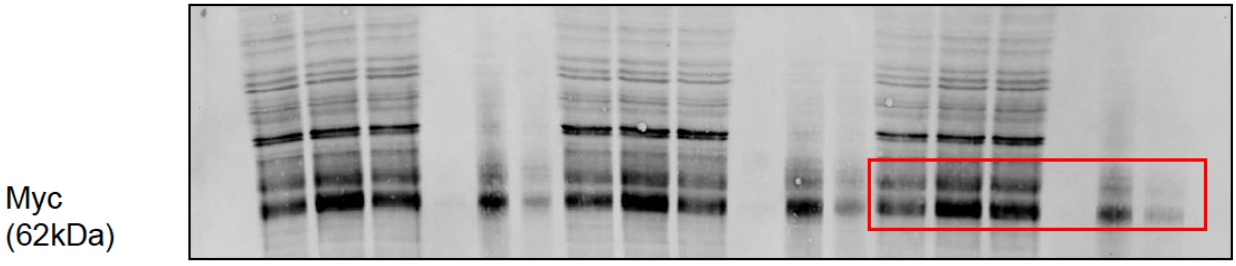

Appendix 3 Figure 6: Raw Image of Blot in Figure 4.3d

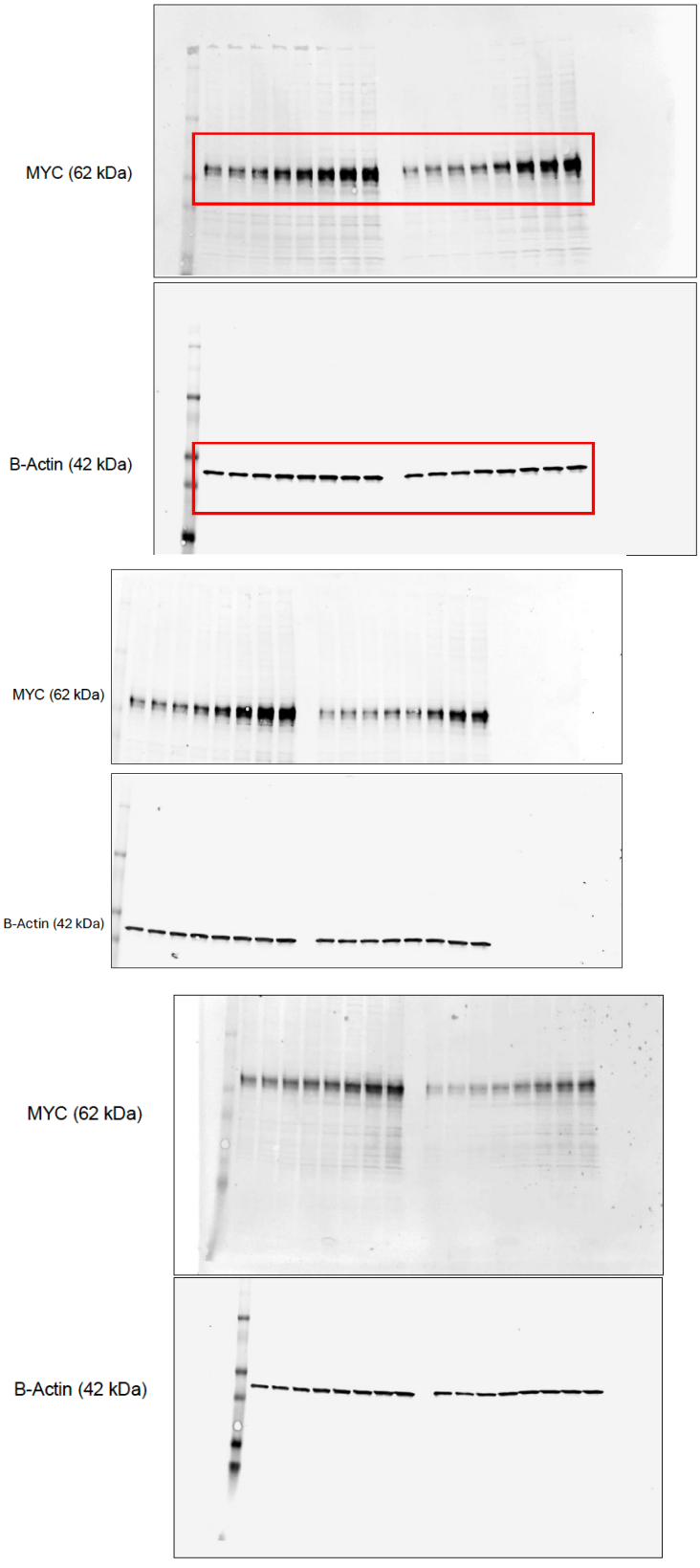

Appendix 3 Figure 7: Raw Image for Blot in Figure 3.6a

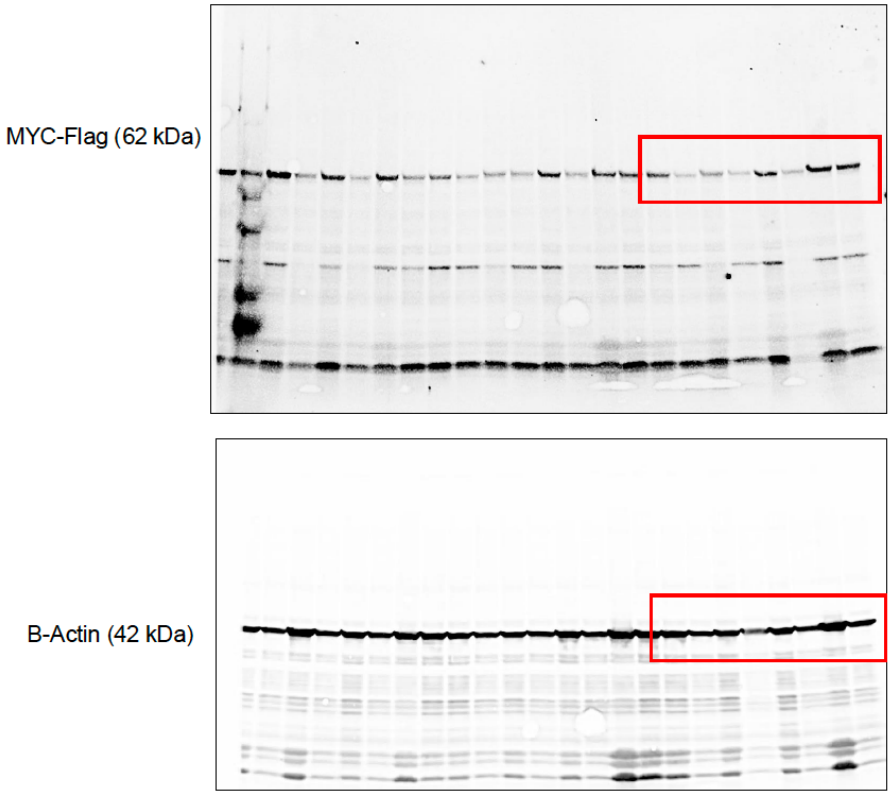

Appendix 3 Figure 8: Raw Image for Blot in Figure 4.6c

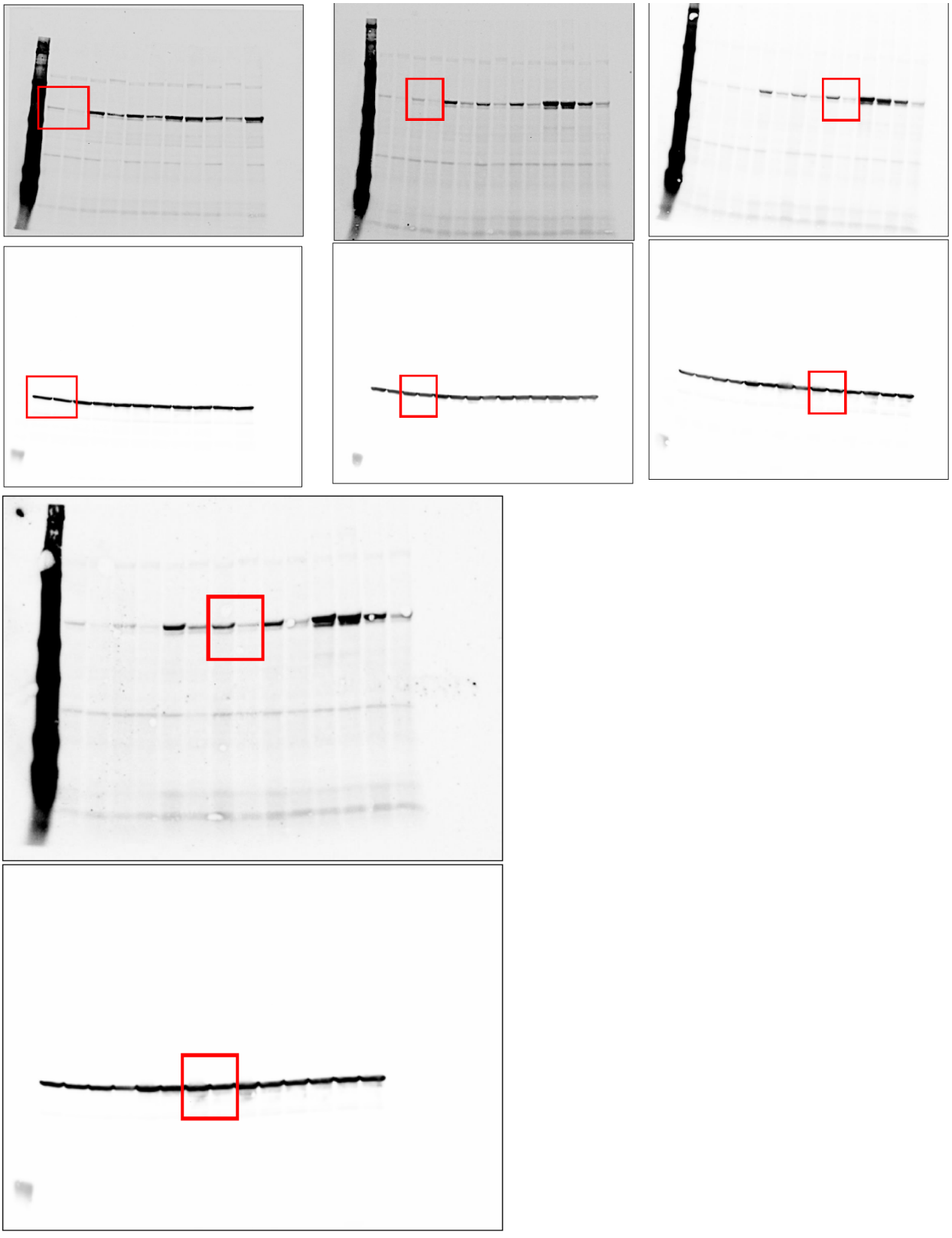

Appendix 3 Figure 9: Raw Image of Blot in Figure 3.9a

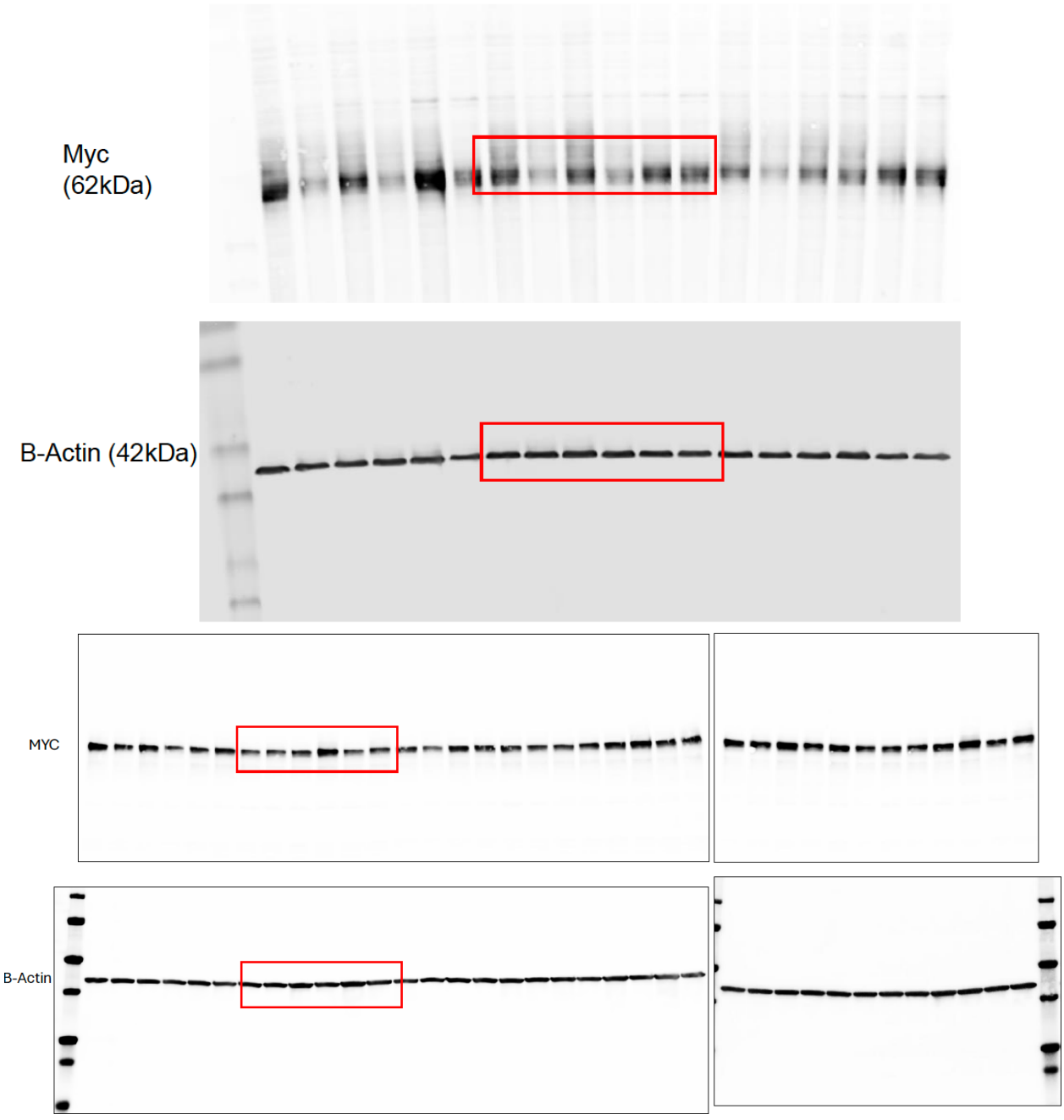

Appendix 3 Figure 10: Raw Image for Blot in Figure 3.12a

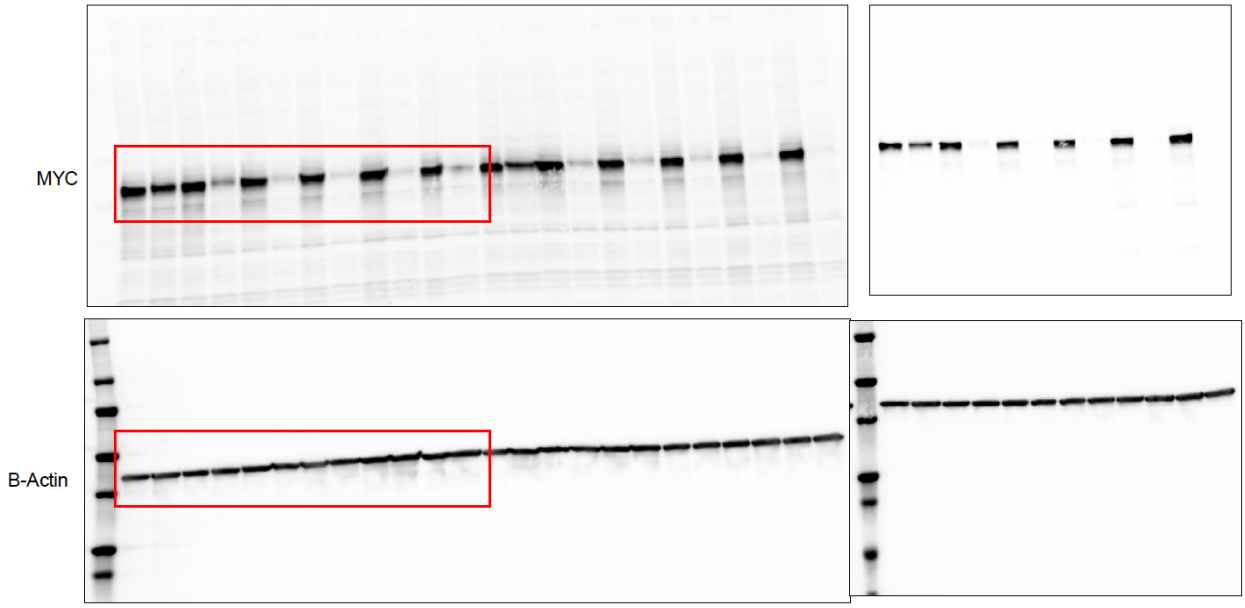

Appendix 3 Figure 11: Raw Image for Blot in Figure 3.14c

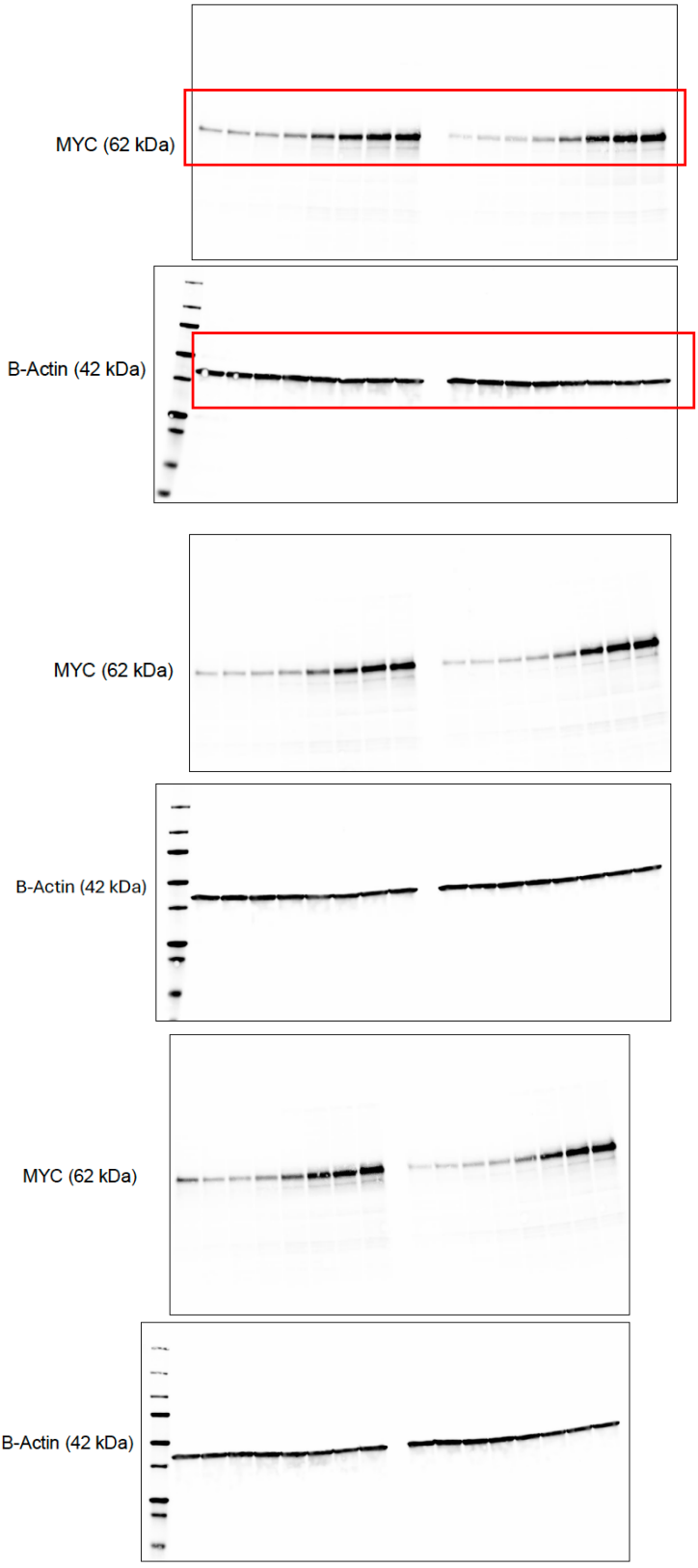

Appendix 3 Figure 12: Raw Image for Blot in Figure 3.14f

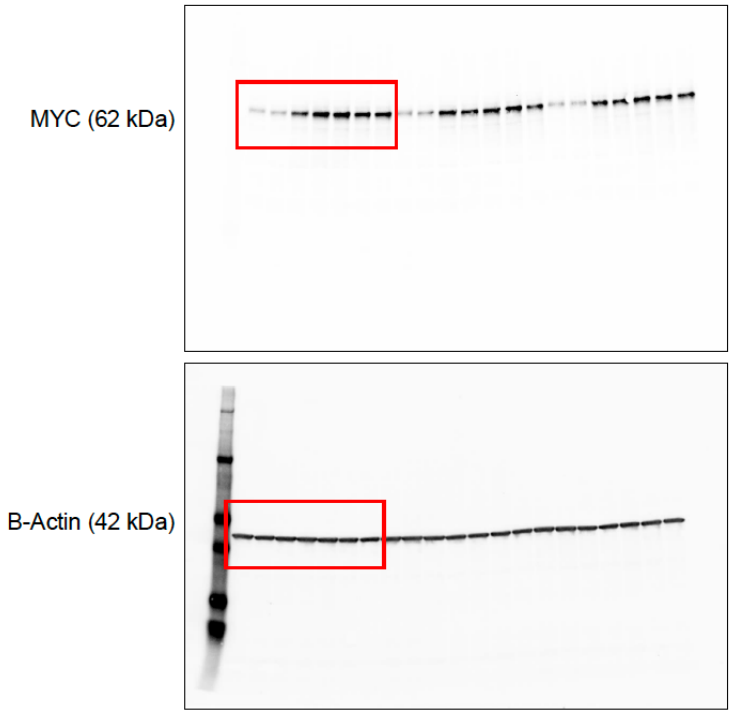

Appendix 3 Figure 13: Raw Image for Blot in Figure 3.15a

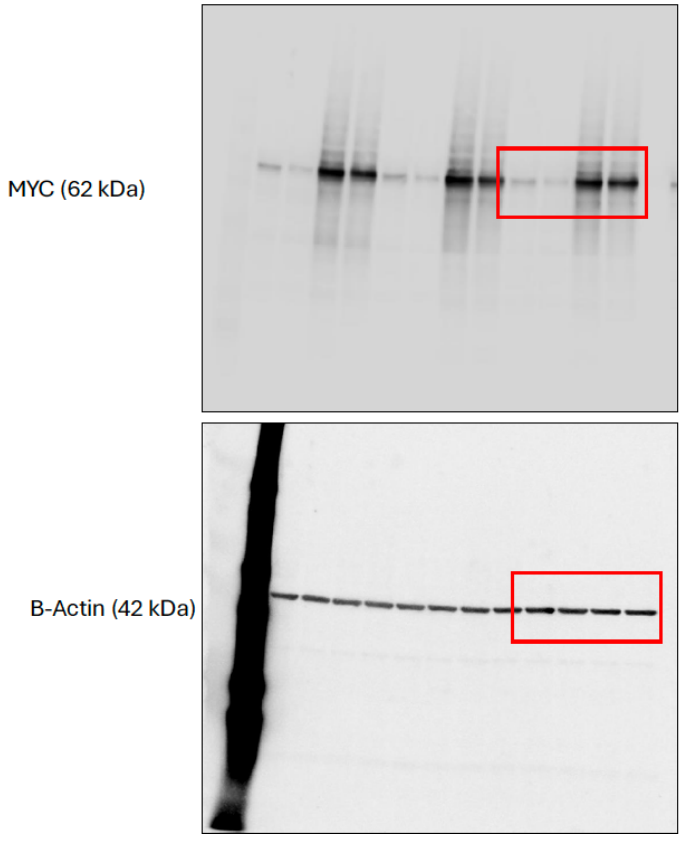

Appendix 3 Figure 14: Raw Image for Blot in 3.16a

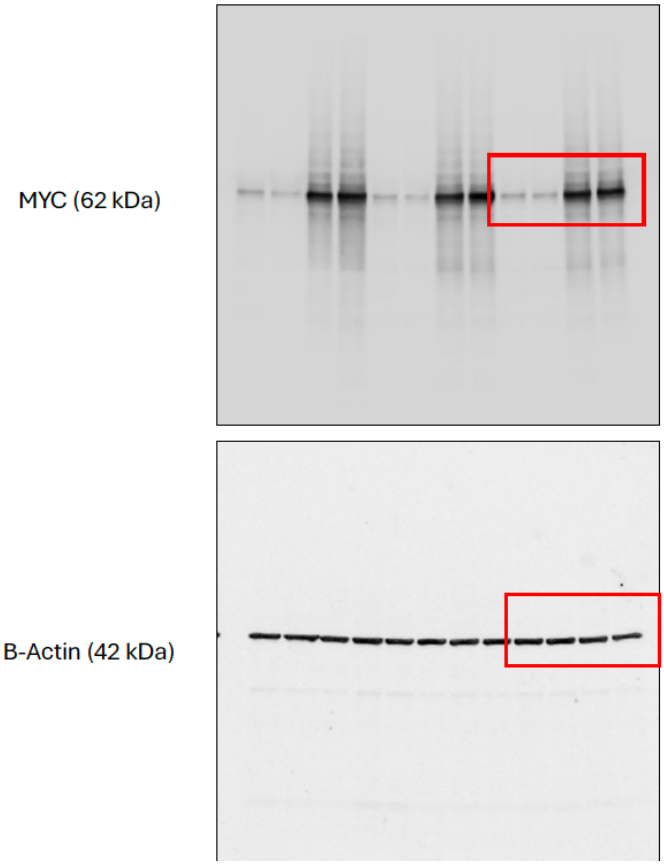

Appendix 3 Figure 15: Raw Image for Blot in 3.16c

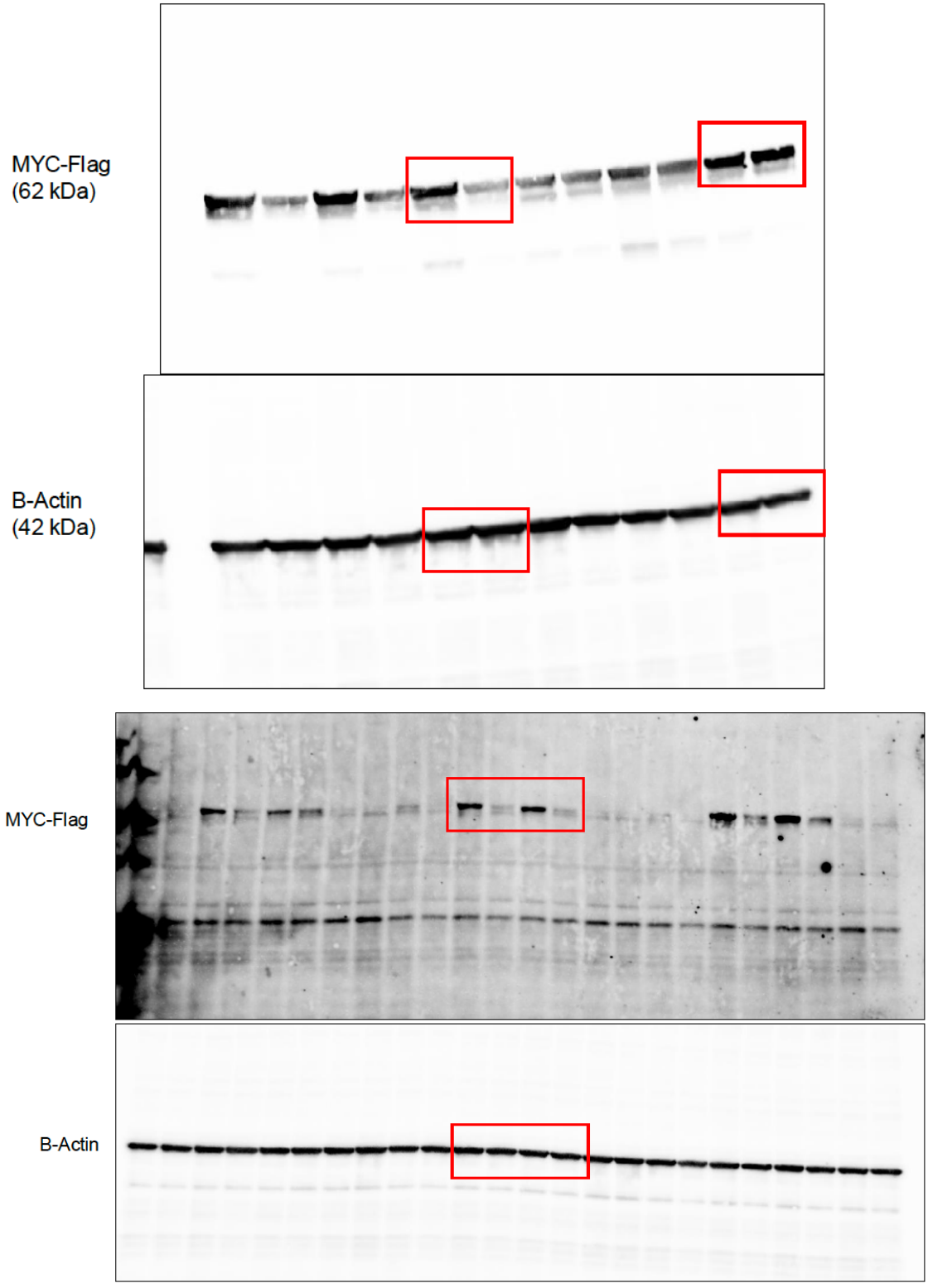

Appendix 3 Figure 16: Raw Image for Blot in Figure 3.17a

Appendix 4: NMR Spectra

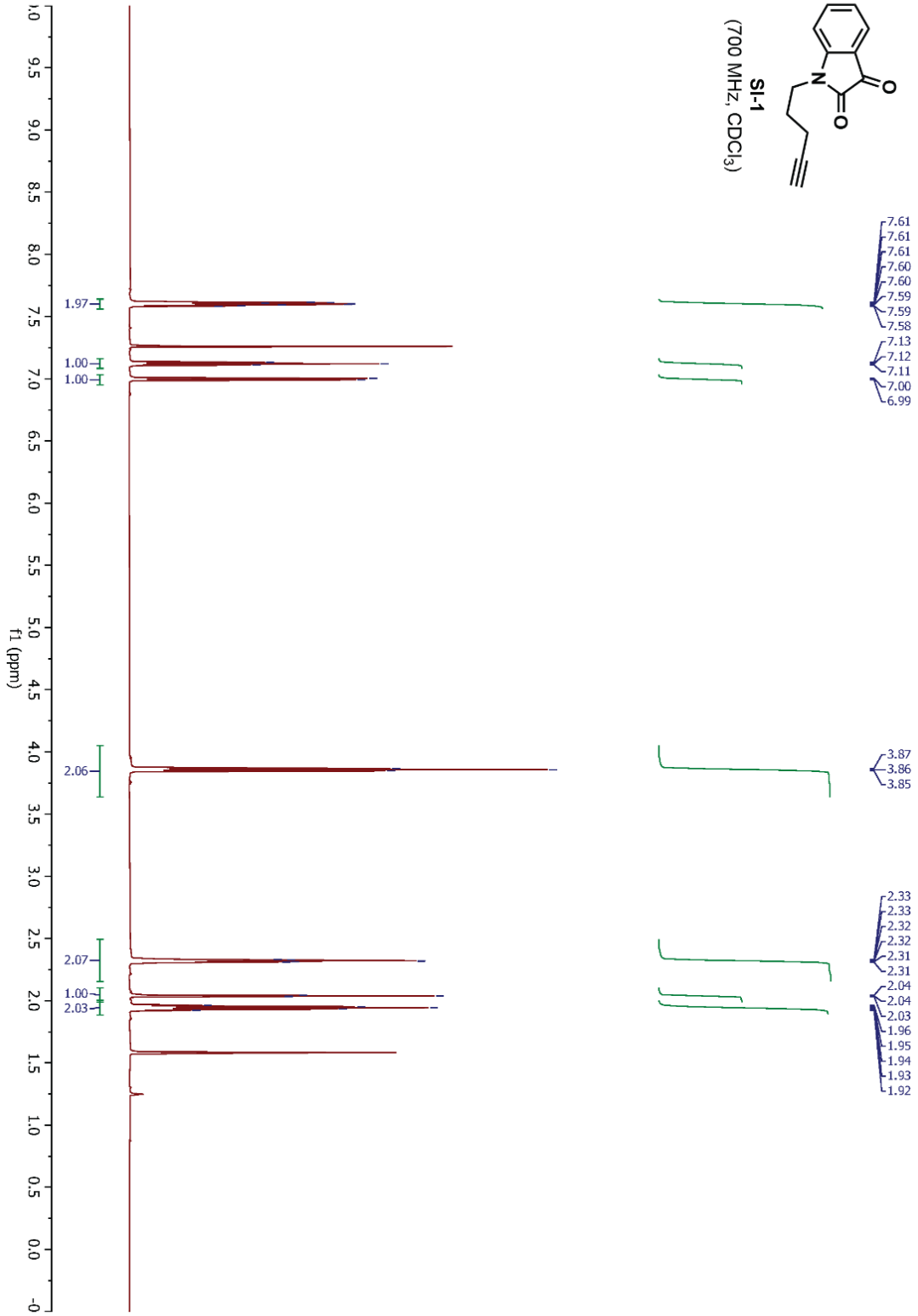

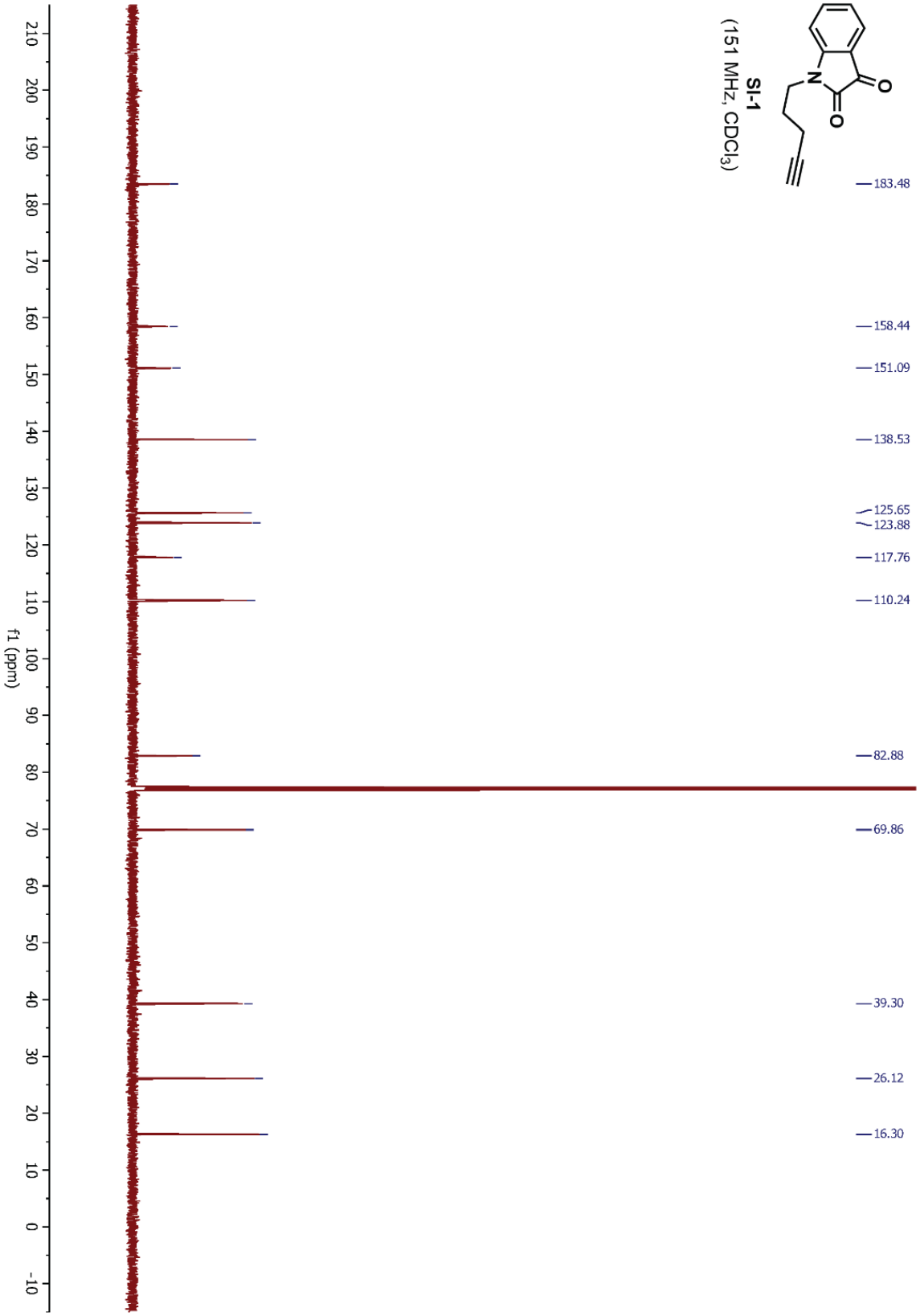
SI-1
(151 MHz, CDCl3)
183.48
158.44
151.09
138.53
125.65
123.88
117.76
110.24
82.88
69.86
39.30
26.12
16.30
f1 (ppm)

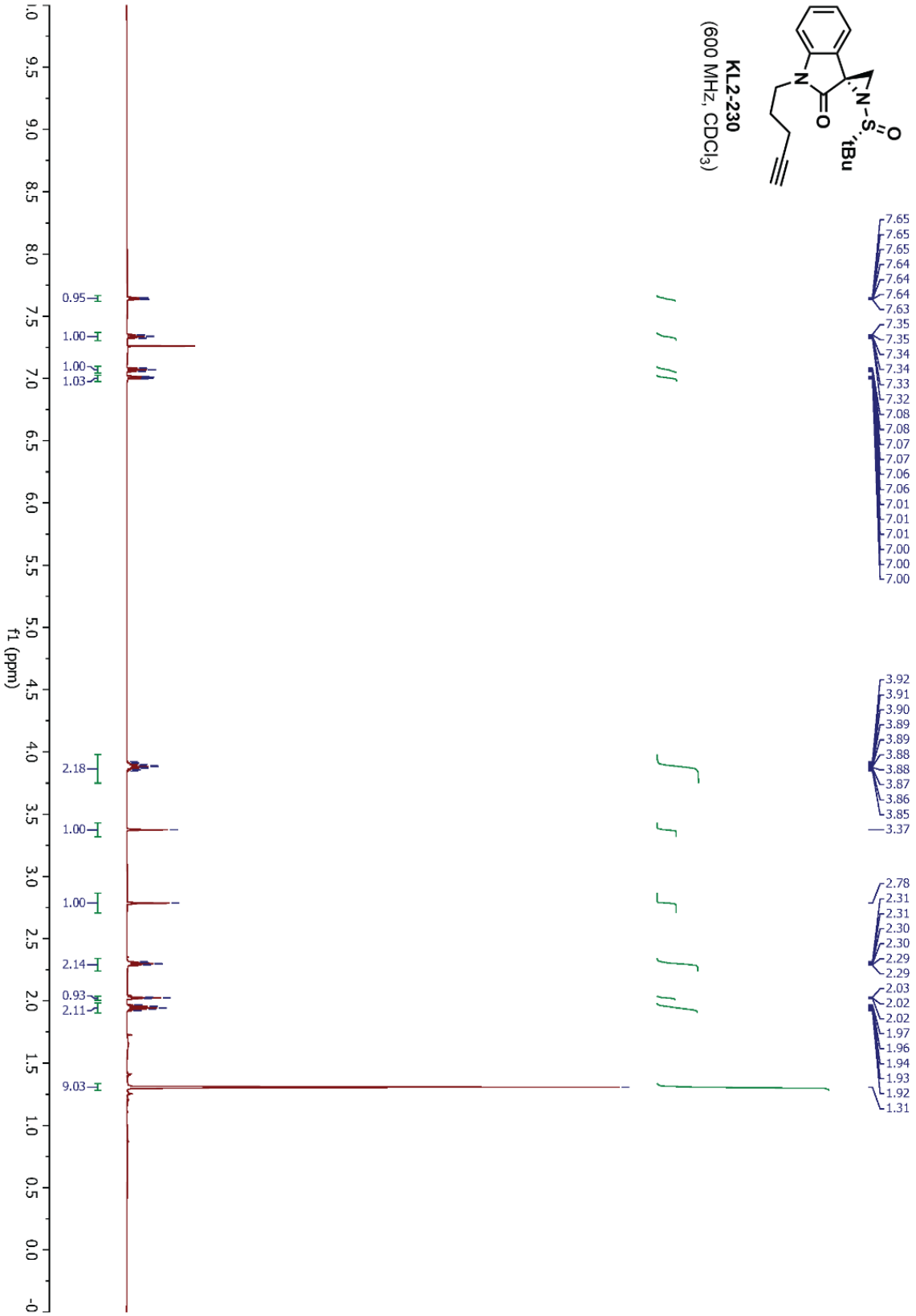
KL2-230
(600 MHz, CDCl3)
f1 (ppm)
0.95
1.00
1.00
1.03
2.18
1.00
1.00
2.14
0.93
2.11
9.03
7.65
7.65
7.65
7.64
7.64
7.64
7.63
7.35
7.35
7.34
7.34
7.33
7.32
7.08
7.08
7.07
7.07
7.06
7.06
7.01
7.01
7.01
7.00
7.00
7.00
3.92
3.91
3.90
3.89
3.89
3.88
3.88
3.87
3.86
3.85
3.37
2.78
2.31
2.31
2.30
2.30
2.29
2.29
2.03
2.02
2.02
1.97
1.96
1.94
1.93
1.92
1.31

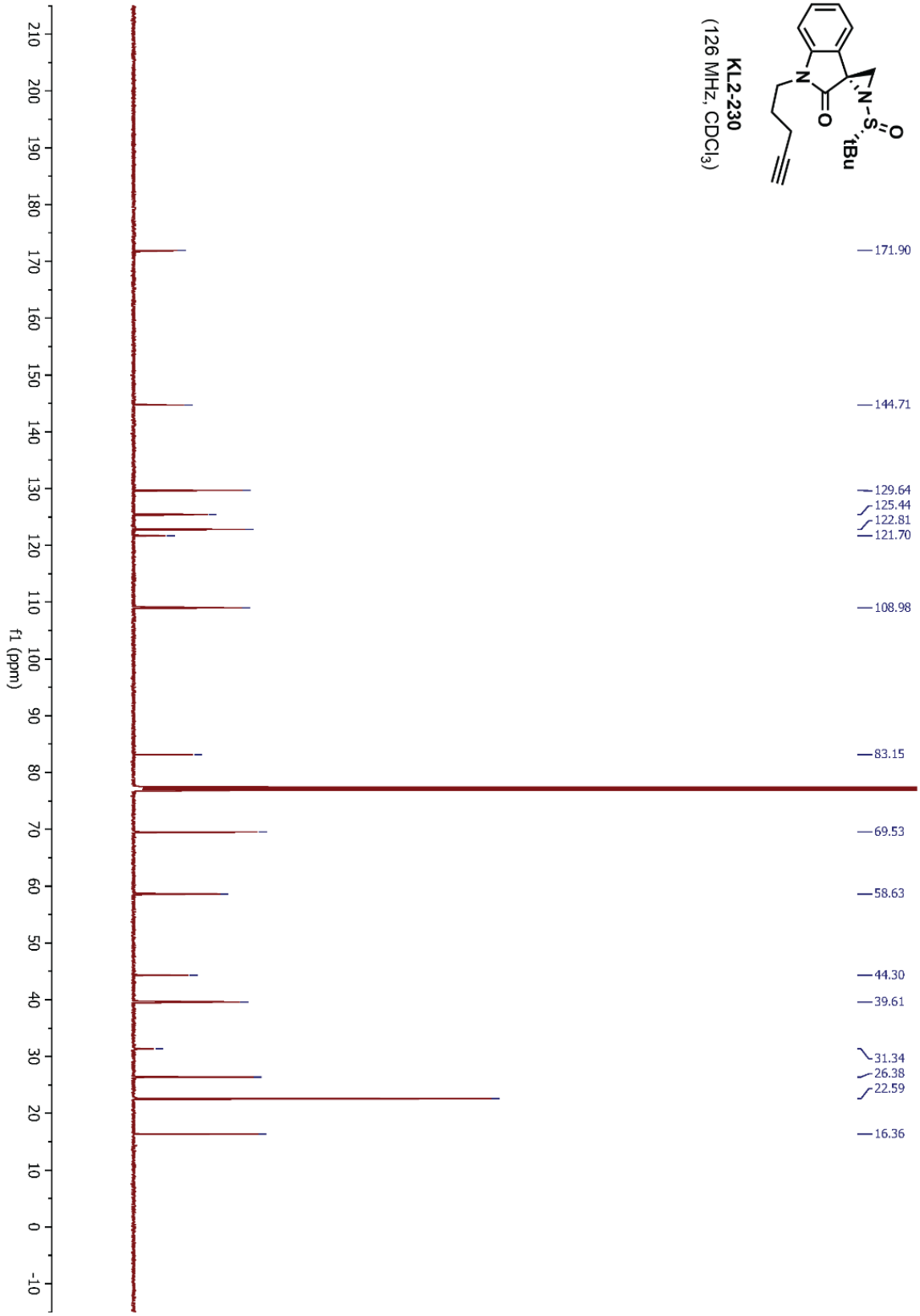
KL2-230
(126 MHz, CDCl3)
171.90
144.71
129.64
125.44
122.81
121.70
108.98
83.15
69.53
58.63
44.30
39.61
31.34
26.38
22.59
16.36
f1 (ppm)

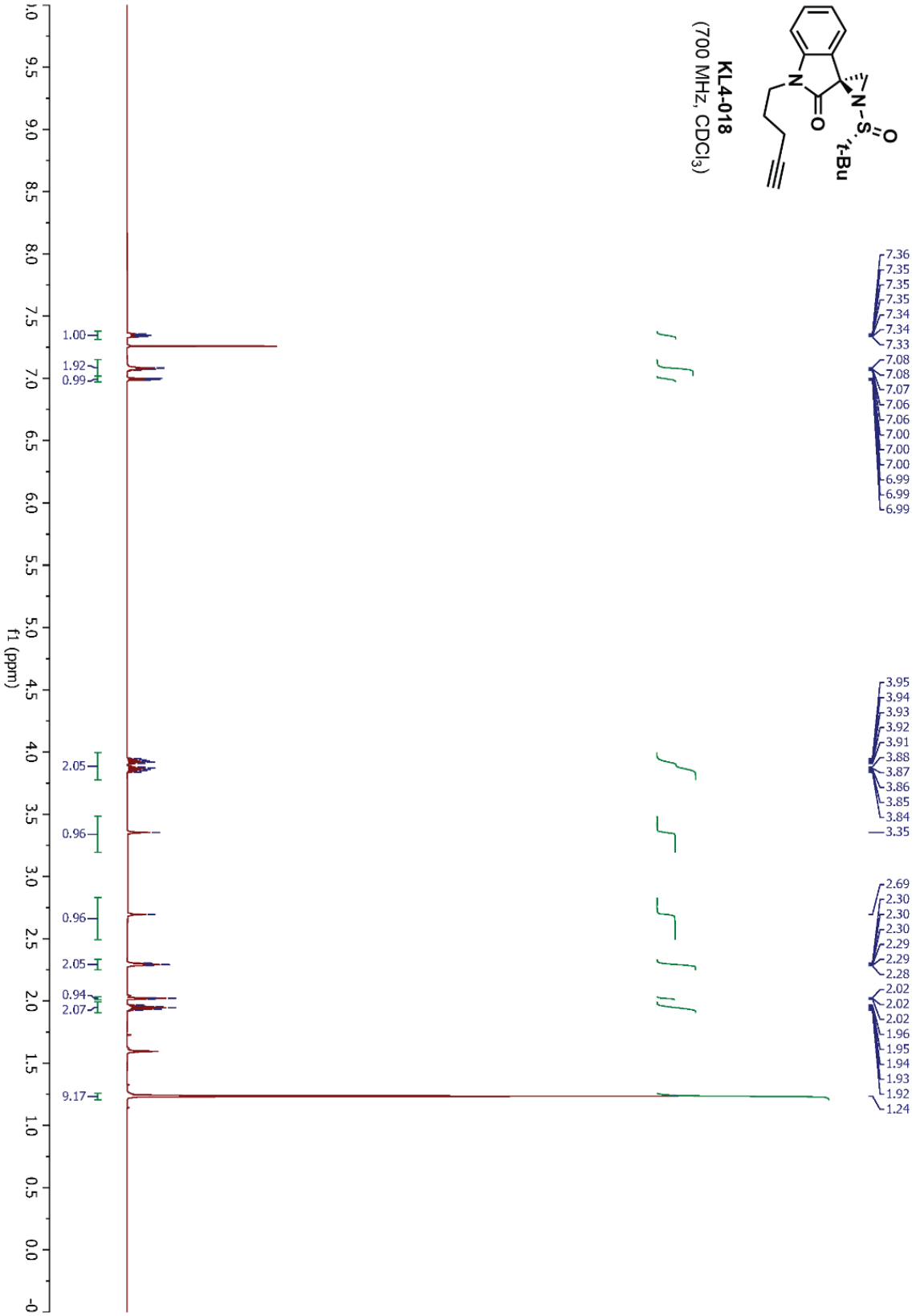
KL4-018
(700 MHz, CDCl3)
N
O
N-S
O
t-Bu
f1 (ppm)
1.00
1.92
0.99
2.05
0.96
0.96
2.05
0.94
2.07
9.17
7.36
7.35
7.35
7.35
7.34
7.34
7.33
7.08
7.08
7.07
7.06
7.06
7.00
7.00
7.00
6.99
6.99
6.99
3.95
3.94
3.93
3.92
3.91
3.88
3.87
3.86
3.85
3.84
3.35
2.69
2.30
2.30
2.30
2.29
2.29
2.28
2.02
2.02
2.02
1.96
1.95
1.94
1.93
1.92
1.24

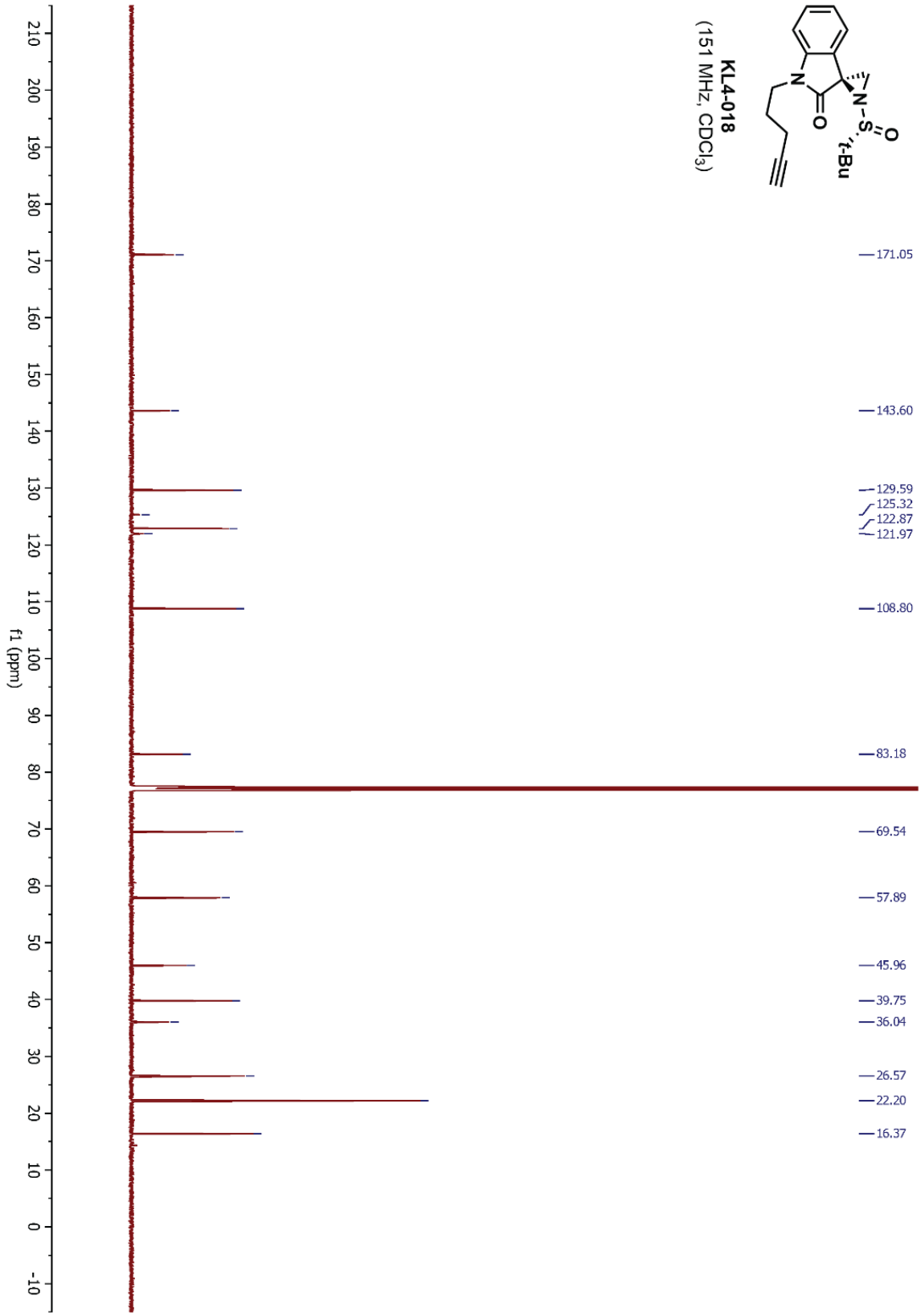
KL4-018
(151 MHz, CDCl3)
171.05
143.60
129.59
125.32
122.87
121.97
108.80
83.18
69.54
57.89
45.96
39.75
36.04
26.57
22.20
16.37
f1 (ppm)

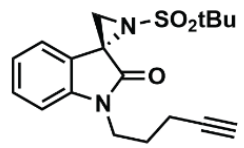

KL2-168
(700 MHz, $CDCl_3$)

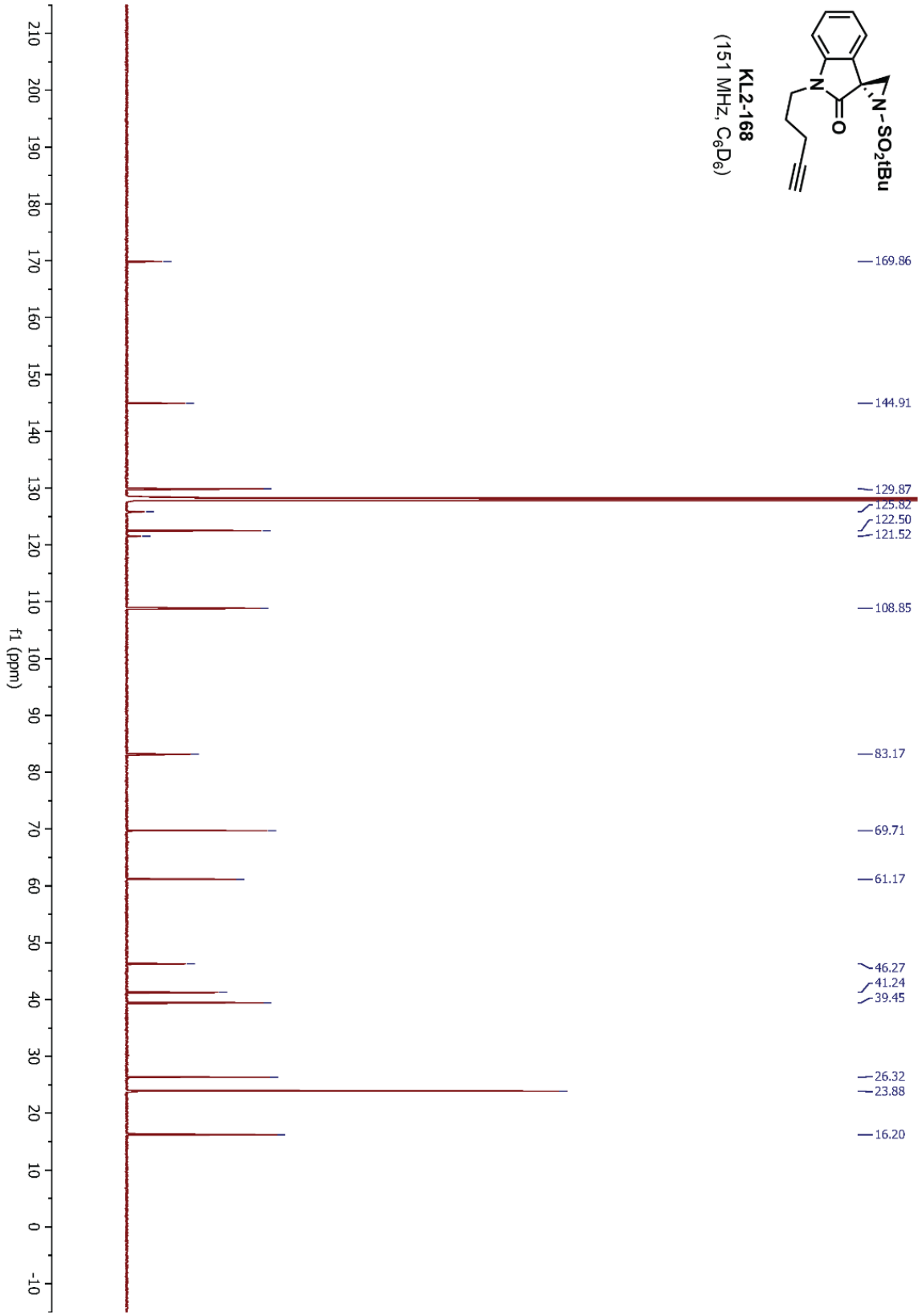
KL2-168
(151 MHz, C6D6)
N-SO2tBu
O
169.86
144.91
129.87
125.82
122.50
121.52
108.85
83.17
69.71
61.17
46.27
41.24
39.45
26.32
23.88
16.20
f1 (ppm)

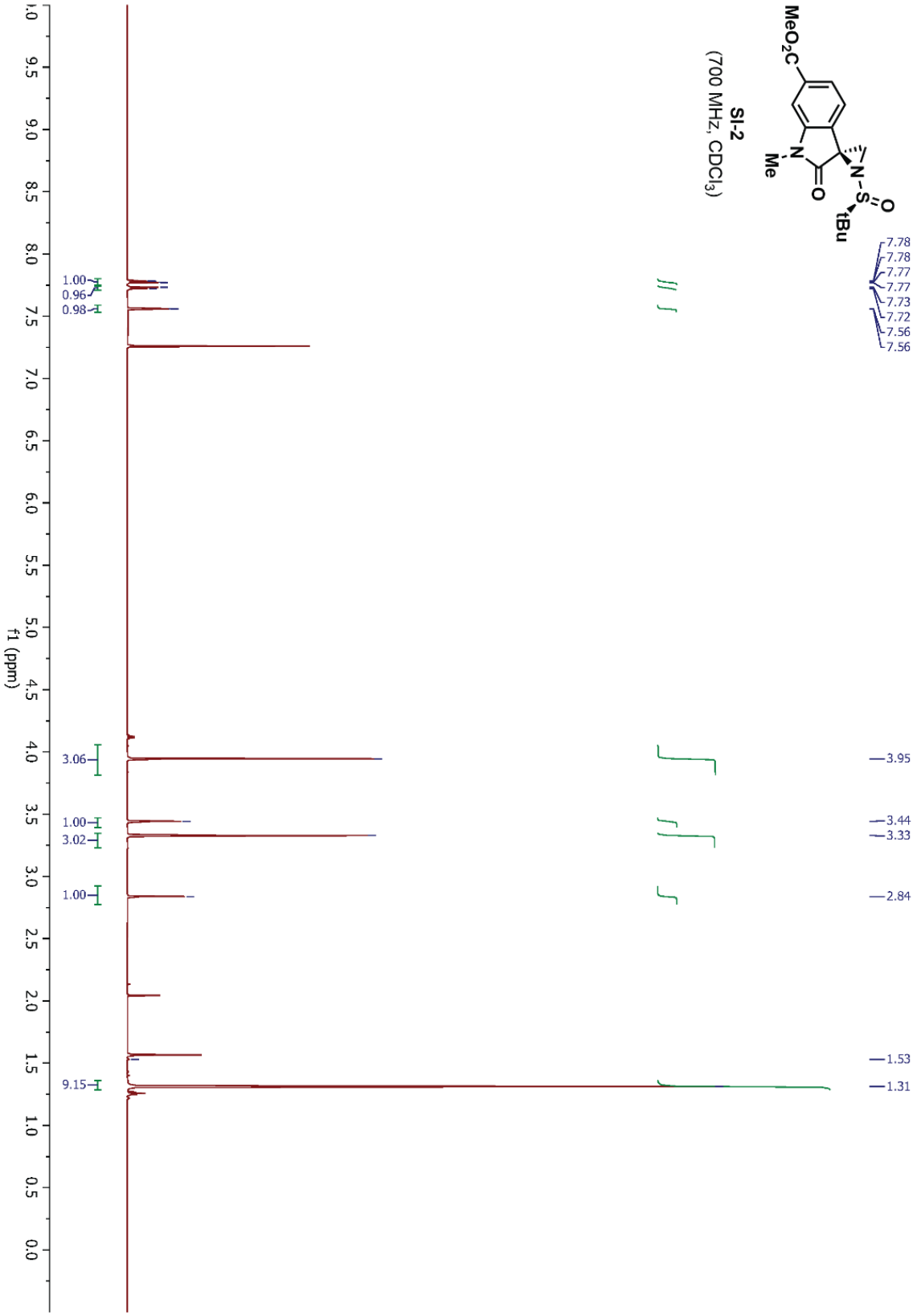
SI-2
(700 MHz, CDCl3)
MeO2C
N
Me
O
N
S
O
tBu
7.78
7.78
7.77
7.77
7.73
7.72
7.56
7.56
3.95
3.44
3.33
2.84
1.53
1.31
1.00
0.96
0.98
3.06
1.00
3.02
1.00
9.15
f1 (ppm)

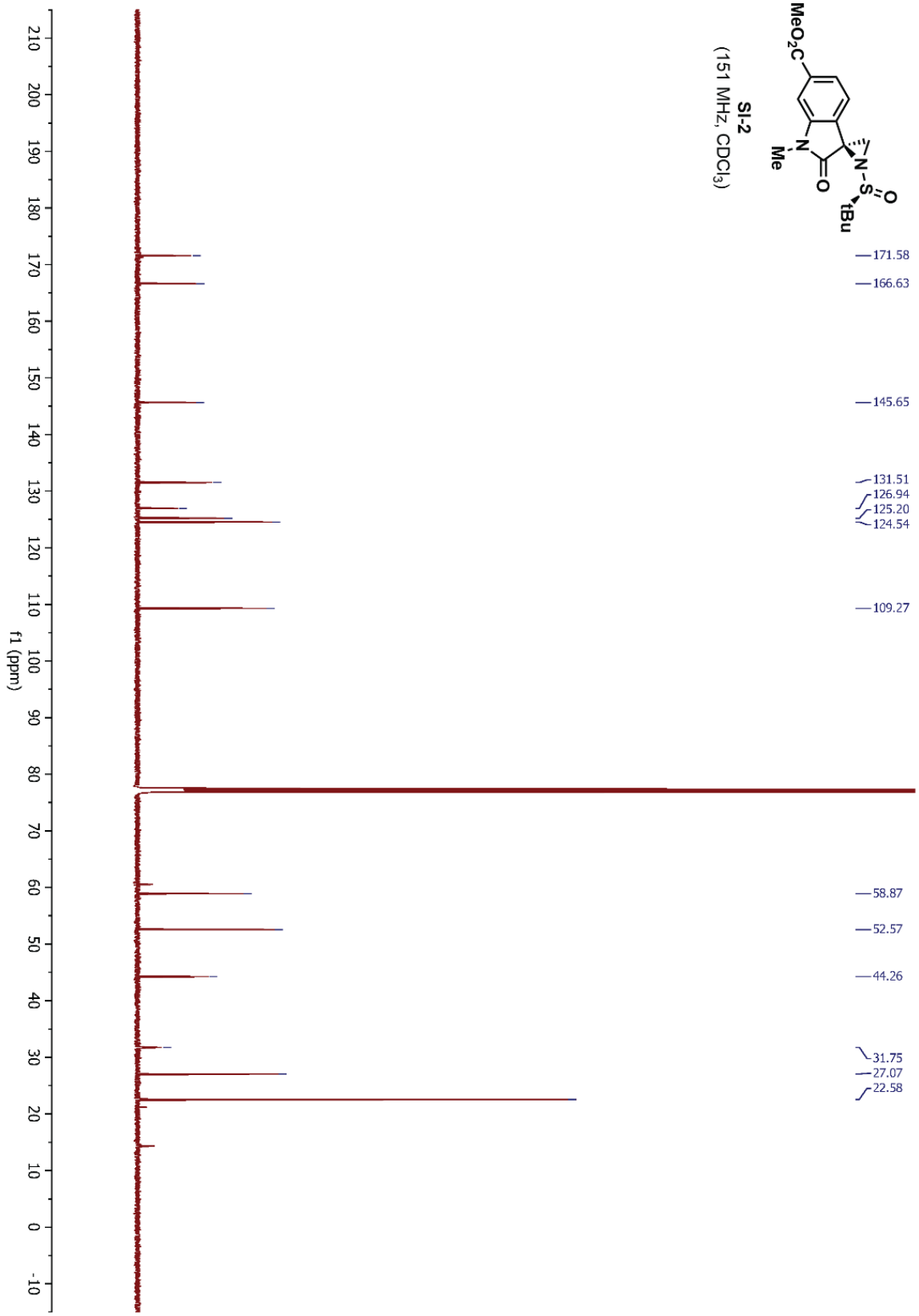
SI-2
(151 MHz, CDCl3)
MeO2C
N
Me
O
N
S
O
tBu
171.58
166.63
145.65
131.51
126.94
125.20
124.54
109.27
58.87
52.57
44.26
31.75
27.07
22.58
f1 (ppm)

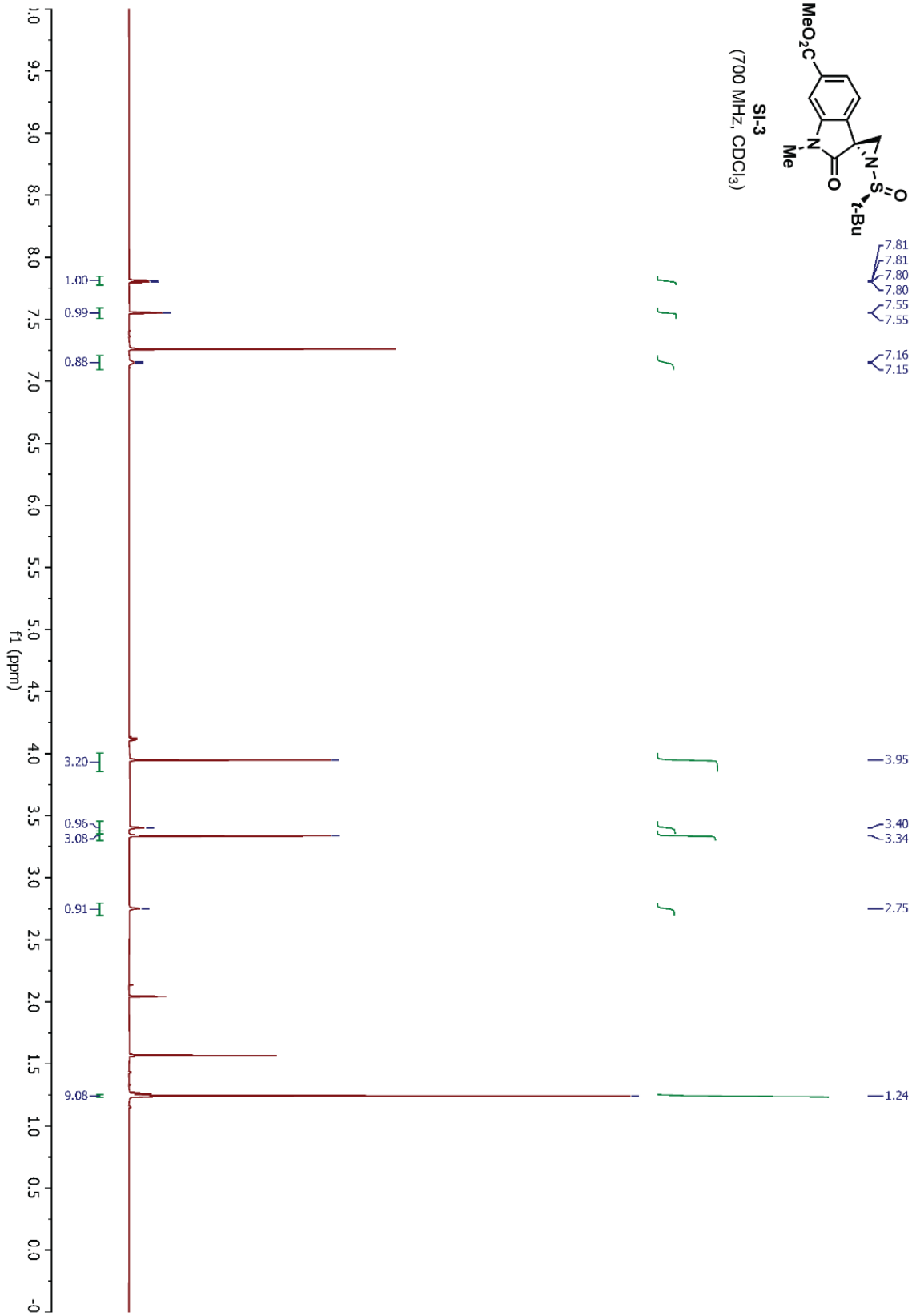
SI-3
(700 MHz, CDCl3)
MeO2C
N
Me
O
N
S
O
t-Bu
7.81
7.81
7.80
7.80
7.55
7.55
7.16
7.15
3.95
3.40
3.34
2.75
1.24
1.00
0.99
0.88
3.20
0.96
3.08
0.91
9.08
f1 (ppm)

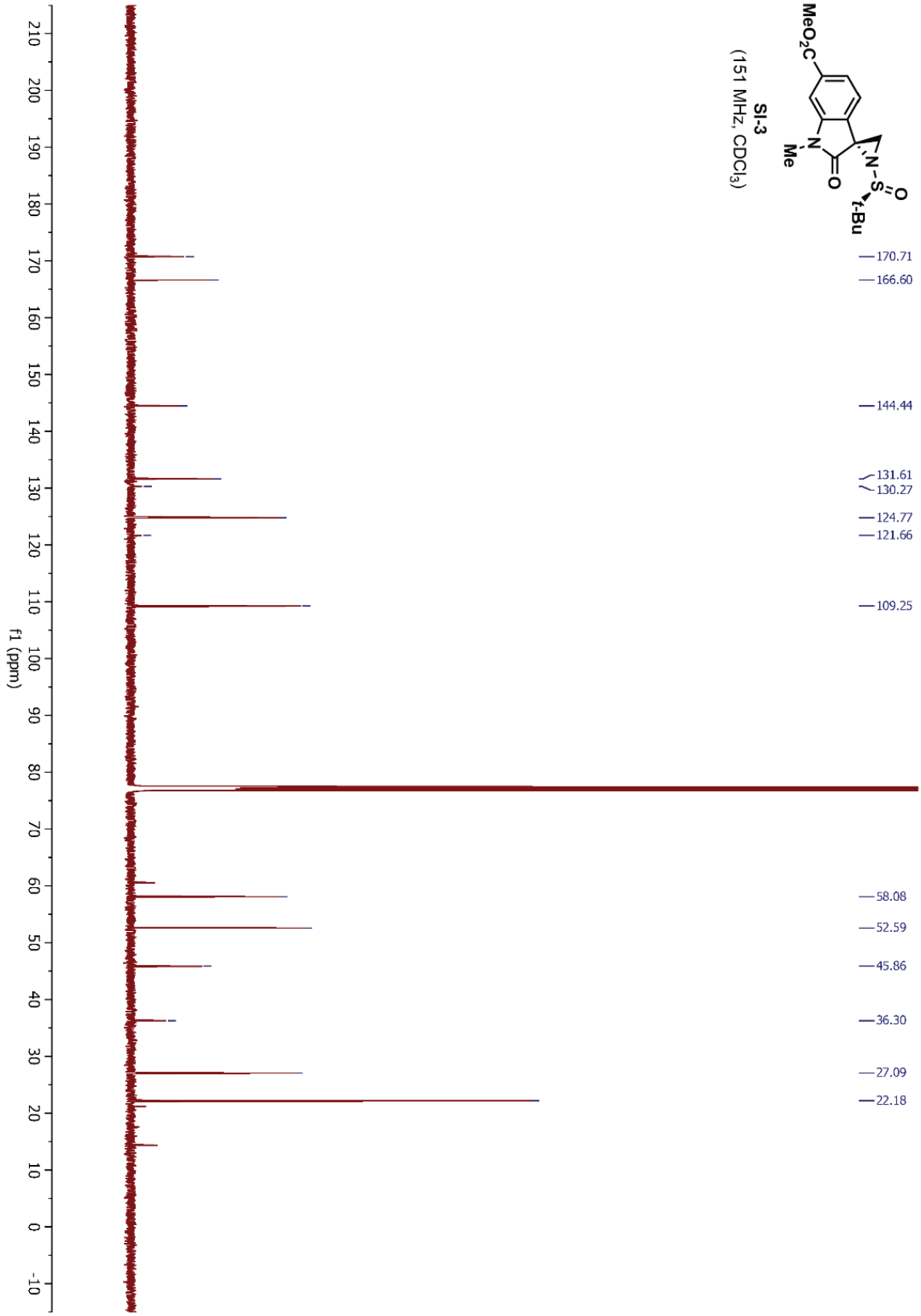
SI-3
(151 MHz, CDCl3)
MeO2C
N
Me
O
N
S
O
t-Bu
170.71
166.60
144.44
131.61
130.27
124.77
121.66
109.25
58.08
52.59
45.86
36.30
27.09
22.18
f1 (ppm)
210
200
190
180
170
160
150
140
130
120
110
100
90
80
70
60
50
40
30
20
10
0
-10

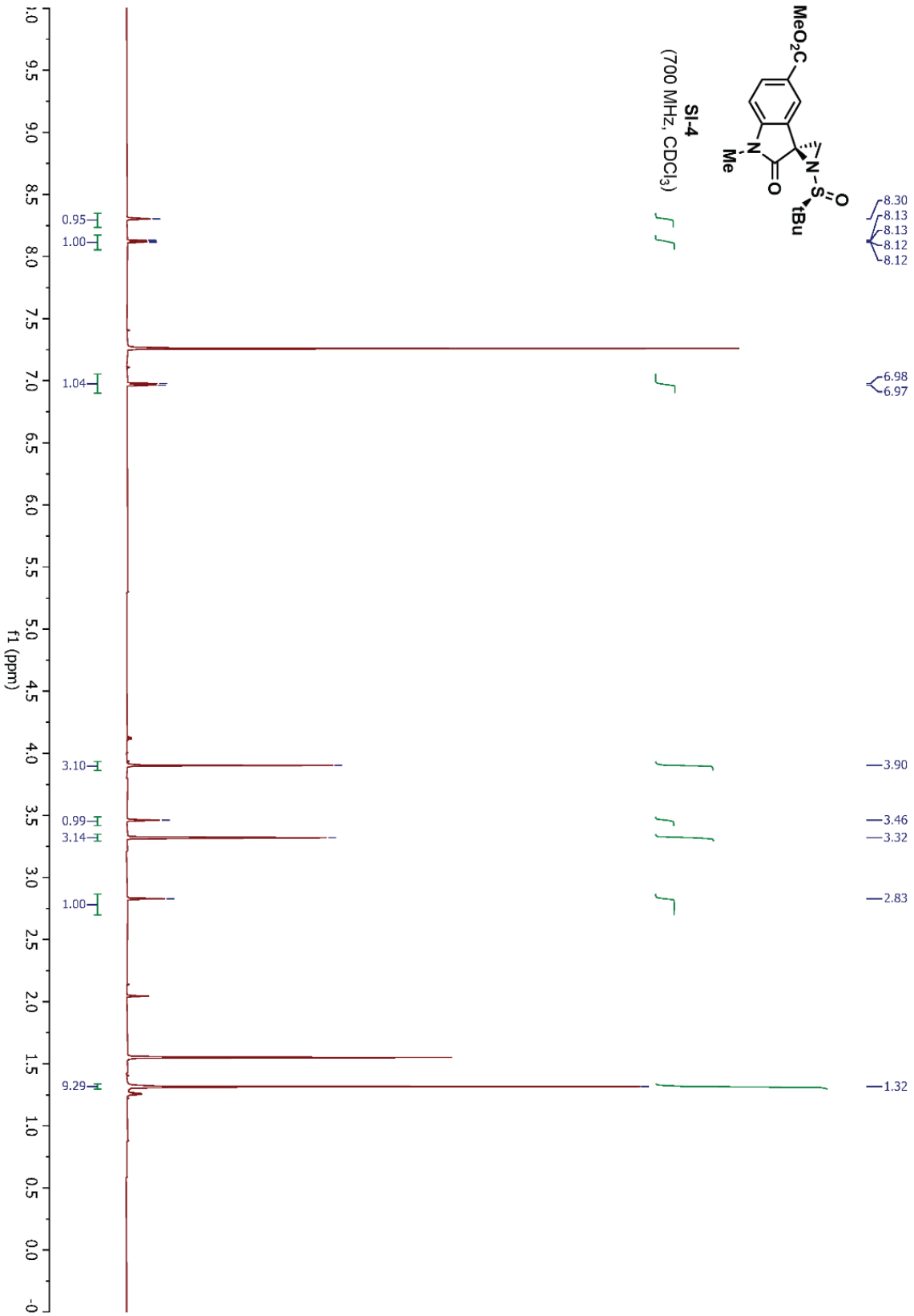
SI-4
(700 MHz, CDCl3)
MeO2C
N
Me
O
N
S
O
tBu
8.30
8.13
8.13
8.12
8.12
6.98
6.97
3.90
3.46
3.32
2.83
1.32
0.95
1.00
1.04
3.10
0.99
3.14
1.00
9.29
f1 (ppm)

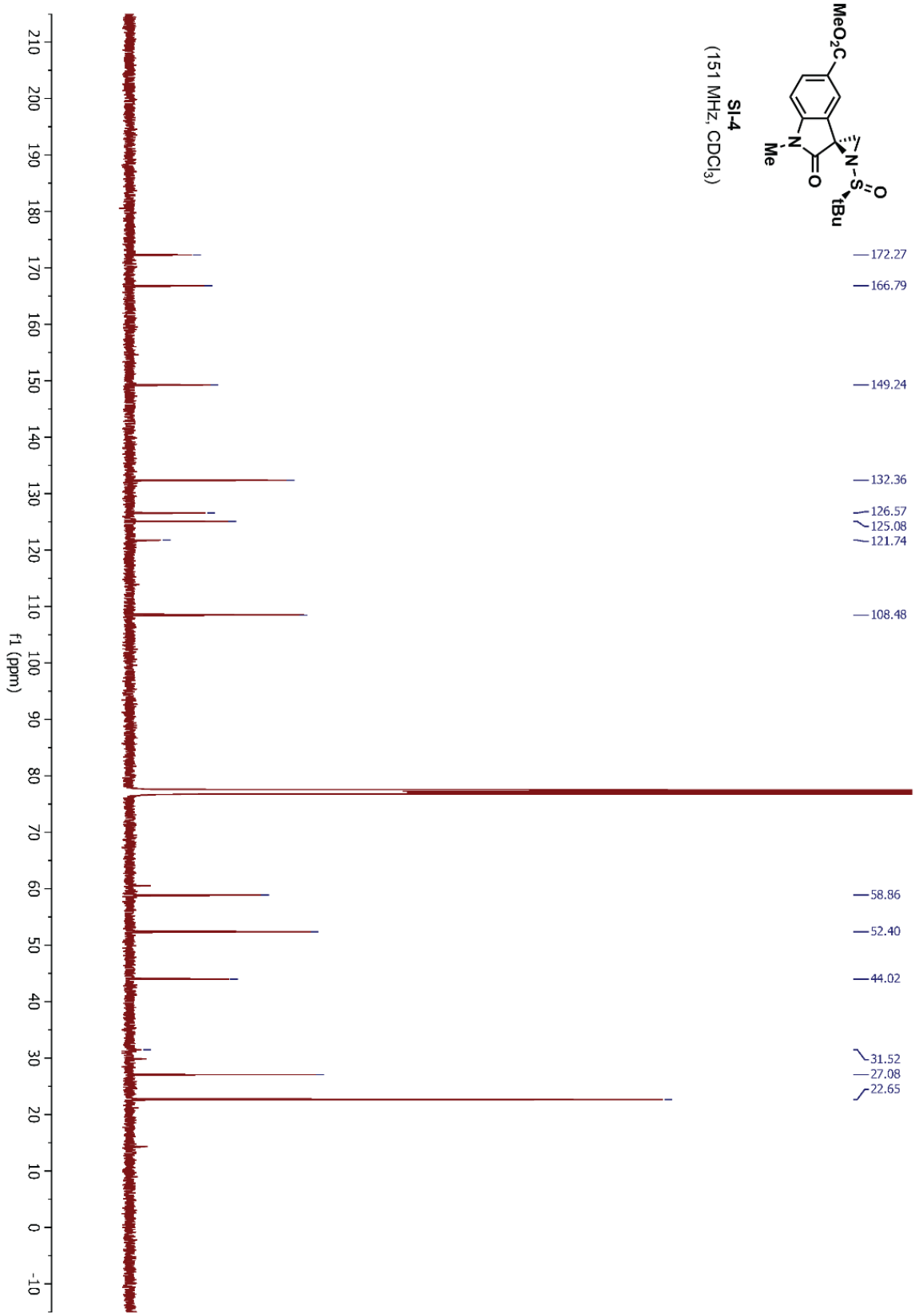
SI-4
(151 MHz, CDCl3)
MeO2C
N
Me
O
N
S
O
tBu
172.27
166.79
149.24
132.36
126.57
125.08
121.74
108.48
58.86
52.40
44.02
31.52
27.08
22.65
f1 (ppm)
210
200
190
180
170
160
150
140
130
120
110
100
90
80
70
60
50
40
30
20
10
0
-10

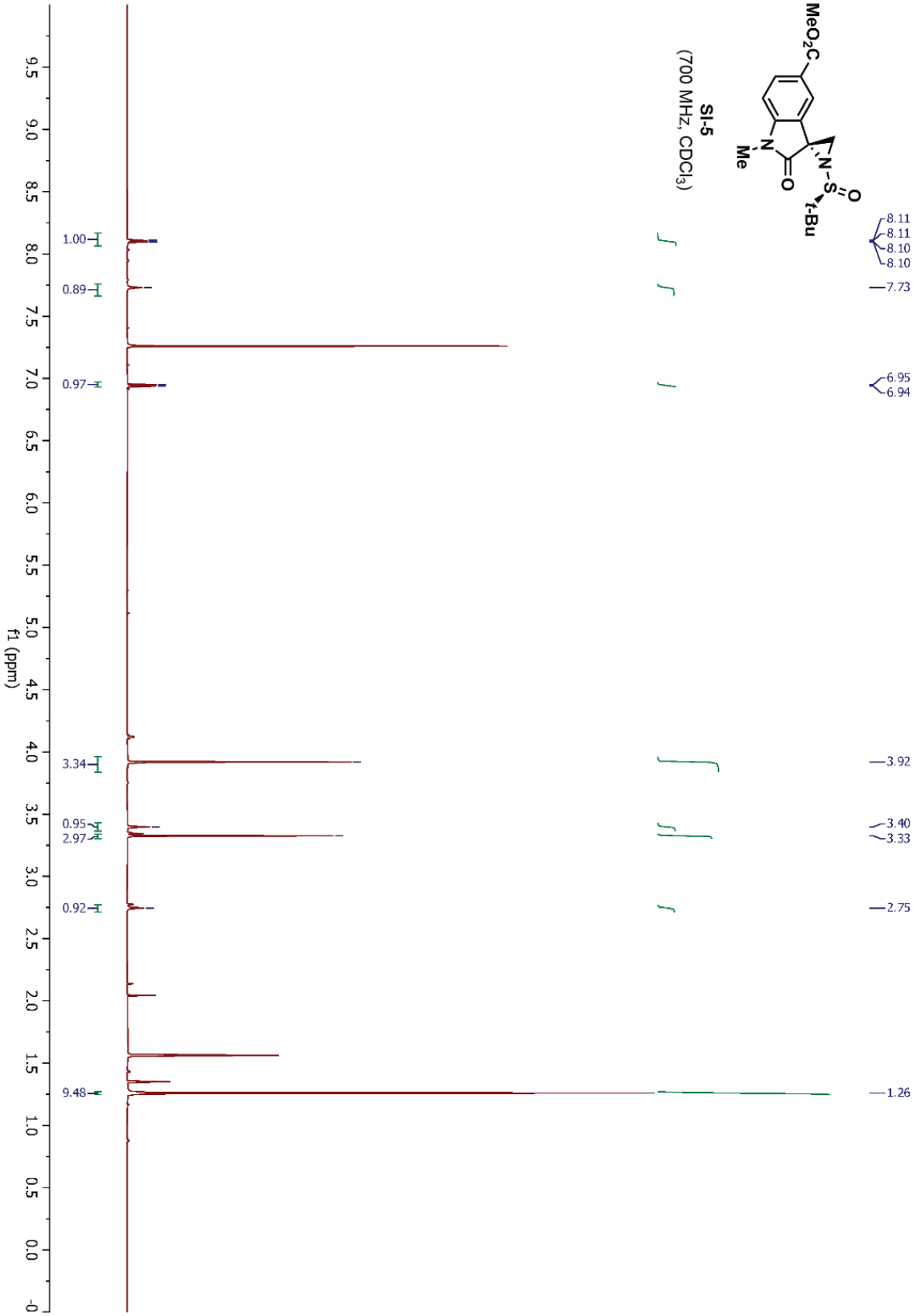
SI-5
(700 MHz, CDCl3)
MeO2C
N
Me
O
N
S
O
t-Bu
8.11
8.11
8.10
8.10
7.73
6.95
6.94
3.92
3.40
3.33
2.75
1.26
1.00
0.89
0.97
3.34
0.95
2.97
0.92
9.48
f1 (ppm)

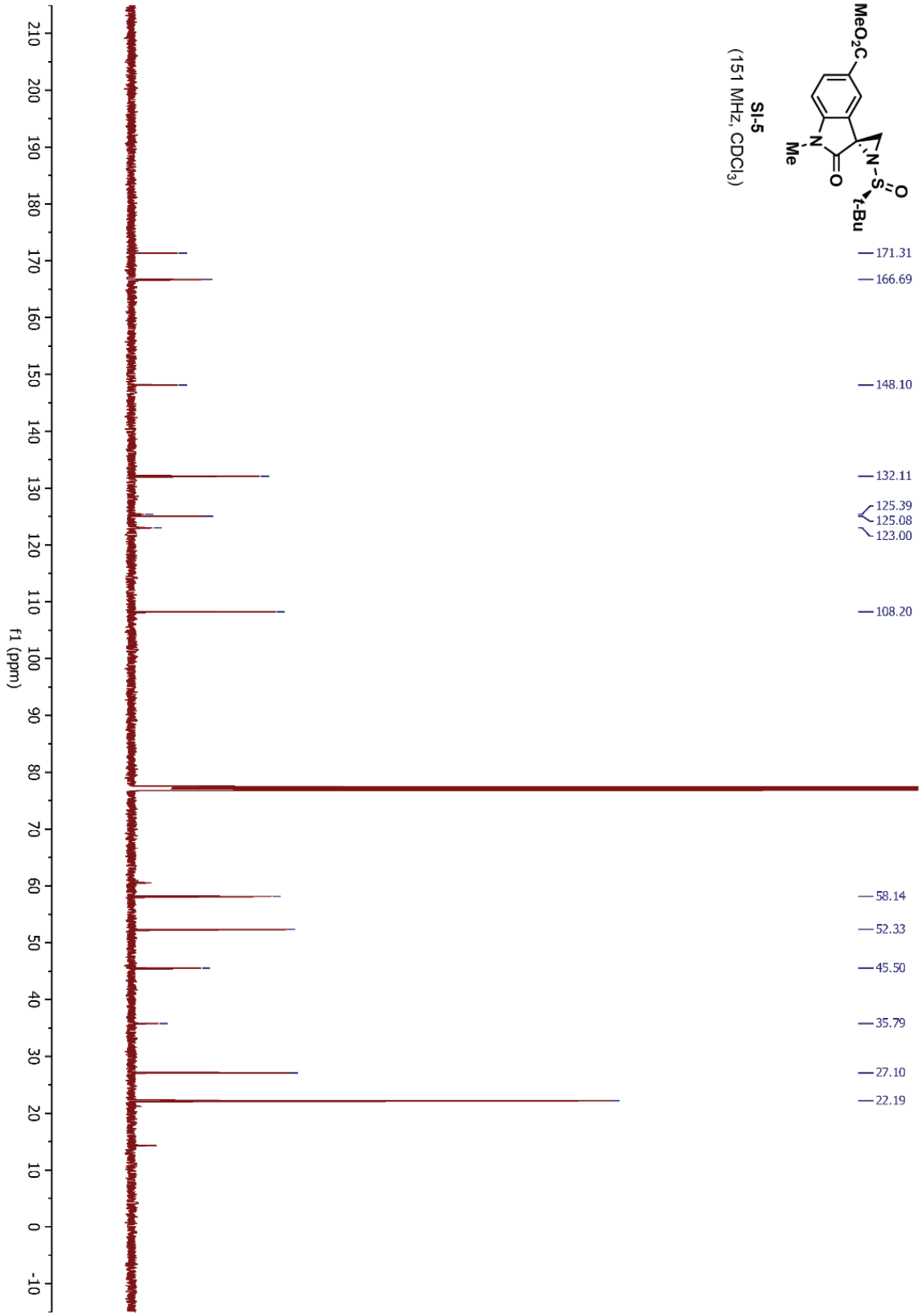
SI-5
(151 MHz, CDCl3)
MeO2C
N
Me
O
N
S
O
t-Bu
171.31
166.69
148.10
132.11
125.39
125.08
123.00
108.20
58.14
52.33
45.50
35.79
27.10
22.19
f1 (ppm)
210
200
190
180
170
160
150
140
130
120
110
100
90
80
70
60
50
40
30
20
10
0
-10

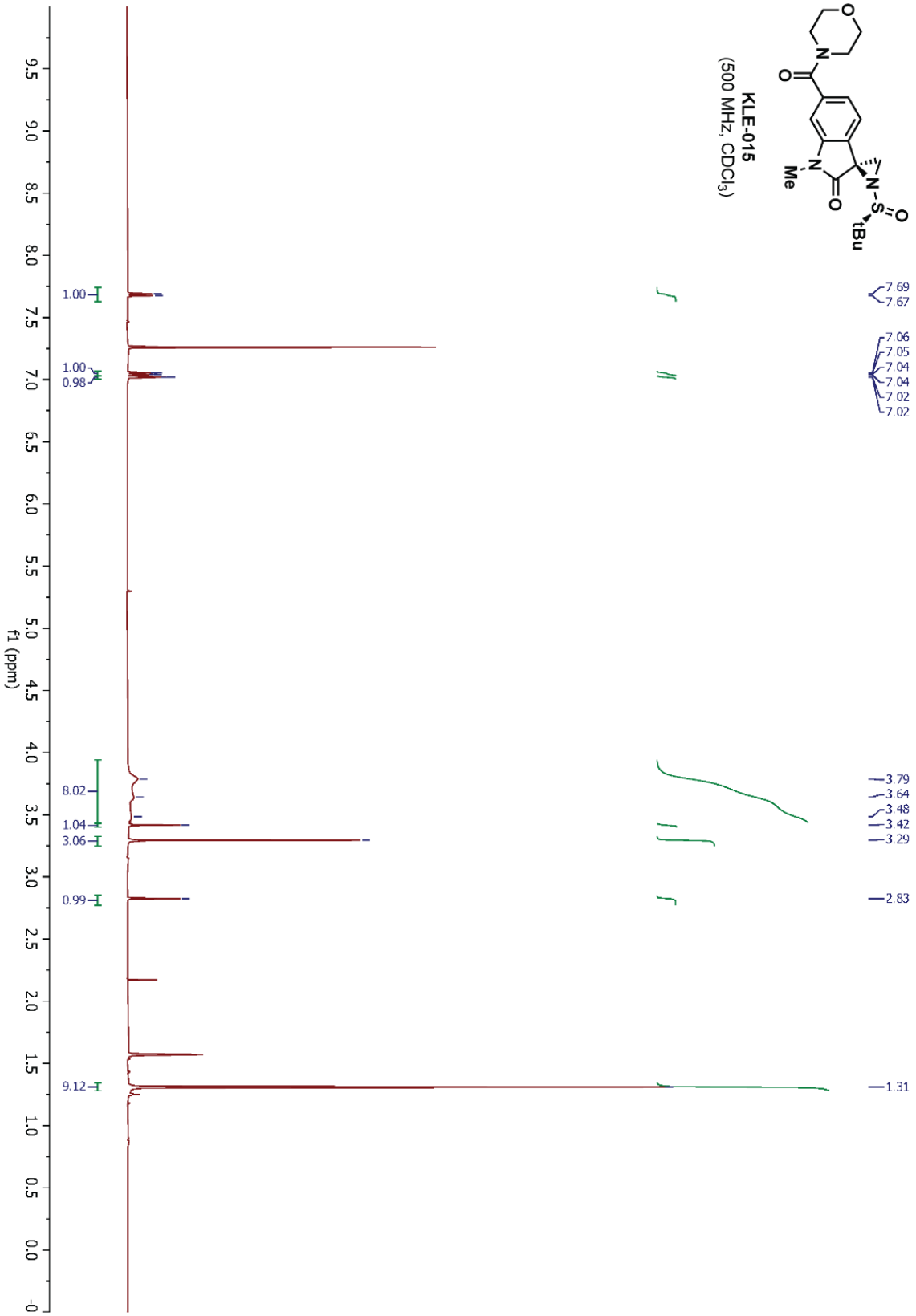
KLE-015
(500 MHz, CDCl3)
f1 (ppm)
1.00
1.00
0.98
8.02
1.04
3.06
0.99
9.12
7.69
7.67
7.06
7.05
7.04
7.04
7.02
7.02
3.79
3.64
3.48
3.42
3.29
2.83
1.31

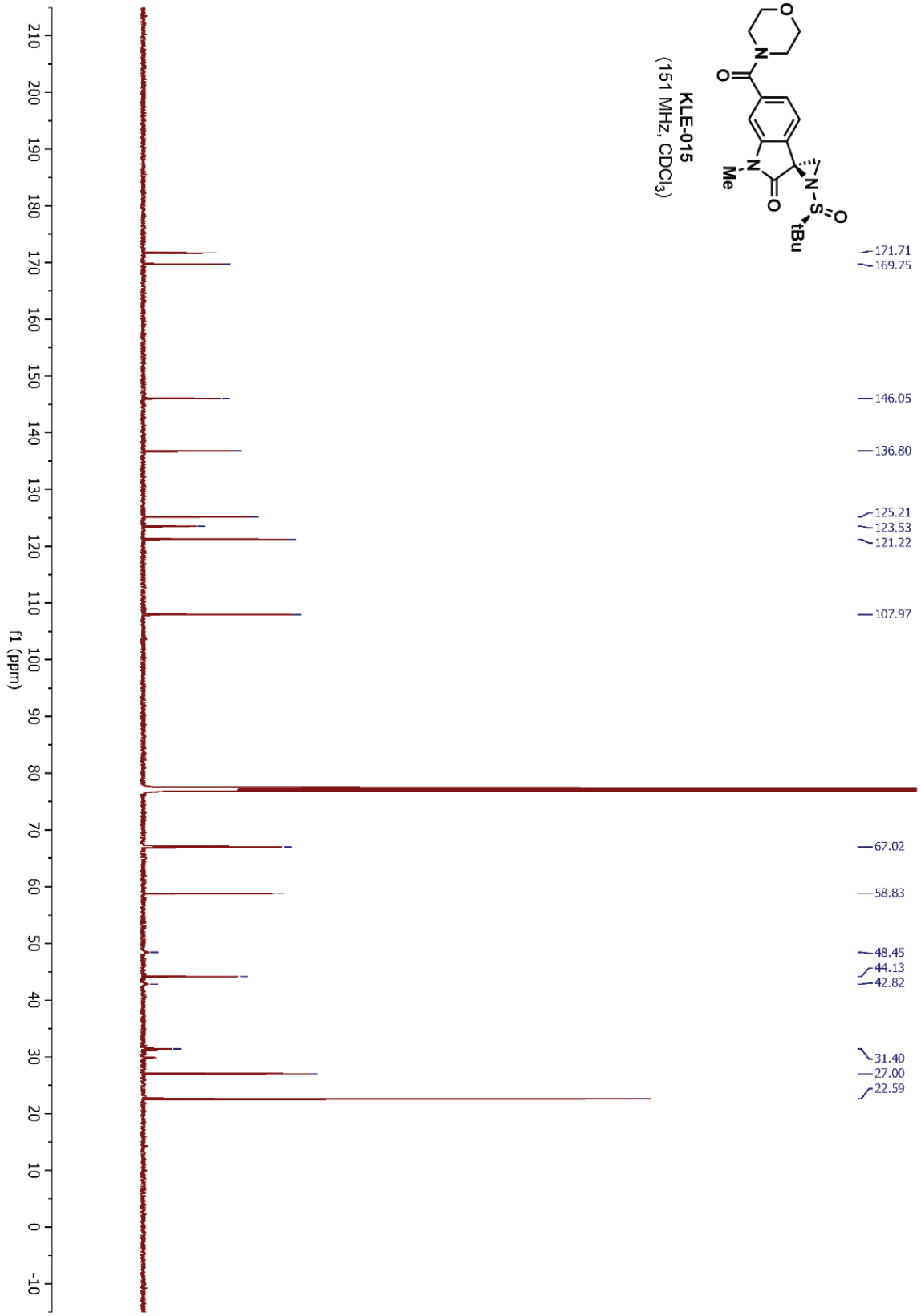
KLE-015
(151 MHz, CDCl3)
Me
tBu
171.71
169.75
146.05
136.80
125.21
123.53
121.22
107.97
67.02
58.83
48.45
44.13
42.82
31.40
27.00
22.59
f1 (ppm)

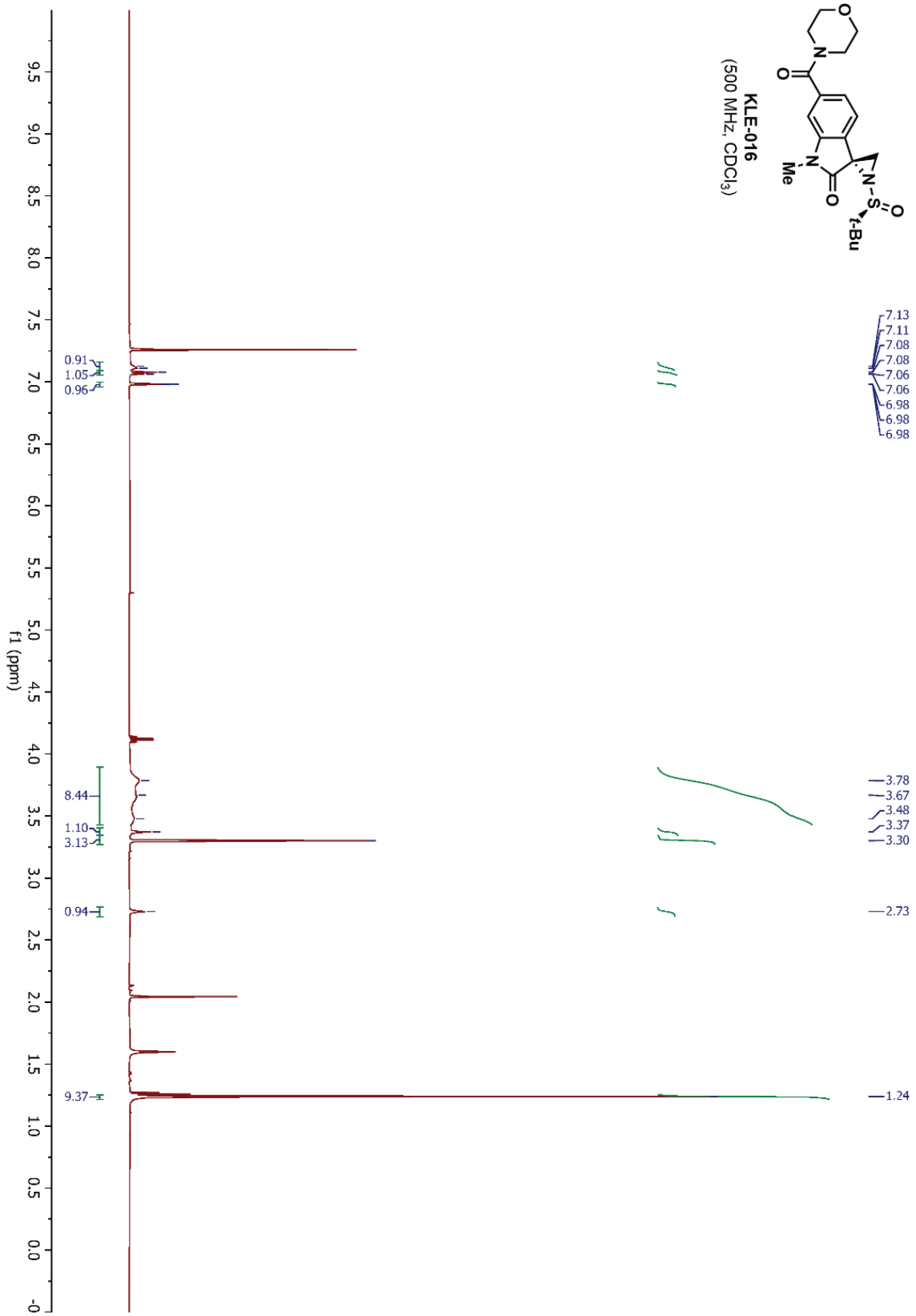
KLE-016
(500 MHz, CDCl3)
f1 (ppm)
0.91
1.05
0.96
8.44
1.10
3.13
0.94
9.37
7.13
7.11
7.08
7.08
7.06
7.06
6.98
6.98
6.98
3.78
3.67
3.48
3.37
3.30
2.73
1.24

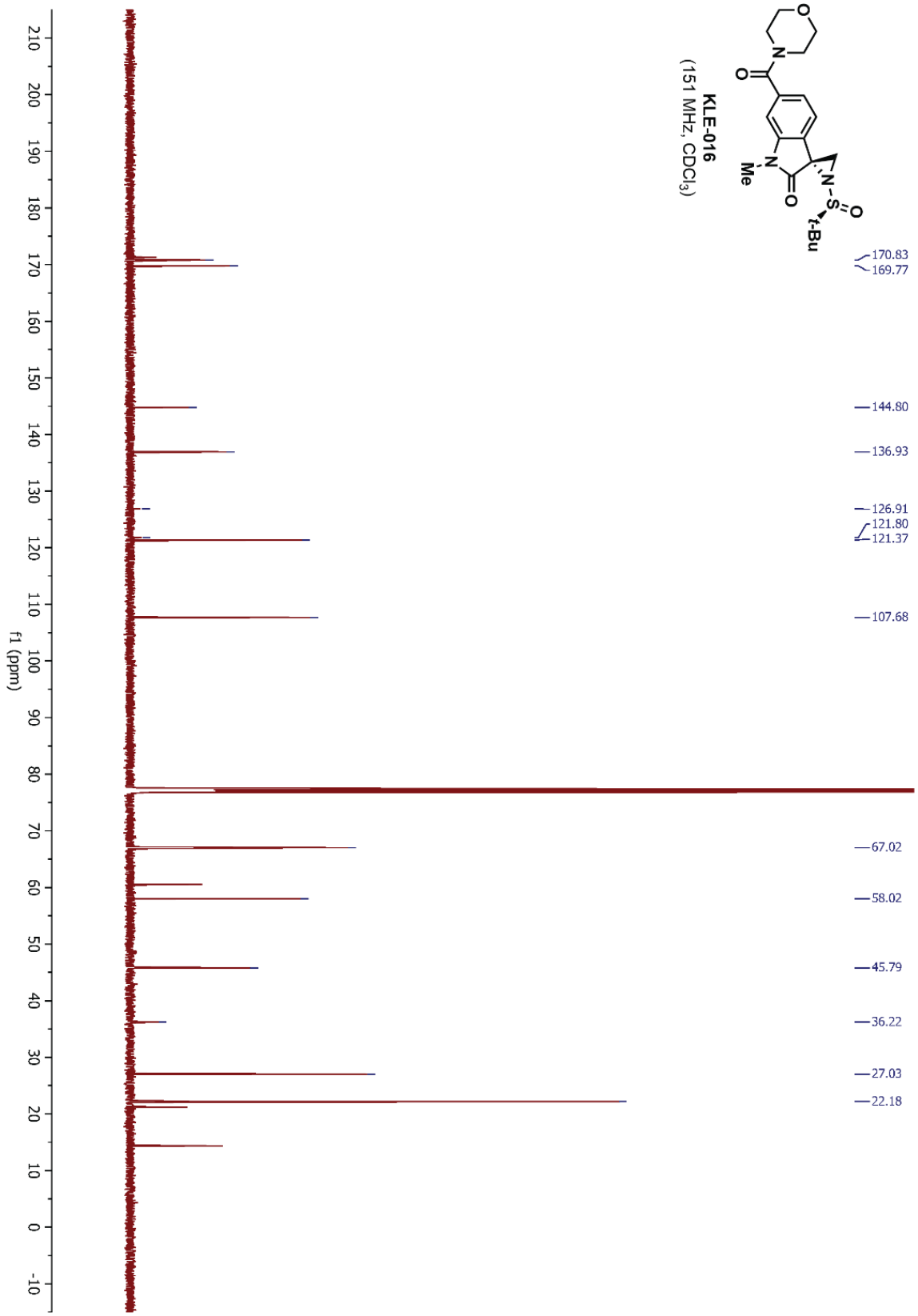
KLE-016
(151 MHz, CDCl3)
Me
t-Bu
170.83
169.77
144.80
136.93
126.91
121.80
121.37
107.68
67.02
58.02
45.79
36.22
27.03
22.18
f1 (ppm)

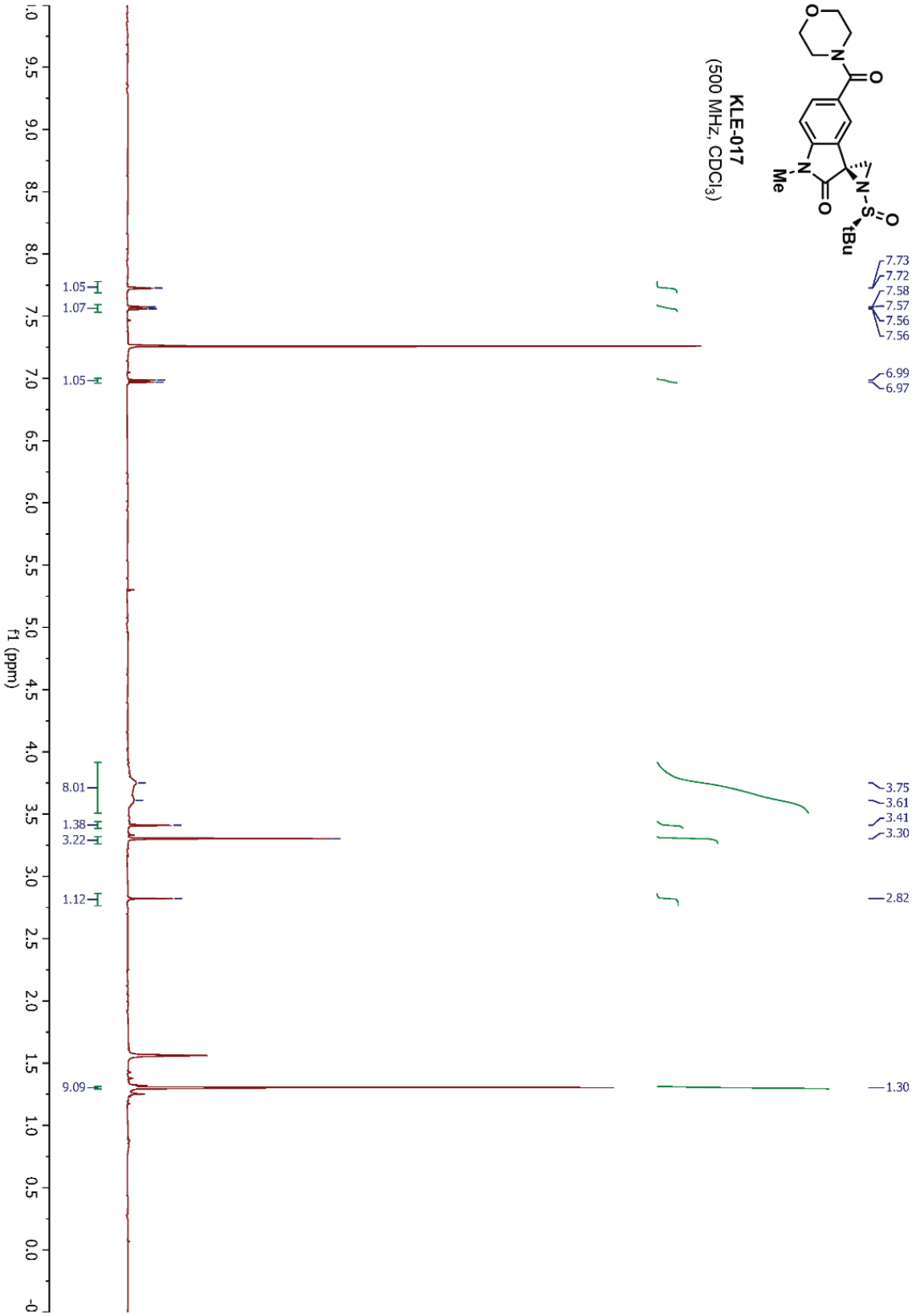
KLE-017
(500 MHz, CDCl3)
Me
tBu
7.73
7.72
7.58
7.57
7.56
7.56
6.99
6.97
3.75
3.61
3.41
3.30
2.82
1.30
1.05
1.07
1.05
8.01
1.38
3.22
1.12
9.09
f1 (ppm)

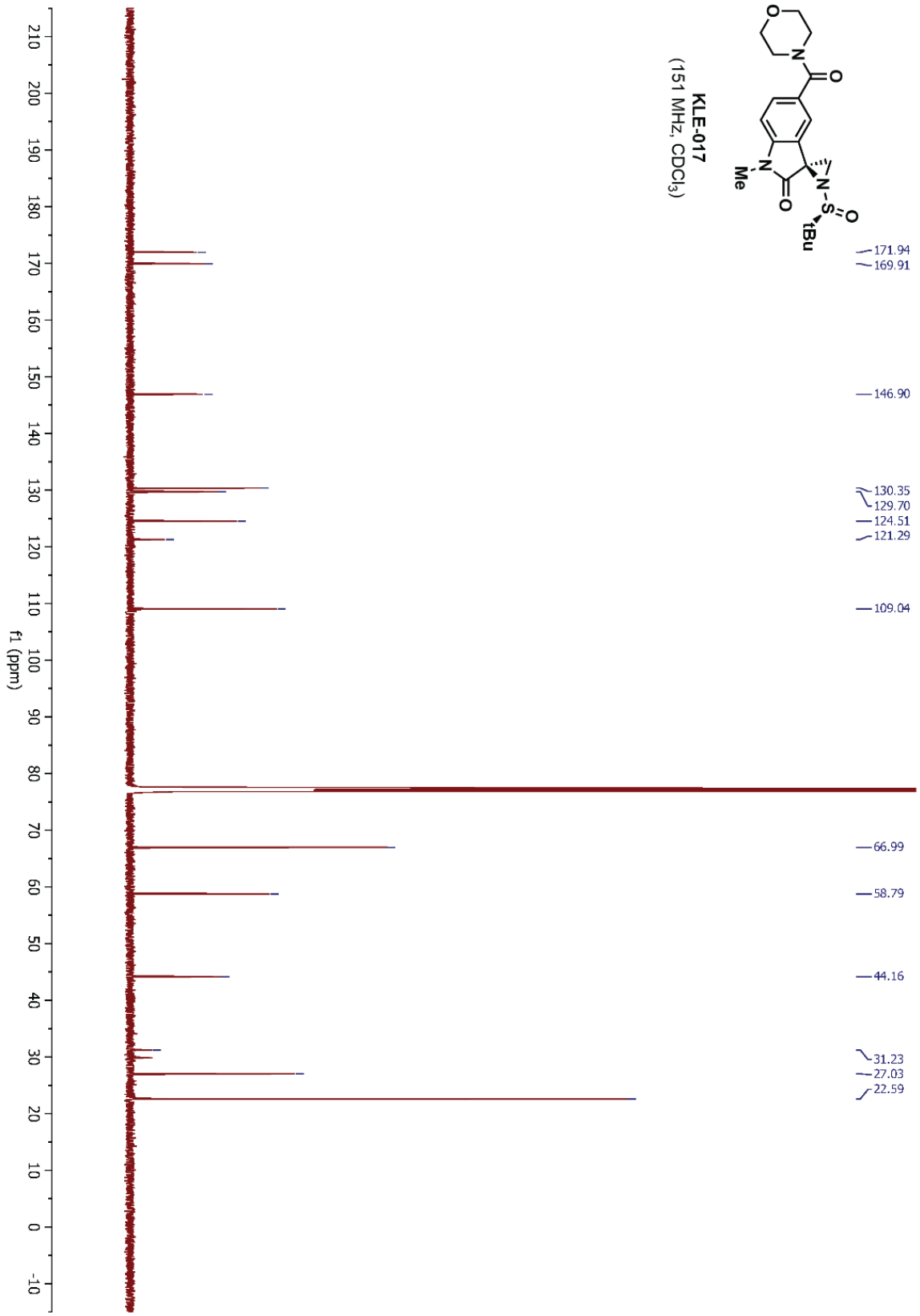
KLE-017
(151 MHz, CDCl3)
Me
tBu
171.94
169.91
146.90
130.35
129.70
124.51
121.29
109.04
66.99
58.79
44.16
31.23
27.03
22.59
f1 (ppm)

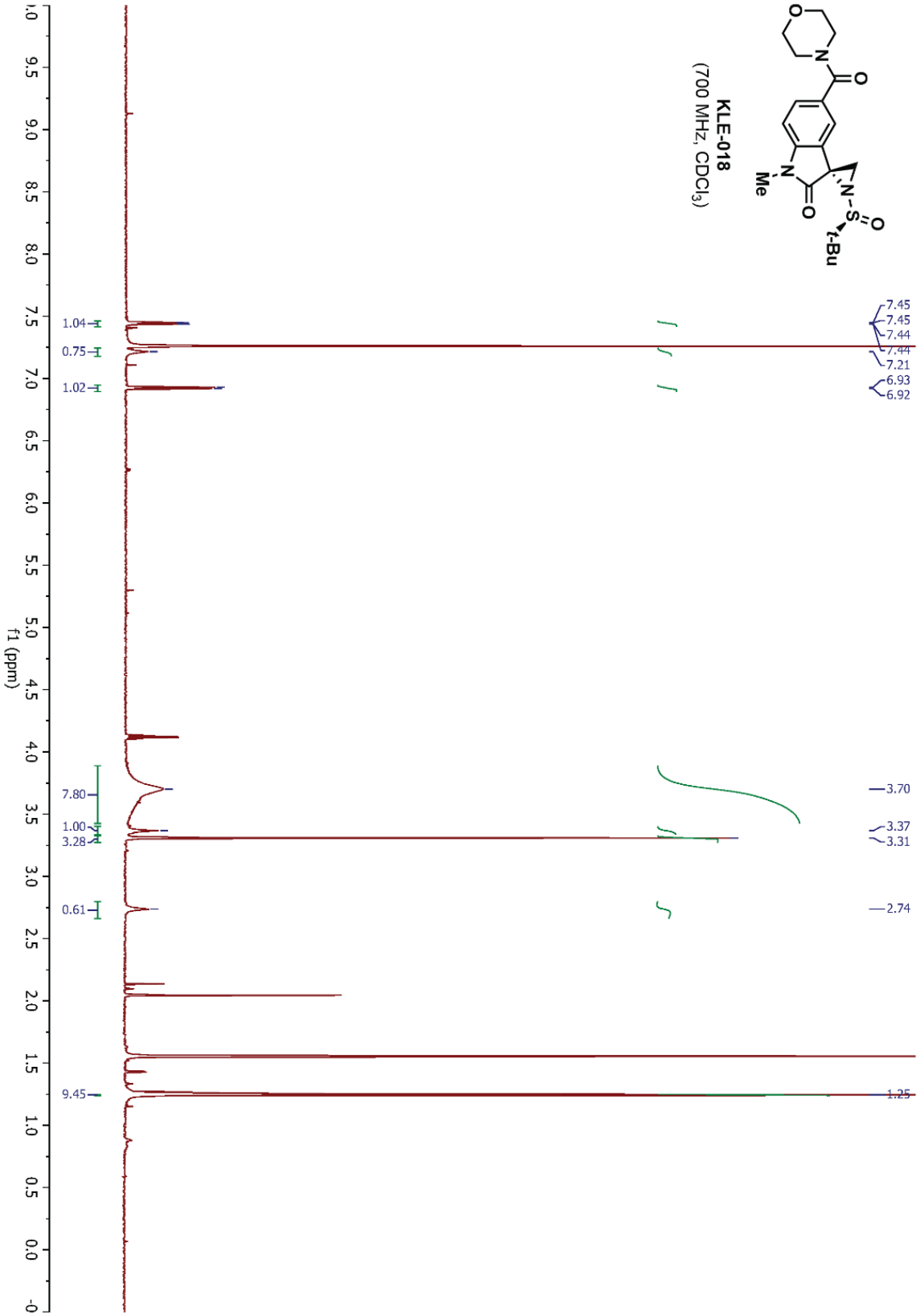
KLE-018
(700 MHz, CDCl3)
Me
t-Bu
f1 (ppm)
1.04
0.75
1.02
7.80
1.00
3.28
0.61
9.45
7.45
7.45
7.44
7.44
7.21
6.93
6.92
3.70
3.37
3.31
2.74
1.25

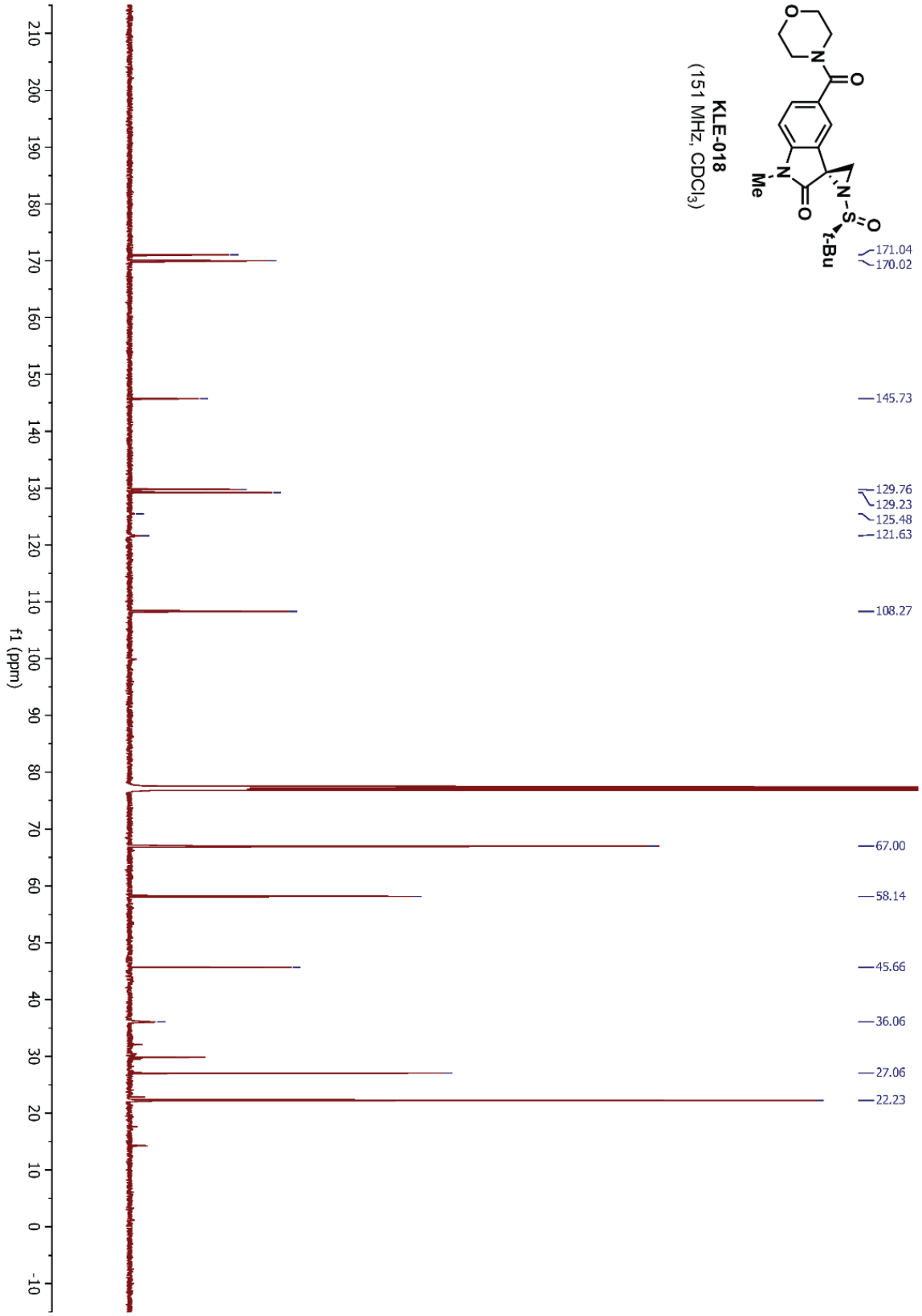
KLE-018
(151 MHz, CDCl3)
Me
t-Bu
171.04
170.02
145.73
129.76
129.23
125.48
121.63
108.27
67.00
58.14
45.66
36.06
27.06
22.23
f1 (ppm)

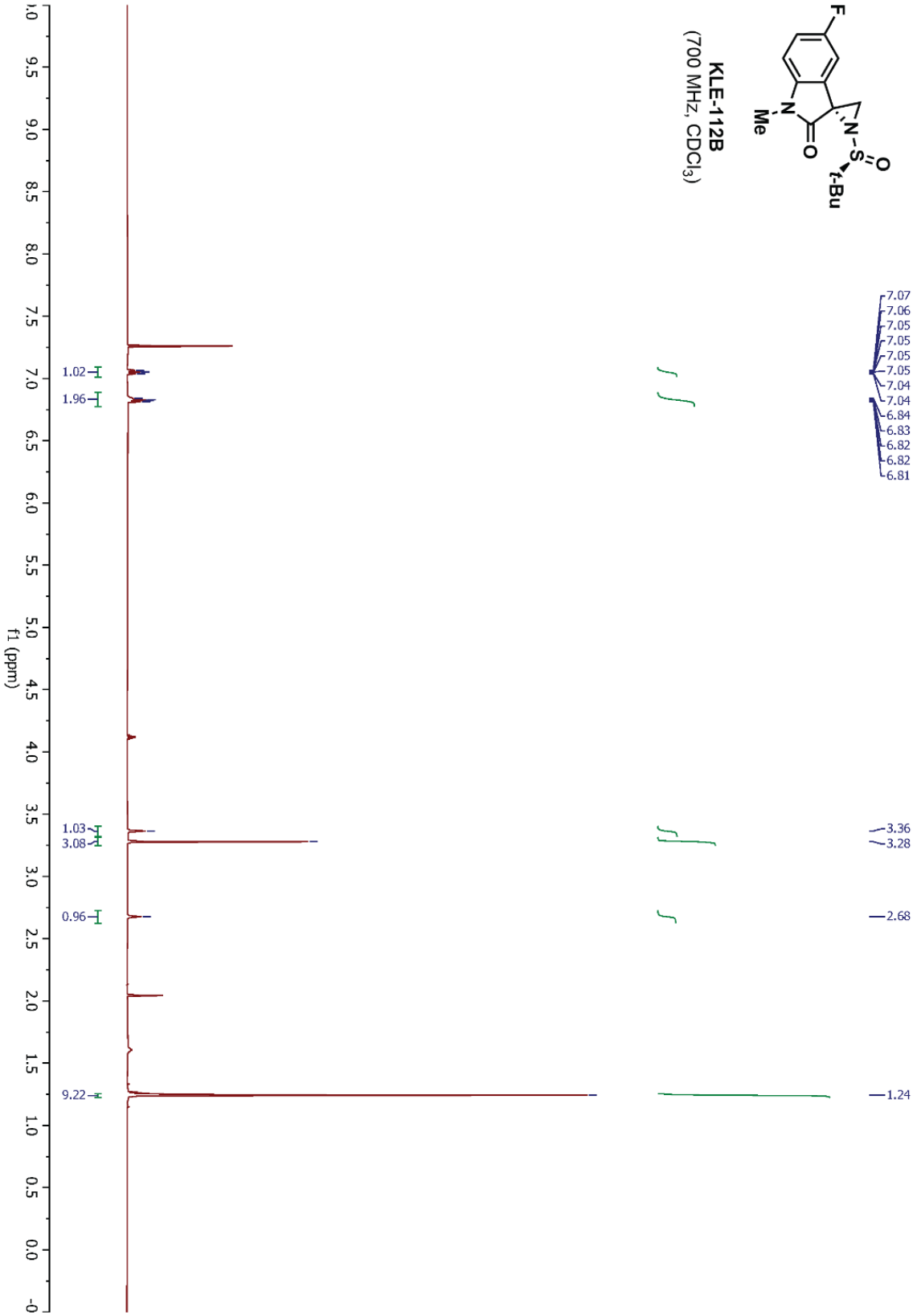
KLE-112B
(700 MHz, CDCl3)
F
N
Me
O
N
S
O
t-Bu
7.07
7.06
7.05
7.05
7.05
7.05
7.04
7.04
6.84
6.83
6.82
6.82
6.81
3.36
3.28
2.68
1.24
1.02
1.96
1.03
3.08
0.96
9.22
f1 (ppm)

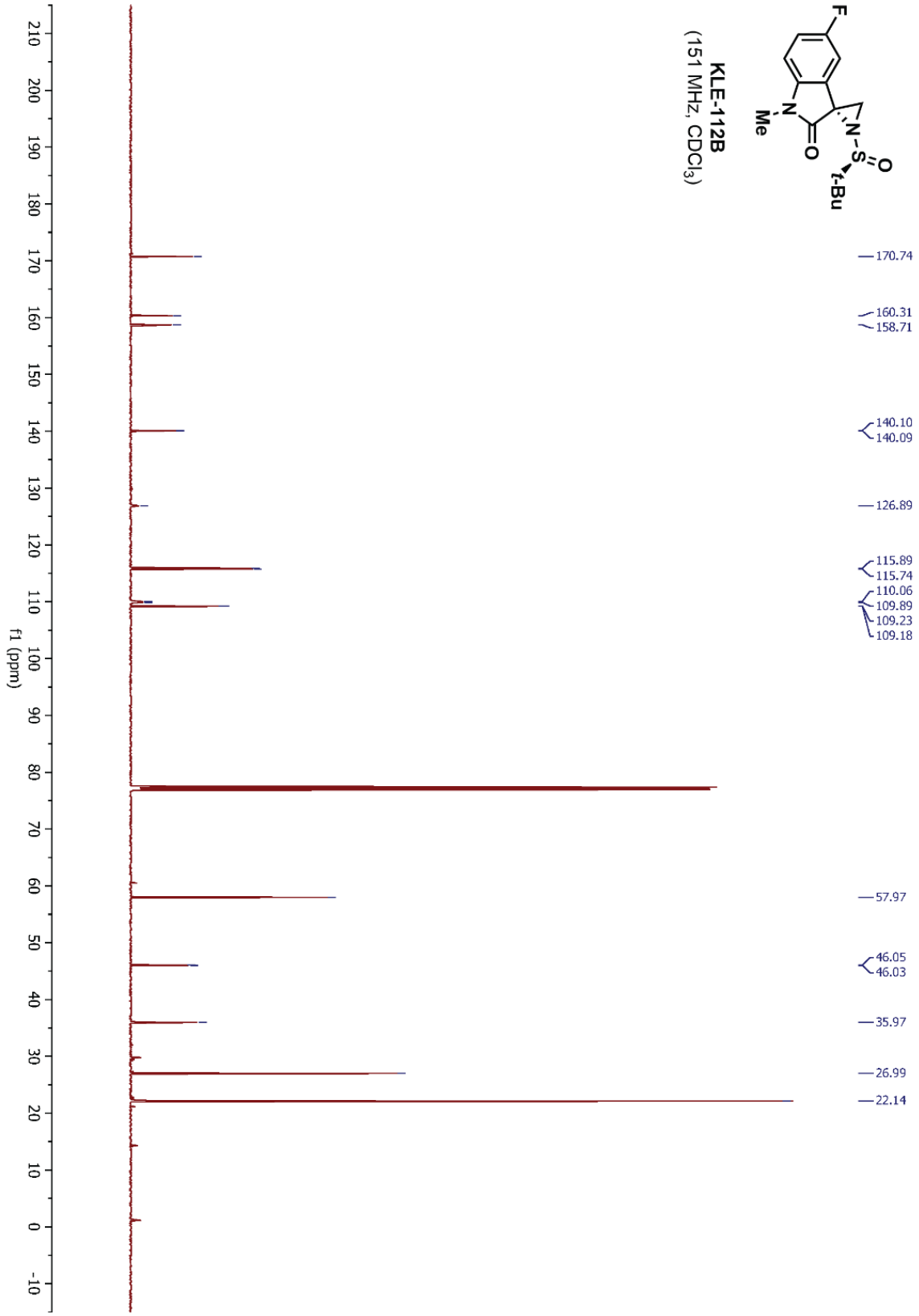
KLE-112B
(151 MHz, CDCl3)
F
N
Me
O
N
S
O
t-Bu
170.74
160.31
158.71
140.10
140.09
126.89
115.89
115.74
110.06
109.89
109.23
109.18
57.97
46.05
46.03
35.97
26.99
22.14
f1 (ppm)
210
200
190
180
170
160
150
140
130
120
110
100
90
80
70
60
50
40
30
20
10
0
-10

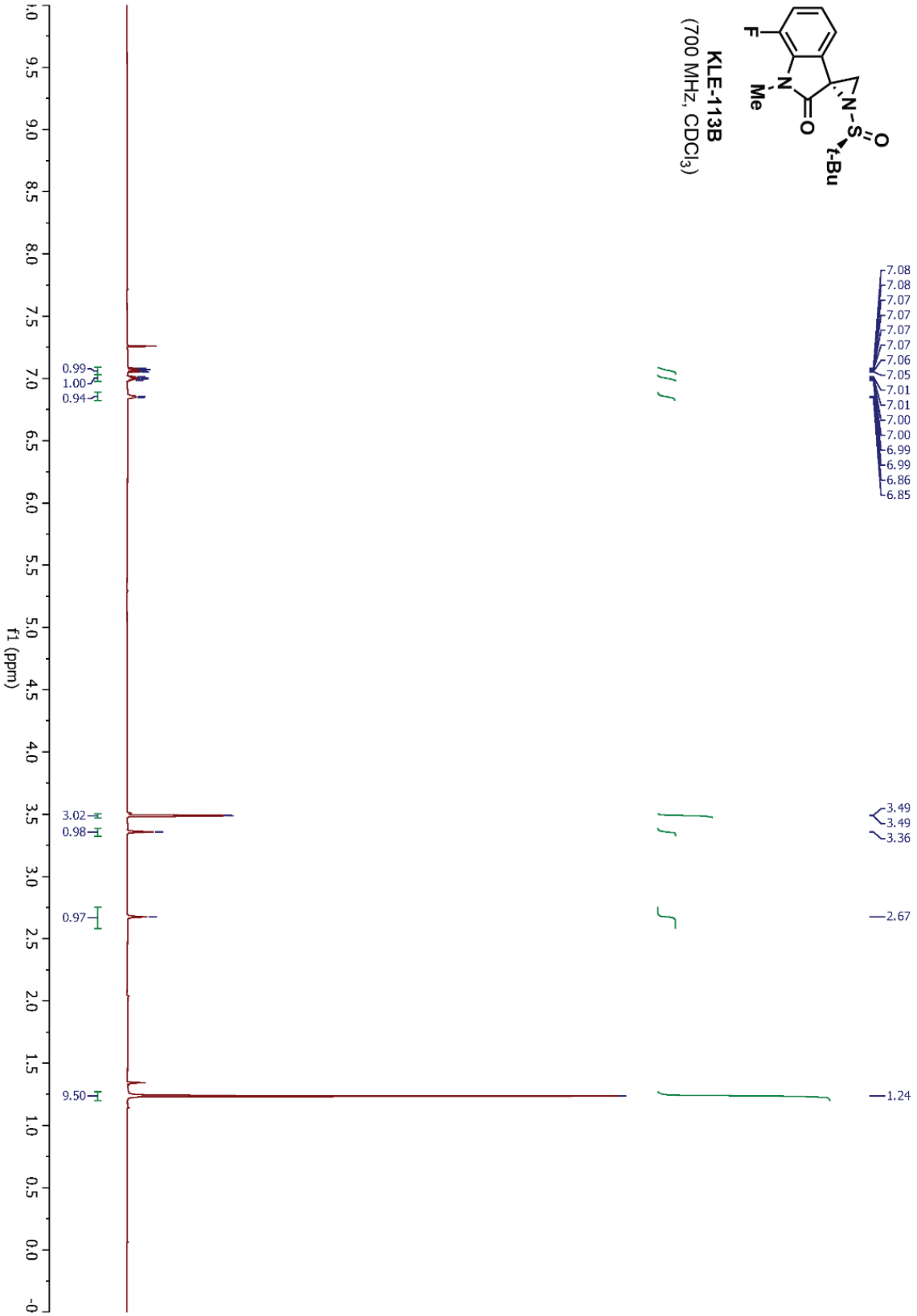
KLE-113B
(700 MHz, CDCl3)
F
N
Me
O
N-S
O
t-Bu
7.08
7.08
7.07
7.07
7.07
7.07
7.06
7.05
7.01
7.01
7.00
7.00
6.99
6.99
6.86
6.85
3.49
3.49
3.36
2.67
1.24
0.99
1.00
0.94
3.02
0.98
0.97
9.50
f1 (ppm)

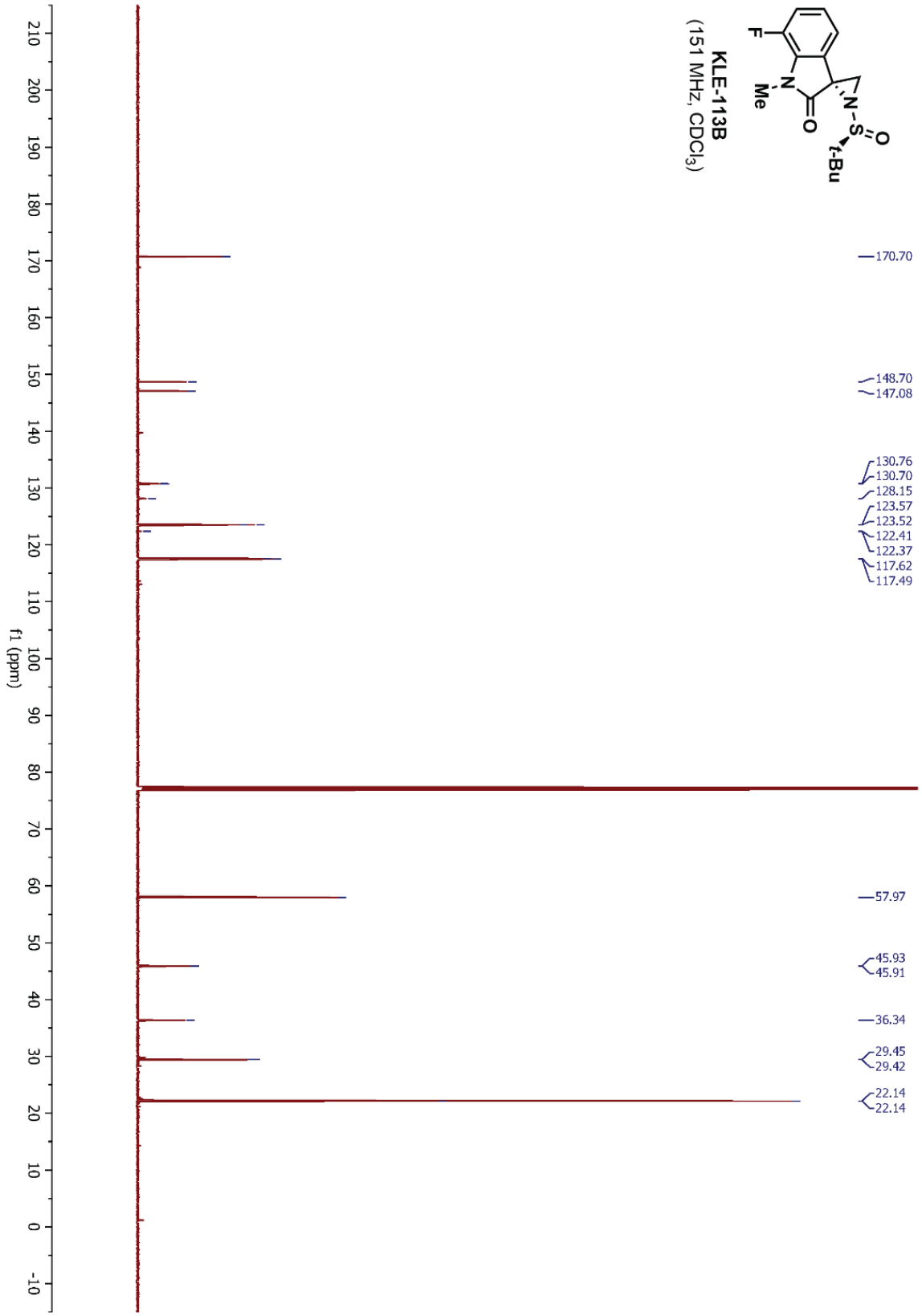
KLE-113B
(151 MHz, CDCl3)
F
N
Me
O
N-S
O
t-Bu
170.70
148.70
147.08
130.76
130.70
128.15
123.57
123.52
122.41
122.37
117.62
117.49
57.97
45.93
45.91
36.34
29.45
29.42
22.14
22.14
f1 (ppm)
210
200
190
180
170
160
150
140
130
120
110
100
90
80
70
60
50
40
30
20
10
0
-10

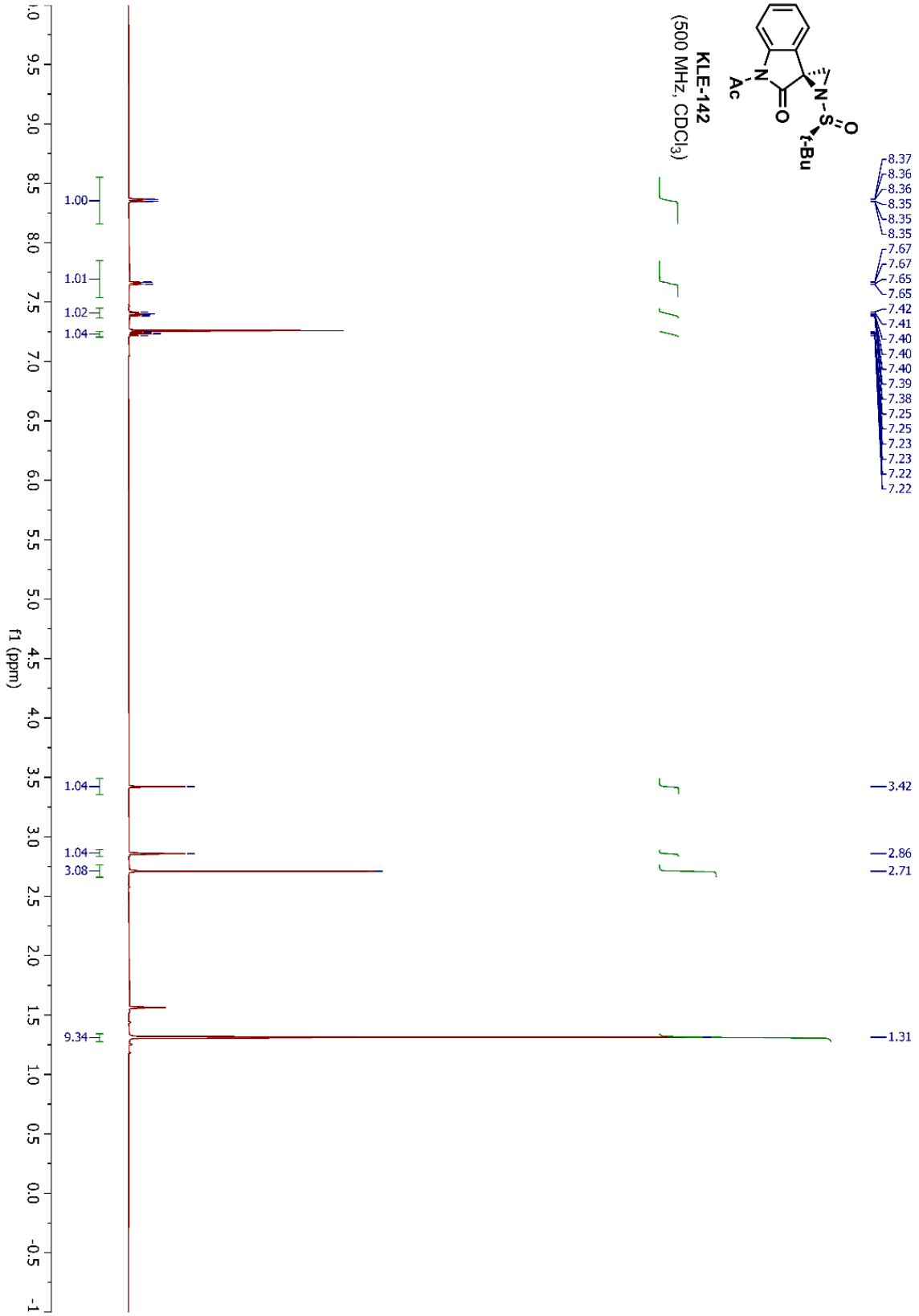
KLE-142
(500 MHz, CDCl3)
f1 (ppm)
1.00
1.01
1.02
1.04
1.04
1.04
3.08
9.34
8.37
8.36
8.36
8.35
8.35
8.35
7.67
7.67
7.65
7.65
7.42
7.41
7.40
7.40
7.40
7.39
7.38
7.25
7.25
7.23
7.23
7.22
7.22
3.42
2.86
2.71
1.31

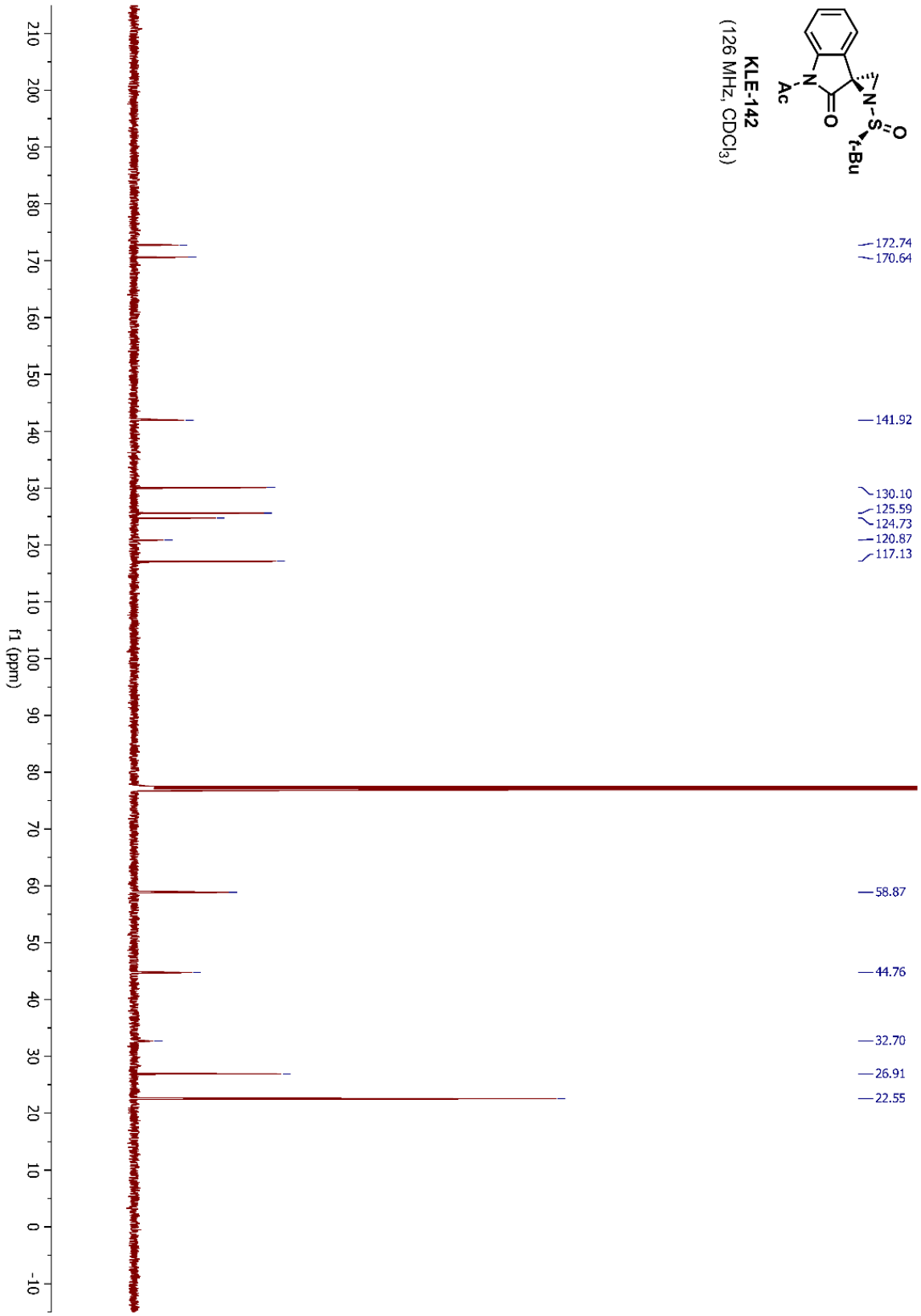
KLE-142
(126 MHz, CDCl3)
Ac
N
O
N
S
O
t-Bu
172.74
170.64
141.92
130.10
125.59
124.73
120.87
117.13
58.87
44.76
32.70
26.91
22.55
f1 (ppm)
210
200
190
180
170
160
150
140
130
120
110
100
90
80
70
60
50
40
30
20
10
0
-10

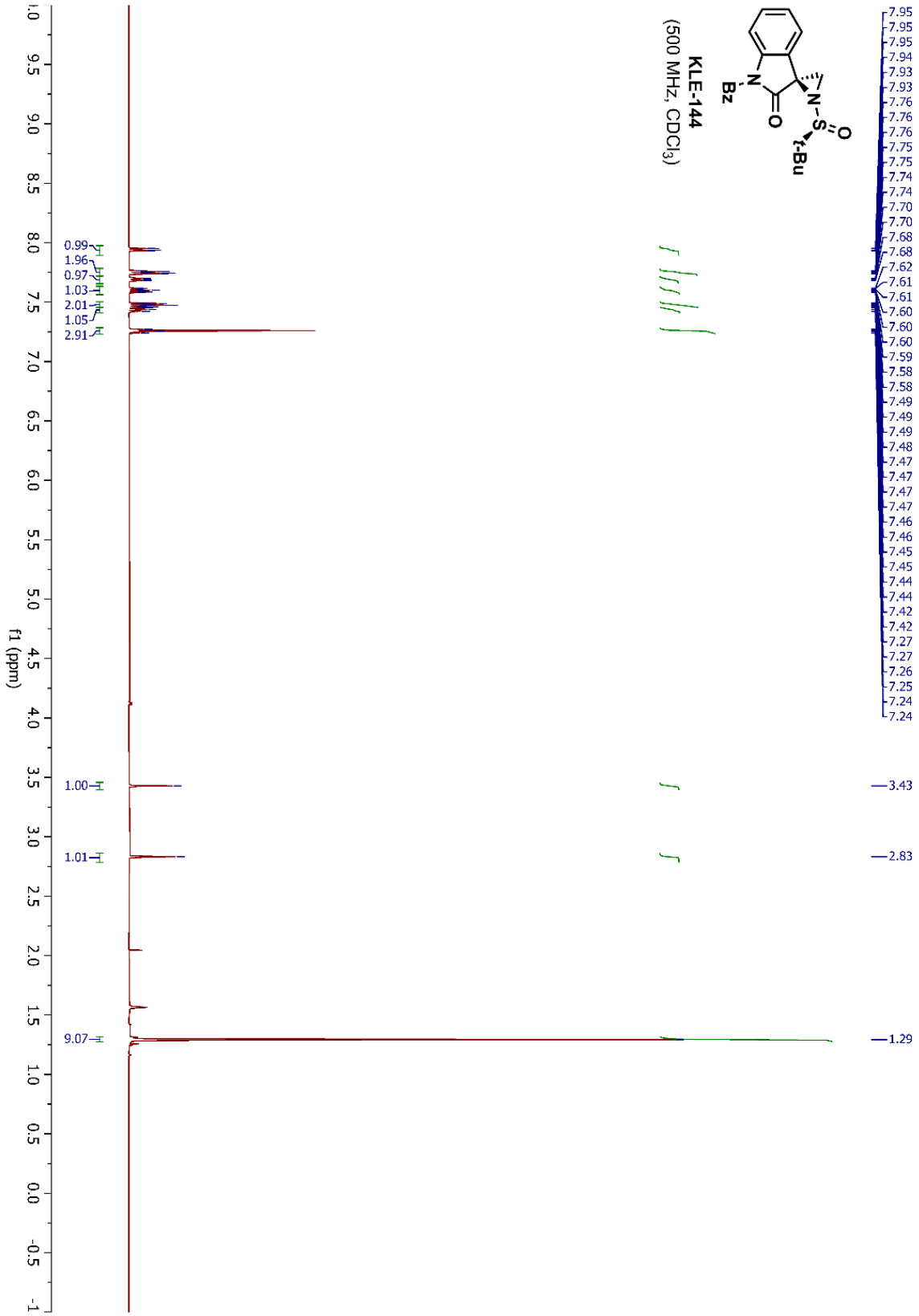
KLE-144
(500 MHz, CDCl3)
Bz
N
O
N
S
O
t-Bu
f1 (ppm)
0.99
1.96
0.97
1.03
2.01
1.05
2.91
1.00
1.01
9.07
3.43
2.83
1.29

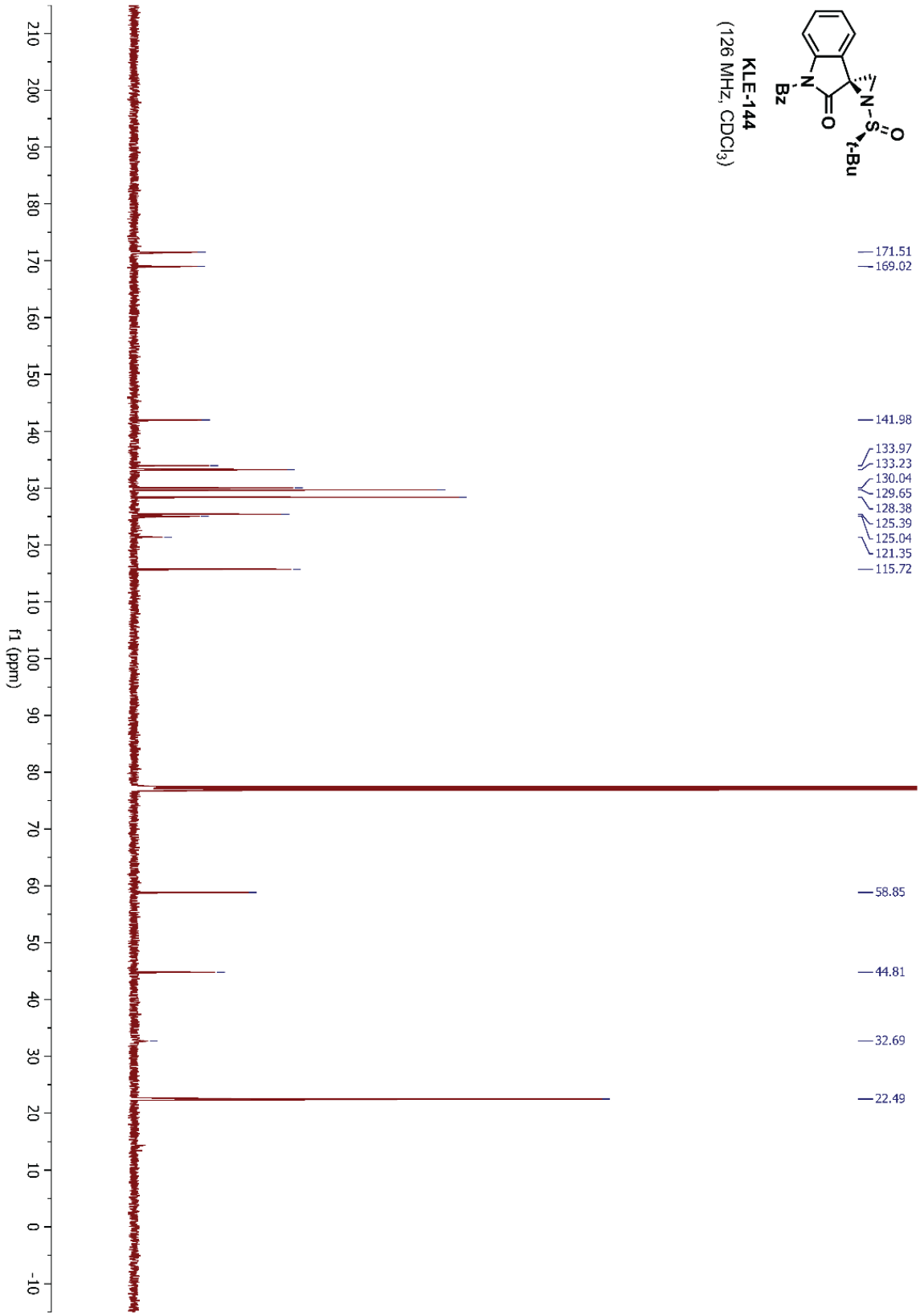
KLE-144
(126 MHz, CDCl3)
Bz
N
O
N
S
O
t-Bu
171.51
169.02
141.98
133.97
133.23
130.04
129.65
128.38
125.39
125.04
121.35
115.72
58.85
44.81
32.69
22.49
f1 (ppm)
210
200
190
180
170
160
150
140
130
120
110
100
90
80
70
60
50
40
30
20
10
0
-10

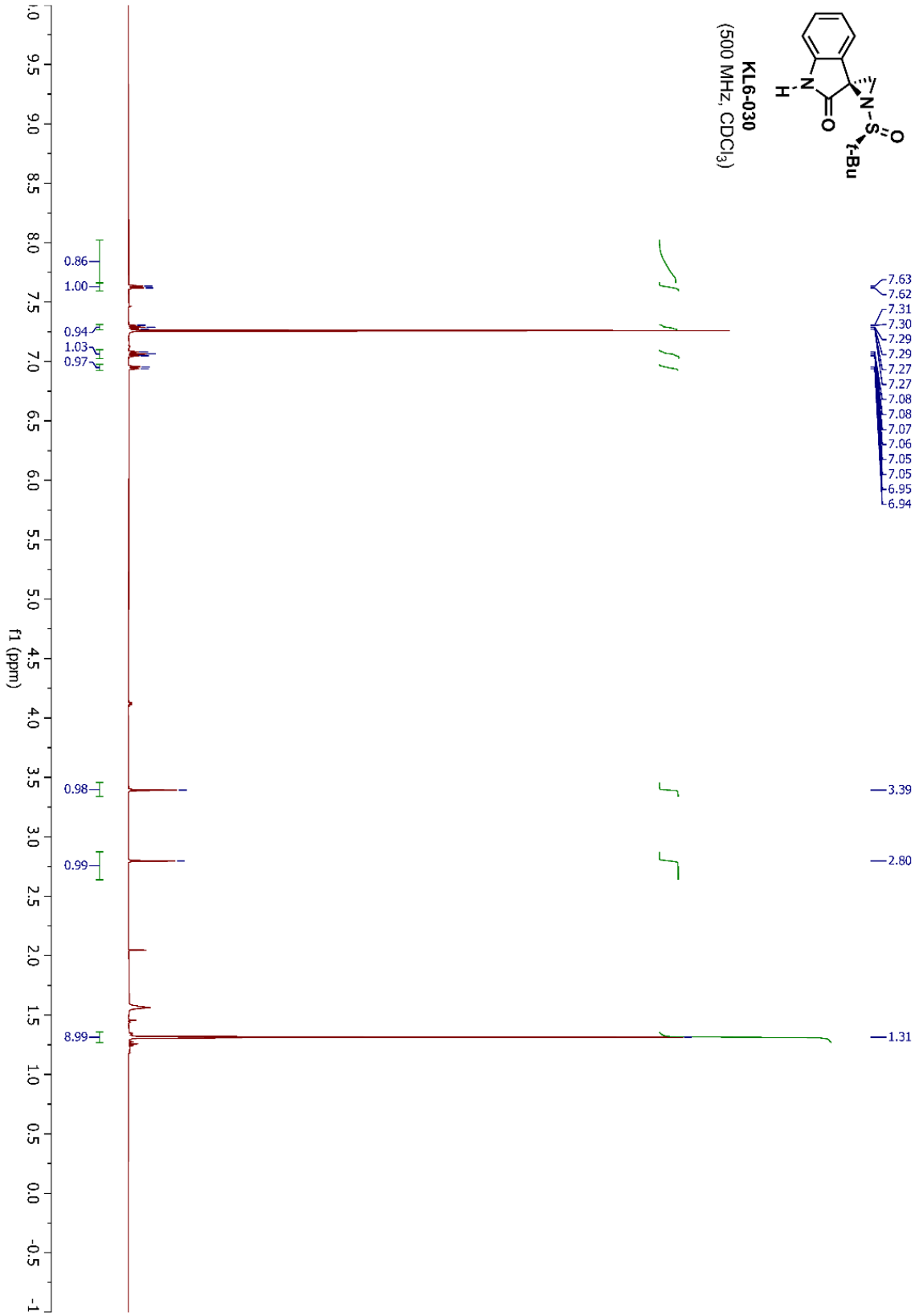
KL6-030
(500 MHz, CDCl3)
f1 (ppm)
0.86
1.00
0.94
1.03
0.97
0.98
0.99
8.99
7.63
7.62
7.31
7.30
7.29
7.29
7.27
7.27
7.08
7.08
7.07
7.06
7.05
7.05
6.95
6.94
3.39
2.80
1.31

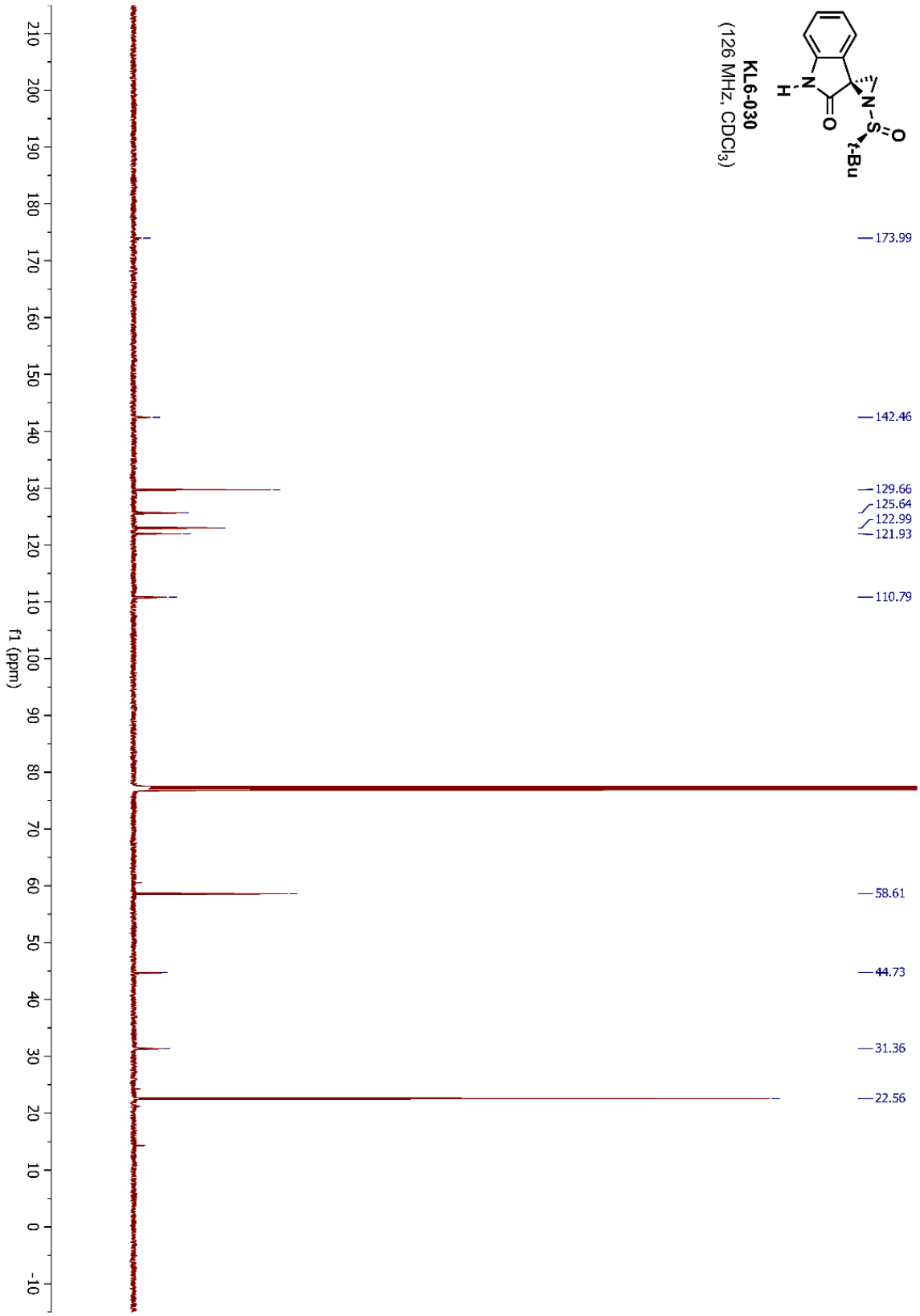
KL6-030
(126 MHz, CDCl3)
173.99
142.46
129.66
125.64
122.99
121.93
110.79
58.61
44.73
31.36
22.56
f1 (ppm)

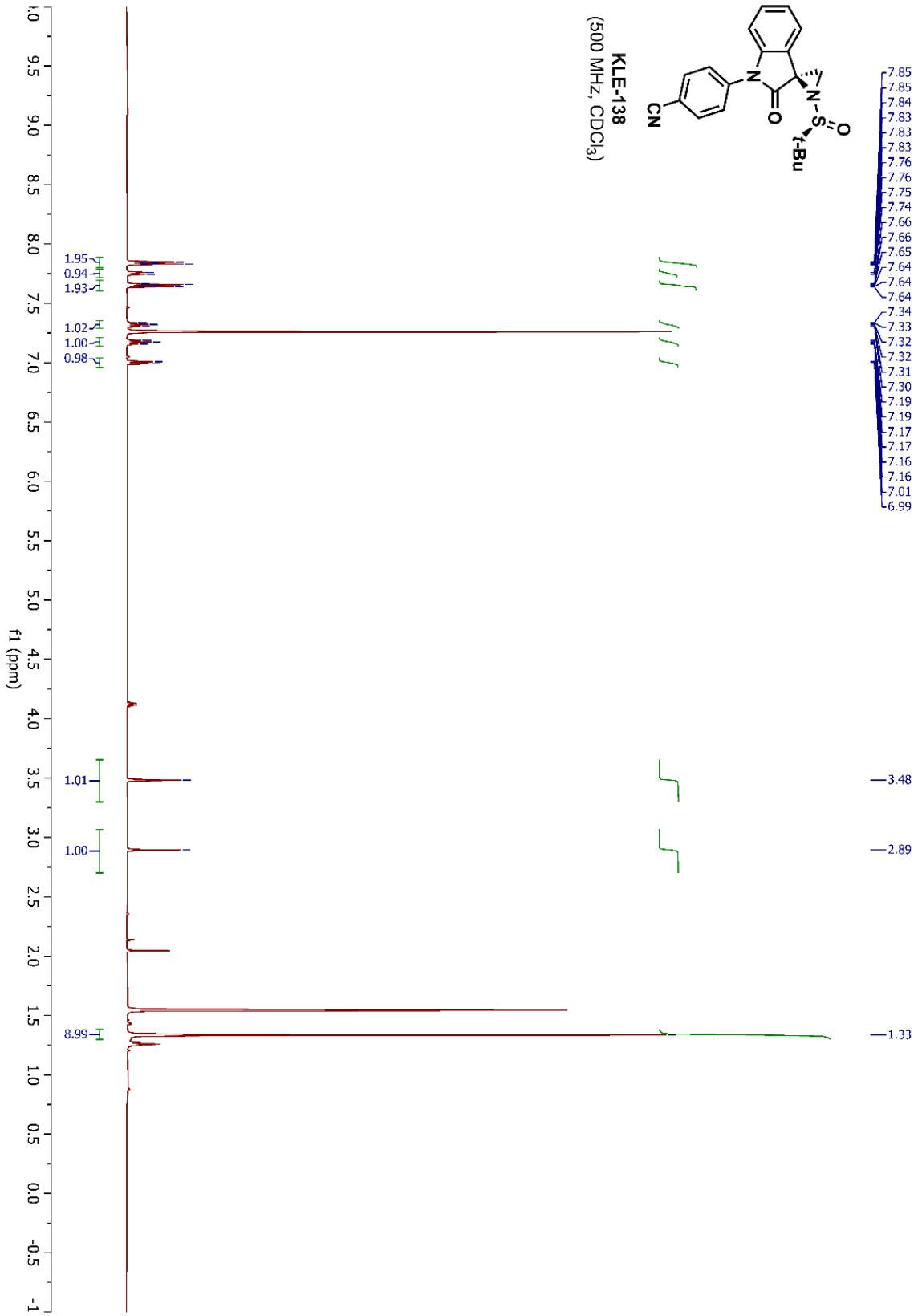
KLE-138
(500 MHz, CDCl3)
CN
N
O
N
S
O
t-Bu
7.85
7.85
7.84
7.83
7.83
7.83
7.76
7.76
7.75
7.74
7.66
7.66
7.65
7.64
7.64
7.64
7.34
7.33
7.32
7.32
7.31
7.30
7.19
7.19
7.17
7.17
7.16
7.16
7.01
6.99
1.95
0.94
1.93
1.02
1.00
0.98
1.01
1.00
8.99
3.48
2.89
1.33
f1 (ppm)

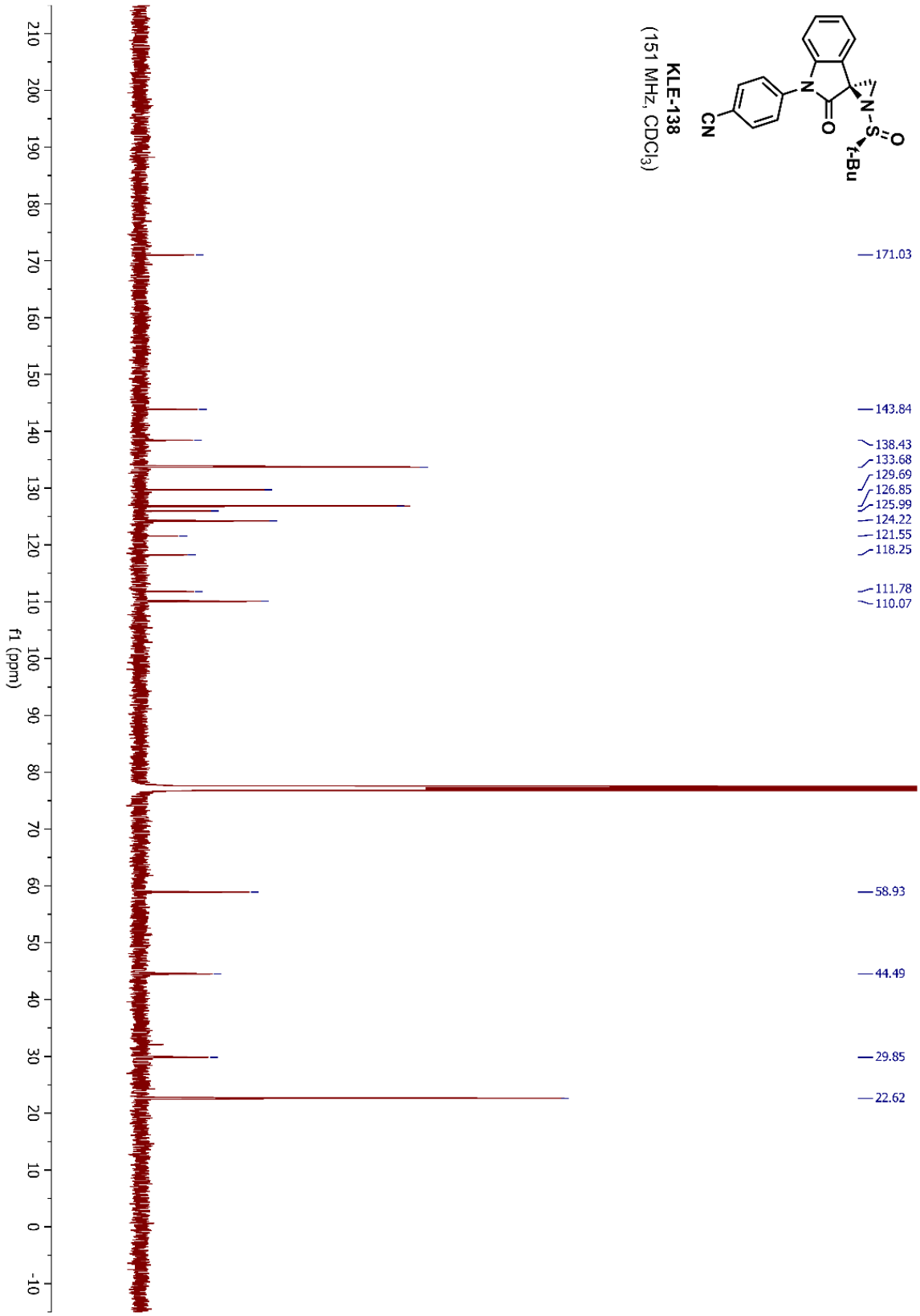
KLE-138
(151 MHz, CDCl3)
CN
N
O
N
S
O
t-Bu
171.03
143.84
138.43
133.68
129.69
126.85
125.99
124.22
121.55
118.25
111.78
110.07
58.93
44.49
29.85
22.62
f1 (ppm)
210
200
190
180
170
160
150
140
130
120
110
100
90
80
70
60
50
40
30
20
10
0
-10

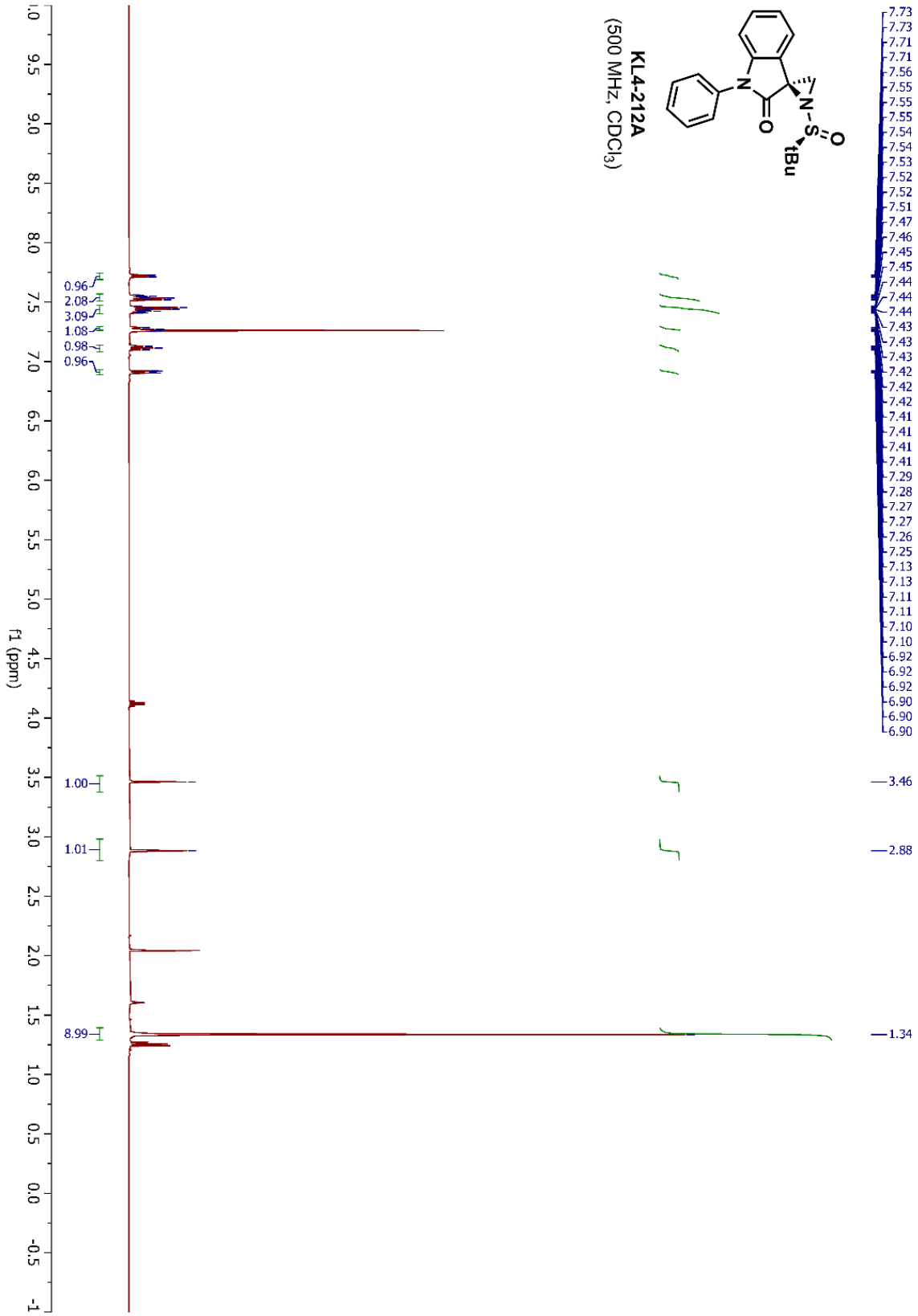
KL4-212A
(500 MHz, CDCl3)
f1 (ppm)
0.96
2.08
3.09
1.08
0.98
0.96
1.00
1.01
8.99
3.46
2.88
1.34

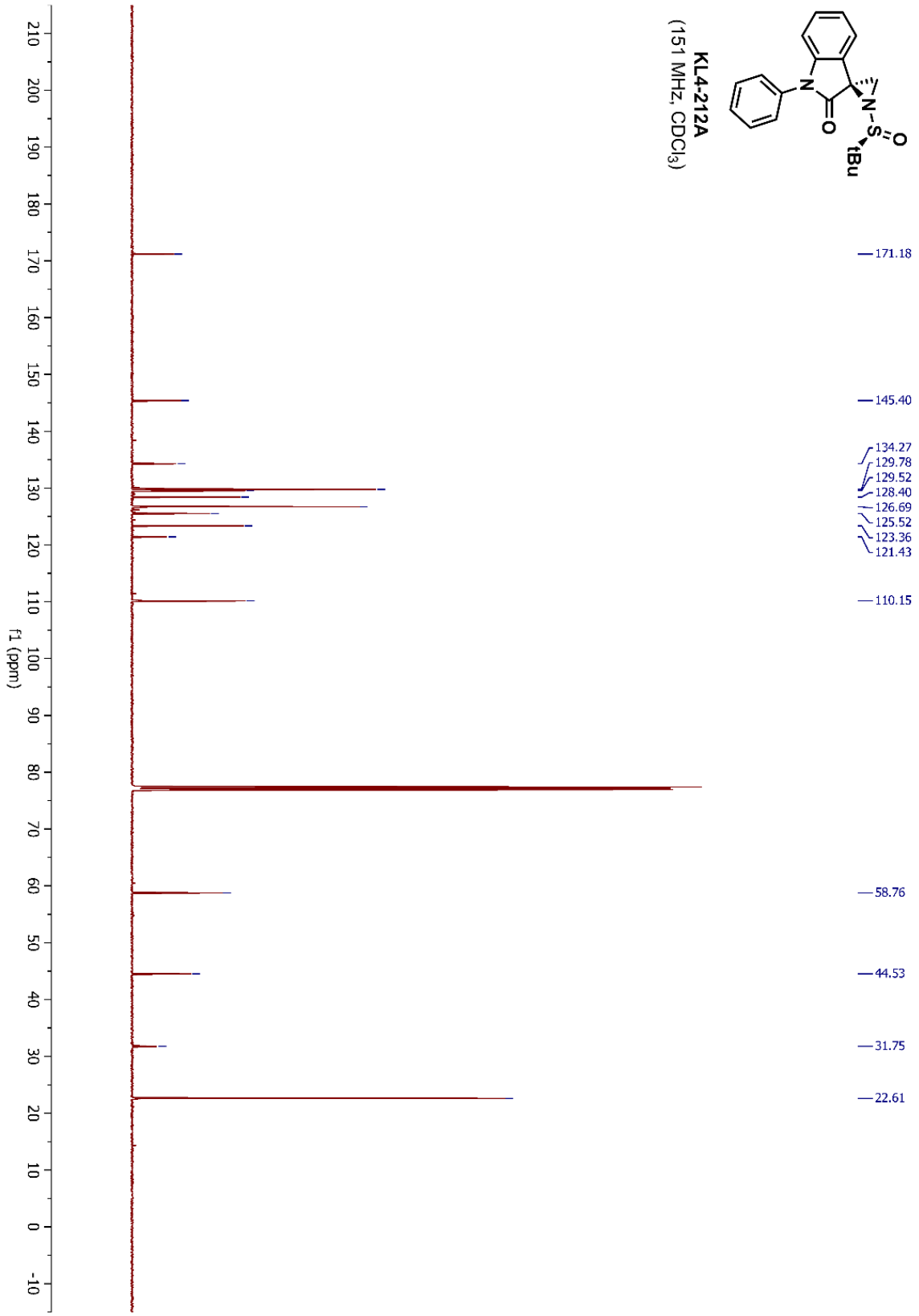
KL4-212A
(151 MHz, CDCl3)
171.18
145.40
134.27
129.78
129.52
128.40
126.69
125.52
123.36
121.43
110.15
58.76
44.53
31.75
22.61
f1 (ppm)

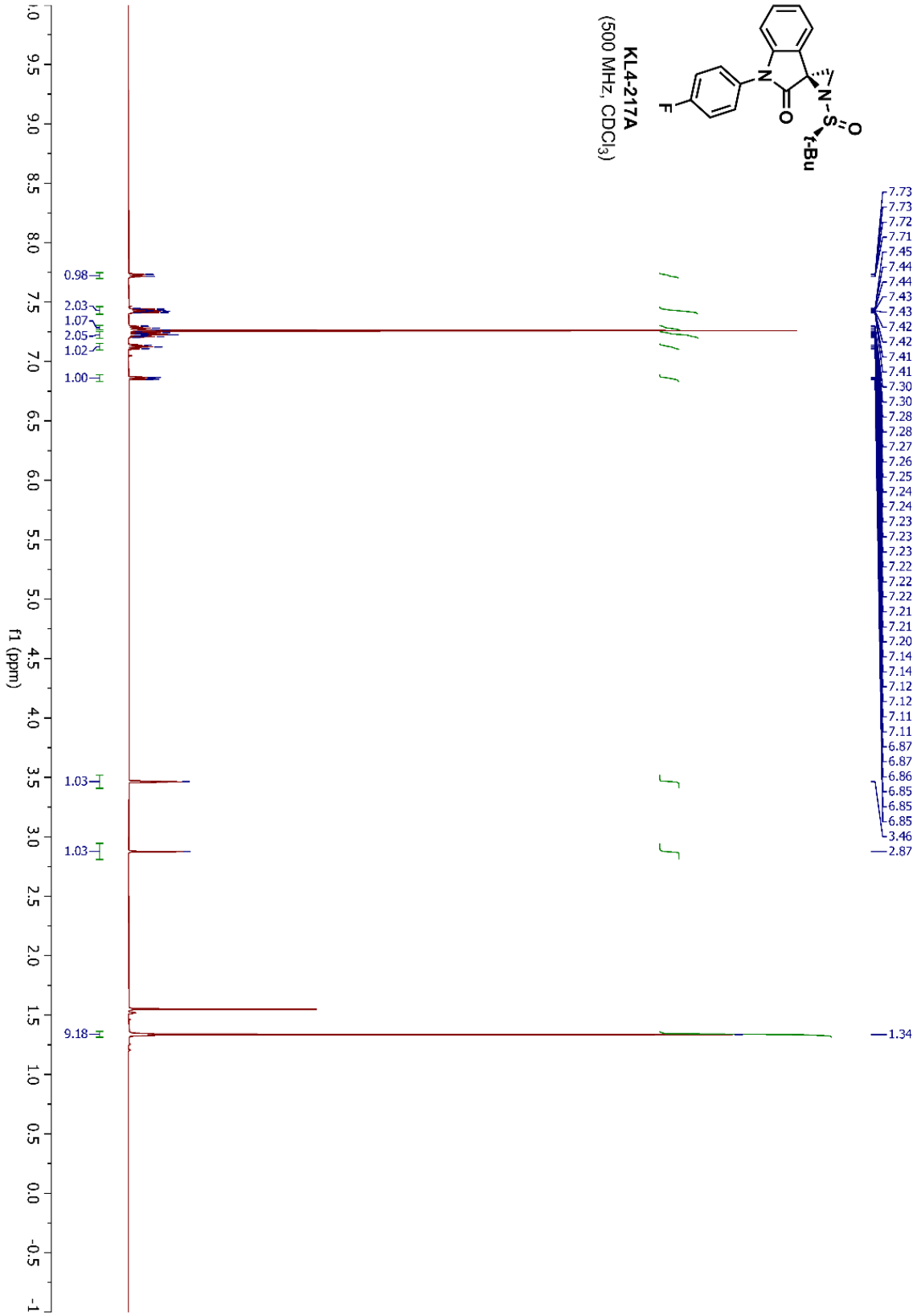
KL4-217A
(500 MHz, CDCl3)
F
N
O
N
S
O
t-Bu
f1 (ppm)
1.0
9.5
9.0
8.5
8.0
7.5
7.0
6.5
6.0
5.5
5.0
4.5
4.0
3.5
3.0
2.5
2.0
1.5
1.0
0.5
0.0
-0.5
-1
0.98
2.03
1.07
2.05
1.02
1.00
1.03
1.03
9.18
7.73
7.73
7.72
7.71
7.45
7.44
7.44
7.43
7.43
7.42
7.42
7.41
7.41
7.30
7.30
7.28
7.28
7.27
7.26
7.25
7.24
7.24
7.23
7.23
7.23
7.22
7.22
7.22
7.21
7.21
7.20
7.14
7.14
7.12
7.12
7.11
7.11
6.87
6.87
6.86
6.85
6.85
6.85
3.46
2.87
1.34

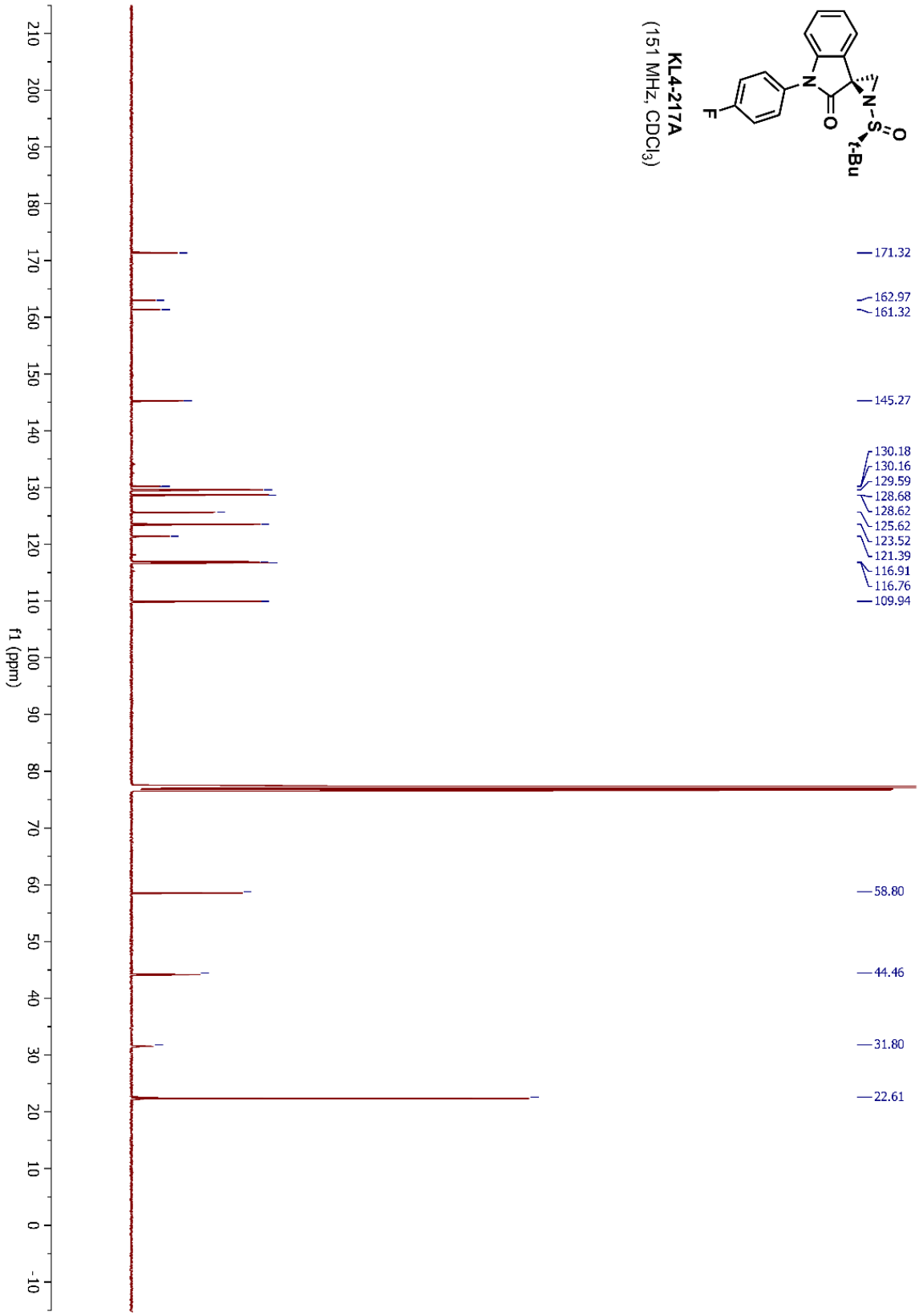
KL4-217A
(151 MHz, CDCl3)
F
N
O
N
S
O
t-Bu
171.32
162.97
161.32
145.27
130.18
130.16
129.59
128.68
128.62
125.62
123.52
121.39
116.91
116.76
109.94
58.80
44.46
31.80
22.61
f1 (ppm)
210
200
190
180
170
160
150
140
130
120
110
100
90
80
70
60
50
40
30
20
10
0
-10

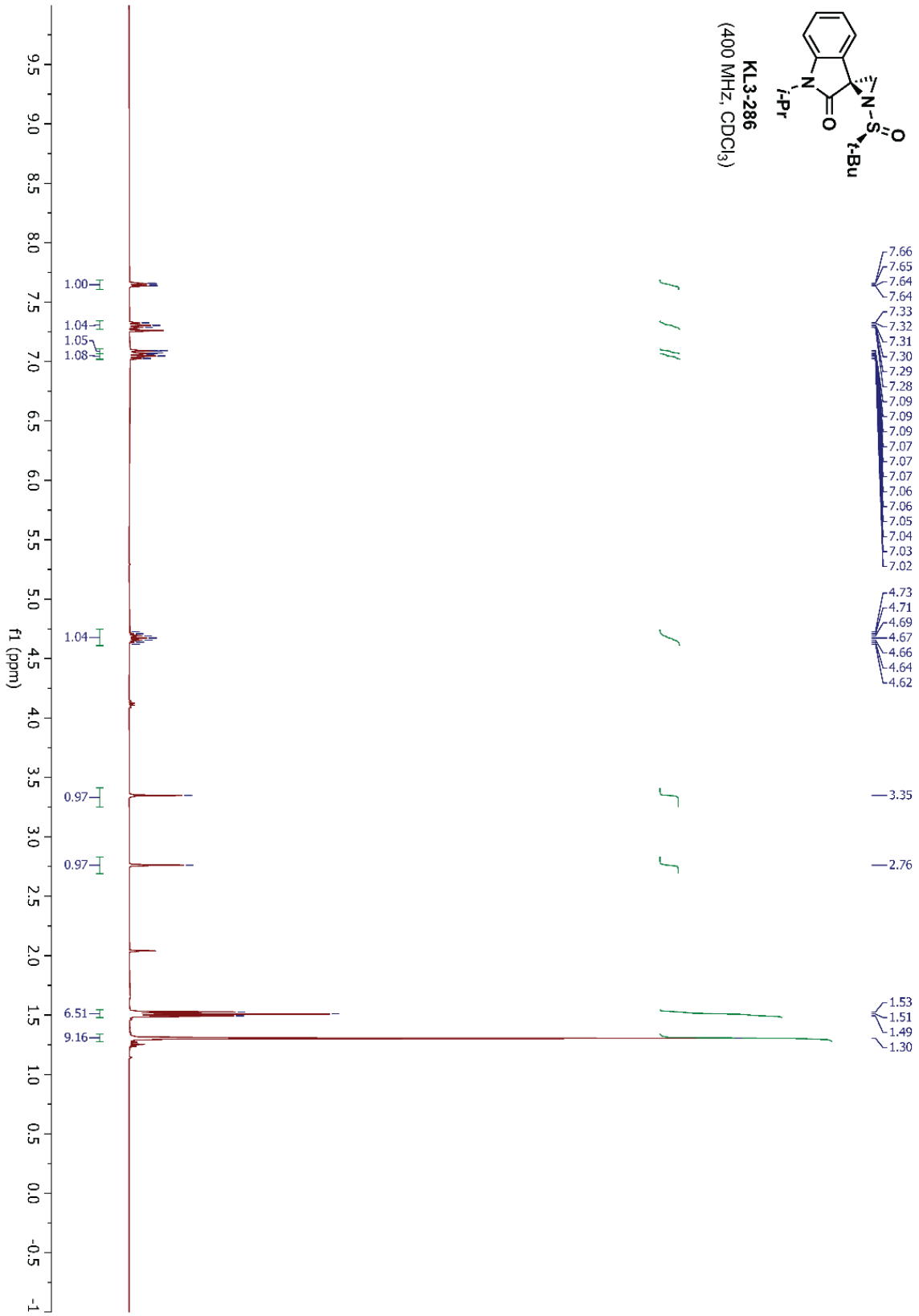
KL3-286
(400 MHz, CDCl3)
i-Pr
t-Bu
f1 (ppm)
1.00
1.04
1.05
1.08
1.04
0.97
0.97
6.51
9.16
7.66
7.65
7.64
7.64
7.33
7.32
7.31
7.30
7.29
7.28
7.09
7.09
7.09
7.07
7.07
7.07
7.06
7.06
7.05
7.04
7.03
7.02
4.73
4.71
4.69
4.67
4.66
4.64
4.62
3.35
2.76
1.53
1.51
1.49
1.30

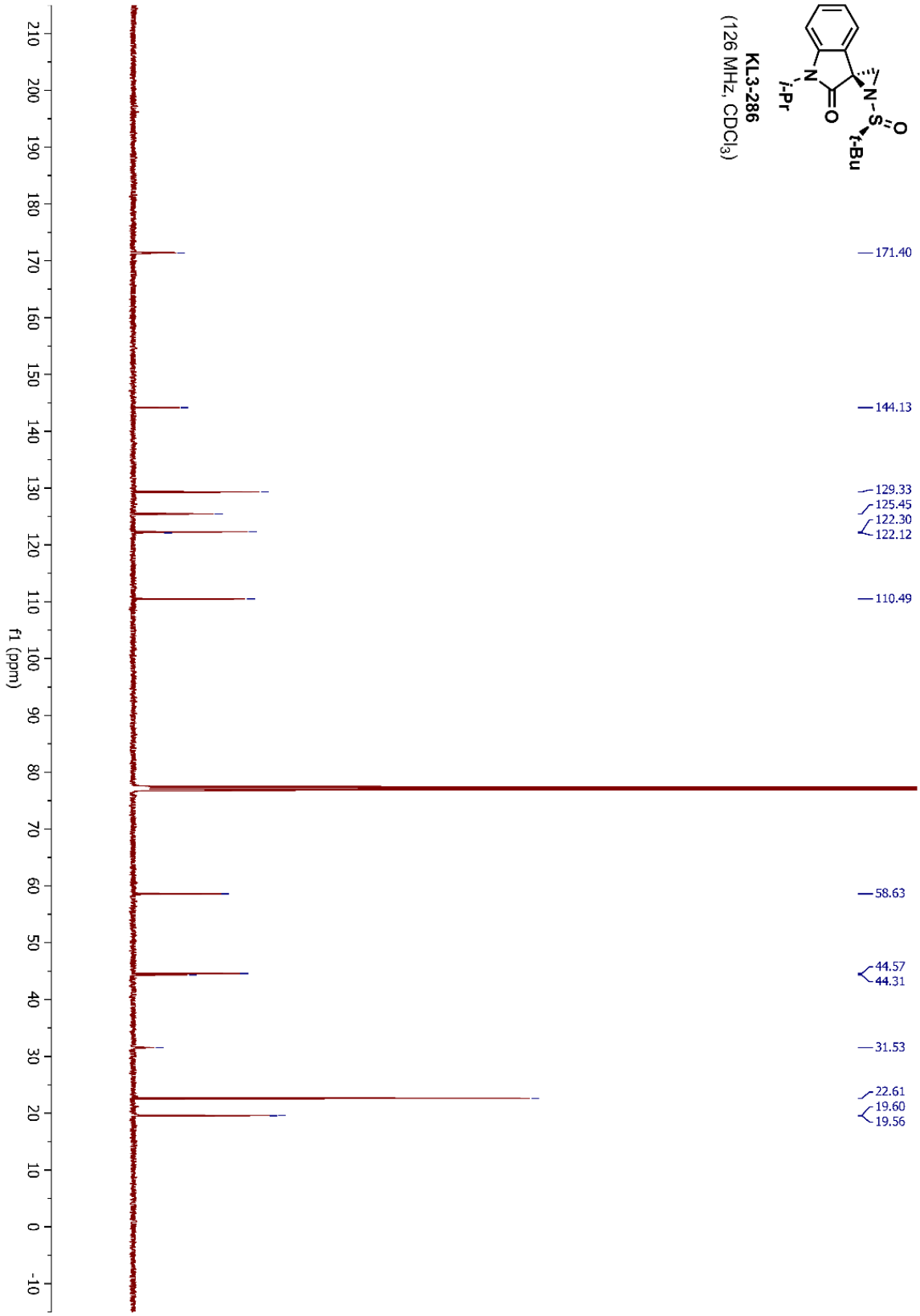
KL3-286
(126 MHz, CDCl3)
i-Pr
t-Bu
171.40
144.13
129.33
125.45
122.30
122.12
110.49
58.63
44.57
44.31
31.53
22.61
19.60
19.56
f1 (ppm)

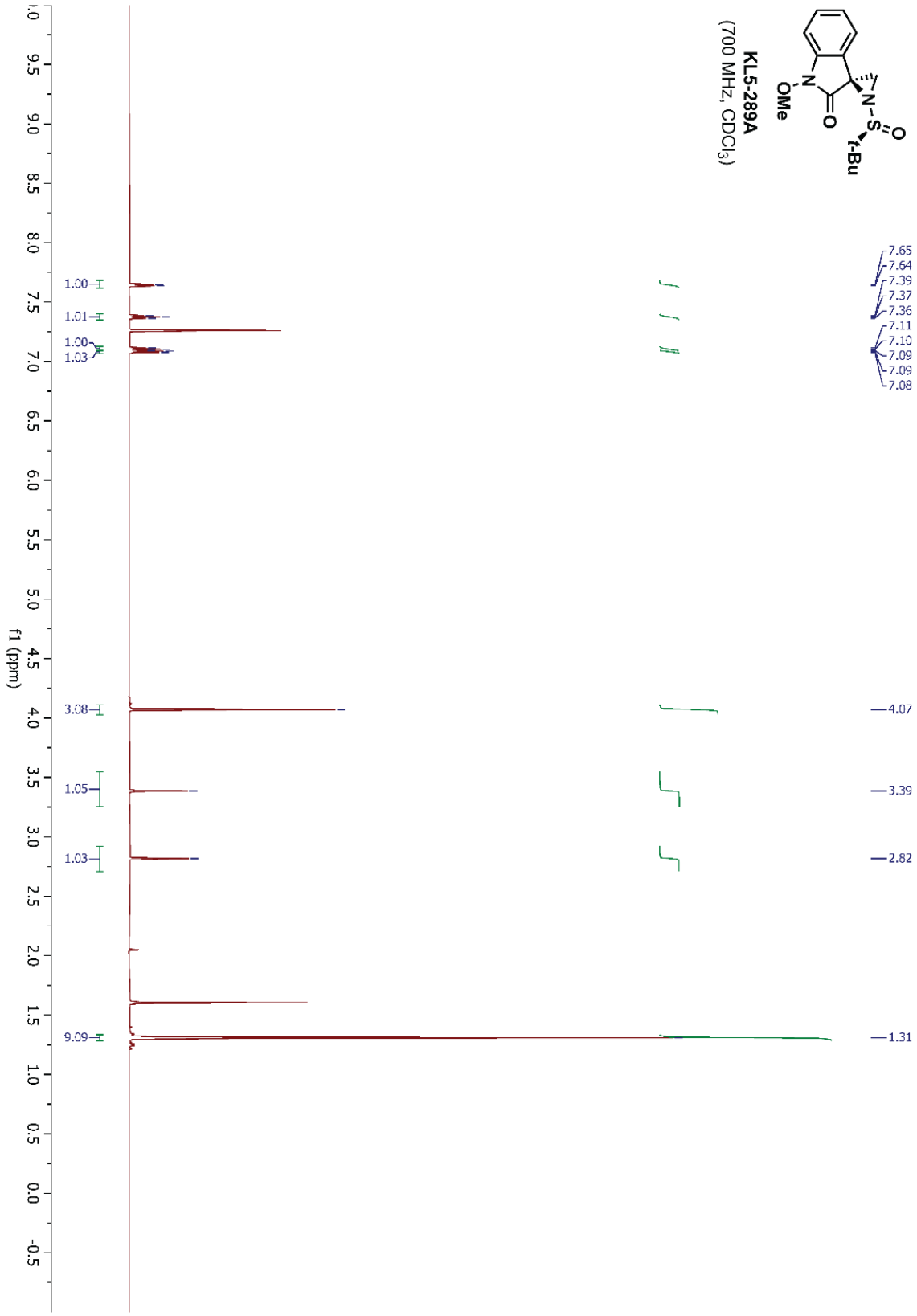
KL5-289A
(700 MHz, CDCl3)
OMe
N
O
N
S
O
t-Bu
7.65
7.64
7.39
7.37
7.36
7.11
7.10
7.09
7.09
7.08
1.00
1.01
1.00
1.03
3.08
1.05
1.03
9.09
4.07
3.39
2.82
1.31
f1 (ppm)

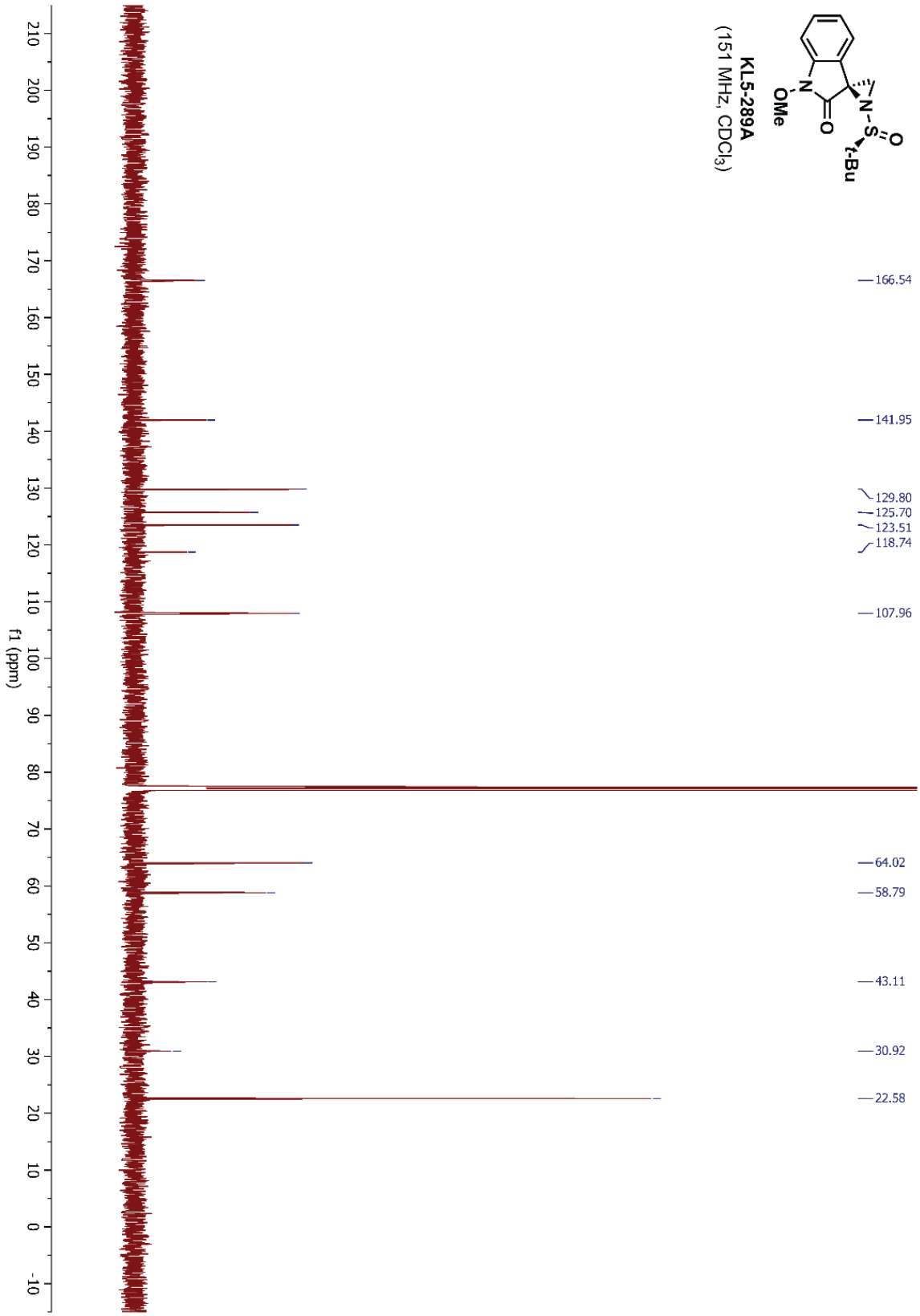
KL5-289A
(151 MHz, CDCl3)
OMe
N
O
N
S
O
t-Bu
166.54
141.95
129.80
125.70
123.51
118.74
107.96
64.02
58.79
43.11
30.92
22.58
f1 (ppm)
210
200
190
180
170
160
150
140
130
120
110
100
90
80
70
60
50
40
30
20
10
0
-10

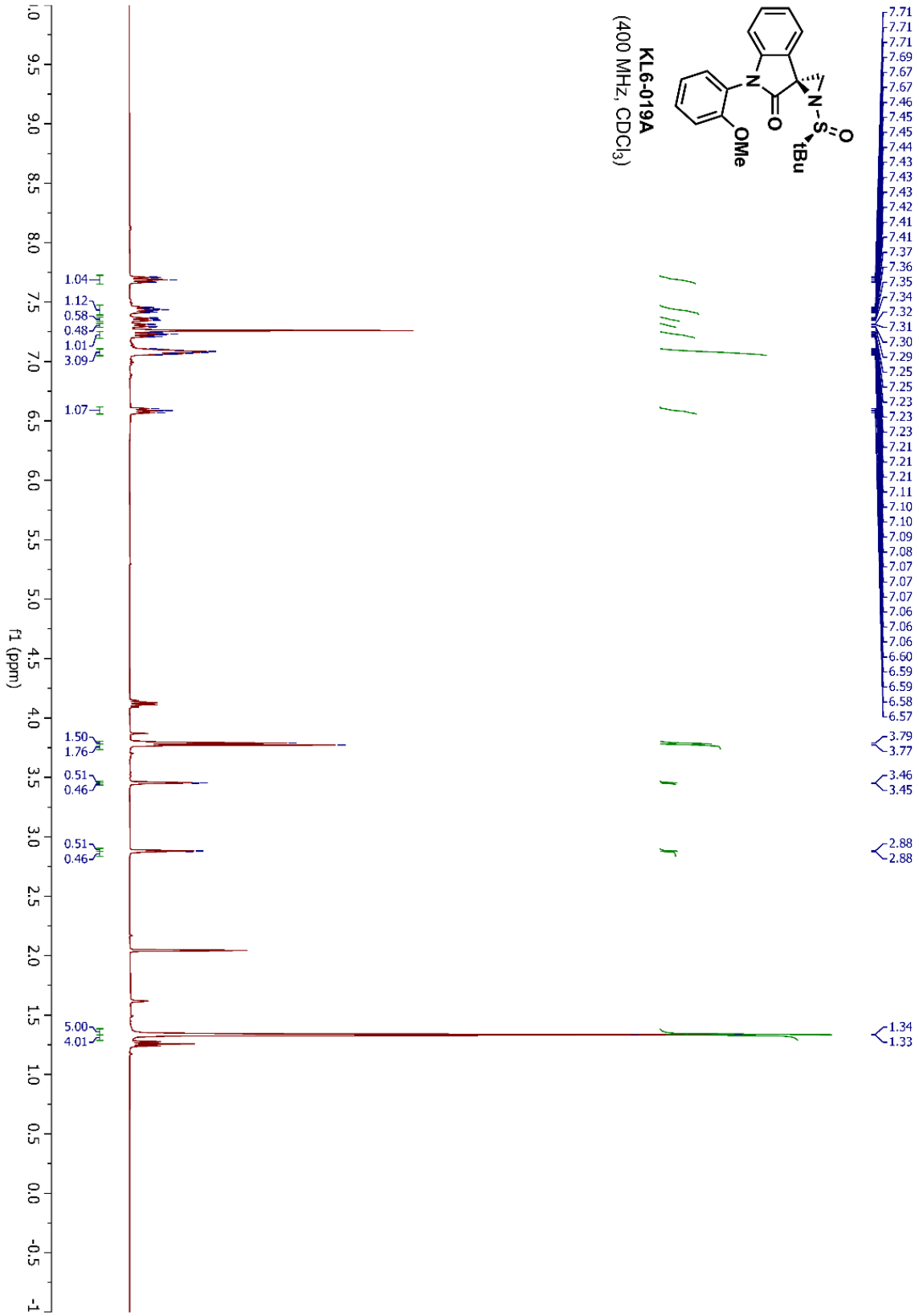
KL6-019A
(400 MHz, CDCl3)
OMe
tBu
f1 (ppm)
1.04
1.12
0.58
0.48
1.01
3.09
1.07
1.50
1.76
0.51
0.46
0.51
0.46
5.00
4.01
7.71
7.71
7.71
7.69
7.67
7.67
7.46
7.45
7.45
7.44
7.43
7.43
7.43
7.42
7.41
7.41
7.37
7.36
7.35
7.34
7.32
7.31
7.30
7.29
7.25
7.25
7.23
7.23
7.23
7.21
7.21
7.21
7.11
7.10
7.10
7.09
7.08
7.07
7.07
7.07
7.06
7.06
7.06
6.60
6.59
6.59
6.58
6.57
3.79
3.77
3.46
3.45
2.88
2.88
1.34
1.33

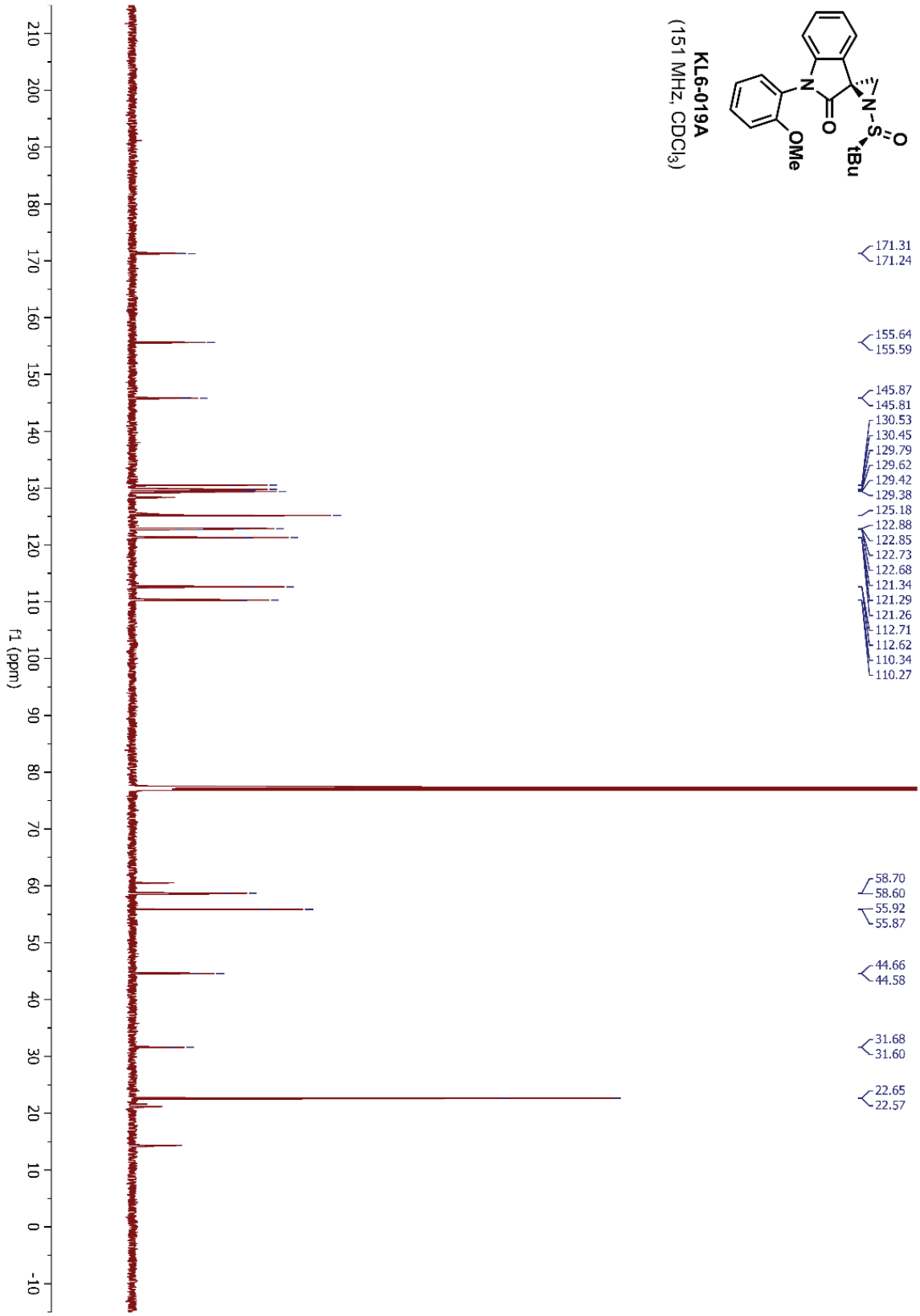
KL6-019A
(151 MHz, CDCl3)
OMe
tBu
171.31
171.24
155.64
155.59
145.87
145.81
130.53
130.45
129.79
129.62
129.42
129.38
125.18
122.88
122.85
122.73
122.68
121.34
121.29
121.26
112.71
112.62
110.34
110.27
58.70
58.60
55.92
55.87
44.66
44.58
31.68
31.60
22.65
22.57
f1 (ppm)

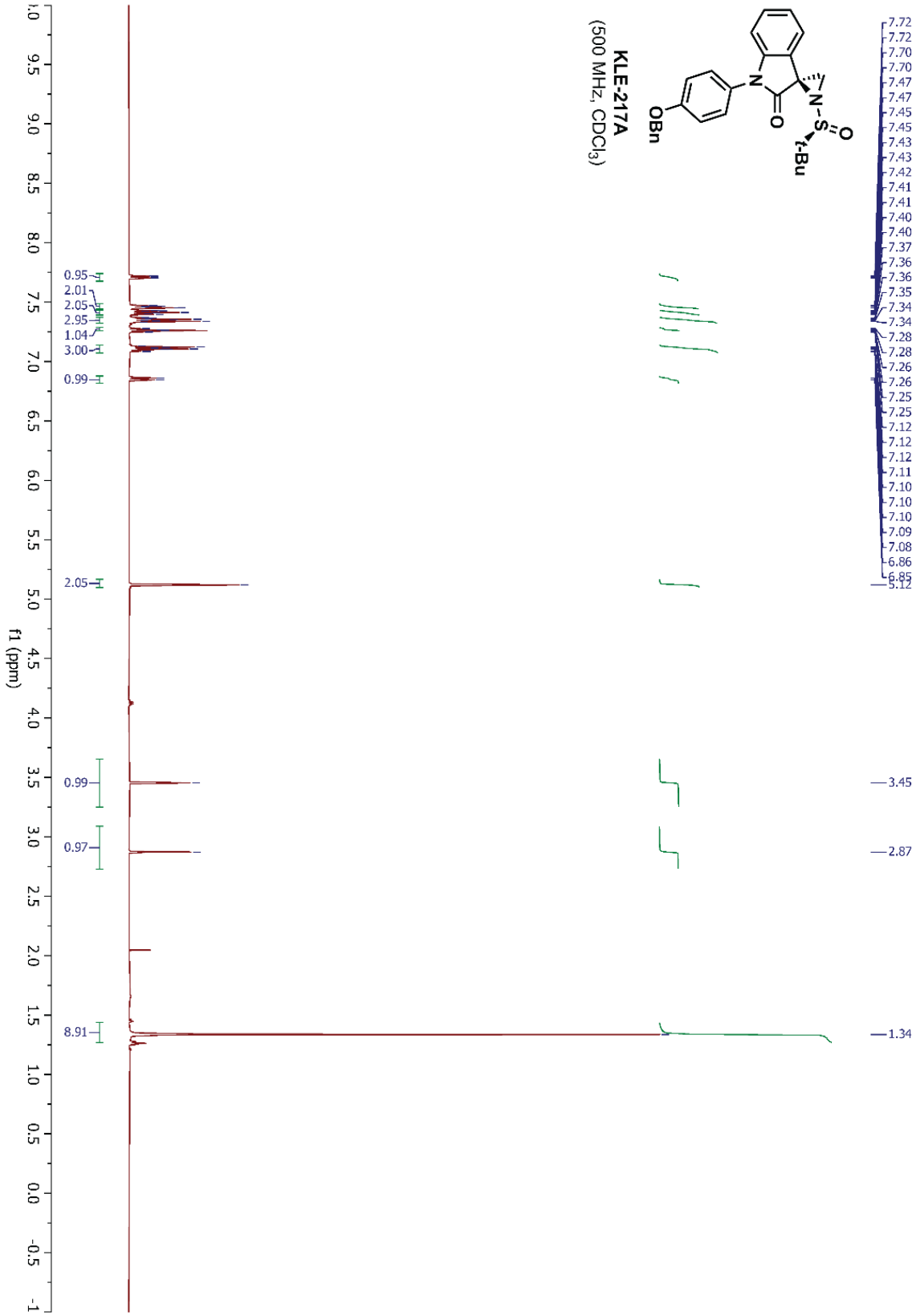
KLE-217A
(500 MHz, CDCl3)
OBn
N
O
N-S
O
t-Bu
7.72
7.72
7.70
7.70
7.47
7.47
7.45
7.45
7.43
7.43
7.42
7.41
7.41
7.40
7.40
7.37
7.36
7.36
7.35
7.34
7.34
7.28
7.28
7.26
7.26
7.25
7.25
7.12
7.12
7.12
7.11
7.10
7.10
7.10
7.09
7.08
6.86
6.85
5.12
3.45
2.87
1.34
0.95
2.01
2.05
2.95
1.04
3.00
0.99
2.05
0.99
0.97
8.91
f1 (ppm)

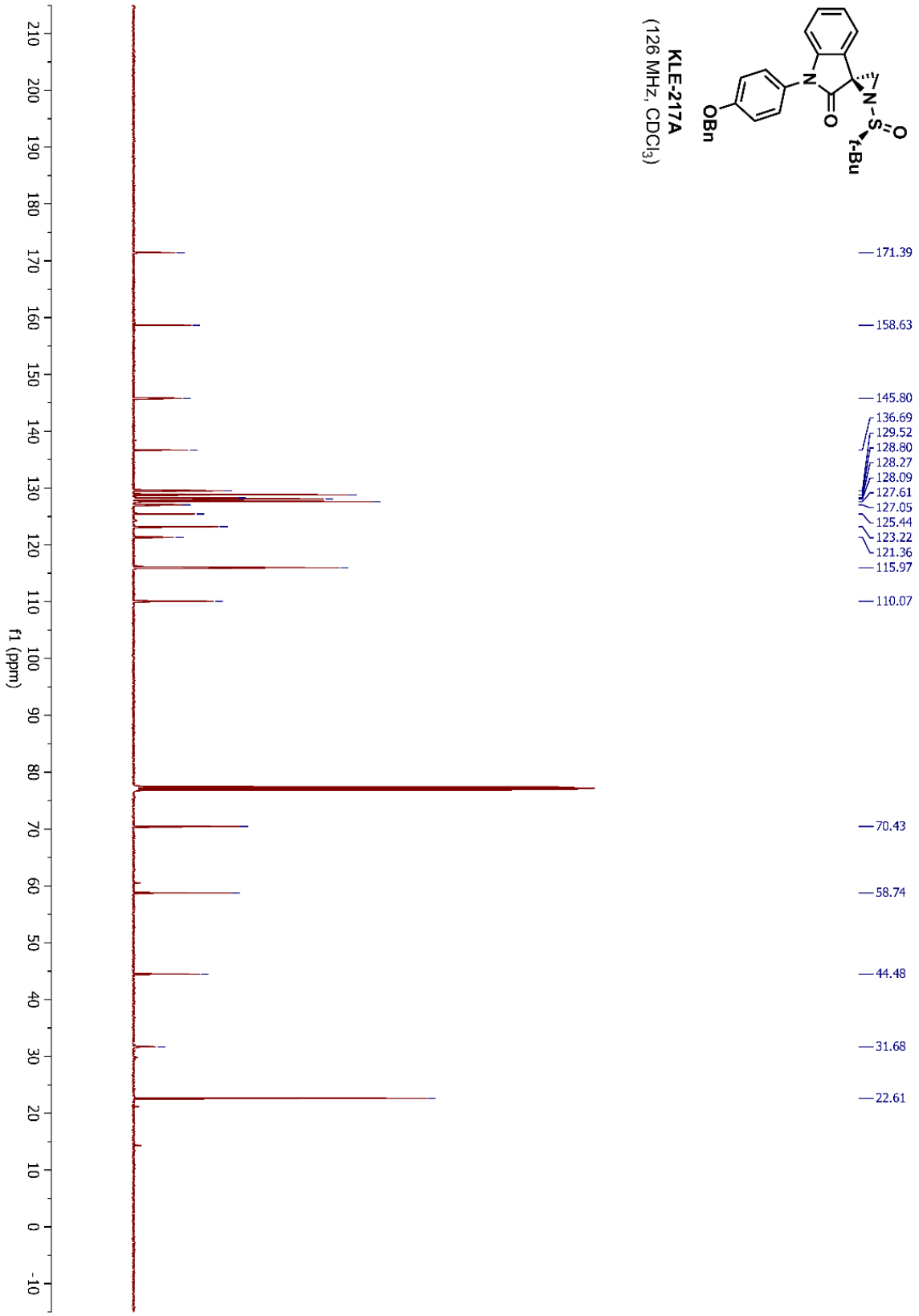
KLE-217A
(126 MHz, CDCl3)
OBn
N
O
N
S
O
t-Bu
171.39
158.63
145.80
136.69
129.52
128.80
128.27
128.09
127.61
127.05
125.44
123.22
121.36
115.97
110.07
70.43
58.74
44.48
31.68
22.61
f1 (ppm)
210
200
190
180
170
160
150
140
130
120
110
100
90
80
70
60
50
40
30
20
10
0
-10

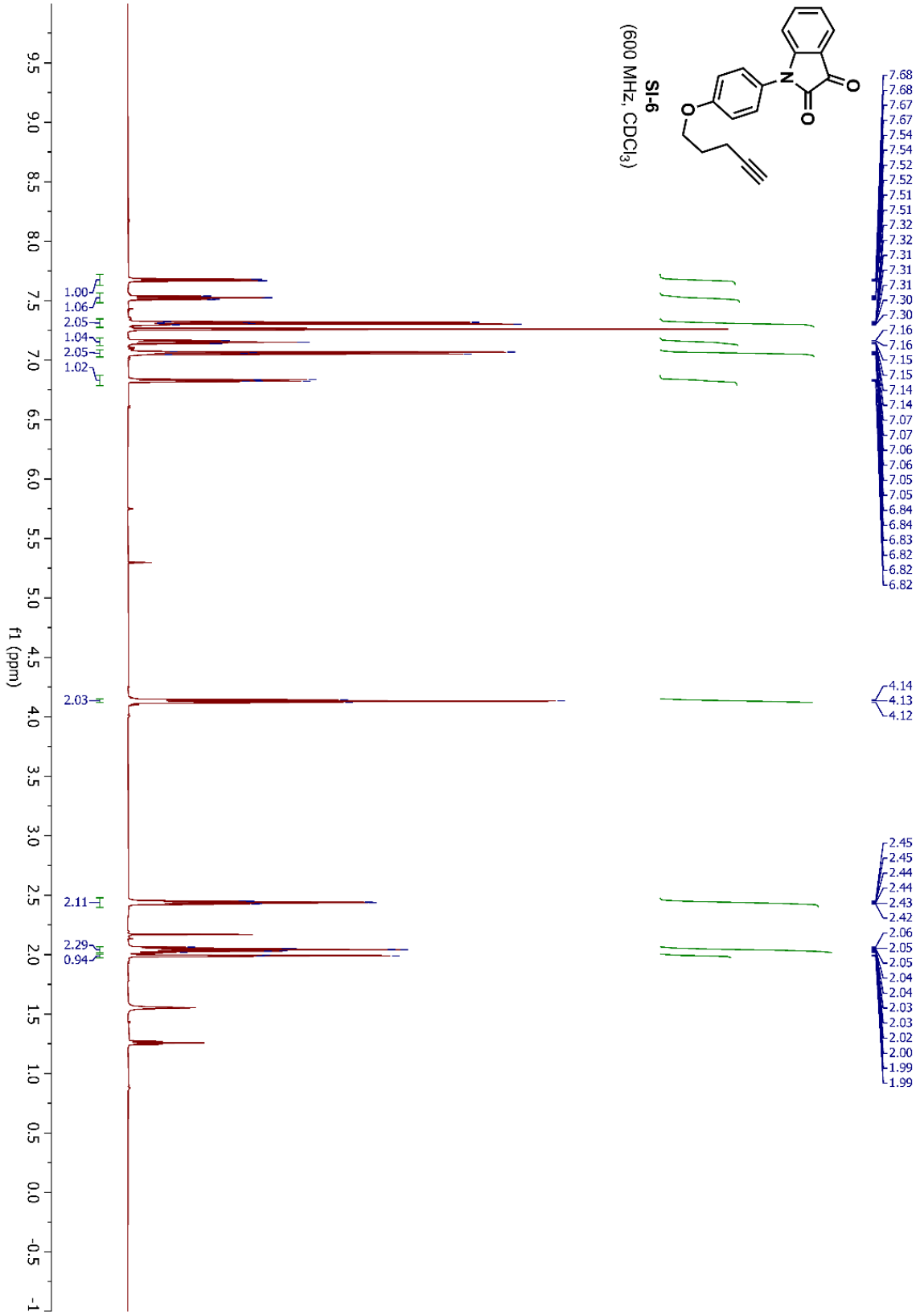
SI-6
(600 MHz, CDCl3)
f1 (ppm)
1.00
1.06
2.05
1.04
2.05
1.02
2.03
2.11
2.29
0.94
7.68
7.68
7.67
7.67
7.54
7.54
7.52
7.52
7.51
7.51
7.32
7.32
7.31
7.31
7.31
7.30
7.30
7.16
7.16
7.15
7.15
7.14
7.14
7.07
7.07
7.06
7.06
7.05
7.05
6.84
6.84
6.83
6.82
6.82
6.82
4.14
4.13
4.12
2.45
2.45
2.44
2.44
2.43
2.42
2.06
2.05
2.05
2.04
2.04
2.03
2.03
2.02
2.00
1.99
1.99

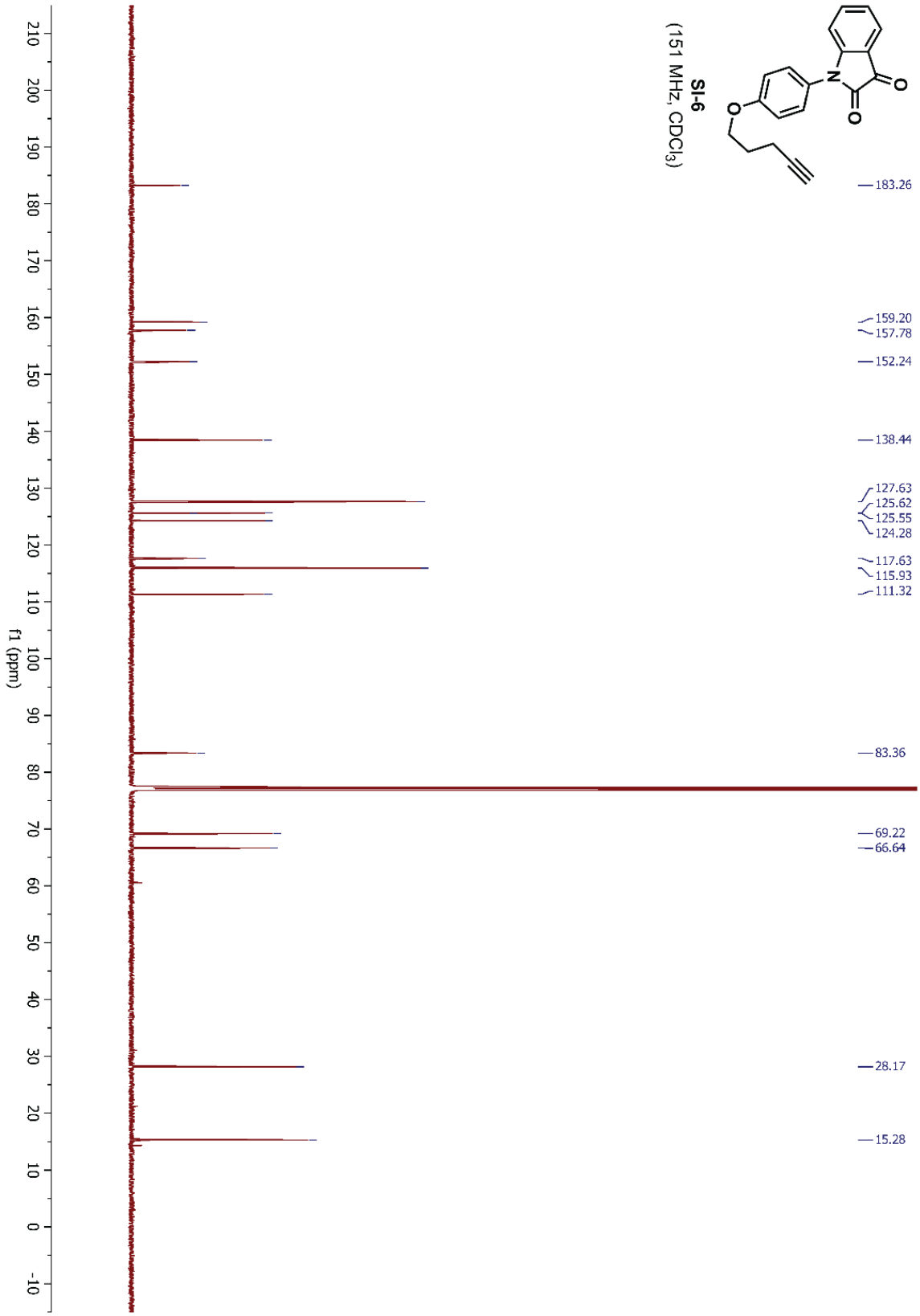
SI-6
(151 MHz, CDCl3)
183.26
159.20
157.78
152.24
138.44
127.63
125.62
125.55
124.28
117.63
115.93
111.32
83.36
69.22
66.64
28.17
15.28
f1 (ppm)

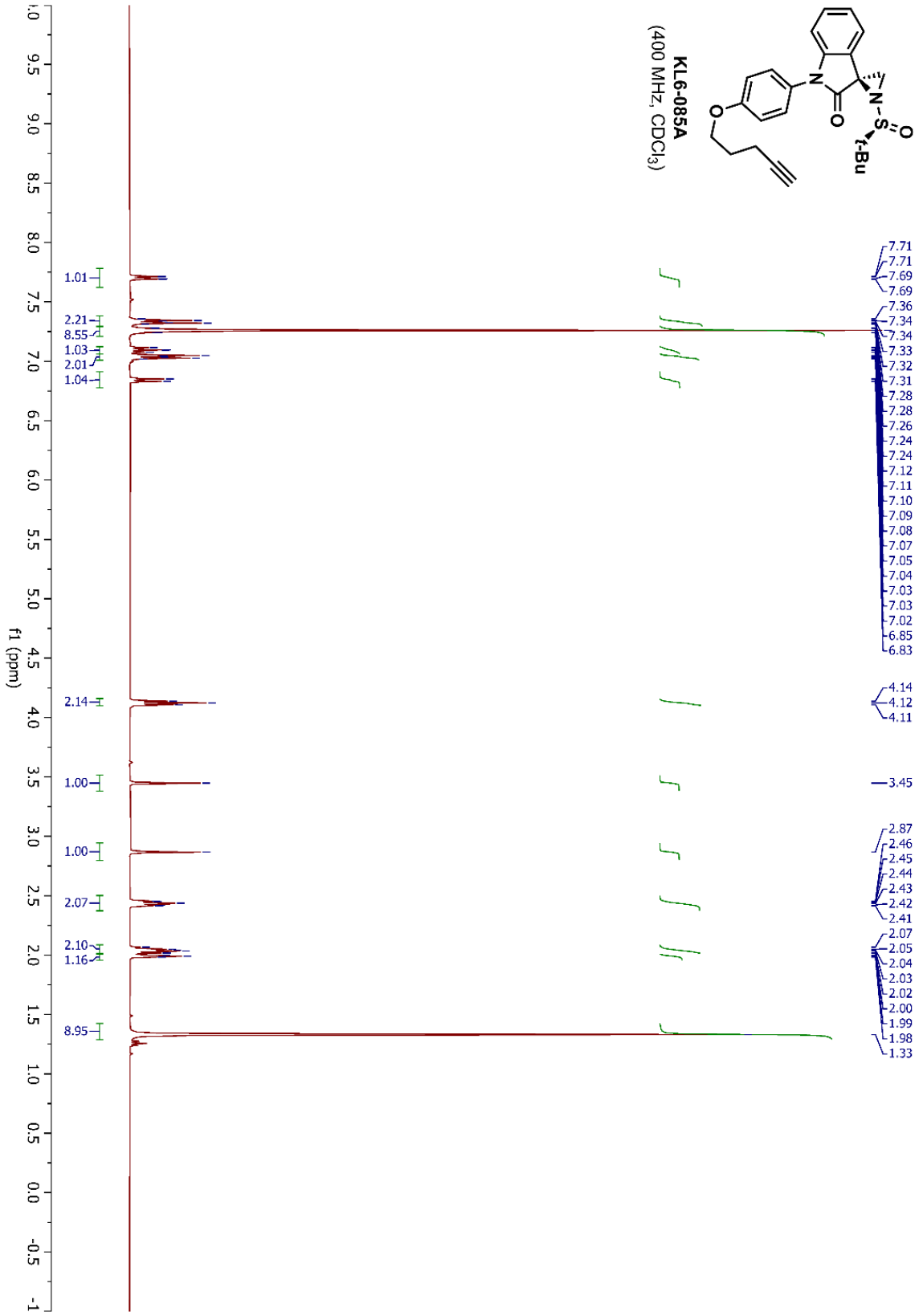
KL6-085A
(400 MHz, CDCl3)
f1 (ppm)
1.01
2.21
8.55
1.03
2.01
1.04
2.14
1.00
1.00
2.07
2.10
1.16
8.95
7.71
7.71
7.69
7.69
7.36
7.34
7.34
7.33
7.32
7.31
7.28
7.28
7.26
7.24
7.24
7.12
7.11
7.10
7.09
7.08
7.07
7.05
7.04
7.03
7.03
7.02
6.85
6.83
4.14
4.12
4.11
3.45
2.87
2.46
2.45
2.44
2.43
2.42
2.41
2.07
2.05
2.04
2.03
2.02
2.00
1.99
1.98
1.33

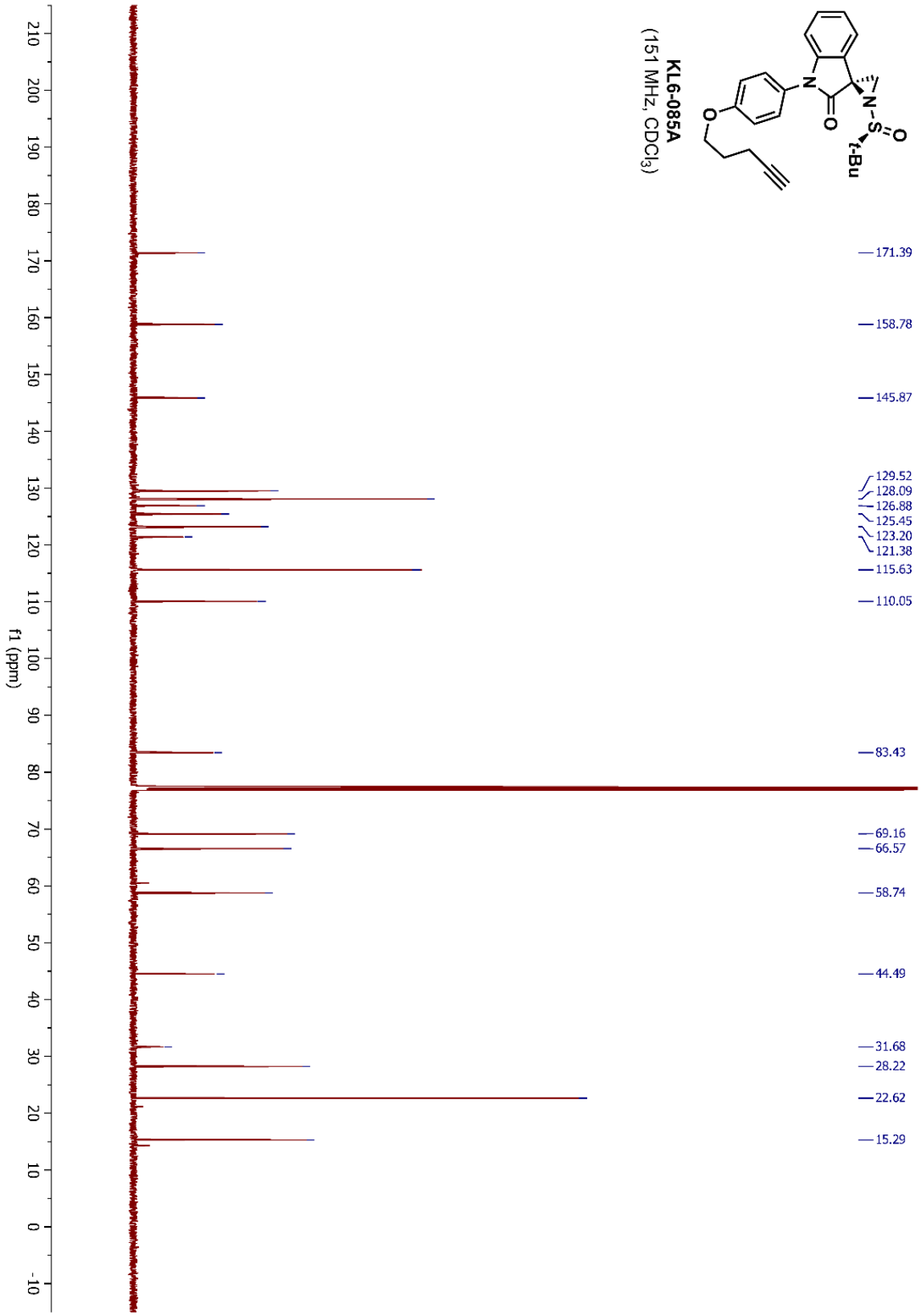
KL6-085A
(151 MHz, CDCl3)
171.39
158.78
145.87
129.52
128.09
126.88
125.45
123.20
121.38
115.63
110.05
83.43
69.16
66.57
58.74
44.49
31.68
28.22
22.62
15.29
f1 (ppm)

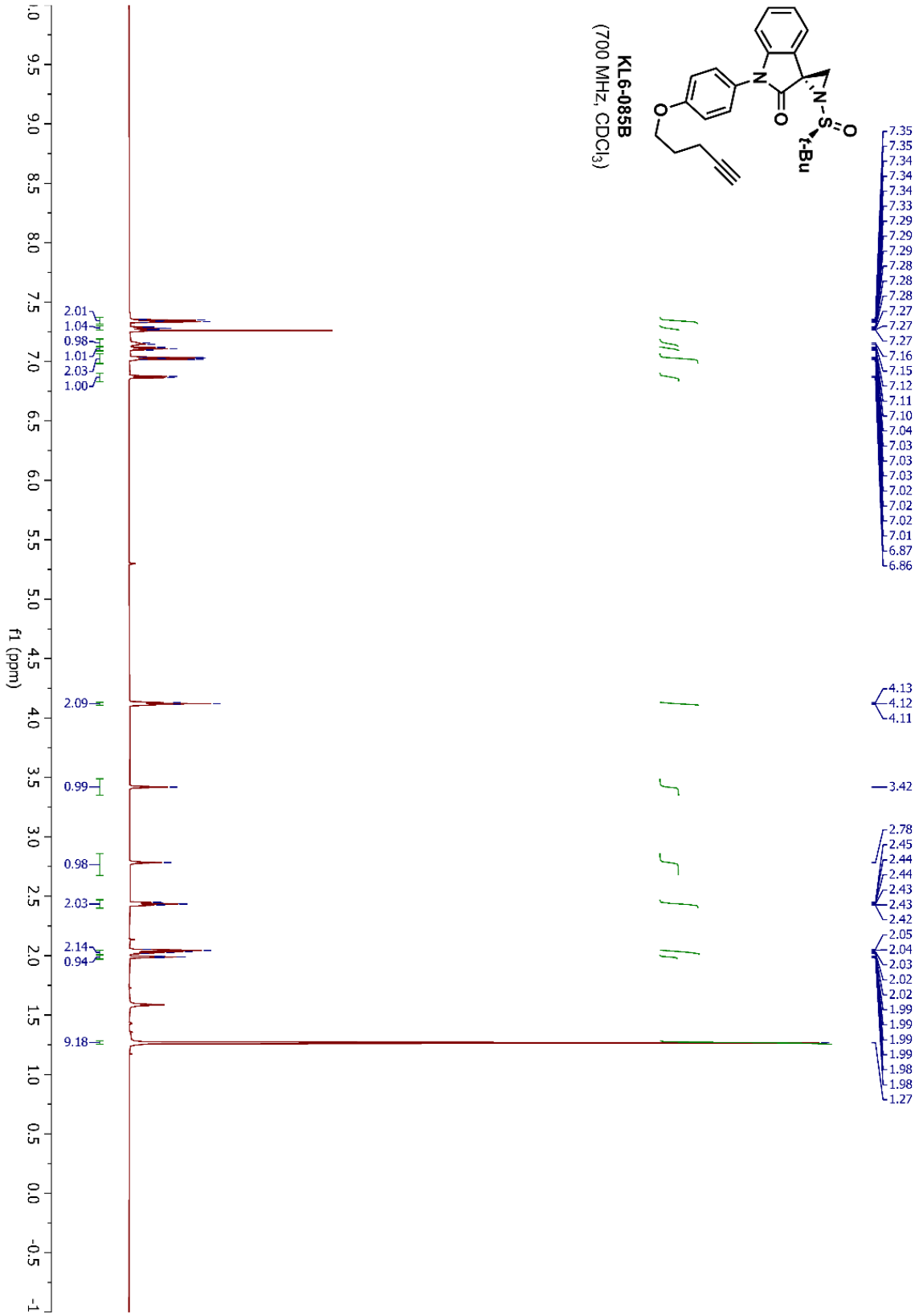
KL6-085B
(700 MHz, CDCl3)
t-Bu
f1 (ppm)
2.01
1.04
0.98
1.01
2.03
1.00
2.09
0.99
0.98
2.03
2.14
0.94
9.18
7.35
7.35
7.34
7.34
7.34
7.33
7.29
7.29
7.29
7.28
7.28
7.28
7.27
7.27
7.27
7.16
7.15
7.12
7.11
7.10
7.04
7.03
7.03
7.03
7.02
7.02
7.02
7.01
6.87
6.86
4.13
4.12
4.11
3.42
2.78
2.45
2.44
2.44
2.43
2.43
2.42
2.05
2.04
2.03
2.02
2.02
1.99
1.99
1.99
1.99
1.98
1.98
1.27

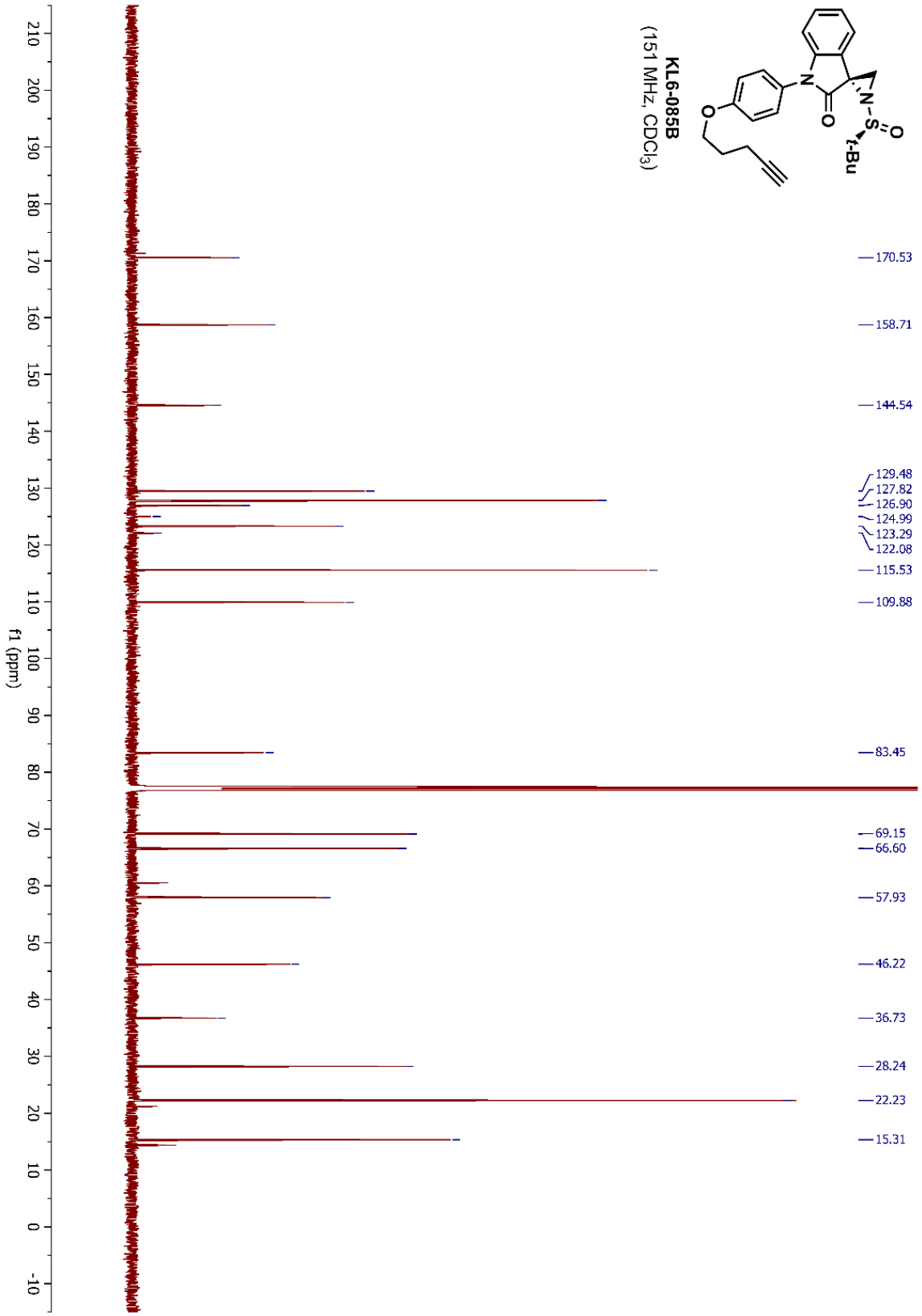
KL6-085B
(151 MHz, CDCl3)
170.53
158.71
144.54
129.48
127.82
126.90
124.99
123.29
122.08
115.53
109.88
83.45
69.15
66.60
57.93
46.22
36.73
28.24
22.23
15.31
f1 (ppm)

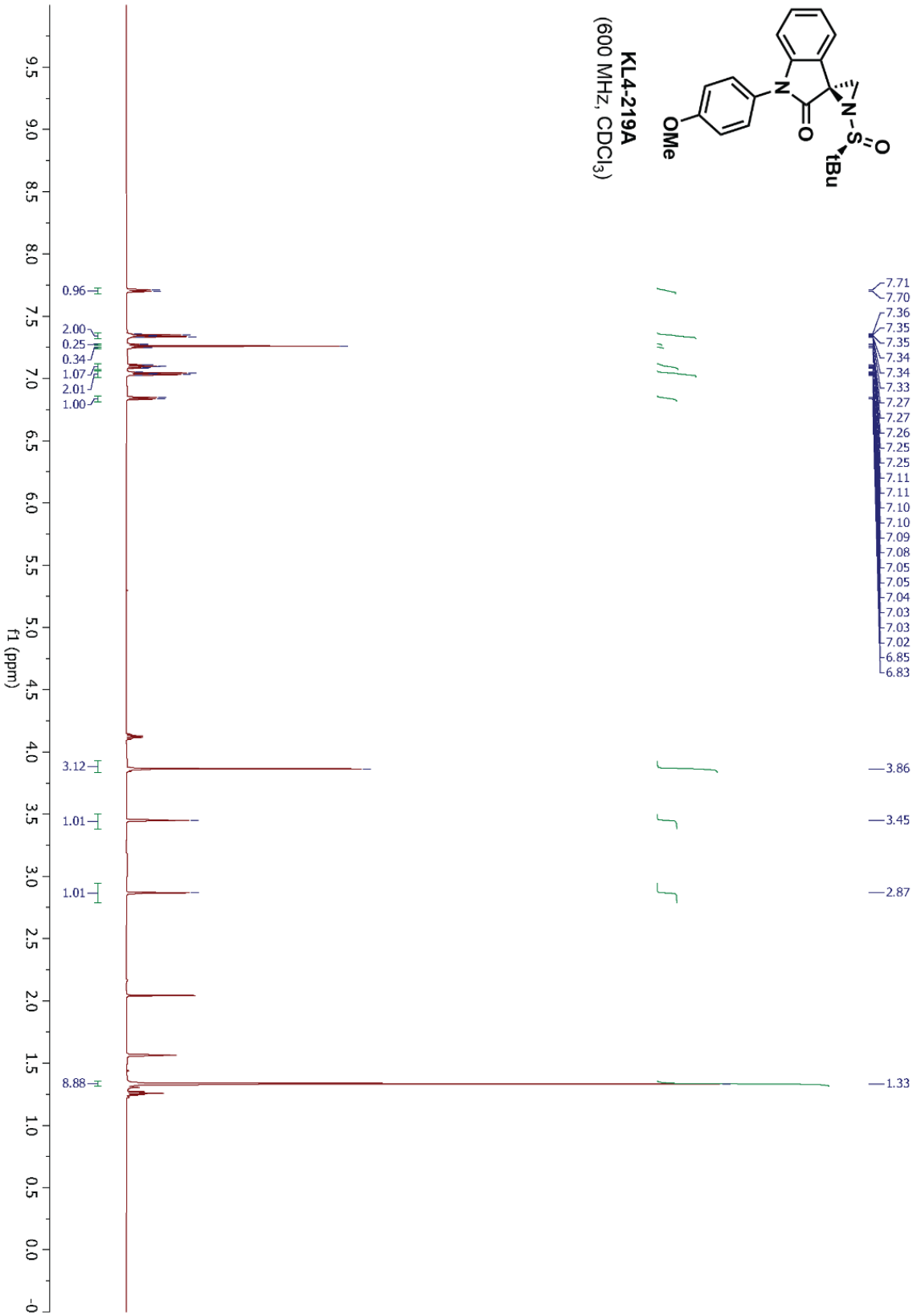
KL4-219A
(600 MHz, CDCl3)
OMe
tBu
f1 (ppm)
0.96
2.00
0.25
0.34
1.07
2.01
1.00
3.12
1.01
1.01
8.88
7.71
7.70
7.36
7.35
7.35
7.34
7.34
7.33
7.27
7.27
7.26
7.25
7.25
7.11
7.11
7.10
7.10
7.09
7.08
7.05
7.05
7.04
7.03
7.03
7.02
6.85
6.83
3.86
3.45
2.87
1.33

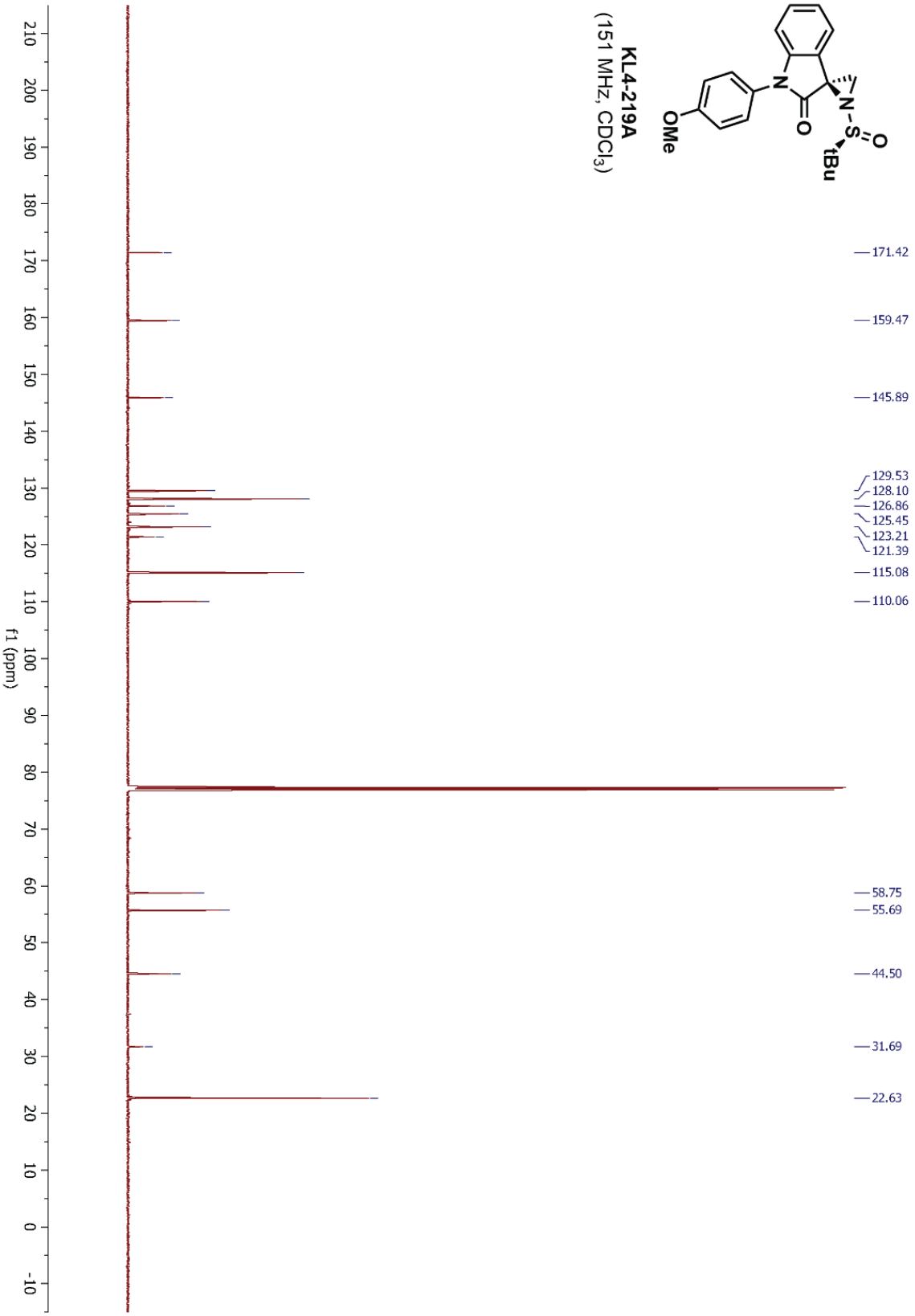
KL4-219A
(151 MHz, CDCl3)
OMe
N
O
N
S
O
tBu
171.42
159.47
145.89
129.53
128.10
126.86
125.45
123.21
121.39
115.08
110.06
58.75
55.69
44.50
31.69
22.63
f1 (ppm)
210
200
190
180
170
160
150
140
130
120
110
100
90
80
70
60
50
40
30
20
10
0
-10

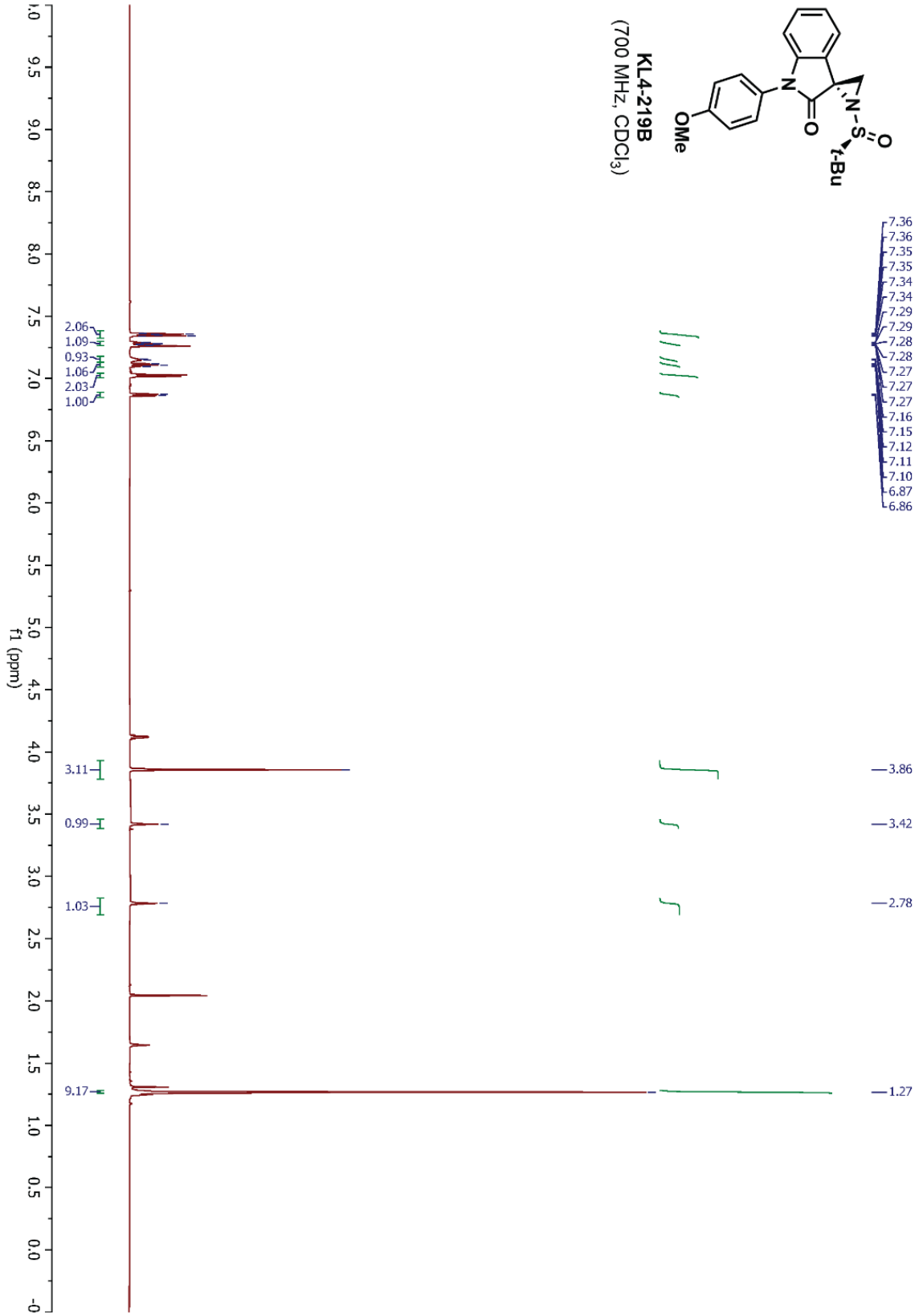
KL4-219B
(700 MHz, CDCl3)
OMe
N
O
N
S
O
t-Bu
7.36
7.36
7.35
7.35
7.34
7.34
7.29
7.29
7.28
7.28
7.27
7.27
7.27
7.16
7.15
7.12
7.11
7.10
6.87
6.86
2.06
1.09
0.93
1.06
2.03
1.00
3.11
0.99
1.03
9.17
3.86
3.42
2.78
1.27
f1 (ppm)

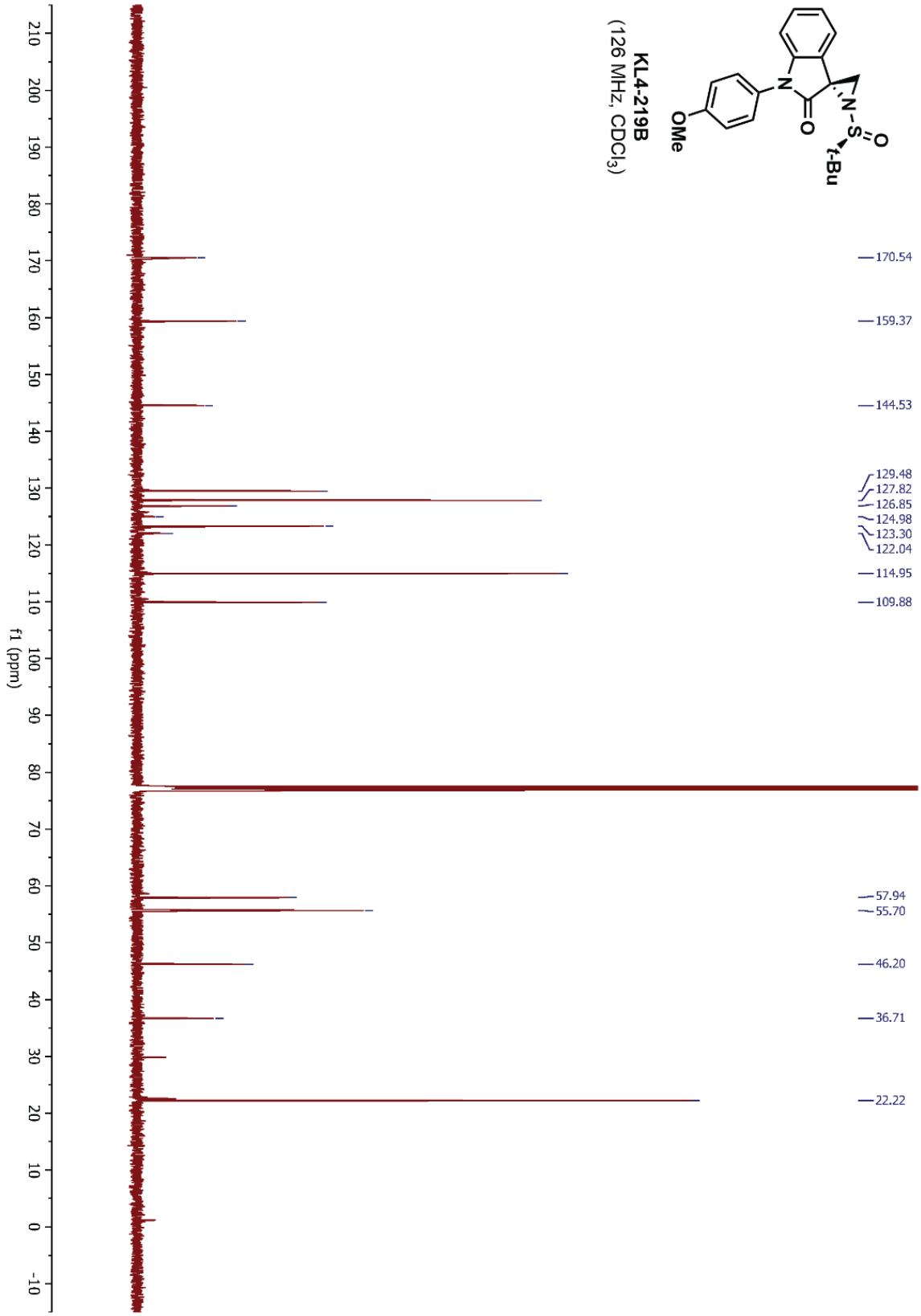
KL4-219B
(126 MHz, CDCl3)
OMe
N
O
N
S
O
t-Bu
170.54
159.37
144.53
129.48
127.82
126.85
124.98
123.30
122.04
114.95
109.88
57.94
55.70
46.20
36.71
22.22
f1 (ppm)
210
200
190
180
170
160
150
140
130
120
110
100
90
80
70
60
50
40
30
20
10
0
-10

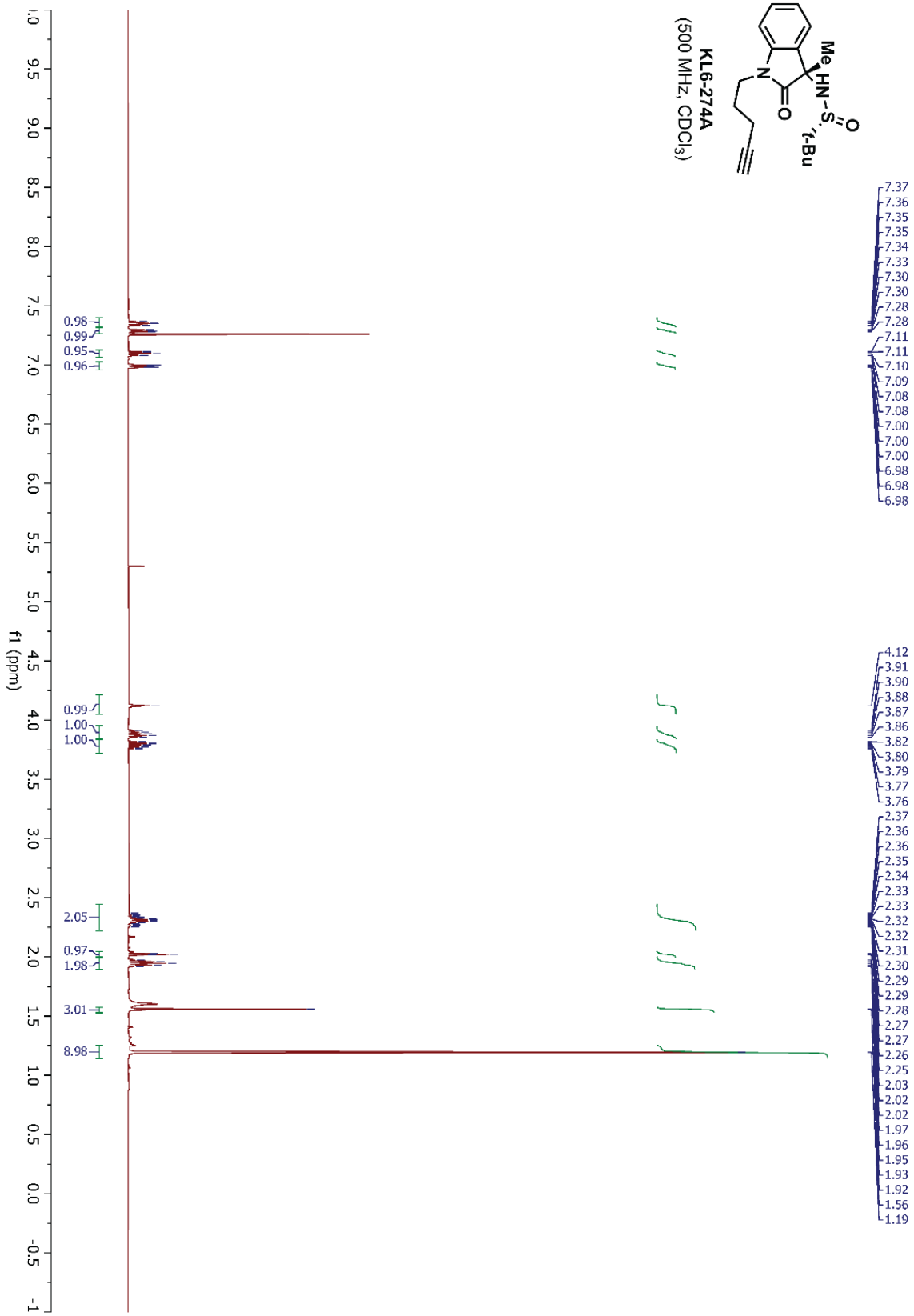
KL6-274A
(500 MHz, CDCl3)
Me
HN
S
O
O
t-Bu
N
O
f1 (ppm)
1.0
9.5
9.0
8.5
8.0
7.5
7.0
6.5
6.0
5.5
5.0
4.5
4.0
3.5
3.0
2.5
2.0
1.5
1.0
0.5
0.0
-0.5
-1
0.98
0.99
0.95
0.96
0.99
1.00
1.00
2.05
0.97
1.98
3.01
8.98
7.37
7.36
7.35
7.35
7.34
7.33
7.30
7.30
7.28
7.28
7.11
7.11
7.10
7.09
7.08
7.08
7.00
7.00
7.00
6.98
6.98
6.98
4.12
3.91
3.90
3.88
3.87
3.86
3.82
3.80
3.79
3.77
3.76
2.37
2.36
2.36
2.35
2.34
2.33
2.33
2.32
2.32
2.31
2.30
2.29
2.29
2.28
2.27
2.27
2.26
2.25
2.03
2.02
2.02
1.97
1.96
1.95
1.93
1.92
1.56
1.19

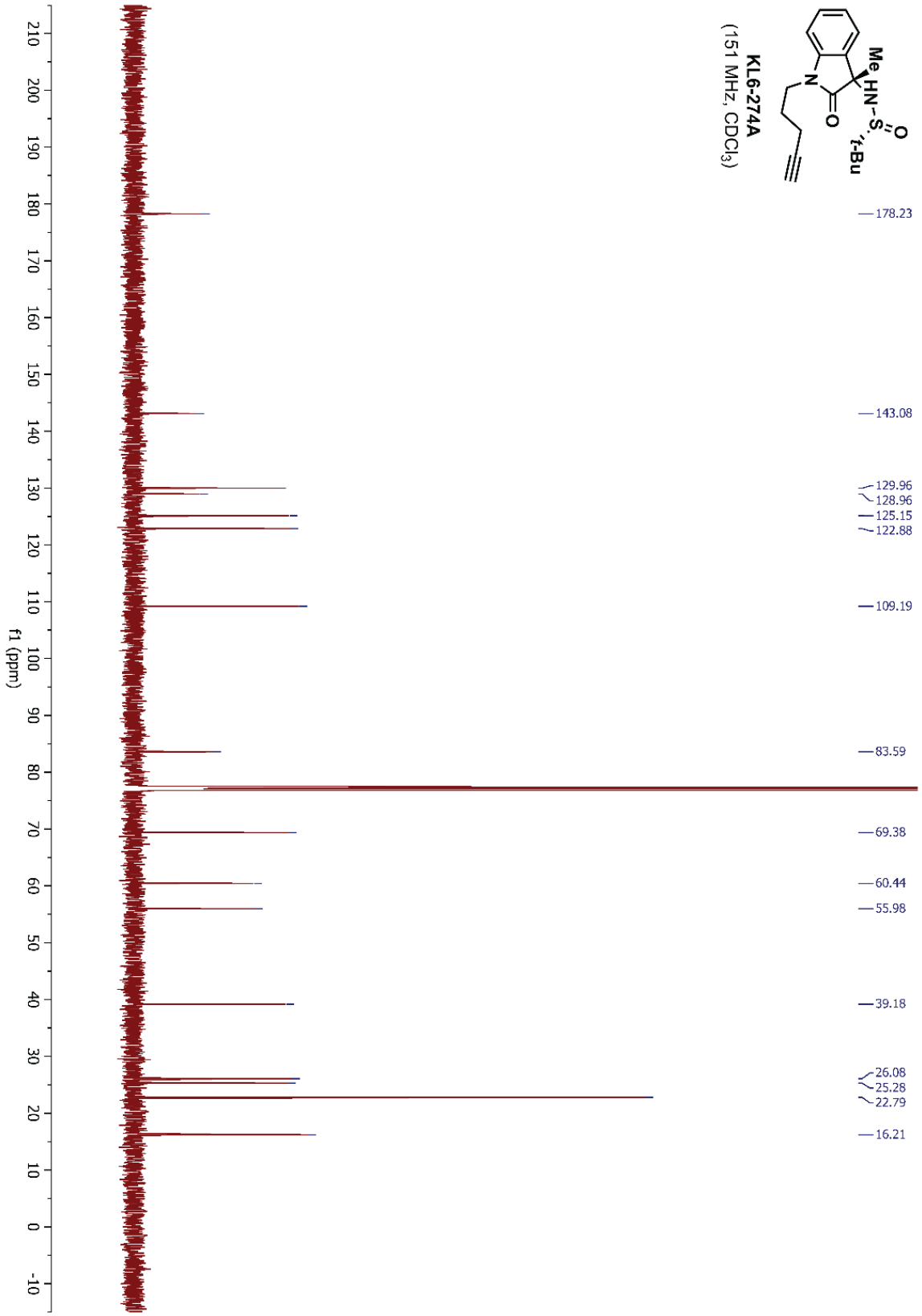
KL6-274A
(151 MHz, CDCl3)
Me
HN
S
O
O
t-Bu
N
O
178.23
143.08
129.96
128.96
125.15
122.88
109.19
83.59
69.38
60.44
55.98
39.18
26.08
25.28
22.79
16.21
f1 (ppm)
210
200
190
180
170
160
150
140
130
120
110
100
90
80
70
60
50
40
30
20
10
0
-10

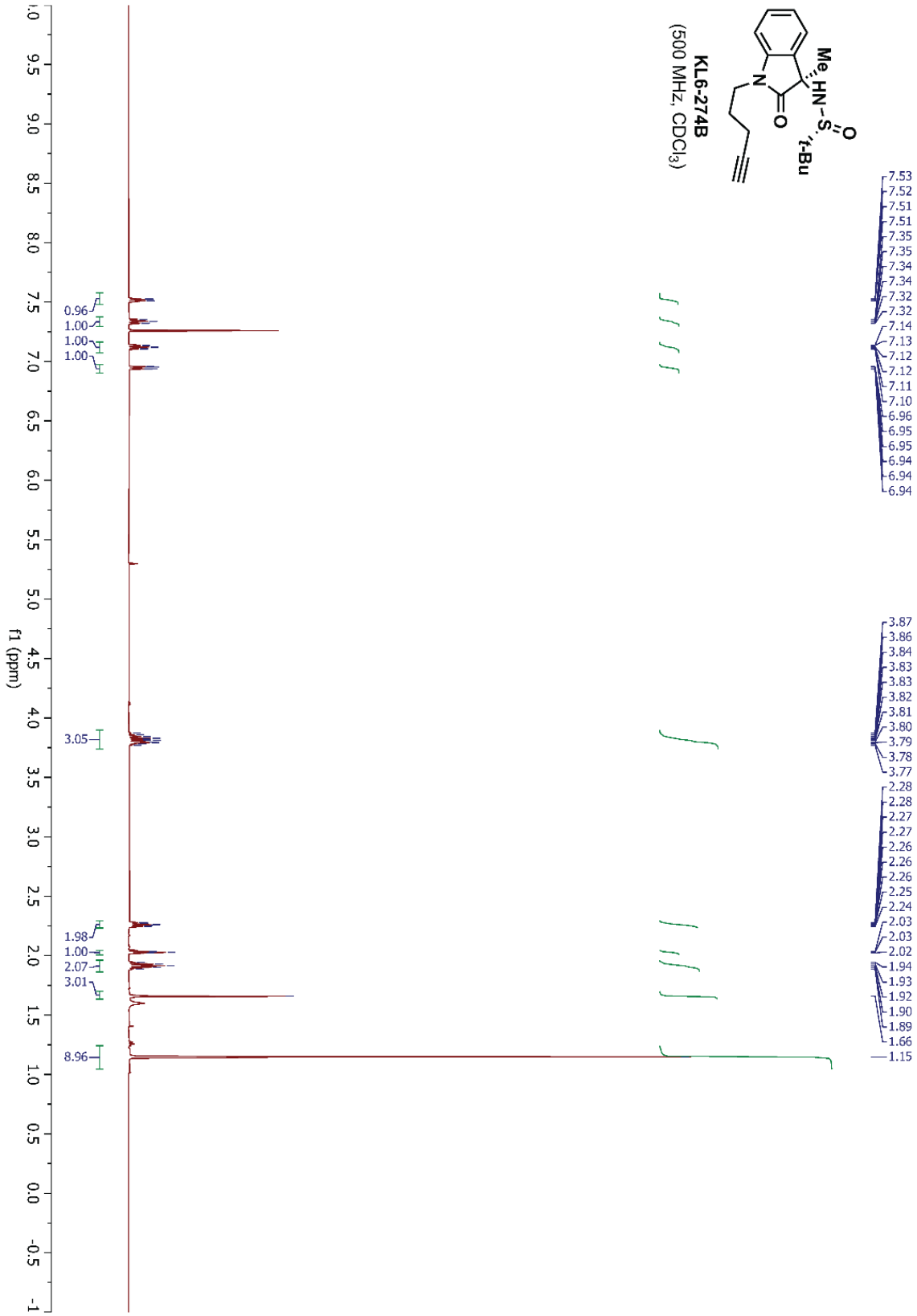
KL6-274B
(500 MHz, CDCl3)
Me
HN
S
O
t-Bu
N
O
f1 (ppm)
0.96
1.00
1.00
1.00
3.05
1.98
1.00
2.07
3.01
8.96
7.53
7.52
7.51
7.51
7.35
7.35
7.34
7.34
7.32
7.32
7.14
7.13
7.12
7.12
7.11
7.10
6.96
6.95
6.95
6.94
6.94
6.94
3.87
3.86
3.84
3.83
3.83
3.82
3.81
3.80
3.79
3.78
3.77
2.28
2.28
2.27
2.27
2.26
2.26
2.26
2.25
2.24
2.03
2.03
2.02
1.94
1.93
1.92
1.90
1.89
1.66
1.15

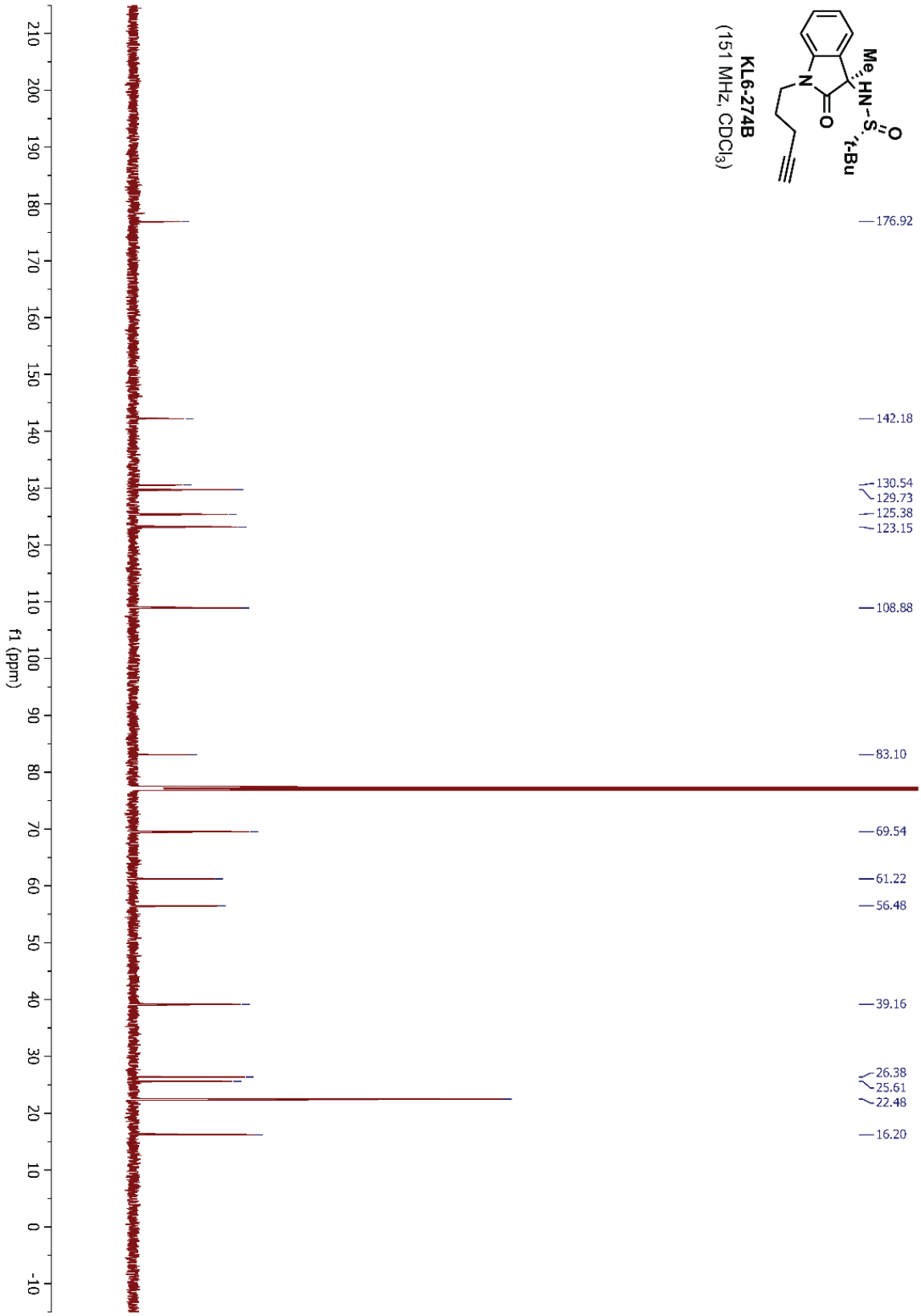
KL6-274B
(151 MHz, CDCl3)
Me
HN
S
O
O
t-Bu
N
O
176.92
142.18
130.54
129.73
125.38
123.15
108.88
83.10
69.54
61.22
56.48
39.16
26.38
25.61
22.48
16.20
f1 (ppm)
210
200
190
180
170
160
150
140
130
120
110
100
90
80
70
60
50
40
30
20
10
0
-10

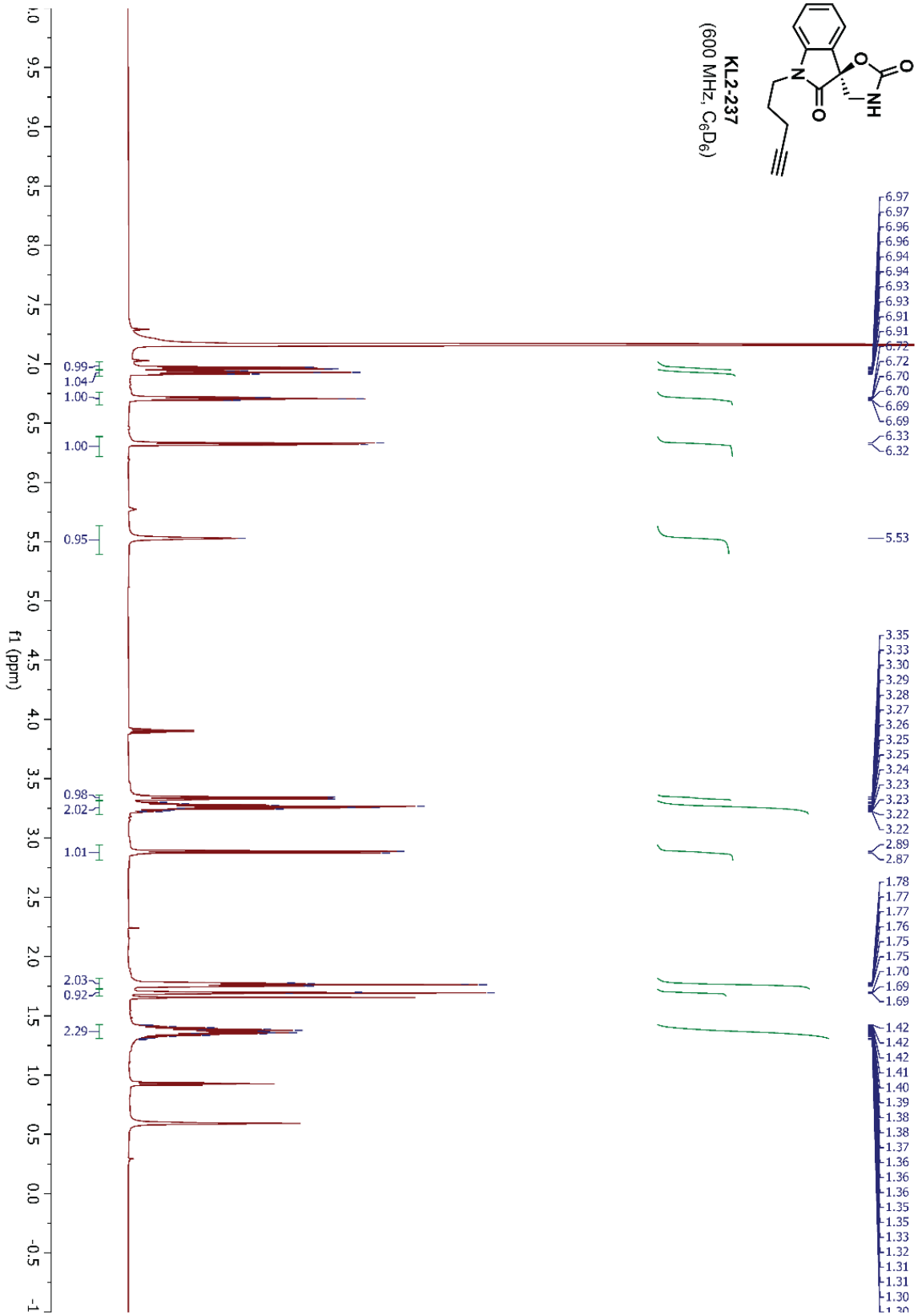
KL2-237
(600 MHz, C6D6)
f1 (ppm)
0.99
1.04
1.00
1.00
0.95
0.98
2.02
1.01
2.03
0.92
2.29
6.97
6.97
6.96
6.96
6.94
6.94
6.93
6.93
6.91
6.91
6.72
6.72
6.70
6.70
6.69
6.69
6.33
6.32
5.53
3.35
3.33
3.30
3.29
3.28
3.27
3.26
3.25
3.25
3.24
3.23
3.23
3.22
3.22
2.89
2.87
1.78
1.77
1.77
1.76
1.75
1.75
1.70
1.69
1.69
1.42
1.42
1.42
1.41
1.40
1.39
1.38
1.38
1.37
1.36
1.36
1.36
1.35
1.35
1.33
1.32
1.31
1.31
1.30

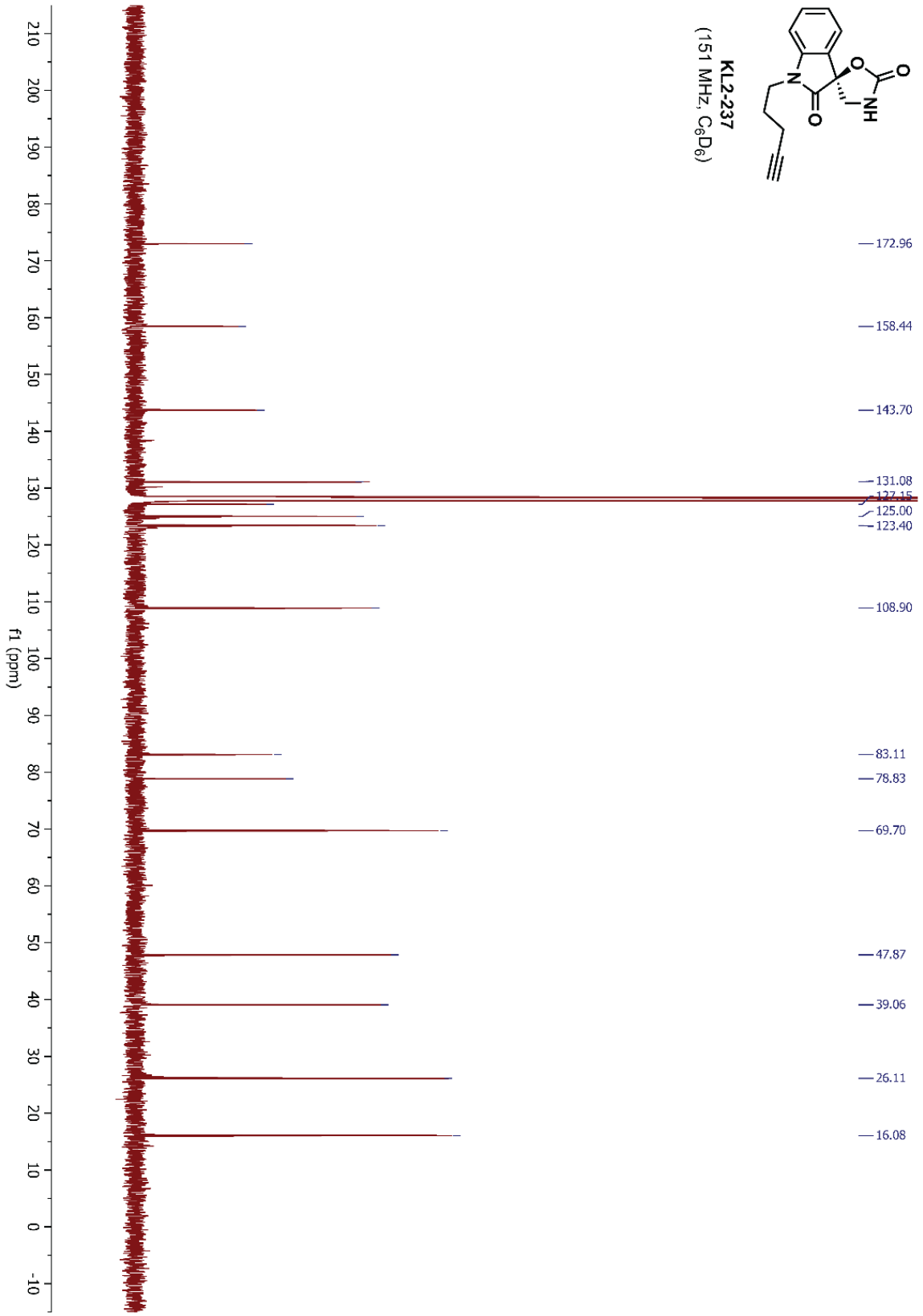
KL2-237
(151 MHz, C_6D_6)
172.96
158.44
143.70
131.08
127.15
125.00
123.40
108.90
83.11
78.83
69.70
47.87
39.06
26.11
16.08
f1 (ppm)

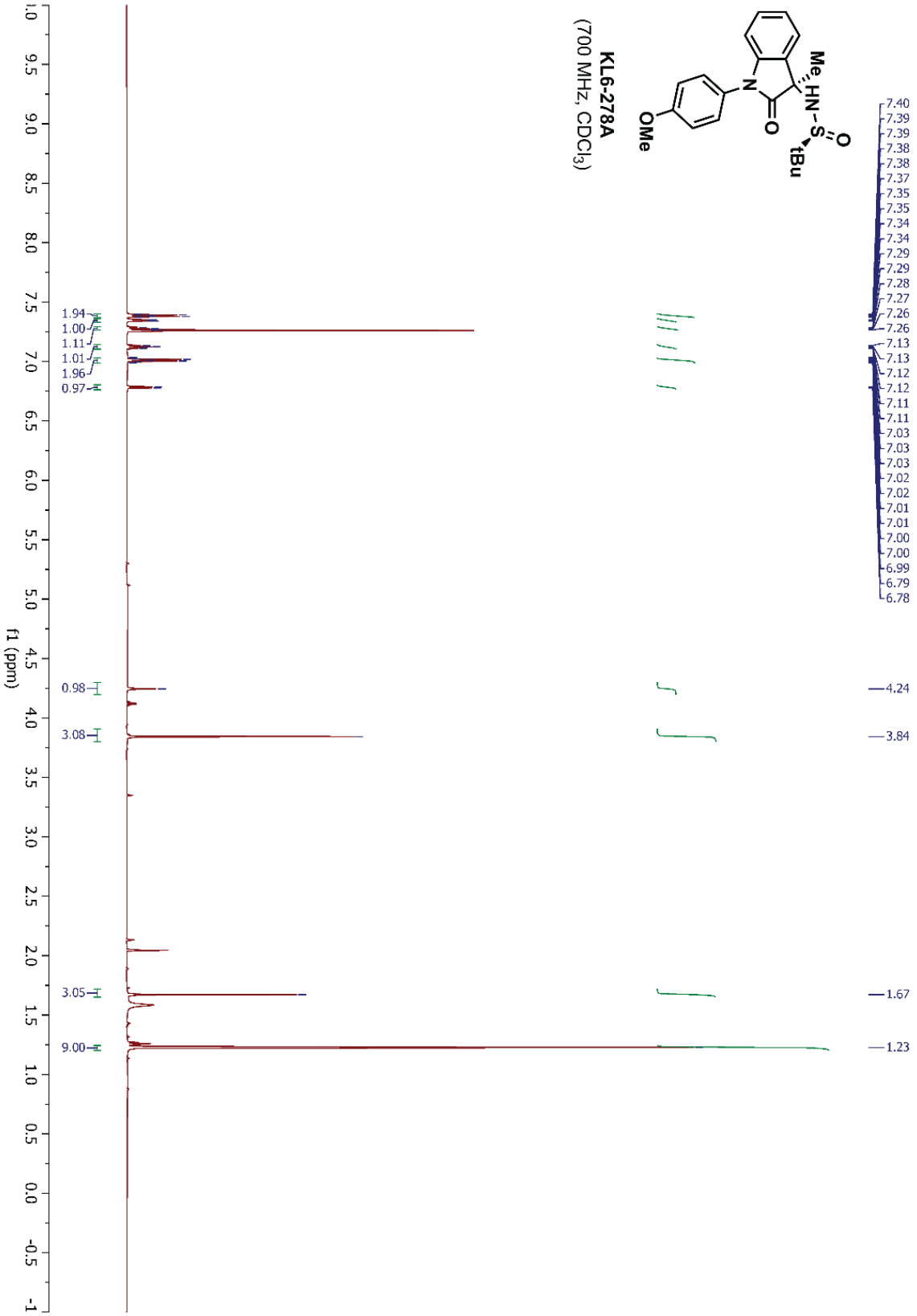
KL6-278A
(700 MHz, CDCl3)
Me
HN
S
O
O
tBu
N
O
OMe
7.40
7.39
7.39
7.38
7.38
7.37
7.35
7.35
7.34
7.34
7.29
7.29
7.28
7.27
7.26
7.26
7.13
7.13
7.12
7.12
7.11
7.11
7.03
7.03
7.03
7.02
7.02
7.01
7.01
7.00
7.00
6.99
6.79
6.78
1.94
1.00
1.11
1.01
1.96
0.97
0.98
3.08
3.05
9.00
4.24
3.84
1.67
1.23
f1 (ppm)

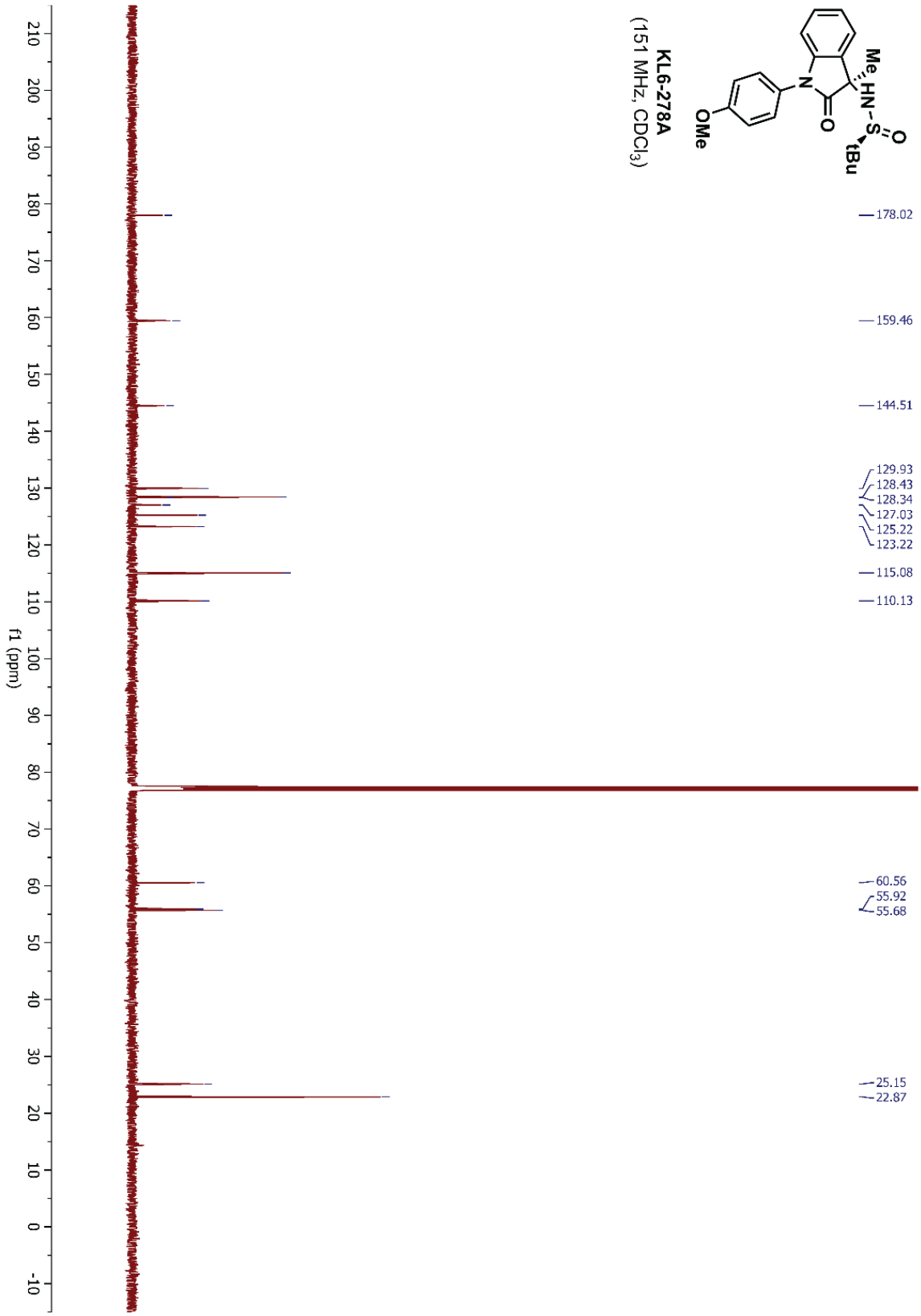
KL6-278A
(151 MHz, CDCl3)
OMe
N
O
Me
HN
S
O
tBu
178.02
159.46
144.51
129.93
128.43
128.34
127.03
125.22
123.22
115.08
110.13
60.56
55.92
55.68
25.15
22.87
f1 (ppm)
210
200
190
180
170
160
150
140
130
120
110
100
90
80
70
60
50
40
30
20
10
0
-10

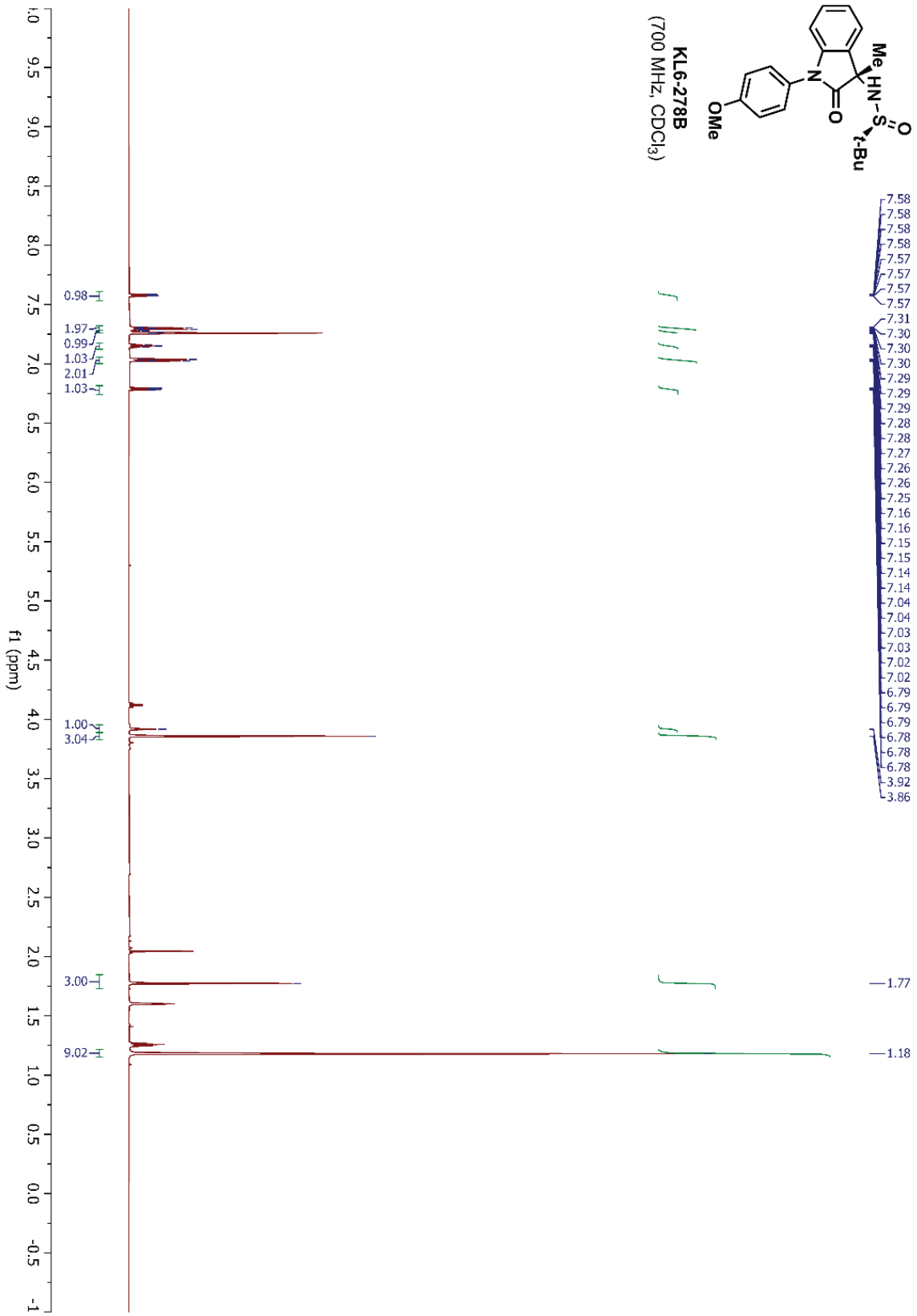
KL6-278B
(700 MHz, CDCl3)
Me
HN
S
O
t-Bu
N
O
OMe
7.58
7.58
7.58
7.58
7.57
7.57
7.57
7.57
7.31
7.30
7.30
7.30
7.29
7.29
7.29
7.28
7.28
7.27
7.26
7.26
7.25
7.16
7.16
7.15
7.15
7.14
7.14
7.04
7.04
7.03
7.03
7.02
7.02
6.79
6.79
6.79
6.78
6.78
6.78
3.92
3.86
1.77
1.18
0.98
1.97
0.99
1.03
2.01
1.03
1.00
3.04
3.00
9.02
f1 (ppm)

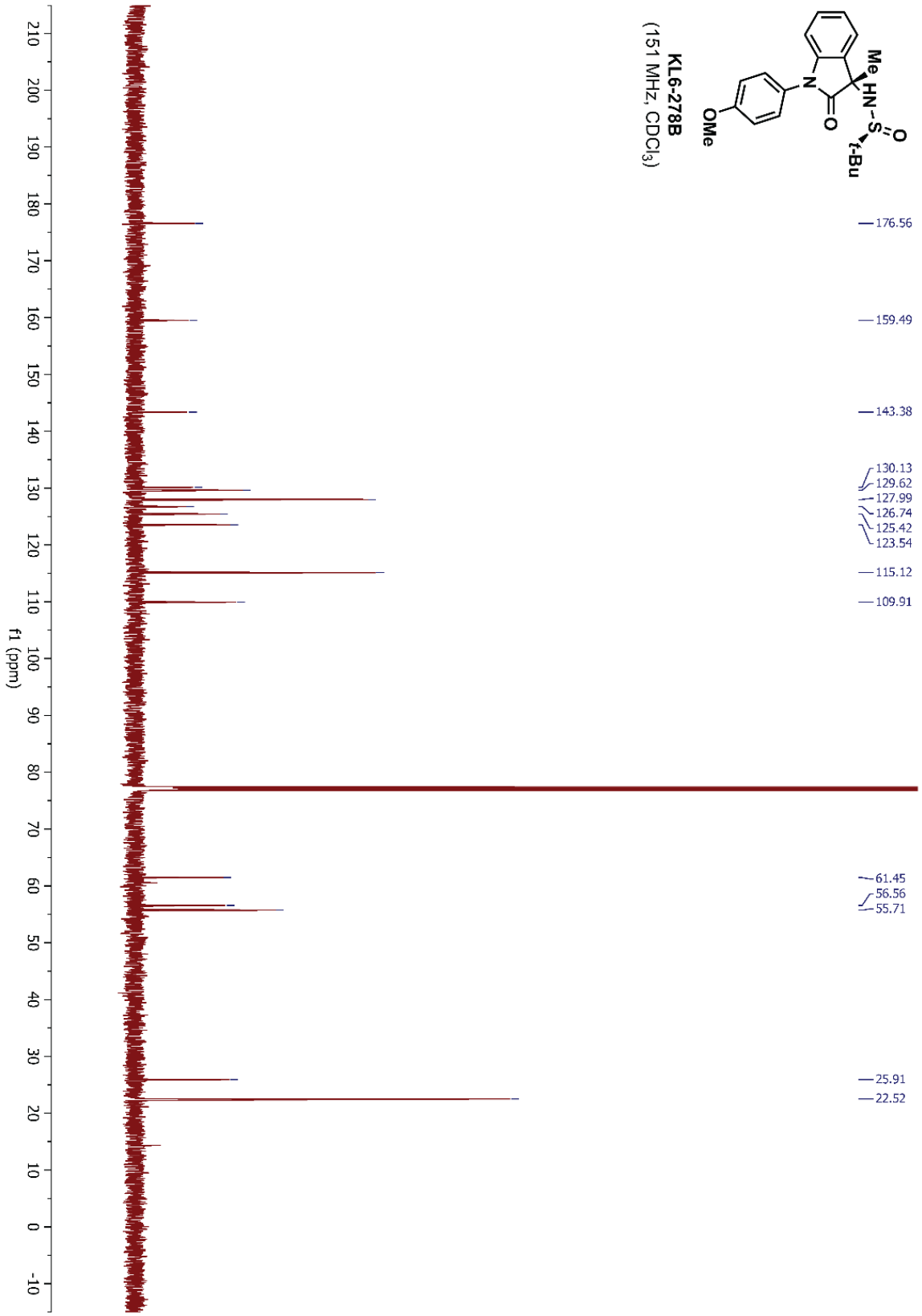
KL6-278B
(151 MHz, CDCl3)
OMe
Me
HN
S
O
O
t-Bu
176.56
159.49
143.38
130.13
129.62
127.99
126.74
125.42
123.54
115.12
109.91
61.45
56.56
55.71
25.91
22.52
f1 (ppm)